Cooperative Localization and Control In Multi-Robot Systems With Event-Triggered Mechanism: Theory and Experiments

by

Tohid Kargar Tasooji

A thesis submitted in partial fulfillment of the requirements for the degree of

Doctor of Philosophy
in
Control Systems

Department of Electrical and Computer Engineering

University of Alberta

Abstract

With the rapid development of mobile robots in practical applications, single robots are generally unable to carry out complex tasks in a large-scale dynamic environment. Therefore, cooperative robotics have grown in recent years as a new research branch that focuses on the problem of coordinating mobile robot teams, such as exploration of multi-robots and coordination of robotic networks. In multi-robot system, the accurate localization of each robot in the team is essential for a successful operation. Existing cooperative localization approaches neglect some realistic limitations of mobile robots, such as battery capacity and communication bandwidth. Especially, this issue is important when the number of sensors, actuators, and robots in the team increases. To this end, event-triggered sampling, as an alternative to time-triggered mechanism, has been employed. Using this framework, the energy consumption of sensors can be reduced and the average updating period of the actuators will be larger. In this aperiodic paradigm, the fundamental idea is that data is sent through the channel only when needed. Mathematically speaking, the system components do not exchange information unless a pre-set triggering condition is satisfied.

The first part was motivated by these realistic limitations of mobile robots and it suggests a new approach for cooperative localization based on event-triggered mechanism. Motivated by the aforementioned discussion, our objective is to design and implement the event-triggered cooperative localization for a group of e-puck2 robots. Our theoretical analysis and experimental results show that we achieve a tradeoff between localization accuracy and communication resources. The second part addresses the problem of decentralized event-triggered cooperative localization

(DECL) for a group of mobile robots in the presence of time delays. We introduce a DECL algorithm for multi-robot systems under time delays. We consider two different scenarios (i) time-stamped (ii) non time-stamped that leads to different DECL algorithms. Then, we provide the stochastic boundedness of filtering error considering bounded random delays. We show that if the delay due to multi-robot communication is sufficiently small, then by choosing proper event-triggering parameters, the filtering error and covariance remain bounded while reducing the transfer of information. In third part of thesis, we study the problem of a secure decentralized event-triggered cooperative localization (SDECL) for a team of mobile robots in an adversarial environment, where the objective is to perform localization in the presence of a malicious attacker. We consider a scenario in which the attacker is able to attack the communication channels between the exteroceptive sensors and filter of the robot and between two robots independently. In forth part of thesis, we investigate the problem of event-triggered consensus control for a group of mobile robots based on cooperative localization (CL). In our framework, each robot employs the position estimates from CL to jointly achieve consensus. An event-triggered mechanism based on a mixed-type condition is adopted in order to reduce the frequency of control updates and unnecessary transmission of information between system components. Our goal is to design an event-triggered consensus controller based on CL such that the closed-loop system achieves the prescribed consensus in spite of inaccurate sensor measurements. We provide sufficient conditions that guarantee the desired consensus using eigenvalues and eigenvectors of the Laplacian matrix. In last part of thesis, we investigate the secure consensus control problem for multi-robot systems with event-triggered communication strategy under aperiodic energy-limited denial of-service (DoS) attacks, where DoS attacks prevent the transmission of information between robots. Based on above discussion, our goal is to design a secure control scheme based on cooperative localization (CL) with event-triggered mechanism and investigate under what conditions the N robots can move cooperatively to the desired consensus position despite the presence of DoS attacks.

Preface

This thesis is an original work by Tohid Kargar Tasooji. As detailed in the following, some chapters of this thesis have been published, accepted or submitted for publication as scholarly articles in which Professor Horacio J. Marquez was the supervisory author and has contributed to concepts formation and the manuscript composition.

- The results of Chapter 3 has been published in the article: T. K. Tasooji and H. J. Marquez, "Cooperative Localization in Mobile Robots Using Event-Triggered Mechanism: Theory and Experiments," *IEEE Trans. Autom. Sci. Eng.*, vol. 19, no. 4, pp. 3246-3258, Oct. 2022, doi: 10.1109/TASE.2021.3115770.

- The results of Chapter 4 has been published in the article: T. K. Tasooji and H. J. Marquez, "Decentralized Event-Triggered Cooperative Localization in Multirobot Systems Under Random Delays: With/Without Timestamps Mechanism," in *IEEE-ASME Trans. Mechatronics*, September 2022, doi: 10.1109/TMECH.2022.3203439.

- The results of Chapter 5 has been published in the article: T. K. Tasooji and H. J. Marquez, "A Secure Decentralized Event-Triggered Cooperative Localization in Multi-Robot Systems Under Cyber Attack," in *IEEE Access*, vol. 10, pp. 128101-128121, 2022, doi: 10.1109/ACCESS.2022.3227076.

- The results of Chapter 6 has been published in the article: T. K. Tasooji and H. J. Marquez, "Event-Triggered Consensus Control for Multi-Robot Systems with Cooperative Localization" *IEEE Trans. Ind. Electron.*, July 2022, doi: 10.1109/TIE.2022.3192673.

- The results of Chapter 7 has been submitted in the article: T. K. Tasooji and H. J. Marquez, "Event-Based Secure Consensus Control for Multi-Robot

Systems with Cooperative Localization Against DoS Attacks " *IEEE-ASME Trans. Mechatronics*, Oct 2022.

To my parents

To my wife

For their endless love and support

The future belongs to those who believe in the beauty of their dreams

– Eleanor Roosevelt

Acknowledgements

First, I would like to express my sincere appreciation to my supervisor, Professor Horacio. J. Marquez, for his guidance and support during my PhD. program.

My deepest gratitude to my parents, who are always there for me and taught me lessons that nobody else could have.

Last but not least, to my beloved wife, I simply could not have done this without her, Words can not express how grateful I am to her.

Contents

List of Tables

List of Figures

List of Symbols

List of Acronyms

DoS Denial of Service

CL Cooperative Localization

CPSs Cyber Physical Systems

LMI Linear Matrix Inequality

FDI False Data Injection

MASs Multi Agent Systems

NCSs Networked Control Systems

DECL Decentralized Event-Triggered Cooperative Localization

SDECL Secure Decentralized Event-Triggered Cooperative Localization

EKF Extended Kalman Filter

SLAM Simultaneous Localization and Mapping

DR Dead Reckoning

ETM Event-Triggered Mechanism

MRSs Multi-Robot Systems

TCP Transmission Control Protocol

ROS Robot Operating System

AR Augmented Reality

RSSI Received Signal Strength Indicator

Chapter 1

Introduction

I Background

In recent years, multi-robot systems (MRSs) have received growing attention due to their significant advantages in accomplishing complex tasks compared with single robots, especially in hazardous and unknown environments and applications such as surveillance, monitoring, search, location, etc [111]-[112]. Critical to the proper operation of a multi-robot team is the reliable localization of each robot in the group, including both its position and orientation. Since these variables are very difficult or impossible to measure in any practical application, the position and orientation of each robot need to be estimated using cooperative localization (CL), a problem that presents significant challenges [62]. Cooperative localization requires information exchange between robots in the team. As the number of sensors, actuators, and robots in the team increases, the amount of information that needs to be transferred in real-time increases exponentially [62]. Two problems associated with this increase are (i) energy consumption, and (ii) bandwidth use. Energy consumption is always important when using battery-operated mobile devices and can be critical when operating small robots with limited energy resources [62]. Similarly, bandwidth constraints may impose an upper limit on communication rates thus compromising system performance. An increase in communication exchange between agents may result in packet losses if the number of packets in the transmission is greater than the available bandwidth. Thus, the the frequency at which sensors operate needs to be adjusted to not exceed the available bandwidth [62]. This inspires us to consider intermittent communication between neighboring robots. To this end, event-triggered sampling, as an alternative to the time-triggered mechanism, has been employed. Using this framework, the energy consumption of sensors can be reduced and the

average updating period of the actuators will be larger. In this aperiodic paradigm, the fundamental idea is that data is sent through the channel only when needed. Mathematically speaking, the system components do not exchange information unless a pre-set triggering condition is satisfied. The main problem is then to design the event-triggered cooperative localization in a way that the desired stability and/or performance is achieved, a problem that is nontrivial and more difficult compared with the periodic counterpart. This is also more challenging when practical issues such as packet dropouts and communication delays happen during data transmission through the communication channel. Cyber attacks are an increasing threat to the security of networked multi-robot systems. More specifically, communication between different robots can be affected by injecting malicious packets and blocking messages through communication channels, which creates another challenge for multi-robot cooperative localization. Therefore, this problem requires designing cooperative localization algorithms that can recover the states of multi-robot system from corrupted measurements.

One of the fundamental problems studied in the control of MRSs is the so-called *consensus problem*. The consensus problem refers to the development of control protocols for a group of robots equipped with onboard sensors to reach an agreement on a task of interest, such as following a trajectory of reaching a position, using only local interactions. In recent years, the consensus control problem of multi-agent systems (MASs) has been the subject of much research [64]-[75]. Consensus control protocols require reliable localization of each robot in the team. In most MRSs applications, each robot typically employs its own proprioceptive sensors to perform self-localization. These sensors, however, rely on physical measurements such as wheel dimensions, etc, and therefore accumulate error over time, and therefore are not sufficiently accurate to achieve precise consensus. The Global Positioning System (GPS) and simultaneous localization and mapping (SLAM) can provide significantly better localization. However, the use of GPS can be challenging in cluttered urban environments, open areas, and an indoor applications [33]. *Cooperative localization* (CL) can provide a good alternative solution. In CL, a team of robots improves localization using relative observations between robots and the flow of positioning information. In this approach, each robot equipped with exteroceptive sensors can local positioning with other robots in order to improve localization. Different estimation approaches for the CL problem have been presented in [1]-[35].

CL methods have been also applied to the consensus control problem, showing much improved results [96]. While the use of cooperative localization can improve the localization of robots, the use of CL does bring some additional complexity into the system and consequent problems. Two of those problems worthy of mention are additional communication between robots, which may lead to excessive energy consumption, and the potential of cyber attacks interrupting the flow of communication and thus the ability to benefit from cooperative localization. The first problem can be critical in battery-operated robots with limited power range, while the second is common to all applications that work using a communications network.

II Literature review

II.1 Cooperative Localization

Precise localization is one of the key criteria for mobile robot autonomy [1]. Indoors and outdoors, mobile robots need to know their exact position and orientation (pose) in order to accomplish their required tasks. There have been several approaches to the localization problem utilizing different types of sensors [2] and a variety of techniques (e.g., [3]–[5]). The idea of exploiting relative robot-to-robot measurements for localization can be traced back to [6], where members of a mobile robotic team were divided into two groups, which alternated remaining stationery as landmarks for the others. Later, [7] removed the necessity of some robots to be stationary and also introduced the term CL to refer to this localization technique.

CL technique has attracted much attention among researchers because of its performance to improve localization accuracy in multi-robot Systems. Most of the studies found in the literature address one or more of the following issues:

- Multi-robot cooperative localization. Multiple approaches have been proposed, including dead reckoning (DR), extended Kalman filter (EKF), maximum a posteriori (MAP) estimator, simultaneous localization and mapping (SLAM), simultaneous localization and object tracking based on particle filters, split covariance intersection filter, robust extended H_∞ filtering (REHF) and Unscented Kalman filter.

- Relative measurement mechanism: including how the number of robots affects localization accuracy.

- Finite-range sensing and communication problems.

Roumeliotis et al. [8] presented a distributed multi-robot localization problem in which they decompose the extended Kalman filter (EKF) into a number of filters such that each robot can perform the prediction step of the EKF locally. They showed how the propagation of the covariance matrix can be factored using singular-value decomposition such that each robot individually can compute the factored terms using their own odometry data. The factored terms only require to be combined before a measurement update, which then requires full network connectivity. Nerurkar et al. [9] performed cooperative localization using a distributed maximum a posteriori (MAP) estimator. Kia et al. [10] proposed a novel distributed CL algorithm in which each robot localizes itself by local dead reckoning, and corrects its pose (position and orientation) estimate whenever it receives a relative measurement update message from a server. The server only needs to compute and transmit update messages when an inter-robot measurement is received. Madhavan et al. [11] propose a framework for localization and terrain mapping for a team of robots operating in uneven and unstructured environments. For cases where all robots of the team may not have absolute positioning capabilities, they showed how cooperative localization and mapping can be performed using robots with heterogeneous sets of sensors. Howard et al. [12] investigated the performance of multi-robot simultaneous localization and mapping (SLAM), where each robot is unaware of the other's initial pose and begins state estimation in a decentralized manner. When robots detect each other for the first time, their individual maps are merged into a common map. The mapping process then continues as robots transmit new observations to each other. Ahmad et al. [13] present a unified framework for multi-robot cooperative simultaneous localization and object tracking based on particle filters. This approach is scalable with respect to the number of robots in the team. Li et al. [14] propose a new cooperative multi-vehicle localization approach using split covariance intersection filter. The basic idea of the proposed method is that each vehicle keeps an estimate of a decomposed group state and this estimate is shared with neighboring vehicles; the estimated state of the decomposed group is updated with both the sensor data of the ego-vehicle and the estimates sent from other vehicles. A split covariance intersection filter is used for data fusion purposes. Kim et al. [15] propose cooperative localization and sea currents estimation using multiple Autonomous Underwater Vehicles (AUVs). The authors acknowledge that dead reckoning (DR) is not reliable for localization due to error accumulation. To

reduce error accumulation, they propose a navigation algorithm that allows multiple AUVs to simultaneously estimate their navigation states and unknown sea currents. They propose the combination of an Unscented Kalman filter and a linear Kalman filter for joint estimation of the navigation states and unknown sea currents. Zhuang et al. [16] proposed a robust approach for multi-robot cooperative localization based on the Metric-based The iterative Closest Point (MbICP) algorithm could provide relative observations more accurately and conveniently, even in a dynamic or semi-structured indoor environment. To deal with the inherent non-linearities in the multi-robot kinematic models and the relative observations, the authors have developed a robust extended H_∞ filtering (REHF) approach, which could handle the non-Gaussian process and measurement noises with respect to robot navigation in unknown dynamic scenes.

Rekleitis et al. [17] investigated how sensing mechanisms and the number of robots influence localization performance with multiple robots. The sensing mechanism included range only, bearing only, range and bearing, and full pose sensing (range, bearing, and relative orientation). The results showed that the full pose measurement mechanism gives slightly better results than the range and bearing measurement mechanism, as well as the range-only measurement mechanism. Increasing the number of robots also indicated better localization results. However, bearing-only measurement mechanisms performed poorly, regardless of the number of robots used. Roumeliotis et al. [18] analytically quantified the benefit of cooperative localization. They showed how the number of robots can affect localization performance. Furthermore, they discovered that increasing the number of robots reduced the uncertainty of localization. Safavi et al. [19] provide a linear distributed algorithm to localize an arbitrary number of mobile robots moving in a bounded region. They assume that each robot can measure a noisy version of its motion as well as its distance to the neighboring nodes.

To process every inter-agent relative measurement, the robots need to communicate with each other. The objective of a decentralized algorithm is to eliminate the need for all-to-all communication in order to reduce the communication burden. The communication cost however can still be high if the robots take measurements from every robot in their measurement zone. The problem of computation/communication cost reduction via smart management of inter-robot relative measurements has been studied in [20]–[21]. One of the approaches used is to de-

termine the optimal measurement frequency given resource constraints [20], [21]. Wanasinghe et al. [22] present a framework to address the finite-range sensing problem of leader-assistive localization. The proposed framework consists of a method to virtually enhance the leader robots' sensing range, and a novel graph search algorithm to avoid possible double counting of the same information when multiple leader robots attempt to provide the localization data to a given child robot. It was shown in [5] that given a limited set of relative measurements from a network of robots in a formation, localizing the robots (and determining the correct formation) is an NP-hard problem. The methods employed in [20] and [21] assume a fixed sensing topology and utilize covariance upper bound analysis to determine the relative measurement frequency in the team. In these methods, the steady-state covariance upper bound obtained by the Discrete-time Algebraic Riccati Equation (DARE) and the corresponding Continuous Algebraic Riccati Equation (CARE). The observability of the system is necessary for the convergence of the Riccati recursion [20], [21], which means there must be at least one robot accessing absolute positioning information such as GPS signals or known landmarks [23]. The methods employed in [24]-[26] consider the cost management in CL via measurement scheduling, in which robots get restricted to take only a certain number of relative measurements but they have to choose their landmark robots in a way that the positioning uncertainty is minimized. It is known in the literature that the optimal measurement scheduling for CL is an NP-hard problem [26], [27]. Therefore, the main effort is on proposing sub-optimal solutions with reasonable computational complexity. The studies in [24], and [25] use some form of greedy algorithms to perform the landmark robot selections. Sullivan et al. [28] investigate the CL algorithm under varying sensor qualities (position accuracy, yaw accuracy, sample rate), communication rates, and a number of robots for both homogeneous and heterogeneous multi-robot systems. Zhu et al. [29] proposed two decentralized multi-agent CL algorithms to guarantee filter consistency and reduce communication costs. In the first algorithm, they consider unknown inter-agent correlations via an upper bound on the joint covariance matrix of the agents. In the second method, they employ an optimization framework to estimate the unknown inter-agent cross-covariance matrix. Trawny et al. [30] proposed quantizing measurement mechanism to reduce the communication cost of CL algorithm. By quantizing measurements to 4 bits, results were practically the same compared to using actual measurements in a MAP estimator. Leung et al. [31]

present a decentralized state-estimation algorithm guaranteed to work in dynamic robot networks without connectivity requirements. They confirm that a robot only requires to consider its own knowledge of network topology to produce an estimate equivalent to the centralized state estimate whenever possible while ensuring that the same can be carried out by all other robots in the network.

Recent research in networked controls and cyber-physical systems has shown that event-triggered algorithms are an attractive tool capable of significantly reducing communication overhead in the area of distributed control and estimation problems. The main idea is that, unlike typical periodic (time-triggered) control and estimation algorithms that require transmission at regular time intervals, event-triggered algorithms require the transmission of information whenever certain events happen, usually if some signal related to states of interest fall outside a certain threshold. Therefore, information is only communicated when it is required and control/estimation routines can still be performed in the absence of explicit information being sent/received by processors in the network [32]. Yan et al. [33], working with robots with limited battery life and communication bandwidth, presented a novel method based on relative measurement scheduling that allows each robot to choose its landmark robots locally in polynomial time. The authors claim their method does not assume full-observability of the CL algorithm, nor does require inter-robot communication at the scheduling stage. Zhang *et al.* [34] address the problem of distributed event-triggered state estimation in sensor networks with the send-on-delta scheme on both the sensor-to-estimator and estimator-to-estimator channels. Liu *et al.* [35] investigate a distributed event-triggered filtering problem using the send-on-delta protocol in which the sensor node transmits the data to its neighbors only when the local innovation violates the triggering condition. Recently, Ouimet et al. [32] presented a Covariance Intersection (CI)-based cooperative localization algorithm for a team of unmanned robotic vehicles in which agents only send measurements to their neighboring agents when the expected innovation for state estimation is higher than a certain threshold. The authors consider an "Innovation-Level-Based" event-trigger condition, based on the difference between the current measurement and the predicted measurement. The limitation of this triggering condition, however, is that requires feedback communication from the local filter to the sensor in order to obtain the predicted measurements. A consequence of this approach is that it suffers from network-induced imperfections such as delays

and packet dropouts. We consider a different approach and employ a mixed-type event-triggering condition in which feedback communication from the estimator is not needed.

II.2 Cooperative localization under time delays

Time delays are inherent in multi-robot systems, arising from multiple factors, including communication delays [36]-[38], event-detecting delays, [39], and camera latency and image processing delays in vision-based systems [36]. Since CL relies on communication with agents via a network, communication delays have a significant effect on time delays [40]. Therefore in this work, we mainly focus on communication delays that occur due to limited bandwidth in the network. Also, communication delays are most likely to happen randomly due to the unpredictable nature of stochastic factors such as latency, percentage of out-of-ordered packets in the communication channel, and re-transmitted packets [40]. The majority of the literature on *cooperative localization* to date considers ideal communication networks, where the inter-agent packet data is transmitted instantly, and only a few scattered results consider networked-induced time delays. Fu *et al.* [41] consider the problem of communication delays and packet loss for Unmanned Aerial Vehicle (UAV) and propose two separate CL algorithms assuming a one-step random delay. Zhang *et al.* [42] investigate CL for a leader–follower problem under time delays. The authors compensate the effect of communication delays to improve localization accuracy. Phung *et al.* [43] consider the localization problem of mobile robots in the presence of communication delays and packet losses. Shan *et al.* [44] propose a particle filter to track multiple agents cooperatively considering time-delayed observations. Yao *et al.* [45] investigate the problem of CL for Multiple Autonomous Underwater Vehicles (MAUVs) in the presence of communication delays. Zhang *et al.* [46] investigate the problem of distributed Kalman filtering for a consensus of leader-following in the presence of communication delays. Most of the aforementioned works assume that the local filter in each robot receives sensor measurements periodically to update the pose estimate. However, periodic sampling may result in unnecessary data transmission with corresponding network congestion, especially when the robots have limited communication resources. To overcome this limitation, *event-triggered* sampling has emerged as an alternative to *time-triggered* or periodic sampling.

II.3 Related works on secure state estimation against cyber attacks

Most of the literature on the subject considers the problem of secure state estimation against cyber-attacks for single-agent systems. Mo *et al.* [47] consider the problem of secure state estimation against integrity attacks (or FDI attacks) where the attacker intentionally manipulates the sensor measurements. Fawzi *et al.* [48] study the problem of secure estimation and control for linear systems where the attacker hijacks the sensor measurements and actuators. The authors design a resilient state estimator and a state-feedback controller such that the state of a system is recovered accurately and improves the system's resilience against deception attacks. Shoukry *et al.* [49] consider a state reconstruction for discrete-time linear systems under *sparse sensor attacks/noise*. Li *et al.* [50] study the problem of remote state estimation where a malicious attacker launches a jamming signal on the communication channel between the sensor and remote estimator. Zhang *et al.* [51] propose an optimal DoS attack scheduling strategy where the attacker decides when or where to attack the communication channel in order to degrade the performance of the remote estimator. Su *et al.* [52] investigates malicious attack detection and secure state estimation for CPSs with sensor attacks. Lin *et al.* [53] derive an optimal estimator for CPSs whose communication channels are subject to mixed DoS and FDI attacks.

Unlike [47]-[53] which focus on single agent systems, some related works consider secure state estimation for MASs. Liu *et al.* [54] studies event-triggered distributed state estimation for discrete-time linear systems with multiple communication channels under DoS attacks. Using the covariance intersection fusion framework, the authors designed distributed Kalman filters resilient against DoS attacks. Liu *et al.* [55] further extend the results for nonlinear systems and design resilient event-triggered distributed state estimation filters against DoS attacks where the attack duration is bounded. Chen *et al.* [56] address the distributed resilient filtering problem for power systems against DoS attacks. Chen *et al.* [57] consider a saturated innovation update mechanism for resilient distributed state estimators against sensor attacks. An *et al.* [58] study the problem of distributed secure state estimation for discrete-time linear systems under sparse sensor attacks. The authors also implement the proposed algorithm over a multi-agent network. Lu *et al.* [59] investigate secure state estimation of MASs with both faulty and malicious agents.

Different from [54]-[59] where each agent reconstructs the states without cooperation in the presence of attacks, few works consider the secure cooperative state estimation under malicious attackers. Su *et al.* [60] consider resilient cooperative state estimation in unreliable multi-agent networks. A gradient descent scheme is adopted for each agent based on local measurements. In this approach, each agent transmits its updates to the other agents in the neighborhood. Lu *et al.* [61] address distributed secure state estimation where a group of agents estimates the states cooperatively under malicious attacks. A distributed switched gradient descent scheme is adopted to reconstruct the states in the presence of malicious nodes.

II.4 Related works on decentralized event-triggered cooperative localization in multi-robot systems

The event-triggered cooperative localization problem for multi-robot systems has received some attention. Ouimet et al. [32] propose a decentralized cooperative localization algorithm using ETM to reduce unnecessary packets exchanged between agents. Tasooji and Marquez [62] propose a new decentralized event-triggered cooperative localization (DECL) algorithm for a group of mobile robots where the objective is to perform localization with limited communication resources and study the effect. Reference [63] extends the results and considers the effect of random delays in the event-triggered cooperative localization.

II.5 Consensus control in multi-agent systems

Some recent research has focussed on the effect of noise affecting consensus control protocols. Cheng *et al.* [64] propose an average consensus control for double-integrator multi-agent systems (MASs) with measurement noises. Li *et al.* [65] consider the problem of distributed consensus control affected by relative state-dependent measurement noises. Chen *et al.* [66] investigate robust consensus of MASs in the presence of transmission nonlinearity and noises by using a nonsmooth Lyapunov function. Wang and Zhang [67] design a new consensus protocol using Kalman filtering and information fusion to handle the system and measurement noises. Wang *et al.* [68] investigate the problem of bounded consensus control for linear MASs with both additive system and communication noises. The authors make use of Kalman filters to estimate the state of neighbor agents. Ma *et al.* [69] design an output-feedback controller for a class of nonlinear discrete time-varying

stochastic MASs. The authors establish a framework based on recursive linear matrix inequalities to achieve the desired consensus performance satisfying both $\mathcal{H}_\infty$ and mean-square consensus. Wang *et al.* [70] focus on stochastic consensus control and performance improvement of a group of agents with linear or linearized dynamics over Markovian randomly switching topologies. Li *et al.* [71] investigate the problem of bounded consensus using event-triggered control for stochastic MASs with communication delay, as well as process and measurement noise. Cao *et al.* [72] address the event-triggered consensus of stochastic MASs. The authors develop a stochastic convergence analysis technique to achieve the desired consensus. Zou *et al.* [73] investigate the problem of event-triggered consensus tracking for a class of stochastic nonlinear MASs, where the agents' dynamics are subject to arbitrary and asynchronous switchings. Ding *et al.* [74] consider the problem of the event-triggered consensus control for a class of discrete-time stochastic MASs with state-dependent noises. The authors consider an absolute triggering condition and propose a simultaneous design of the consensus control gain and threshold of the triggering condition by solving a set of parameter-dependent matrix inequalities. Ma *et al.* [75] consider an event-triggered mean-square consensus control problem based on the triggering threshold matrix for a class of discrete time-varying stochastic MASs under sensor saturation. Ge *et al.* [76] investigate the problem of leader-following consensus for networked MASs in the presence of limited communication resources and unknown-but-bounded process and measurement noise. The authors develop a new event-triggered scheme based on a time-varying threshold parameter to schedule the transmission of sensor measurements through the communication network.

II.6 Secure consensus control in multi-agent systems under DoS attacks

Although most of the existing results on the subject consider the problem of designing secure control in the presence of DoS attacks for single-agent systems [85]-[88], some related works studied secure consensus control for MASs against DoS attacks. Feng et al. [76] introduce an event-based secure control framework for linear MASs under DoS attacks to achieve secure consensus under certain conditions for the duration and frequency of attacks. Xu et al. [77] adopt an input-based triggering approach to investigate the secure consensus problem in MASs under DoS attacks.

The authors propose an event-triggered control scheme based on the estimated relative state for a secure consensus problem. Yang et al. [78] study the problem of distributed secure consensus control for linear leader-following MASs with an event-triggered mechanism under DoS attacks. The authors consider an observer-based controller during the DoS attack instead of setting a control signal of either zero or constant. Xu et. al [79] investigate the problem of event-triggered secure consensus for MASs subject to periodic energy-limited DoS attacks. The authors develop the event-triggering condition based on two different combination measurements corresponding to leader–followers, and follower–followers. Xu et. al [82] develop a fully distributed framework to investigate the cooperative behavior of MASs under DoS attacks launched by multiple adversaries. The authors considered two types of communication mechanisms, that is, *time-triggered* and *event-triggered* communication mechanisms. Zhang and Ye [81] consider the event-triggered consensus problem for MASs under intermittently random DoS attacks. Xu et. al [83] investigate the leader-follower consensus problem with event/self-triggered mechanisms under DoS attacks. The authors construct synchronous and asynchronous updated strategies of control protocols to achieve leader-follower consensus under DoS attacks. Dong et. al [80] investigate the event-triggered leader-follower secure consensus for second-order MASs with nonlinear dynamics in the presence of DoS attacks. The authors obtain an upper bound for the duration and frequency of DoS attacks and design a controller to ensure that the tracking error between the leader and followers converges to zero. Liu et al. [84] focus on event-based secure leader-follower consensus control for MASs with multiple cyber attacks, which include replay attacks and DoS attacks. The authors model replay attacks and DoS attacks as Bernoulli processes.

III Statement of contribution

Most of the literature on event-triggered systems deals with the control problem, including closed-loop stability and various forms of systems performance for both linear and nonlinear systems. Central to the design problem and the properties of the final design is the type of triggering condition used in the implementation. Most event-triggered mechanisms (ETMs) proposed in the literature can be classified as (i) absolute (also called *send-on-delta* [89]), (ii) relative [90], or (iii) mixed [91]. Both absolute and relative ETMs are simple to use and although they have been successfully applied in multiple applications, they can result in excessive triggering

events in the presence of noise and/or disturbances. Mixed-type ETM, on the other hand, is more challenging to design but can eliminate the shortcomings of simpler ETMs and can perform better in the presence of noise or disturbances. An event-based estimation has also received attention, including event-triggering versions of the Kalman filter, and various extensions. Relevant to this work, however, the problem of event-triggering cooperative localization of multi-robot networks has not yet received much attention, perhaps due to the challenges involved in some of the practical aspects of the event-triggered mechanism. Our main contribution can be summarized as follows:

In *chapter 3*, we present a complete, novel solution to the event-triggered cooperative localization problem for multi-robot systems. Our work involves both the theoretical development of the solution and the practical implementation of a team of robots. The main challenges involved in the event-triggered formulation of our DECL algorithm include: (i) designing an event-triggering mechanism that guarantees satisfactory performance of the DECL algorithm while reducing communication rate; and (ii) application of the proposed algorithm to a practical system of multi-robots. Our solution employs a mixed-type event-triggered mechanism which can significantly reduce the communication rate between sensor and filter while maintaining the estimation error bounded. The use of a mixed-type event-triggering mechanism implies that our solution includes both the send-on-delta and relative-type triggering mechanisms of previous references as special cases. Also, we address the tradeoff between the quality of estimation and communication rate between components by posing the design of the triggering rule as an optimization problem that minimizes the communication rate subject to an upper bound on the error covariance. We also provide a mathematical relationship between energy consumption and event-triggered parameters to prove our claim. We show that by tuning the event-triggered parameters, we can reduce the amount of information transmitted in the network in order to minimize the energy consumption of each robot. Unlike current literature which validates the results by simulations, we endeavor on the practical application and validation of the results using a team of four e-puck2 robots. Comparative experiments are carried out for different choices of triggering parameters. The results illustrate that satisfactory localization performance can be achieved at a reduced average sampling rate. We emphasize that the practical application of the results is nontrivial and brings up a multiplicity of challenges,

including limited communication bandwidth, power constraints, synchronizing the timestamps of messages, and time delays in multi-robot systems.

In *chapter 4*, our main interest is the problem of designing a DECL algorithm that can deliver reliable performance in the presence of time delays. Our study is based on the DECL architecture proposed in our previous work [62], but our main results and approach are valid in any other architecture. Our main focus is in the effect of time delays, including the design of the event-triggered mechanism (ETM) and Kalman gain in the presence of time delays. Second, we consider the implementation of the proposed algorithm to a practical system of multi-robots considering the challenges of limited communication bandwidth, power constraints, and synchronizing timestamps. we investigate the effect of time delays in designing the DECL algorithm and propose a solution that guarantees satisfactory performance in the presence of time delays while reducing the communication rate. Considering time delays leads to a different set of assumptions and a different structure of the DECL design with respect to our previous work [62] and current literature [1]-[35]. Our solution allows multiple-step random delays in the DECL algorithm design, unlike [41]-[44], which are limited to a one-step delay. Furthermore, different from our previous work [62] where the higher order terms in the Taylor series expansion were ignored during the filter design, in this work we explicitly account for the higher order terms as a norm-bounded uncertain term, which improves the robustness of the design. *Second*, our solution considers two separate scenarios, thus leading to two separate DECL algorithms assuming (i) time-stamped and (ii) no time-stamped information. In the first case, the local filter does not have information pertinent to the time delays affecting the signals received. Thus, our solution relies on probabilistic models. We then consider the case where information data packets are time-stamped and propose a DECL algorithm that takes advantage of the information available. Time-stamped technology offers a convenient way to reorder delayed measurements [92]. However, non-time-stamped technology is simpler to use and can be an appropriate way to reduce communication costs in the case of limited communication bandwidth compared to time-stamped technology [92]. *Third*, different from our previous work [62], which is limited to designing the DECL algorithm, we prove the efficiency of the proposed DECL algorithm by computing the stochastic boundedness of the filter error under random delays. We obtain sufficient conditions that ensure convergence and stochastic stability of the proposed DECL algorithm.

We show that if the maximum delay due to agent-agent interaction is sufficiently small, then choosing proper event-triggering parameters the filtering error and its covariance remains bounded while reducing the average transmission rate of information between the sensor and filter. In other words, this work deals with the convergence analysis and design of the event-triggering mechanism under random delays and system nonlinearities, which extends our previous work [62] in a non-trivial manner. *Finally*, in addition to the theoretical developments, we tackle the practical implementation of our results using a fleet of e-puck2 mobile robots with inherent time delay. This time delay is the effect of camera latency, image processing, event-detector, and communication network delays. In our experiments, we employ time-stamped technology to transmit packets including sensor measurements and communication between multiple robots.

In *chapter 5*, we investigate the problem of event-triggered cooperative localization for multi-robot systems in the presence of cyber attacks. Departing from our previous work in references [62]-[63], we modify our DECL algorithm to account for the effect of cyber attacks. Our work involves both the theoretical development of the solution and practical implementation using a fleet of e-puck2 robots. The experimental results are expected to provide a preliminary effort toward bridging the gap between theoretical analysis and experimental validation. The main challenges involved in this work include (1) designing a secure CL algorithm against cyber attacks that guarantees satisfactory localization performance while maintaining a low communication volume between system components, and (2) implementing the solution using a multi-robot hardware platform and verifying the effectiveness of the algorithm. Compared with the existing literature on *cooperative localization* [1]-[35] and our previous works on *decentralized event-triggered cooperative localization* [62]-[63], this work investigates secure decentralized event-triggered cooperative localization for multi-robot systems operating with an unreliable communication network subject to DoS and FDI attacks. Also, we consider a scenario in which each robot can sense and communicate with other robots simultaneously within a certain range, extending the results of our previous works [62]-[63]. Contrary to the case of secure state estimation against a single type of attack (either DoS or FDI) for a single agent system as in references [47]-[52], we consider secure state estimation for MASs in the presence of mixed DoS and FDI attacks. Different from [54]-[59] where agents reconstruct states without cooperation, we design a resilient state estimation

scheme in which agents reconstruct the states cooperatively in the presence of mixed attacks. In contrast to [56]-[61] that employ periodic sampling, our solution relies on a mixed-type event-triggered mechanism which significantly reduces the average transmission of information through the network. Moreover, our approach to secure communication is different from [54], [56], [58], [59]. In our approach, we consider a detector for each robot based on received *innovations* to decide whether the measurements received have been attacked or not. Also, the majority of the literature on secure state estimation uses simulations to justify the proposed solution. In this work, we tackle the actual implementation of our solution using a group of mobile robots. The implementation is not trivial and brings up multiple challenges. *First*, we introduce an SDECL algorithm for a group of mobile robots explicitly focusing on the problem of cyber attacks. We consider a scenario in which the adversary is able to attack the communication channels between the exteroceptive sensors and the robot's filter and between two robots independently. *Second*, we prove the effectiveness of the proposed algorithm by computing the stochastic boundedness of the estimation error in the mean square for the SDECL algorithm under cyber attacks. We provide sufficient conditions that ensure the resiliency and convergence of the proposed algorithm when the attacker signal is bounded. We show that by choosing a proper event-triggered condition, the estimation error and covariance of the state estimator remain bounded while reducing the data transmission between the sensor and the filter. *Third*, when the attack signals are unbounded we introduce an attack detection mechanism capable of detecting the presence of an attack. *Finally*, comparative experiments are carried out using a team of four e-puck2 robots to validate the corresponding theoretical results. The experimental results show the effectiveness and robustness of the SDECL algorithm in the presence of cyber attacks.

In *chapter 6*, we consider the problem of event-triggered consensus control for multi-robot systems in the presence of sensor noise. Different from [93]-[95] where the impact of sensor measurement noise is ignored, our consensus control protocol employs a CL algorithm in which each mobile robot estimates its state cooperatively using onboard sensors and relative measurements. Unlike [64]-[70] which consider a time-triggered scheme in consensus control problems, our solution employs an event-triggering mechanism to reduce the amount of transmitted information by each agent. Also, our proposed event-triggering scheme depends only on the state

estimate of each robot, but the neighboring state estimates are not required to check the event-triggering condition which reduces the communication and computational cost in each robot. This formulation is therefore simpler and different from previous works in references [93]-[95], [74]. In addition, we consider a scenario in which each robot can take relative measurements and can communicate with multiple robots simultaneously within a certain communication range, thus improving the estimation performance compared with our own previous work [62]. Different from [93]-[95], [64]-[65], [67]-[69], [71], [72], [74], [75] which assume a fixed communication topology, we consider a realistic scenario in multi-robot systems in which communication between robots can be switched randomly over the time due to random link failures, or limited communication range. Also, our work relaxes the assumption in references [93]-[95], [64]-[69], [71]-[75] where they assume that all communication graphs are connected. Removing this assumption is important because, due to the limited communication range, agents may fail to maintain a connected communication topology. Finally, much of the existing works reported in the MASs literature, including references [64]-[69], [71]-[75], illustrate their findings using computer simulations. While computer simulations are unquestionably important, there are a number of issues very difficult to capture in computer simulations. In this work, we explicitly tackle the practical implementation of the consensus results using a group of e-puck2 mobile robots. Much of our work is, in fact, motivated by the challenges encountered in this application, including communication bandwidth, power constraints, wheel velocity constraints, time delays in the communication of multi-robot systems and packet losses. Our experimental results show the effectiveness and robustness of the proposed consensus algorithm in the presence of these challenges. The main challenges encountered in this work include (i) the development of the event-triggered consensus control for multi-robot systems capable of coping with sensor noise while reducing computation burden as well as the average communication rate, and (ii) establishing a framework to design the consensus control gain, filter gain and parameters of event-triggered mechanism simultaneously. Motivated by the above challenges, our main contribution can be summarized as follows: *First*, we develop a novel event-triggered consensus protocol for a team of mobile robots based on cooperative localization (CL). Our solution employs a mixed-type triggering condition to reduce the frequency of control updates and significantly reduce the transmission of information between robots. *Second*, we provide sufficient

conditions to ensure bounded consensus in mean square sense and compute the consensus bound of multi-robot systems. *Third*, we propose a simultaneous design of the consensus control gain, the filter gain and the parameters of the event-triggered mechanism, that reflects the desired consensus performance. Our solution is cast using linear matrix inequalities (LMI) which can be solved using efficient numerical tools. *Finally*, we implement the proposed method experimentally on group of four e-puck2 robots to validate our theoretical results.

In *chapter 7*, In this work, our interest is in the study of resilient consensus control of MRSs under DoS attacks with an event-triggered communication strategy. More specifically, we consider a scenario in which each robot equipped with proprioceptive and exteroceptive sensors estimates its states cooperatively by taking relative measurements and exchanging local positioning information with other robots using an unreliable communication network that is susceptible to DoS attacks. Position estimates from cooperative localization (CL) are also collected from neighbouring robots through the unreliable network to update the control signal and achieve consensus. Different from [93]-[95], [76]-[80], [82]-[83] where the effect of noise in sensor measurements and controller design is neglected, we consider a scenario in which each robot can estimate its own state using the CL algorithm and jointly perform consensus. Unlike some existing references that either take a zero control signal or set the control signal as a constant value [76], [82], [85], [88] during the DoS attack intervals, our control strategy employs the predicted state of its neighbouring robots to improve resiliency and secure consensus during DoS attack intervals. Different from [76]-[79] where it is assumed that the adversary launch the attacks to all communication links simultaneously, we consider a scenario where the adversary has limited energy resources and may attack some partial communication links during the attack interval. Compared to the periodic DoS attacks investigated in [79], we consider a case where DoS attacks occur aperiodically. Different from the event-triggered communication strategy proposed in [76], [78], [83], [84], where continuous communication is required in order to check the triggering condition and update the control signal, our proposed event-triggered mechanism relies only on state estimates of the agent itself and other agents state estimates are not required. Also, our triggering condition is structurally different from [76], [78], [83], [84]. In addition, the CL algorithm proposed here extends the previous works [1]-[35], where each agent is able to take relative measurements and communicate with multiple

neighbouring agents simultaneously and reconstruct its current state in the presence of DoS attacks to improve localization performance. To the best of our knowledge, the problem of event-triggered consensus control with cooperative localization has not been investigated for multi-robot systems in the presence of DoS attacks. In this work, we extend the result of our prior work in [93] to account for the effect of DoS attacks in the communication network. We deal with the following challenges in this work *(1) How to develop a framework to solve a consensus problem of multi-robot systems by simultaneously considering the limited communication resources and unreliable communication network? (2) how to design the gain of the consensus control protocol and filter gain as well as the parameters of the event-triggered scheme simultaneously to ensure a secure consensus in the presence of DoS attacks. (3) how to establish an optimization framework to maximize the attack duration that the multi-robot system can tolerate without losing consensus performance?* Inspired by the aforementioned challenges, the main contribution of our work is summarized as follows: *First*, we develop a secure consensus control for multi-robot systems where each robot localizes itself cooperatively and reaches consensus in the presence of DoS attacks. An event-based protocol based on mixed-type triggering conditions is employed to reduce data transmission between agents and the frequency of control updates. *Second*, we obtain sufficient conditions to guarantee secure consensus of MRSs in exponentially mean square sense. *Third*, we provide an optimization framework to maximize the attack duration such that MRSs reach secure consensus by designing the control and filter gains as well as the parameters of the event-triggered scheme simultaneously. *Finally*, we implement the designed event-based secure consensus control experimentally on a team of four e-puck2 mobile robots and validate the effectiveness of the proposed controller in the presence of DoS attacks.

Chapter 2

Preliminaries

I Graph Theory

Graph theory is used in the multi-robot localization and control for the information exchange among group of mobile robots. The topology is modeled as a graph in which robots can be considered as nodes and links such as communication and sensing can be considered as edges [97]. Graph theory is the mathematical structure utilized in order to model pairwise relations between objects. A graph consists of nodes that are connected by edges. There are different types of graphs including undirected and directed graphs, [98]. An illustration of these directed and undirected graphs are represented in Figure 2.1. An undirected graph is a graph in which edges do not have orientations. Mathematically, an undirected graph is an ordered pair $G = (V, E)$ comprising:

1. V, a set of nodes (also called points).
2. $E \subseteq \{\{x, y\} \mid x, y \in V \text{ and } x \neq y\}$, a set of edges (also called links) which are unordered pairs of nodes.

A directed graph or digraph is a graph in which edges have orientations. Mathematically, directed graph is an ordered pair $G = (V, E)$ comprising:

1. V, a set of nodes (also called points).
2. $E \subseteq \{(x, y) \mid (x, y) \in V^2 \text{ and } x \neq y\}$, a set of edges (also called directed links or directed edges) which are ordered pairs of nodes.

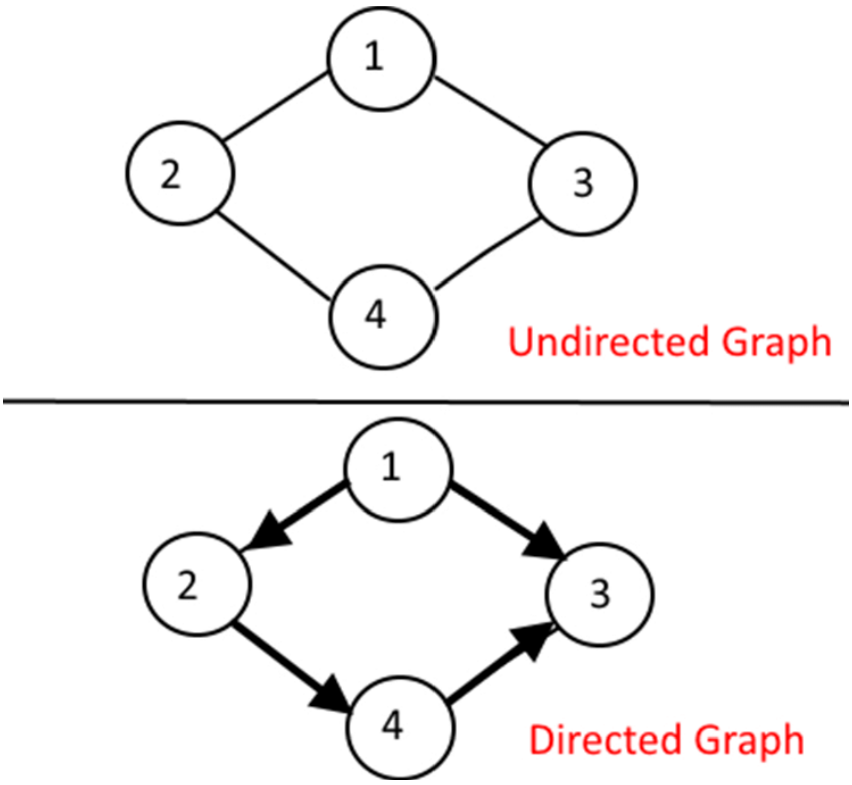

Figure 2.1: Directed graph vs Undirected graph

II Lyapunov stability

In this section, we provide an outline of the Lyapunov stability theorem that will be needed in later sections. First, we introduce time-dependent positive definite functions. We consider a scalar function $W : R^n \times R \to R$ with variables $x \in R^n$ and time t. Assuming this function is continuous and has continuous partial derivatives with respect to its arguments, then the function $W(x,t)$ is said to be positive semi-definite if it satisfies the following conditions [99]:

1. $W(0,t) = 0,\ \forall t \in R^+$
2. $W(x,t) \geq 0,\ \forall x \neq 0,\ x \in R^n$

$W(x,t)$ is said to be positive definite if conditions (1)-(3) above are satisfied, and there exists a time-invariant positive definite function $V_1(x)$ such that:

$V_1(x) \leq W(x,t),\ \forall x \in R^n$

Similarly, $W(x,t)$ is said to be negative definite (semi-definite) if $-W(x,t)$ is positive definite (semi-definite).

$W(x,t)$ is said to be *decrescent* if there exists a positive definite function $V_2(x)$

such that: $\mid W(x,t) \mid \leq V_2(x),\ \forall x \in R^n$. $W(x,t)$ is said to be radially unbounded if $W(x,t) \to \infty$ as $x \to \infty$ uniformly on t.

Now, consider the system $\dot{x} = f(x,t),\ f : R^n \times R^+ \to R^n$ and assume that the origin is an equilibrium state: $f(0,t) = 0,\ \forall t \in R$. Then if in a neighborhood D of the equilibrium state $x = 0$ there exist a differentiable function $W(.,.) : D \times [0,\infty) \times R$ such that:

1. $W(x,t)$ is positive definite.
2. The derivative of $W(.,.)$ along any solution of $\dot{x} = f(x,t)$ is negative semi definite in D.

then, the equilibrium state is stable. Moreover, if $W(x,t)$ is also *decrescent* then the origin is uniformly stable. The equilibrium state is uniformly asymptotically stable if

1. $W(x,t)$ is positive definite and decrescent.
2. The derivative of $\dot{W}(x,t)$ is negative definite in D

If there exists a differentiable function $W(.,.) : R^n \times [0,\infty) \to R$ such that:

1. $W(x,t)$ is positive definite, decrescent, and radially unbounded $\forall x \in R^n$ and that
2. The derivative of $\dot{W}(x,t)$ is negative definite in $\forall x \in R^n$, then

the equilibrium state at $x = 0$ is globally uniformly asymptotically stable. Suppose that the equilibrium state $x = 0$ is uniformly asymptotically stable, and in addition assume that there exist positive constants K_1, K_2 and K_3 such that:

1. $K_1\|x\|^p \leq W(x,t) \leq K_2\|x\|^p$.
2. $\dot{W}(x,t) \leq -K_3\|x\|^p$

Then the origin is exponentially stable. When the above conditions hold globally, then the equilibrium state $x = 0$ is globally exponentially stable.

III Linear Matrix Inequality (LMI)

The history of LMIs in the analysis of dynamic systems goes back more than 100 years, when Lyapunov published his seminal work introducing what we now call Lyapunov theory. He showed that the differential equation

$$\frac{d}{dt}x(t) = Ax(t) \tag{2.1}$$

is stable (i.e., all trajectories converge to zero) if and only if there exists a positive-definite matrix P such that

$$A^T P + PA < 0 \tag{2.2}$$

The requirement $P > 0$, $A^T P + PA < 0$ is what we now call a Lyapunov inequality on P, which is a special form of an LMI. Lyapunov also showed that this first LMI could be explicitly solved. Indeed, we can pick any $Q(x) = Q^T(x)$ and then solve the linear equation $A^T P + PA = -Q(x)$ for the matrix P, which is guaranteed to be positive-definite if the system (2.1) is stable. In summary, the first LMI used to analyze the stability of a dynamical system was the Lyapunov inequality (2.2), which can be solved analytically (by solving a set of linear equations) [138].

A linear matrix inequality (LMI) has the form

$$F(x) = F_0 + \sum_{i=1}^{m} x_i F_i > 0 \tag{2.3}$$

where $x \in R^m$ is the variable and the symmetric matrices $F_i = F_i^T \in R^{n\times n}$, $i = 0, ..., m$, are given. The inequality symbol in (2.3) means that $F(x)$ is positive-definite, i.e., $u^T F(x)u > 0$ for all nonzero $u \in R^n$. Of course, the LMI (2.3) is equivalent to a set of n polynomial inequalities in x, i.e., the leading principal minors of $F(x)$ must be positive.

We will also encounter nonstrict LMIs, which have the form

$$F(x) \geq 0 \tag{2.4}$$

The strict LMI (2.3) and the nonstrict LMI (2.4) are closely related, but here we consider strict LMIs.

The LMI (2.3) is a convex constraint on x, i.e., the set $\{x|F(x) > 0\}$ is convex. Although the LMI (2.3) may seem to have a specialized form, it can represent a wide variety of convex constraints on x. In particular, linear inequalities, (convex) quadratic inequalities, matrix norm inequalities, and constraints that arise in control

theory, such as Lyapunov and convex quadratic matrix inequalities, can all be cast in the form of an LMI.

Multiple LMIs $F^{(1)}(x) > 0, ..., F^{(p)}(x) > 0$ can be expressed as the single LMI $\mathbf{diag}(F^{(1)}(x), ..., F^{(p)}(x)) > 0$. Therefore we will make no distinction between a set of LMIs and a single LMI, i.e., "the LMI $F^{(1)}(x) > 0, ..., F^{(p)}(x) > 0$" will mean " the LMI $\mathbf{diag}(F^{(1)}(x), ..., F^{(p)}(x)) > 0$".

When the matrices F_i are diagonal, the LMI $F(x) > 0$ is just a set of linear inequalities. Nonlinear (convex) inequalities are converted to LMI form using Schur complements [100]. The basic idea is as follows: the LMI

$$\begin{bmatrix} Q(x) & S(x) \\ S^T(x) & R(x) \end{bmatrix} > 0 \tag{2.5}$$

where $Q(x) = Q^T(x)$, $R(x) = R^T(x)$, and $S(x)$ depend on x, is equivalent to

$$R(x) > 0, \quad Q(x) - S(x)R(x)^{-1}S(x)^T > 0 \tag{2.6}$$

In other words, the set of nonlinear inequalities (2.6) can be represented as the LMI (2.5).

IV EKF Algorithm

Time Update

1. Initialization of the filter at $k = 0$:

$$\begin{cases} \hat{x}_0^+ = E(x_0) \\ P_0^+ = E[(x_0 - \hat{x}_0^+)(x_0 - \hat{x}_0^+)^T] \end{cases} \tag{2.7}$$

   where represents the expected value and the $+$ in superscript implies an *a posteriori* estimate.

2. Computation of the partial-derivation matrices for $k = 1, 2, \ldots$:

$$\begin{cases} F_{k-1} = \frac{\partial f_{k-1}}{\partial x}|_{\hat{x}_{k-1}^+} \\ L_{k-1} = \frac{\partial f_{k-1}}{\partial w}|_{\hat{x}_{k-1}^+} \end{cases} \tag{2.8}$$

3. Computation of the time update of the state estimate and estimation-error covariance ($k = 1, 2, \dots$):

$$\begin{cases} P_{k-1}^{-} = F_{k-1} P_{k-1} F_{k-1}^{T} + L_{k-1} Q_{k-1} L_{k-1}^{T} \\ \hat{x}_{k}^{-} = f(\hat{x}_{k-1}, u_{k-1}, 0) \end{cases} \tag{2.9}$$

Measurement Update

1. Computation of the partial-derivation matrices for $k = 1, 2, \dots$:

$$\begin{cases} H_{k-1} = \frac{\partial h_k}{\partial x}|_{\hat{x}_k^-} \\ M_{k-1} = \frac{\partial h_{k-1}}{\partial v}|_{\hat{x}_k^-} \end{cases} \tag{2.10}$$

2. Computation of the measurement update of the state estimate and estimation-error covariance ($k = 1, 2, \dots$):

$$\begin{cases} K_k = P_k^- H_k^T (H_k P_k^- H_k^T + M_k R_k M_k^T)^{-1} \\ \hat{x}_k^+ = \hat{x}_k^- + K_k[y_k - h_k(\hat{x}_k^-, 0)] \\ P_k^+ = (I - K_k H_k) P_k^- \end{cases} \tag{2.11}$$

V The e-Puck2 System

The e-puck2 is a small (7cm in diameter) differential drive robot developed at the Swiss Federal Institute of Technology in Lausanne (EPFL) in collaboration with GCtronic. The hardware and software of e-puck2 are fully open source, providing low-level access to every electronic device and offering unlimited extension possibilities. The e-puck2 is powered by an STM32F4 microcontroller and features a large number of sensors: IR proximity, sound I/O, 9×IMU, ToF distance sensor, camera, and uSD storage. The robot is a full system with a USB hub, debugger/programmer, and Wi-Fi module [101]. Figure 2.2 shows what the e-puck2 robot is made up of, featuring sensors, actuators, a microcontroller, and a few other components. Due to its elegant design, flexibility, user friendly, and low cost, a lot of research work has been implemented using this robot, especially in the area of multi-agent systems. Eight infrared sensors placed around the e-puck2 measure closeness of obstacles in a 6 cm range and front real distance sensor, the Time of flight (ToF), measure up to 2 meters, and the camera in front of the e-puck2 measure up to 1m. The robot has two

lateral wheels which can rotate in both directions. The internal computer is able to count the number of pulses generated by encoders which are installed on each wheel for estimating the distance traversed by each wheel. An inertial measurement unit (imu) consists of a gyroscope (3DOF) and an accelerometer (3DOF) and can have a magnetometer (3DOF) as well [101], [102]. The system is integrated with the Webots simulation software for programming, simulation, and control of the robot. An early implementation can be found in [103] where a swarm of e-pucks is remotely controlled by external users over the internet using Web Services communication protocol. Each e-puck2 runs a modular piece of software built using a Robot Operating System (ROS) framework. ROS is an open-source system that provides a message-passing structure between different processes (or nodes) across a network (inter-process communication). The available support for ROS makes it even more suitable for robotics research in multi-agent systems as it provides easy access to the robot's sensors and actuators, as well as easy communication via Bluetooth or Wi-Fi among robots.

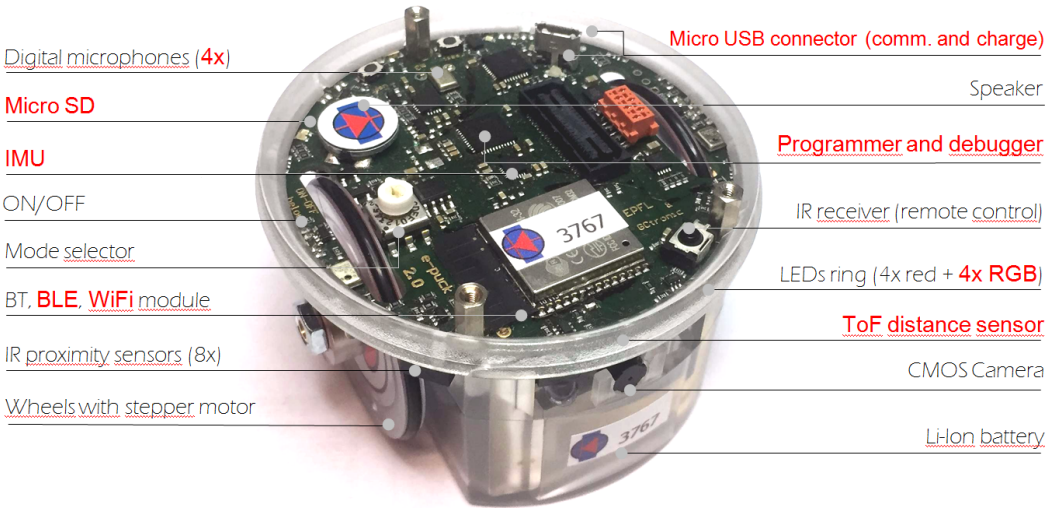

Figure 2.2: The main components offered by the e-puck2 robot

VI ZED Stereo camera

In multi-robot applications such as locomotion, and path planning, where the accurate posture of robots is essential, localization can be challenging especially when using small-sized low-cost robots such as the e-puck2. One of the common strategies to localize these robots is the use of an overhead camera with some detecting

algorithms that can detect markers mounted on the robots. An example is in [104] where an effective vision-based system is proposed to accurately track mobile robots' true pose using multiple overhead cameras. Their system can localize multiple mobile robots simultaneously in a 3m $\times$6m arena with each robot assigned a symbol marker for identification. In [106], an overhead camera is used to localize a group of e-puck2 robots to address the formation control problem using Model Predictive Control. During the experiment, pose estimates of the robots are sent to the PC in real time via the video camera attached for the computer to calculate optimal inputs to the robots. Due to hardware limitations and real-time image processing, the position and orientation of each robot estimated by the camera are subject to delays. In this work, we employ the proposed EKF to fuse the information obtained from the odometry sensors (filter propagation) along with the information from the overhead camera (filter updating) to improve localization accuracy. The combination of both odometry and camera sensors combines the advantages of each type of sensor. ZED is a a passive stereo camera that reproduces the way human vision works. Using its two "eyes" and through triangulation, the ZED creates a three-dimensional model of the scene it observes, introducing for the first time indoor and outdoor long-range depth perception and positional tracking [105]. Figure 2.3 shows the ZED stereo camera, it has an integrated 2.0m USB3.0 cable, with minimum system requirements of USB3.0 port, CUDA 6.5, NVIDIA GPU with compute capability greater than 2.0, 4GB RAM, Dual-core 2,3GHz, and windows 7 or Ubuntu 14.04 or later to run the system development toolkit provided by StereoLabs. The camera can be interfaced with multiple third-party libraries and environments such as OpenCV, ROS, PyTorch, TensorFlow, and MATLAB, just to name a few. We chose ZED camera as a measurement update in our localization algorithm because it can be interfaced with ROS, which makes it easy to communicate pose estimates to our localization algorithm (in the host computer).

Figure 2.3: ZED Stereo camera

VII The Robot Operating System (ROS)

Robots need to communicate with the localization algorithm (in the host computer) to get their respective pose estimate messages and communicate with other robots in the group to achieve consensus. Therefore, a reliable system is required for robots to interact with the camera and other robots, and one of such system is the Robot Operating System (ROS). ROS is a modular open-source framework for writing robot software. ROS is a collection of tools, libraries, and conventions that aim to simplify the task of creating complex and robust robot behavior across a wide variety of robotics platforms [107]. It provides functionality for hardware abstraction, communication between processes over multiple machines, and great tools for visualization. It also provides the flexibility to work with heterogeneous devices in a shared environment. Control of individual robots and communication between robots and other devices is realized using some software processes called "nodes" that can register with the ROS master node. Nodes can execute tasks independently or by communicating with other nodes within the system. The communication mechanism used by ROS is through sending and receiving messages grouped into specific categories called topics. A message is defined by the type of message and data format, a node can send data by publishing it on a defined topic and receive data by subscribing to the topic of interest. Also, Fig. 2.4 shows a general schematic of a ROS-based robotics system in which all the sensors are exposed to ROS and can be also sent commands back to the robot through ROS. The benefits of ROS include being an ecosystem that allows to introduce of a new sensor (or a node) easily and having simultaneous data from different sensors.

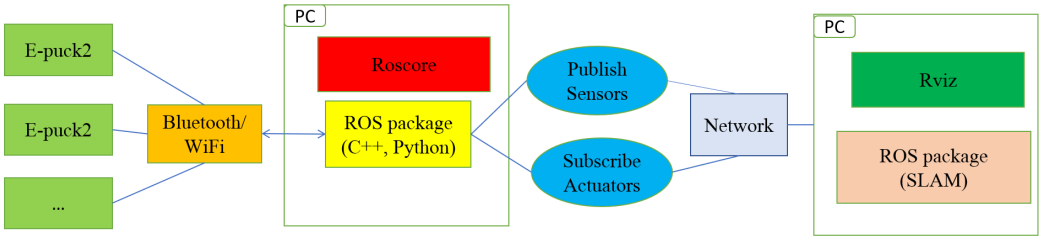

Figure 2.4: A general schematic of a ROS-based robotics system

VIII Markers

An important step in implementing our work is finding a way to estimate the pose of robots through the camera and transmit it to our localization algorithm. With the ZED camera, we use visual localization to estimate the pose of each robot within the field of view of the camera. Visual localization involves the problem of determining the camera pose of one or multiple query images in a database scene. This problem is highly relevant for a wide range of applications, including autonomous robots, augmented reality (AR), loop closure detection re-localization, SLAM, and Structure-from-Motion (SFM) systems [108]. The complexities associated with detecting our robots can be avoided using patterns designed to be reliably detected by computer vision, such patterns are termed "fiducial markers" (see Figure 2.5). A lot of research papers have employed the use of fiducial markers to localize robots, or to improve localization accuracy. An example is in [109] where AR Tag markers are used for robot localization with an overhead camera viewing the robots from above with a unique marker mounted on each robot. To solve a formation control problem, [110] uses the overhead camera to determine the pose estimates of a group of e-puck2 robots by mounting patterns on each of the robots. In our work, we employ the use of AR Tag markers, a square pattern of size 5 by 5 printed on a flat surface with black and white patches, and a relatively thick solid outer boundary. These tags are provided by the ar track Alvar package, which is a ROS wrapper for Alvar, an open-source AR tag-tracking library.

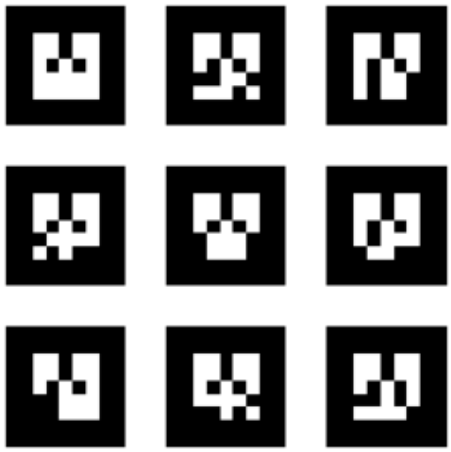

Figure 2.5: AR tags

Chapter 3

Cooperative Localization in Mobile Robots Using Event-Triggered Mechanism: Theory and Experiments

I Introduction

In this chapter, we address a new cooperative localization problem for a team of mobile robots subject to limited communication resources. First, we develop a decentralized event-triggered cooperative localization (DECL) algorithm for the multi-robot system such that each robot localizes itself with minimum communication exchange between robots. Then, using an event-triggered mechanism we propose an optimization framework to achieve the balance between estimation performance and communication rate. Simulation results show the main benefits of the event-triggered mechanism. Also, experimental results using four e-puck2 mobile robots demonstrate the effectiveness of the proposed method.

The rest of this chapter is as follows. In Section II, we describe the problem statement and introduce the dynamics of the multi-robot system and the architecture of the event-triggering data-transferring mechanism. In section III we discuss the proposed event-based cooperative localization method. In section IV, we discuss the performance of the proposed localization algorithm. In Section V, we present the relationship between the event-triggered data-transferring mechanism and energy consumption. In Section VI, we present our simulation and experimental results. Finally, in Section VII we provide some final conclusions.

Notation: $\mathbb{R}^{n^i}$ and $\mathbb{S}^{n^i}$ represent the set of n^i-dimensional real vectors and $n^i \times n^i$

real matrices, respectively. Matrix I is the identity matrix of the appropriate size. For a matrix A, A^T represents its transpose. $\text{diag}\{A^1, A^2, ..., A^N\}$ refers to the block diagonal matrix where $A^1, A^2, ..., A^N$ are the main diagonal matrix blocks. The subscript $m \in \{1, 2, ..., M\}$ is the m^{th} dimension of sensor measurement which will be dropped. The subscript i and j are used to represent robot i and robot j. Also, $i-$, $j-$ and $ij-$ denote the time prediction of the corresponding filter and $i+$, $j+$ and $ij+$ represent the measurement update. $E[x]$ represents the expectation of random variable x.

II Problem statement and Preliminaries

II.1 Dynamic of multi-robot systems

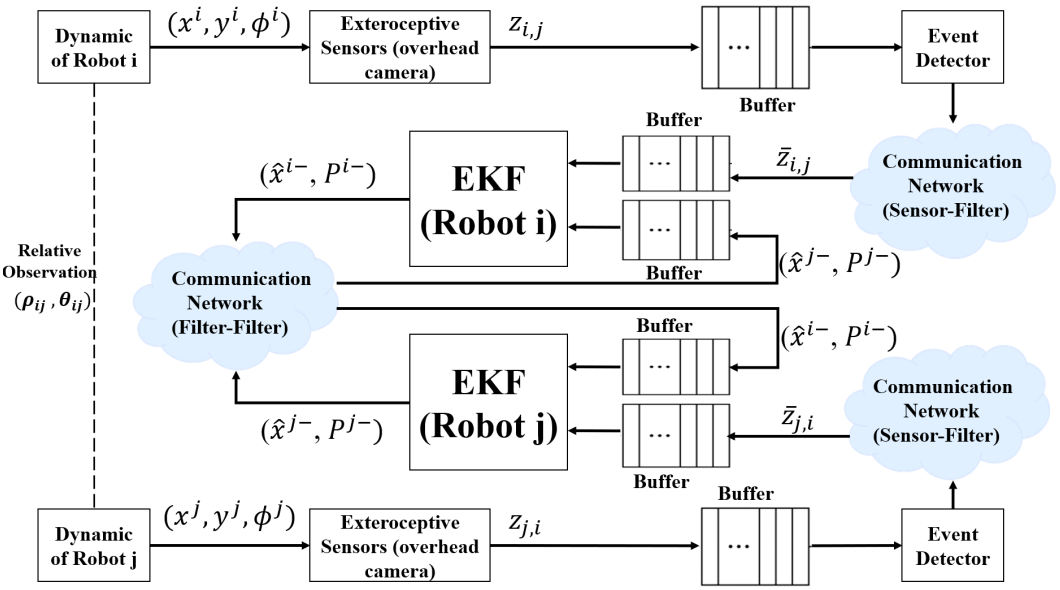

Figure 3.1: Block diagram of decentralized event-triggered cooperative localization (DECL) algorithm in two dimensions

We consider a group of N robots $\vartheta = \{1, 2, ..., N\}$, each capable of sensing and communicating with the rest of the group. We assume a general nonlinear system model for the motion of robots ([29])

$$\boldsymbol{x}^i(k) = \boldsymbol{f}^i(\boldsymbol{x}^i(k-1), \boldsymbol{u}_c^i(k-1)), \tag{3.1}$$

where the state vector $\boldsymbol{x}^i(k) = [x^i(k), y^i(k), \phi^i(k)]^T$ represents the pose of robot i consist of the Cartesian coordinates $(x^i(k), y^i(k))$ and orientation $\phi^i(k)$, and $\boldsymbol{u}_c^i$ is the control input. We will assume throughout that $\boldsymbol{u}_c^i = \boldsymbol{u}^i + \boldsymbol{\eta}^i$, is the measured velocity

of robot i obtained from the odometry and inertial sensors, where $\boldsymbol{u}^i$ represents the actual velocity and $\boldsymbol{\eta}^i$ is contaminating noise. Each robot uniquely detects the other robots in the team use exteroceptive sensors (overhead camera in this work) and take relative measurements, e.g., range or bearing or both. The relative measurement taken by robot i from robot j at time k is described by the following equation ([29])

$$\boldsymbol{z}_{i,j}^m(k) = \boldsymbol{h}_{i,j}^m(\boldsymbol{x}^i(k), \boldsymbol{x}^j(k)) + \boldsymbol{\nu}_m^i(k), \tag{3.2}$$

where $\boldsymbol{h}_{i,j}^m(.)$ is the measurement model and $\boldsymbol{\nu}_m^i$ is measurement noise. The noises $\boldsymbol{\eta}^i$ and $\boldsymbol{\nu}^i$, $i \in \vartheta$ are independent zero-mean white Gaussian processes with known positive definite variances $\boldsymbol{Q}^i(k) = E[\boldsymbol{\eta}^i(k)\boldsymbol{\eta}^i(k)^T]$ and $\boldsymbol{R}^i(k) = E[\boldsymbol{\nu}^i(k)\boldsymbol{\nu}^i(k)^T]$. All noises are assumed to be mutually uncorrelated.

II.2 Problem Statement

The block diagram of the proposed decentralized event-triggered cooperative localization (DECL) algorithm is shown in Fig. 3.1. Here, the exteroceptive sensors (overhead camera) provide relative measurements, $\boldsymbol{z}_{i,j}(k)$ (range and bearing) in a periodic manner. Sensor outputs are sent to the event detector which decides whether or not the current measurement is to be transmitted through the communication channel to the estimator, based on a triggering rule. All robots exchange information regarding their propagated estimates (namely; state and covariance) across the communication network in order to update the filters. Note that the communication graph of robots changes randomly over time. We assume throughout that the communication network is reliable, therefore, new packets will be stored in the buffers with no packet losses.

II.3 Event-Triggered Data Transferring Mechanism

We consider a scenario in which, due to limited onboard resources, only a limited number of relative measurements per robot are allowed during the update stage. The event-detector works as follow: let $\boldsymbol{z}_{i,j}(k)$ represent the current sensor measurement and $\bar{\boldsymbol{z}}_{i,j}(k)$ the last measurement transmitted through the channel. The triggering rule works as follows. Define the binary decision variable $\boldsymbol{\gamma}_m^i(k)$:

$$\boldsymbol{\gamma}_m^i(k) = \begin{cases} \mathbf{1}, & \textbf{if} \quad \|\boldsymbol{e}_i^m(k)\| \geq \delta_m^i(k) \left\|\boldsymbol{z}_{i,j}^m(k)\right\| + \xi_m^i(k) \\ \\ \mathbf{0}, & \textbf{otherwise}. \end{cases} \tag{3.3}$$

where $\boldsymbol{e}_i^m(k) = \boldsymbol{z}_{i,j}^m(k) - \bar{\boldsymbol{z}}_{i,j}^m(k-1)$ is the error between the last transmitted measurement and the current measurement at time k. $\delta_m^i(k)$, $\xi_m^i(k) > 0$ are design parameters in the event-triggered mechanism. The smaller the event-triggering parameters $\delta_m^i(k)$, $\xi_m^i(k)$ are chosen, the more the events will be triggered. When the parameters $\delta_m^i(k)$, $\xi_m^i(k)$ are sufficiently approaching zero, the event-triggered mechanism performs as a time-triggered one. This triggering rule is a discrete-time a version of the so-called mixed triggering mechanism introduced in [91]. Note that we can obtain send-on-delta and relative type triggering conditions as special cases of (3.3). Indeed, setting $\delta_m^i(k) = 0$ we obtain a send-on-delta type condition, whereas setting $\xi_m^i(k) = 0$ we obtain a relative-type condition. From Eq. (3.3), we see that the measurement $\boldsymbol{z}_{i,j}^m(k)$ will be sent to the estimator when $\boldsymbol{\gamma}_m^i(k) = 1$; otherwise no signal is transmitted. Then the measurement used to update the state at time instant k can be written as follows:

$$\bar{\boldsymbol{z}}_{i,j}^m(k) = \boldsymbol{\gamma}_m^i(k)\boldsymbol{z}_{i,j}^m(k) + (\boldsymbol{I} - \boldsymbol{\gamma}_m^i(k))\bar{\boldsymbol{z}}_{i,j}^m(k-1). \tag{3.4}$$

Thus, if $\boldsymbol{\gamma}_m^i(k) = 1$, then $\boldsymbol{z}_{i,j}^m(k)$ will is used to update the state. If $\boldsymbol{\gamma}_m^i(k) = 0$, only the old measurement is used.

III Design decentralized event-triggered cooperative localization

In this section, we design a cooperative localization algorithm for multi-robot systems with event-triggered data transmission. We consider the mixed-type triggering condition (3.3) in our solution. Our proof makes use of the following lemma and assumptions:

Lemma III.1. *For any two vectors u, $v \in \mathbb{R}^n$, there exists a scalar $\varepsilon \in \mathbb{R}$ such that the following inequality holds [113]:*

$$uv^T + vu^T \leq \varepsilon uu^T + \varepsilon^{-1}vv^T. \tag{3.5}$$

Assumption 1. *All robots in the team are identical with the same motion and measurement models.*

Assumption 2. *The robots move in a limited area and thus they move in the sensing and communication range from each other.*

Theorem III.2. *Consider the nonlinear discrete-time system (3.1) and (3.2) with the event-triggered communication scheme (3.3), the CL algorithm via the EKF for robot i can be recursively executed as follows:*

Time update:

$$\hat{\boldsymbol{x}}^{i-}(k) = \boldsymbol{f}^i(\hat{\boldsymbol{x}}^{i+}(k-1), \boldsymbol{u}_c^{i+}(k-1)) \tag{3.6}$$

$$\begin{aligned}\boldsymbol{P}^{i-}(k) = &\boldsymbol{A}^i(k-1)\boldsymbol{P}^{i+}(k-1)\boldsymbol{A}^i(k-1)^T \\ &+\boldsymbol{G}^i(k-1)\boldsymbol{Q}^i(k-1)\boldsymbol{G}^i(k-1)^T\end{aligned} \tag{3.7}$$

where $\hat{\boldsymbol{x}}^{i-}(k)$ and $\boldsymbol{P}^{i-}(k)$ are the predicted state and error covariance for each robot.

Measurement update:

$$\begin{aligned}\hat{\boldsymbol{x}}^{i+}(k) = &\hat{\boldsymbol{x}}^{i-}(k) + \boldsymbol{K}_i(k)(\boldsymbol{z}_{i,j}(k) - (\boldsymbol{I} - \boldsymbol{\gamma}^i(k))\boldsymbol{e}_i(k) \\ &-\hat{\boldsymbol{z}}_{i,j}(k))\end{aligned} \tag{3.8}$$

$$\begin{aligned}\bar{\boldsymbol{P}}^{i+}(k) = &(1+\varepsilon_1)(\boldsymbol{I} - \boldsymbol{K}_i(k)\boldsymbol{H}_i^i(k))\boldsymbol{P}^{i-}(k)(\boldsymbol{I} - \boldsymbol{K}_i(k) \\ &\times\boldsymbol{H}_i^i(k))^T - (\boldsymbol{I} - \boldsymbol{K}_i(k)\boldsymbol{H}_i^i(k))\boldsymbol{P}^{ij-}(k)\boldsymbol{H}_j^i(k)^T \\ &\times\boldsymbol{K}_i(k)^T - \boldsymbol{K}_i(k)\boldsymbol{H}_j^i(k)\boldsymbol{P}^{ij-}(k)(\boldsymbol{I} - \boldsymbol{K}_i(k)\boldsymbol{H}_i^i(k))^T \\ &+\boldsymbol{K}_i(k)\boldsymbol{H}_j^i(k)\boldsymbol{P}^{j-}\boldsymbol{H}_j^i(k)^T\boldsymbol{K}_i(k)^T \\ &+(1-\varepsilon_2)\boldsymbol{K}_i(k)\boldsymbol{R}^i(k)\boldsymbol{K}_i(k)^T \\ &+(1+\varepsilon_1^{-1}-\varepsilon_2^{-1})\boldsymbol{K}_i(k)(\boldsymbol{I} - \boldsymbol{\gamma}^i(k))\boldsymbol{\delta}_i(k)\boldsymbol{I} \\ &\times(\boldsymbol{I} - \boldsymbol{\gamma}^i(k))^T\boldsymbol{K}_i(k)^T\end{aligned} \tag{3.9}$$

where $\hat{\boldsymbol{x}}^{i+}(k)$ and $\bar{\boldsymbol{P}}^{i+}(k)$ are the estimated state and upper bound of the error covariance for each robot.

Kalman gain:

$$\begin{aligned}\boldsymbol{K}_i(k) = &[(1+\varepsilon_1)\boldsymbol{P}^{i-}(k)\boldsymbol{H}_i^i(k)^T + \boldsymbol{P}^{ij-}(k)\boldsymbol{H}_j^i(k)^T)] \\ &\times[(1+\varepsilon_1)\boldsymbol{H}_i^i(k)\boldsymbol{P}^{i-}(k)\boldsymbol{H}_i^i(k)^T \\ &+\boldsymbol{H}_i^i(k)\boldsymbol{P}^{ij-}(k)\boldsymbol{H}_j^i(k)^T + \boldsymbol{H}_j^i(k)\boldsymbol{P}^{ij-}(k)\boldsymbol{H}_i^i(k)^T \\ &+\boldsymbol{H}_j^i(k)\boldsymbol{P}^{j-}(k)\boldsymbol{H}_j^i(k)^T + (1-\varepsilon_2)\boldsymbol{R}_i(k) \\ &+(1+\varepsilon_1^{-1}-\varepsilon_2^{-1})(\boldsymbol{I} - \boldsymbol{\gamma}^i(k))\boldsymbol{\delta}_i(k)\boldsymbol{I}(\boldsymbol{I} - \boldsymbol{\gamma}^i(k))^T]^{-1}\end{aligned} \tag{3.10}$$

Proof. The CL algorithm via the EKF is obtained by applying the EKF over the joint system motion model $\boldsymbol{x}^i(k+1) = (\boldsymbol{f}^1(\boldsymbol{x}^1, \boldsymbol{u}^1), ..., \boldsymbol{f}^N(\boldsymbol{x}^N, \boldsymbol{u}^N)) + \text{diag}\{\boldsymbol{g}^1(\boldsymbol{x}^1), ..., \boldsymbol{g}^N(\boldsymbol{x}^N)\}\boldsymbol{\eta}(k)$ and the relative measurement model (3.2). Let $\boldsymbol{x}^{i+}(0) \in \mathbb{R}^{n^i}$, $\boldsymbol{P}^{i+} \in \mathbb{S}^{n^i}$, $\boldsymbol{P}_{i,j}^{+} = \boldsymbol{0}_{n^i \times n^j}$, $i \in \vartheta$ and $j \in \vartheta \backslash \{i\}$.

The prediction error for robot i at time instant k can be defined as follows:

$$\tilde{\boldsymbol{x}}^{i-}(k) = \boldsymbol{x}^i(k) - \hat{\boldsymbol{x}}^{i-}(k) \tag{3.11}$$

where the predicted state $\hat{\boldsymbol{x}}^{i-}(k)$ is given by:

$$\hat{\boldsymbol{x}}^{i-}(k) = \boldsymbol{f}^i(\hat{\boldsymbol{x}}^{i+}(k-1), \boldsymbol{u}_c^{i+}(k-1)) \tag{3.12}$$

Expanding $\boldsymbol{f}^i(\boldsymbol{x}^i(k-1), \boldsymbol{u}_c^i(k-1))$ from (3.1) in Taylor Series around $\hat{\boldsymbol{x}}^{i+}(k-1)$ we get:

$$\begin{aligned}\boldsymbol{f}^i(\boldsymbol{x}^i(k-1), \boldsymbol{u}_c^i(k-1)) \approx \boldsymbol{f}^i(\hat{\boldsymbol{x}}^{i+}(k-1), \boldsymbol{u}_c^i(k-1)) \\ +\boldsymbol{A}^i(k-1)(\boldsymbol{x}^i(k-1) - \hat{\boldsymbol{x}}^{i+}(k-1))\end{aligned} \tag{3.13}$$

where $\boldsymbol{A}^i = \frac{\partial \boldsymbol{f}^i(\hat{\boldsymbol{x}}^{i+}, \boldsymbol{u}_c^i)}{\partial \boldsymbol{x}^i}$. Using (3.11)-(3.13) the predicted error for robots i and j can be computed as follows:

$$\tilde{\boldsymbol{x}}^{i-}(k) = \boldsymbol{A}^i(k-1)\tilde{\boldsymbol{x}}^{i-}(k-1) + \boldsymbol{G}^i(k-1)\boldsymbol{\eta}^i(k-1) \tag{3.14}$$

$$\tilde{\boldsymbol{x}}^{j-}(k) = \boldsymbol{A}^j(k-1)\tilde{\boldsymbol{x}}^{j-}(k-1) + \boldsymbol{G}^j(k-1)\boldsymbol{\eta}^j(k-1) \tag{3.15}$$

where $\boldsymbol{G}^i = \frac{\partial \boldsymbol{f}^i(\hat{\boldsymbol{x}}^{i+}, \boldsymbol{u}_c^i)}{\partial \boldsymbol{\eta}^i}$, $\boldsymbol{G}^j = \frac{\partial \boldsymbol{f}^i(\hat{\boldsymbol{x}}^{j+}, \boldsymbol{u}_c^j)}{\partial \boldsymbol{\eta}^j}$ and $\boldsymbol{A}^j = \frac{\partial \boldsymbol{f}^i(\hat{\boldsymbol{x}}^{j+}, \boldsymbol{u}_c^j)}{\partial \boldsymbol{x}^j}$.

Using (3.14)-(3.15), the predicted error covariance for robot i and cross covariance between two robots (i and j) are given by:

$$\begin{aligned}\boldsymbol{P}^{i-}(k) &= E[(\boldsymbol{x}^i(k) - \hat{\boldsymbol{x}}^{i-}(k))(\boldsymbol{x}^i(k) - \hat{\boldsymbol{x}}^{i-}(k))^T] \\ &= \boldsymbol{A}^i(k-1)\boldsymbol{P}^{i+}(k-1)\boldsymbol{A}^i(k-1)^T \\ &\quad +\boldsymbol{G}^i(k-1)\boldsymbol{Q}^i(k-1)\boldsymbol{G}^i(k-1)^T\end{aligned} \tag{3.16}$$

$$\begin{aligned}\boldsymbol{P}^{ij-}(k) &= E[(\boldsymbol{x}^i(k) - \hat{\boldsymbol{x}}^{i-}(k))(\boldsymbol{x}^j(k) - \hat{\boldsymbol{x}}^{j-}(k))^T] \\ &= \boldsymbol{A}^i(k-1)\boldsymbol{P}^{+}_{i,j}(k-1)\boldsymbol{A}^i(k-1)^T\end{aligned} \tag{3.17}$$

The state estimates for robot i are corrected according to

$$\hat{\boldsymbol{x}}^{i+}(k) = \hat{\boldsymbol{x}}^{i-}(k) + \boldsymbol{K}_i(k)(\boldsymbol{z}_{i,j}(k) - \hat{\boldsymbol{z}}_{i,j}(k)) \tag{3.18}$$

where $\hat{\boldsymbol{z}}_{i,j} = \boldsymbol{h}_{i,j}(\hat{\boldsymbol{x}}^{i-}, \hat{\boldsymbol{x}}^{j-})$ is the estimated measurement. Let the first-order expansion of $\boldsymbol{h}_{i,j}(\boldsymbol{x}^i, \boldsymbol{x}^j)$ around $(\hat{\boldsymbol{x}}^{i-}, \hat{\boldsymbol{x}}^{j-})$ be

$$\boldsymbol{h}_{i,j}(\boldsymbol{x}^i, \boldsymbol{x}^j) \approx \boldsymbol{h}_{i,j}(\boldsymbol{x}^{i-}, \boldsymbol{x}^{j-}) + \boldsymbol{H}_i^i(\boldsymbol{x}^i - \hat{\boldsymbol{x}}^{i-}) + \boldsymbol{H}_j^i(\boldsymbol{x}^j - \hat{\boldsymbol{x}}^{j-}) \tag{3.19}$$

where $\boldsymbol{H}_i^i = \frac{\partial \boldsymbol{h}_{i,j}(\hat{\boldsymbol{x}}^{i-}, \hat{\boldsymbol{x}}^{j-})}{\partial \boldsymbol{x}^i}$ and $\boldsymbol{H}_j^i = \frac{\partial \boldsymbol{h}_{i,j}(\hat{\boldsymbol{x}}^{i-}, \hat{\boldsymbol{x}}^{j-})}{\partial \boldsymbol{x}^j}$. Considering the event-triggered mechanism, the state estimates can be modified as follows:

$$\begin{aligned}\hat{\boldsymbol{x}}^{i+}(k) = \hat{\boldsymbol{x}}^{i-}(k) + \boldsymbol{K}_i(k)(\bar{\boldsymbol{z}}_{i,j}(k) - \hat{\boldsymbol{z}}_{i,j}(k)) = \hat{\boldsymbol{x}}^{i-}(k) \\ +\boldsymbol{K}_i(k)\big(\boldsymbol{z}_{i,j}(k) - (\boldsymbol{I} - \boldsymbol{\gamma}^i(k))\boldsymbol{e}_i(k) - \hat{\boldsymbol{z}}_{i,j}(k)\big)\end{aligned} \tag{3.20}$$

Using (3.11), (3.19) and (3.20), the estimation error for robot i is given by:

$$\begin{aligned}\tilde{\boldsymbol{x}}^{i+}(k) = \boldsymbol{x}^i(k) - \hat{\boldsymbol{x}}^{i+}(k) = \big(\boldsymbol{I} - \boldsymbol{K}_i(k)\boldsymbol{H}_i^i(k)\big)\tilde{\boldsymbol{x}}^{i-}(k) \\ -\boldsymbol{K}_i(k)\boldsymbol{H}_j^i(k)\tilde{\boldsymbol{x}}^{j-}(k) - \boldsymbol{K}_i(k)\boldsymbol{\nu}^i(k) \\ +\boldsymbol{K}_i(k)(\boldsymbol{I} - \boldsymbol{\gamma}^i(k))\boldsymbol{e}_i(k).\end{aligned} \tag{3.21}$$

We now look for an upper bound for the error covariance matrix. Defining constants $\varepsilon_1 > 0$ and $\varepsilon_2 > 0$ and applying Lemma III.1 we obtain:

$$\begin{aligned}&\big(\boldsymbol{I} - \boldsymbol{K}_i(k)\boldsymbol{H}_i^i(k)\big)E[\tilde{\boldsymbol{x}}^{i-}(k)\boldsymbol{e}_i(k)^T](\boldsymbol{I} - \boldsymbol{\gamma}^i(k))^T\boldsymbol{K}_i(k)^T \\ &+\boldsymbol{K}_i(k)(\boldsymbol{I} - \boldsymbol{\gamma}^i(k))E[\boldsymbol{e}_i(k)\tilde{\boldsymbol{x}}^{i-}(k)^T]\big(\boldsymbol{I} - \boldsymbol{K}_i(k)\boldsymbol{H}_i^i(k)\big)^T \leq \\ &\varepsilon_1\big(\boldsymbol{I} - \boldsymbol{K}_i(k)\boldsymbol{H}_i^i(k)\big)E[\tilde{\boldsymbol{x}}^{i-}(k)\tilde{\boldsymbol{x}}^{i-}(k)^T]\big(\boldsymbol{I} - \boldsymbol{K}_i(k)\boldsymbol{H}_i^i(k)\big)^T \\ &+\varepsilon_1^{-1}\boldsymbol{K}_i(k)(\boldsymbol{I} - \boldsymbol{\gamma}^i(k))E[\boldsymbol{e}_i(k)\boldsymbol{e}_i(k)^T](\boldsymbol{I} - \boldsymbol{\gamma}^i(k))^T\boldsymbol{K}_i(k)^T\end{aligned} \tag{3.22}$$

$$
\begin{aligned}
&\boldsymbol{K}_i(k)E[\boldsymbol{\nu}^i(k)\boldsymbol{e}_i(k)^T](\boldsymbol{I}-\boldsymbol{\gamma}^i(k))^T\boldsymbol{K}_i(k)^T\\
&+\boldsymbol{K}_i(k)(\boldsymbol{I}-\boldsymbol{\gamma}^i(k))E[\boldsymbol{e}_i(k)\boldsymbol{\nu}^i(k)^T]\boldsymbol{K}_i(k)^T\\
&\leq \varepsilon_2\boldsymbol{K}_i(k)E[\boldsymbol{\nu}^i(k)\boldsymbol{\nu}^i(k)^T]\boldsymbol{K}_i(k)^T\\
&+\varepsilon_2^{-1}\boldsymbol{K}_i(k)(\boldsymbol{I}-\boldsymbol{\gamma}^i(k))E[\boldsymbol{e}_i(k)\boldsymbol{e}_i(k)^T](\boldsymbol{I}-\boldsymbol{\gamma}^i(k))^T\boldsymbol{K}_i(k)^T
\end{aligned}
\tag{3.23}
$$

Using (3.21)-(3.23), we compute the upper bound error covariance matrix ($\bar{\boldsymbol{P}}^{i+}(k)$) for robot i as a follows:

$$
\begin{aligned}
&\bar{\boldsymbol{P}}^{i+}(k) = E[(\boldsymbol{x}^i(k)-\hat{\boldsymbol{x}}^{i+}(k))(\boldsymbol{x}^i(k)-\hat{\boldsymbol{x}}^{i+}(k))^T]\\
&= (1+\varepsilon_1)\big(\boldsymbol{I}-\boldsymbol{K}_i(k)\boldsymbol{H}_i^i(k)\big)\boldsymbol{P}^{i-}(k)\big(\boldsymbol{I}-\boldsymbol{K}_i(k)\boldsymbol{H}_i^i(k)\big)^T\\
&-\big(\boldsymbol{I}-\boldsymbol{K}_i(k)\boldsymbol{H}_i^i(k)\big)\boldsymbol{P}^{ij-}(k)\boldsymbol{H}_j^i(k)^T\boldsymbol{K}_i(k)^T\\
&-\boldsymbol{K}_i(k)\boldsymbol{H}_j^i(k)\boldsymbol{P}^{ij-}(k)\big(\boldsymbol{I}-\boldsymbol{K}_i(k)\boldsymbol{H}_i^i(k)\big)^T\\
&+\boldsymbol{K}_i(k)\boldsymbol{H}_j^i(k)\boldsymbol{P}^{j-}\boldsymbol{H}_j^i(k)^T\boldsymbol{K}_i(k)^T\\
&+(1-\varepsilon_2)\boldsymbol{K}_i(k)\boldsymbol{R}^i(k)\boldsymbol{K}_i(k)^T\\
&+(1+\varepsilon_1^{-1}-\varepsilon_2^{-1})\boldsymbol{K}_i(k)(\boldsymbol{I}-\boldsymbol{\gamma}^i(k))\boldsymbol{\delta}_i(k)(\boldsymbol{I}-\boldsymbol{\gamma}^i(k))^T\boldsymbol{K}_i(k)^T
\end{aligned}
\tag{3.24}
$$

□ □

Remark 1. *Compared to the classical CL, the event-triggered mechanism brings additional terms affecting the upper and the lower bounds of the estimation error and the estimation error covariance, respectively. The Kalman gain (3.10) is obtained by minimizing the upper bound of the error covariance with respect to the Kalman gain, i.e.,* $\frac{\partial\bar{\boldsymbol{P}}^{i+}(k)}{\partial\boldsymbol{K}_i(k)}=0$.

Remark 2. *In a cooperative localization algorithm, a set of sensors needs to be fused in order to improve localization performance. Therefore, each sensor might capture its data at different rates when compared to the other sensors available on the robot itself or available from other robots within the swarm. The event-triggered mechanism proposed in this work is employed to deal with synchronization problems (handling different rates) within different sensors in the robot itself or other robots.*

Remark 3. *Compared with other localization methods such as Iterated Closets Point Scan and Pose Graph Optimization, our approach based on an extended Kalman filter (EKF) has computational advantages. Also, our approach does not need any external landmark to estimate the pose of robots. However, Pose Graph Optimization is able to better represent large, nonlinear errors in odometry estimates and needs an external landmark to localize the robots. Note that the solution proposed in this work is used to localize robots in the dynamic environment since all the robots in the team are moving and performing the localization task. In other words, localization in a static environment is a special case where neighboring robots perform as a static landmark with a known initial position.*

Algorithm 1 Decentralized Event-Triggered Cooperative Localization Algorithm.

Initialize state estimation and error covariance matrix as Robots $i \in \vartheta$ and $j \in \vartheta \backslash \{i\}$: $\hat{\mathbf{x}}^{i+}(0) \in \mathbb{R}^{n^i}$, $\mathbf{P}^{i+}(0) \in \mathbb{S}^{n^i}$, $\mathbf{P}^{ij+}(0) = \mathbf{0}_{n^i \times n^j}$

repeat

Propagation: Compute the predicted state and error covariance for each robot:

$$\begin{aligned}\hat{\mathbf{x}}^{i-}(k) &= \mathbf{f}^i\big(\hat{\mathbf{x}}^{i+}(k-1), \mathbf{u}_c^{i+}(k-1)\big) \\ \mathbf{P}^{i-}(k) &= \mathbf{A}^i(k-1)\mathbf{P}^{i+}(k-1)\mathbf{A}^i(k-1)^T \\ &\quad + \mathbf{G}^i(k-1)\mathbf{Q}^i(k-1)\mathbf{G}^i(k-1)^T\end{aligned}$$

Update:

if robot $i \in \vartheta$ receive the relative measurement $\mathbf{z}_{i,j}(k)$, then each robot $i \in \vartheta$ exchange relative pose information with the other robot $j \in \vartheta \backslash \{i\}$. The measurement residual and its covariance are as follows:

- if the event-detector transmit the current measurement, then $\boldsymbol{\gamma}^i(k) = 1$

$$\mathbf{r}_i(k) = \mathbf{z}_{i,j}(k) - \mathbf{h}_{i,j}(\hat{\mathbf{x}}^{i-}(k), \hat{\mathbf{x}}^{j-}(k))$$

- otherwise $\boldsymbol{\gamma}^i(k) = 0$, then the last transmitted measurement will be used in the update step.

$$\mathbf{r}_i(k) = \bar{\mathbf{z}}_{i,j}(k) - \mathbf{h}_{i,j}(\hat{\mathbf{x}}^{i-}(k), \hat{\mathbf{x}}^{j-}(k))$$

$$\begin{aligned}\mathbf{S}_{i,j}(k) &= (1+\varepsilon_1)\mathbf{H}_i^i(k)\mathbf{P}^{i-}(k)\mathbf{H}_i^i(k)^T + (1-\varepsilon_2)\mathbf{R}_i(k) \\ &\quad + \mathbf{H}_i^i(k)\mathbf{P}^{ij-}(k)\mathbf{H}_j^i(k)^T + \mathbf{H}_j^i(k)\mathbf{P}^{ji-}(k)\mathbf{H}_i^i(k)^T \\ &\quad + (1+\varepsilon_1^{-1}-\varepsilon_2^{-1})(\mathbf{I}-\boldsymbol{\gamma}^i(k))\boldsymbol{\delta}_i(k)\mathbf{I}(\mathbf{I}-\boldsymbol{\gamma}^i(k))^T \\ &\quad + \mathbf{H}_j^i(k)\mathbf{P}^{j-}(k)\mathbf{H}_j^i(k)^T\end{aligned}$$

Compute optimal Kalman gain:

$$\begin{aligned}\mathbf{K}_i(k) = \big(&(1+\varepsilon_1)\mathbf{P}^{i-}(k)\mathbf{H}_i^i(k)^T \\ &+ \mathbf{P}^{ij-}(k)\mathbf{H}_j^i(k)^T\big)\mathbf{S}_{i,j}^{-1}(k)\end{aligned}$$

If there is no relative measurement, the Kalman gain:

$$\mathbf{K}_i(k) = 0$$

Update state estimation with the current relative measurement:

$$\hat{\mathbf{x}}^{i+}(k) = \hat{\mathbf{x}}^{i-}(k) + \mathbf{K}_i(k)\mathbf{r}_i(k)$$

Update the error covariance:

$$\begin{aligned}\mathbf{P}^{i+}(k) &= \mathbf{P}^{i-}(k) - \mathbf{K}_i(k)\mathbf{S}_{i,j}(k)\mathbf{K}_i(k)^T \\ \mathbf{P}^{ij+}(k) &= \mathbf{P}^{ij-}(k) - \mathbf{K}_i(k)\mathbf{S}_{i,j}(k)\mathbf{K}_j(k)^T\end{aligned}$$

$k \leftarrow k+1$

IV Performance Analysis

In proposing an event-based trigger formulation our goal is to address the trade-off between estimation performance and communication savings. First, we define communication rate as the average number of transmitted sensor measurements when the triggering condition ($\boldsymbol{\gamma}_m^i$) is satisfied [114]:

$$\boldsymbol{\Gamma}_m^i = \lim_{T\to\infty} \frac{1}{T+1} \sum_{k=0}^{T} \boldsymbol{\gamma}_m^i(k) \tag{3.25}$$

Note that this measure ($\boldsymbol{\Gamma}^i$) is a number between zero and one, with one representing the periodic case (*i.e.* $\gamma^i = 1, \forall i$). The smaller the communication rate, the greater the communication savings with respect to the periodic case. Knowledge of the communication rate $\boldsymbol{\Gamma}^i$ of each sensor is necessary to determine the required system bandwidth and the lifetime of each sensor. Our next Theorem provides a mechanism to compute the Kalman gain. Unlike previous references in event-triggered state estimation, we pose the design of the event-triggered rule and Kalman gains simultaneously as an optimization problem, trading off between estimation performance and communication rate.

Theorem IV.1. *The Kalman gain can be found by solving the following optimization problem:*

$$\begin{aligned} \boldsymbol{Y}^i = \min_{m=1,\dots,M} \quad & \sum_{m=0}^{M} \boldsymbol{\Gamma}_m^i \\ \bar{\boldsymbol{P}}^i \le \Delta^i, \quad & \bar{\boldsymbol{P}}^j \le \Delta^i, \quad \bar{\boldsymbol{P}}^{ij} \le \Delta^{ij}, \quad \boldsymbol{Y}^i \ge 0, \\ \text{Inequality } & (3.29) \end{aligned} \tag{3.26}$$

Where

$$\begin{aligned} \Omega_1 &= \bar{\boldsymbol{P}}^i - (1+\varepsilon_1)\big((\boldsymbol{A}_i\bar{\boldsymbol{P}}^i\boldsymbol{A}_i^T + \boldsymbol{Q}^i) - \boldsymbol{K}_i\boldsymbol{H}_i^i(\boldsymbol{A}_i\bar{\boldsymbol{P}}^i\boldsymbol{A}_i^T \\ &\quad + \boldsymbol{Q}^i) - (\boldsymbol{A}_i\bar{\boldsymbol{P}}^i\boldsymbol{A}_i^T + \boldsymbol{Q}^i)\boldsymbol{H}_i^{i^T}\boldsymbol{K}_i^T\big) + \boldsymbol{A}_i\bar{\boldsymbol{P}}^{ij}\boldsymbol{A}_i^T\boldsymbol{H}_j^{i^T}\boldsymbol{\Gamma}_i^T\boldsymbol{K}_i^T \\ &\quad + \boldsymbol{K}_i\boldsymbol{\lambda}_i\boldsymbol{H}_j^i\boldsymbol{A}_i\bar{\boldsymbol{P}}^{ij}\boldsymbol{A}_i^T \\ \Omega_2 &= (1+\varepsilon_1)^{-1}(\boldsymbol{A}_i\bar{\boldsymbol{P}}^i\boldsymbol{A}_i^T + \boldsymbol{Q}^i)^{-1} \\ \Omega_3 &= (\boldsymbol{A}_j\bar{\boldsymbol{P}}^j\boldsymbol{A}_j^T + \boldsymbol{Q}^j)^{-1} \\ \Omega_4 &= (1-\varepsilon_2)^{-1}\boldsymbol{R}_i^{-T} \\ \Omega_5 &= (1+\varepsilon_1^{-1}-\varepsilon_2^{-1})(\boldsymbol{\delta}_i\boldsymbol{I})^{-1} \end{aligned} \tag{3.27}$$

Proof. We first assert the following statements:

1. $\bar{\boldsymbol{P}}^i \le \Delta^i$

2. There exists $0 \leq \bar{\boldsymbol{P}}^i \leq \Delta^i$ such that:

$$\begin{aligned}
&\bar{\boldsymbol{P}}^i \leq (1+\varepsilon_1)(\boldsymbol{I}-\boldsymbol{K}_i\boldsymbol{H}_i^i)(\boldsymbol{A}_i\bar{\boldsymbol{P}}^i\boldsymbol{A}_i^T+\boldsymbol{Q}^i)\\
&\times(\boldsymbol{I}-\boldsymbol{K}_i\boldsymbol{H}_i^i)^T-(\boldsymbol{I}-\boldsymbol{K}_i\boldsymbol{H}_i^i)(\boldsymbol{A}_i\bar{\boldsymbol{P}}^{ij}A_i^T)(\boldsymbol{K}_i\boldsymbol{H}_j^i)^T\\
&+\boldsymbol{K}_i\boldsymbol{R}^i\boldsymbol{K}_i^T-(\boldsymbol{K}_i\boldsymbol{H}_j^i)(\boldsymbol{A}_i\bar{\boldsymbol{P}}^{ij}\boldsymbol{A}_i^T)(\boldsymbol{I}-\boldsymbol{K}_i\boldsymbol{H}_i^i)^T\\
&+(1-\varepsilon_2)(\boldsymbol{K}_i\boldsymbol{H}_j^i)(\boldsymbol{A}_j\bar{\boldsymbol{P}}^j\boldsymbol{A}_j^T+\boldsymbol{Q}^j)(\boldsymbol{K}_i\boldsymbol{H}_j^i)^T\\
&+(1+\varepsilon_1^{-1}-\varepsilon_2^{-1})\boldsymbol{K}_i(\boldsymbol{I}-\boldsymbol{\gamma}^i)\boldsymbol{\delta}_iI(\boldsymbol{I}-\boldsymbol{\gamma}^i)^T\boldsymbol{K}_i^T
\end{aligned} \tag{3.28}$$

   where inequality (3.28) is the form of developed steady-state Kalman filter.

3. $\bar{\boldsymbol{P}}^j \leq \Delta^j$

4. $\bar{\boldsymbol{P}}^{ij} \leq \Delta^{ij}$

Thus, using Schur complement, inequality (3.28) is equivalent to the linear matrix inequality (LMI) in Eq. (3.29). □

Remark 4. *The result of Theorem IV.1 allows designers to reduce the overall communication rate in the system subject to some upper bound on the worst case error covariance.*

$$\begin{bmatrix}
\Omega_1 & \boldsymbol{K}_i\boldsymbol{H}_i^i & \boldsymbol{K}_i\boldsymbol{H}_j^i & \boldsymbol{K}_i\boldsymbol{H}_i^i & \boldsymbol{K}_i\boldsymbol{H}_j^i & \boldsymbol{K}_i & \boldsymbol{K}_i(\boldsymbol{I}-\boldsymbol{\Gamma}^i)\\
\boldsymbol{H}_i^{iT}\boldsymbol{K}_i^T & \Omega_2 & \boldsymbol{0} & \boldsymbol{0} & \boldsymbol{0} & \boldsymbol{0} & \boldsymbol{0}\\
\boldsymbol{H}_j^{iT}\boldsymbol{K}_i^T & \boldsymbol{0} & \Omega_3 & \boldsymbol{0} & \boldsymbol{0} & \boldsymbol{0} & \boldsymbol{0}\\
\boldsymbol{H}_j^{iT}\boldsymbol{K}_i^T & \boldsymbol{0} & \boldsymbol{0} & (\boldsymbol{A}_i\bar{\boldsymbol{P}}^{ij}\boldsymbol{A}_i^T)^{-1} & 0 & \boldsymbol{0} & \boldsymbol{0}\\
\boldsymbol{H}_i^{iT}\boldsymbol{K}_i^T & \boldsymbol{0} & \boldsymbol{0} & \boldsymbol{0} & (\boldsymbol{A}_i\bar{\boldsymbol{P}}^{ij}\boldsymbol{A}_i^T)^{-1} & \boldsymbol{0} & \boldsymbol{0}\\
\boldsymbol{K}_i^T & \boldsymbol{0} & \boldsymbol{0} & \boldsymbol{0} & \boldsymbol{0} & \Omega_4 & \boldsymbol{0}\\
(\boldsymbol{I}-\boldsymbol{\Gamma}^i)^T\boldsymbol{K}_i^T & \boldsymbol{0} & \boldsymbol{0} & \boldsymbol{0} & \boldsymbol{0} & \boldsymbol{0} & \Omega_5
\end{bmatrix} \leq \boldsymbol{0} \tag{3.29}$$

V Relationship between energy consumption and event triggering mechanism

In this section, we analyze the relationship between energy consumption and communication rate with our proposed event-triggered transmission mechanism. To this end, we focus on the average number of transmitted sensor measurements and energy consumption in each mobile robot. We first model the received signal strength indicator (RSSI) considering the position of the transmitter (x_t^i) and receiver (x_r^i) for each mobile robot i. The RSSI is affected by three factors: 1) path loss due to the distance between the transmitter and the receiver, 2) shadowing due to physical

obstacles that block the transmitted signals, and 3) multipath fading due to reflections and refractions of the transmitted signal. We define L_0 as a received power in 1 m. The RSSI, measured in dBm, is given by (see [115]):

$$P(x_s^i, x_r^i) = \underbrace{L_0 - 10n\log_{10}(\|x_t^i - x_r^i\|)}_{Path\ loss} + \underbrace{W(x_t^i, x_r^i)}_{Shadowing} + \underbrace{F}_{Fading} \tag{3.30}$$

Since the fading term in the above formulation is a random variable, we consider the average RSSI in order to compute the energy consumed during communication.

The average communication energy consumed due to data transmission is given by:

$$\bar{E}_i^c(k) = \sum_{k=0}^{T} \boldsymbol{\gamma}^i(k)\bar{P}(x_s^i, x_r^i) \tag{3.31}$$

where $\boldsymbol{\gamma}^i(k)$ is the triggering condition (3.3). Our framework is as follows: whenever robot i receives relative measurement from the camera (event-triggered generator), then robot i computes the updated state estimate and transmits it through the network. Thus, the goal is to reduce the amount of information transmitted by each robot. Since energy consumption is directly proportional to the transmission of information, energy can be saved by reducing the amount of transmitted information. The smaller the event-triggering parameters, the more events are triggered thus leading to higher energy communication consumption. Therefore, it is important to design the event-triggering parameters such that we reduce the communication rate and energy consumption with acceptable localization accuracy.

VI Applications

VI.1 Simulation Results

In this section, the effectiveness of the proposed method is illustrated using computer simulation. Consider four mobile robots whose equations of motion are described by [116]:

$$\begin{cases} x^i(t+1) = x^i(t) + \Delta t(v_m^i(t)\cos(\phi^i(t) + \Delta\phi^i(t)) \\ y^i(t+1) = y^i(t) + \Delta t(v_m^i(t)\sin(\phi^i(t) + \Delta\phi^i(t)) \\ \phi^i(t+1) = \phi^i(t) + \Delta t\omega^i(t) \qquad i \in \{1,2,3,4\}, \end{cases} \tag{3.32}$$

where $v^i(t)$ and $\omega^i(t)$ represent the linear and angular velocity, respectively. Also, we define $\Delta t v_m^i(t) = \frac{\Delta R^i + \Delta L^i}{2}$ and $\Delta\phi^i(t) = \frac{\Delta R^i - \Delta L^i}{2b}$, where ΔL^i, ΔR^i, b and $\Delta\phi^i(t)$ are the distance moved by the left wheel, the distance moved by the

right wheel, the distance between the wheels and uncertainty of the orientation, respectively. The control input for each robot i is given by:

$$u^i(t) = \begin{bmatrix} \Delta L^i \\ \Delta R^i \end{bmatrix} \tag{3.33}$$

Where the control input $u^i(t)$ is obtained from odometry sensor. The relationship between observation measurements, such as range and bearing, of a robot $i \in \{1,2,3,4\}$ relative to robot $j \in \{1,2,3,4\} \setminus \{i\}$ is given by:

$$z_{ij}(t) = \begin{bmatrix} \rho_{ij}(t) \\ \theta_{ij}(t) \end{bmatrix} = \begin{bmatrix} \sqrt{(x^i(t) - x^j(t))^2 + (y^i(t) - y^j(t))^2} \\ \arctan(\frac{y^i(t) - y^j(t)}{x^i(t) - x^j(t)}) \end{bmatrix} \tag{3.34}$$

where:

$\rho_{ij}(t)$ is the relative distance between the mobile robot i and the observed robot j.

$\theta_{ij}(t)$ is the bearing of robot j relative to the robot i.

Where range-bearing measurements $z_{ij}(t)$ are corresponding to overhead camera.

Table 3.1: Average transmission rate for different triggering conditions considering the range of robot i relative to robot j (simulation)

Type of robot	Robot 1	Robot 2	Robot 3	Robot 4
Time-triggered	1	1	1	1
Event-triggered (δ^i, ξ^i)=(0.1,0.1)	0.17	0.12	0.14	0.15
Event-triggered (δ^i, ξ^i)=(0.2,0.2)	0.10	0.09	0.14	0.11

Table 3.2: Average transmission rate for different triggering conditions considering the bearing of robot i relative to robot j (simulation)

Type of robot	Robot 1	Robot 2	Robot 3	Robot 4
Time-triggered	1	1	1	1
Event-triggered (δ^i, ξ^i)=(0.3,0.3)	0.65	0.42	0.55	0.53
Event-triggered (δ^i, ξ^i)=(0.5,0.5)	0.47	0.42	0.44	0.46

We consider additive white noise affecting both control input $u^i(t)$ and relative measurements $z_{ij}(t)$ in order to reflect actual uncertainties associated with the wheel

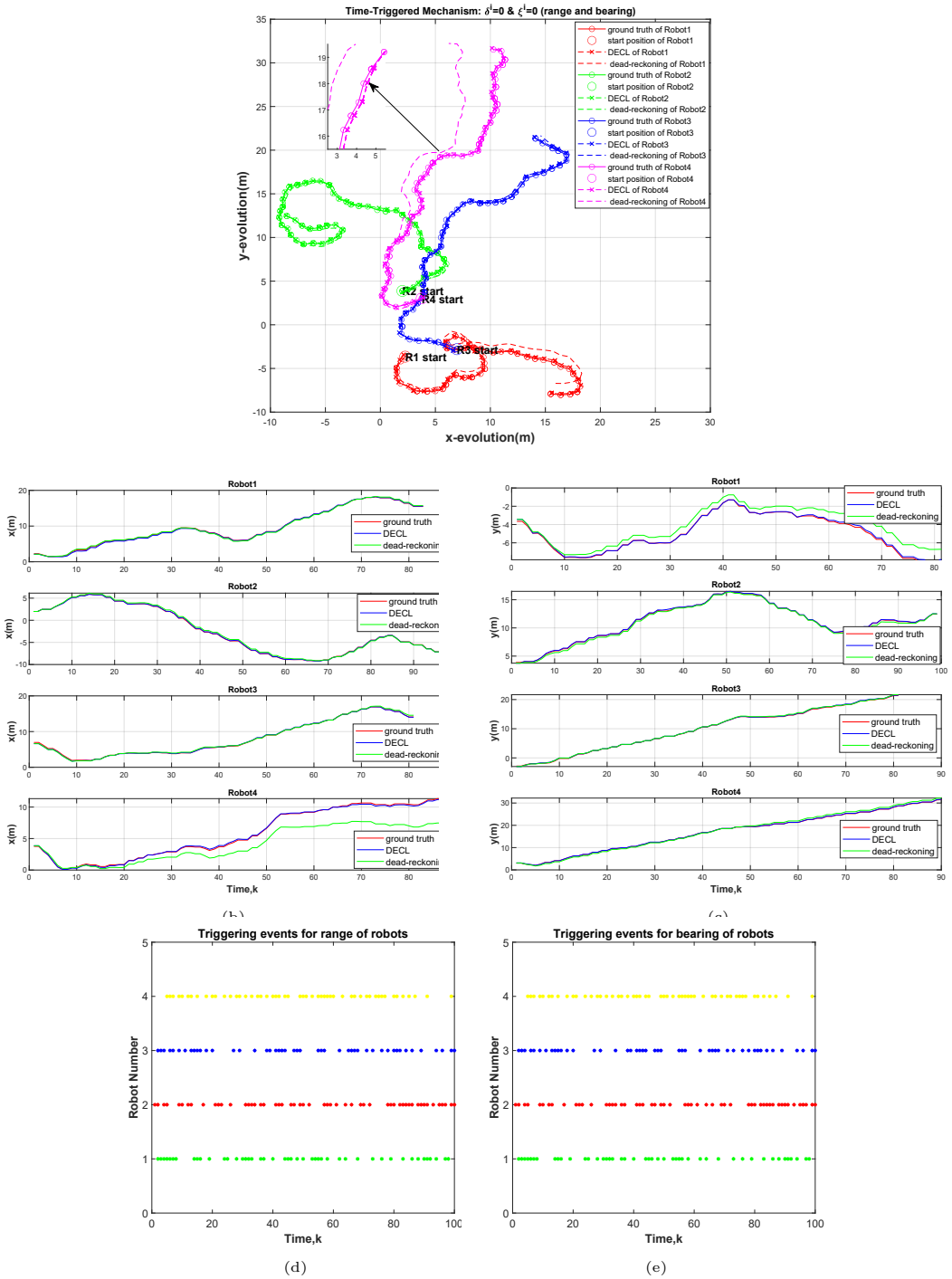

Figure 3.2: Simulation testing results: localization of four robots by DECL algorithm under time-triggered mechanism (a) ground truth, dead-reckoning and DECL trajectories of four robots on the xy-plane (b),(c) ground truth, dead-reckoning and DECL trajectories of four robots respect to time (d), (e) the relationship between the triggered times and time axis for range and bearing of four robots

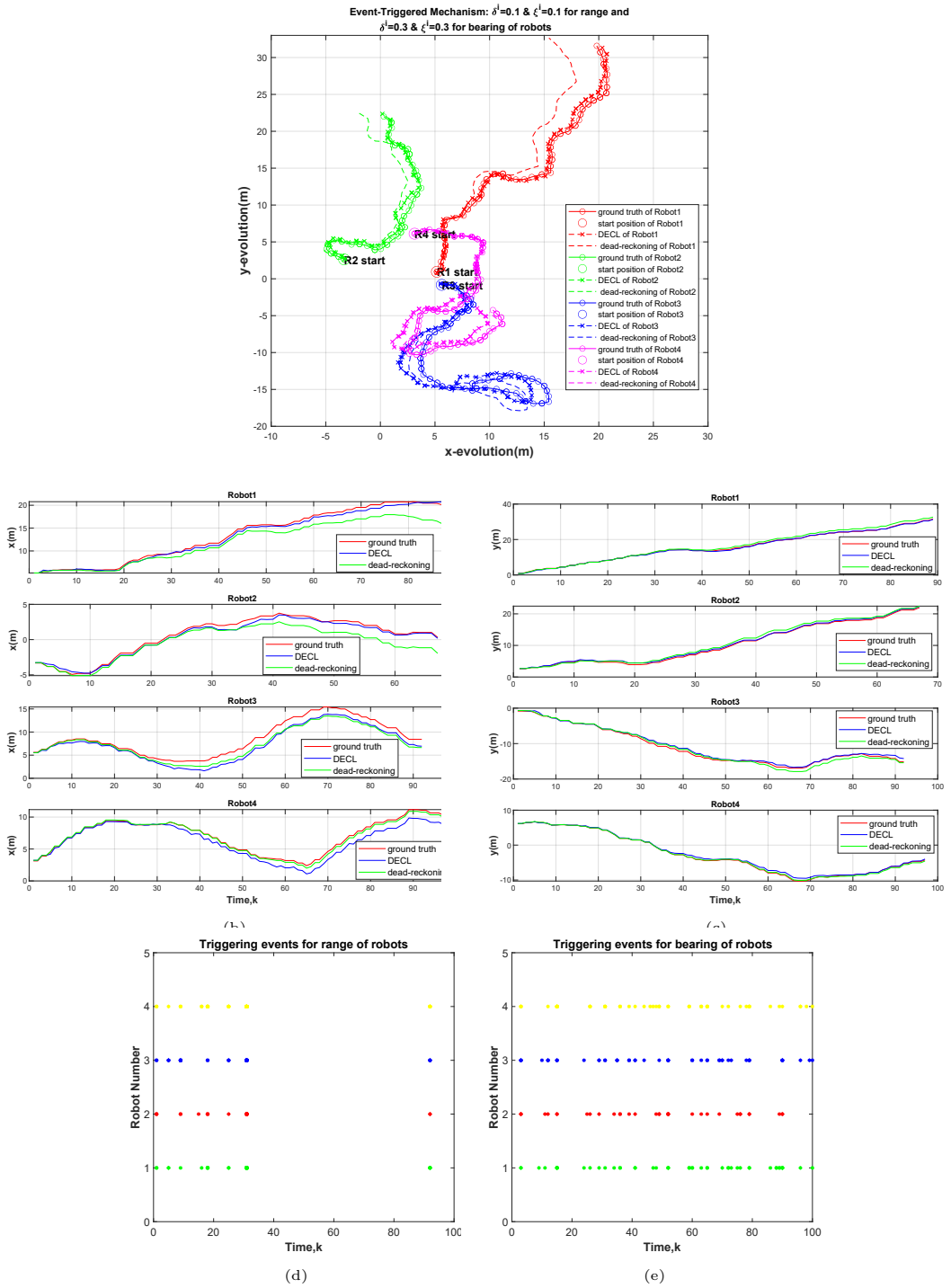

(d) (e)

Figure 3.3: Simulation testing results: localization of four robots by DECL algorithm under event-triggered mechanism ($\delta^i = 0.1$ and $\xi^i = 0.1$ for the range and $\delta^i = 0.3$ and $\xi^i = 0.3$ for the bearings) (a) ground truth, dead-reckoning and DECL trajectories of four robots on the xy-plane (b),(c) ground truth, dead-reckoning and DECL trajectories of four robots respect to time (d), (e) the relationship between the triggered times and time axis for range and bearing of four robots

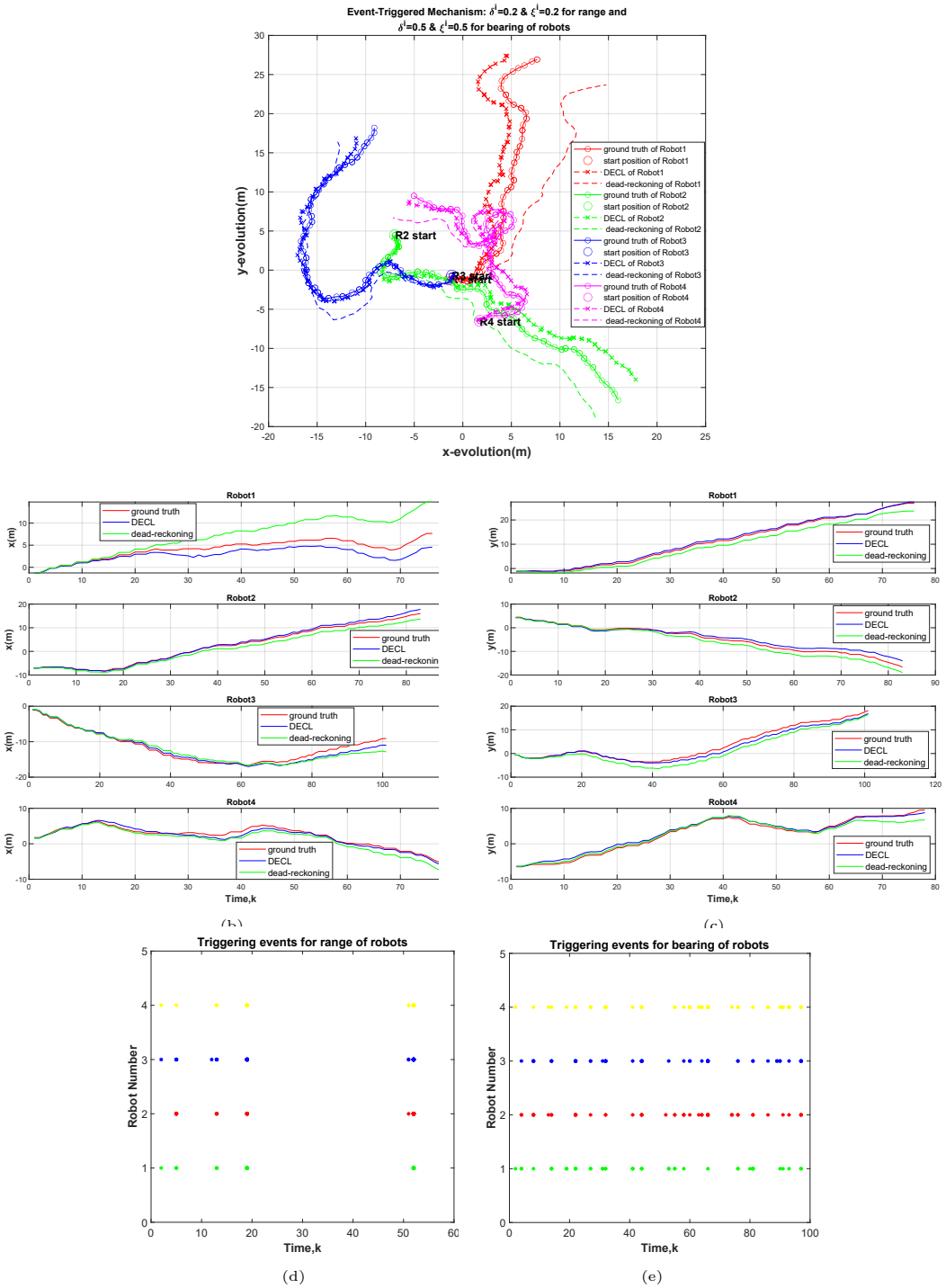

(b) (c)

(d) (e)

Figure 3.4: Simulation testing results: localization of four robots by DECL algorithm under event-triggered mechanism ($\delta^i = 0.2$ and $\xi^i = 0.2$ for the range and $\delta^i = 0.5$ and $\xi^i = 0.5$ for the bearings) (a) ground truth, dead-reckoning and DECL trajectories of four robots on the xy-plane (b),(c) ground truth, dead-reckoning and DECL trajectories of four robots respect to time (d), (e) the relationship between the triggered times and time axis for range and bearing of four robots

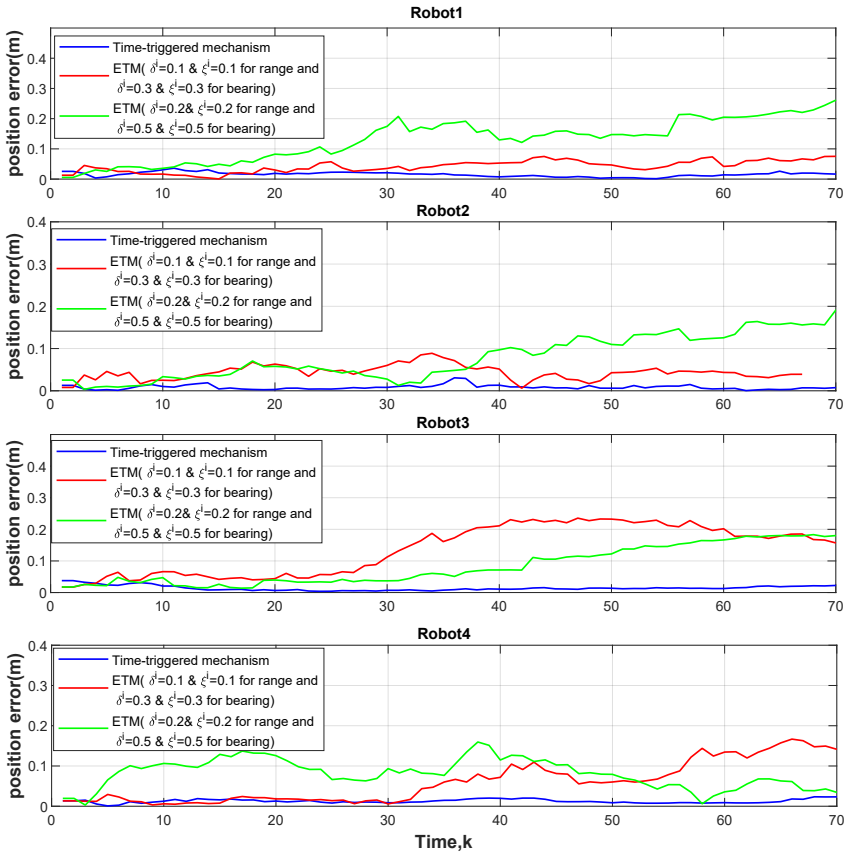

Figure 3.5: Simulation testing results: the estimated position error of each robot for different triggering conditions; the blue curve shows the time-triggered mechanism, the red and green curves represent event-triggered mechanism with different triggering conditions

encoders and overhead camera. To proceed with our simulation, we assume that the distance between wheels is $b = 0.4m$. The control input $u^i(t)$, covariance matrix of the control input, R^i, and covariance matrix for the relative measurements, Q_{ij} are given by:

$$\begin{aligned} u^i(t) &= [\Delta L^i; \Delta R^i] = [0.25m; 0.25m], \\ R^i &= \text{diag}\{(0.05\Delta L^i)^2; (0.05\Delta R^i)^2\}, \\ Q_{ij} &= \text{diag}\{0.1m^2; 0.1rad^2\}. \end{aligned}$$

In our simulations, we consider the following pose estimates:

1. Actual position of each robot,
2. pose estimate obtained using filter propagation,
3. pose estimate obtained using the DECL algorithm 1.

We assume that as robots $i \in \{1, 2, 3, 4\}$ are in motion, at least one of them rests and performs as a stationary robot. Robots then use their exteroceptive sensors to update their localization through relative observations of stationary robots. The moving robots receive the predicted position and associated error covariance of each observed stationary robot over a communication network.

Fig. 3.2, Fig. 3.3, and Fig. 3.4 show the results of our simulations. We first examine localization performance using dead-reckoning where each robot uses the wheel encoders to estimate pose independently without the exchange of information between robots. The results show that without relative measurements the position estimator cannot accurately track trajectories.

In Fig. 3.2 we consider a time-triggered scenario in which each robot continuously receives relative measurement and corrects its pose estimation. Fig. 3.2(a) shows the localization of four robots using DECL on the xy plane, Fig. 3.2(b) and Fig. 3.2(c) show the localization of four robots using DECL with respect to time. Figs. 3.2(d)-(e) display the triggering instants times for range and bearing of the four robots. Note that in the case of the time-triggered mechanism, the absence of triggering instances in Fig. 3.2(d) and Fig. 3.2(e), means that robot i is performing as a stationary robot. As seen in Fig. 3.2, the pose estimation from the DECL algorithm closely tracks the reference trajectory.

In Fig. 3.3 and Fig. 3.4 we study the effect of the event-triggered solution proposed here for different values of the triggering parameters δ and ξ. In Fig. 3.3 we set $\delta^i = 0.1$ and $\xi^i = 0.1$ for the range of each robot and $\delta^i = 0.3$ and $\xi^i = 0.3$ for the bearings. In Fig. 3.4 we choose $\delta^i = 0.2$ and $\xi^i = 0.2$ for range and $\delta^i = 0.5$ and $\xi^i = 0.5$ for bearings of each robot. Figs. 3.3(a)-(c) and Figs. 3.4(a)-(c) show how the pose obtained from the filter using the DECL algorithm change in relation to the actual position and the xy plane and also for different event-triggered parameters. Also, in Figs. 3.3(d)-(e) and Figs. 3.4(d)-(e) we display the triggering times for different event-triggered parameters. As in the previous case, the absence of triggering instances in Fig. 3.3(d)-(e) and Fig. 3.4(d)-(e), indicates that the amount of transmitted sensor measurements are reduced due to the event-triggering mechanism and just a few intervals represent robot i performing as a stationary robot.

To compare the filter performance for the different triggering conditions we use position error for each robot. The norm of position error for each robot at time k

is given by $\mathrm{SE^i(k)} = \sqrt{(x^i(k) - \hat{x}^{i+}(k))^2 + (y^i(t) - \hat{y}^{i+}(k))^2}$ where $x^i(k)$ and $\hat{x}^{i+}(k)$ are the actual and estimated position in the x direction, respectively, and $y^i(k)$ and $\hat{y}^{i+}(k)$ are the actual and estimated position in the y direction, respectively. Fig. 3.5 shows the estimated position error of each robot for different triggering conditions. As expected, large parameters of event-triggering conditions reduce the transfer of information with an increase in the estimated position error. Table 3.1 and Table 3.2 show the comparison between the value of the event-triggered mechanism parameters and the average communication rate of the range-bearing sensor measurements. Smaller values of the average communication rate result in reduced transmission with respect to the periodic case. Comparing tracking results and average communication rate (Table 3.1 and Table 3.2), we can summarize the results as follows:

1. Increasing the parameters of the event-triggering mechanism can reduce the average transmission rate of relative measurements significantly while sacrificing slightly the localization quality.

2. By tuning properly the parameters of the event-triggered mechanism, the desired localization quality can be achieved while drastically reducing the communication rate.

VI.2 Experimental Validation

In this section, we implement and test the performance of our algorithm experimentally. Our testbed consists of a set of one overhead ZED camera, a host computer (Ubuntu 18.04.5 LTS, Intel Core i7-10750H CPU @ 2.60GHz $\times$ 12 processors, GeForce RTX 2070 with Max-Q Design/PCIe/SSE2 graphics), and four e-puck2 robots (see Fig. 3.6). This testbed is equipped with Melodic Robot Operating System (ROS). Our computer vision system uses the ArUco image processing library [117] to track the pose (position and orientation) of the four e-puck2 robots. The host computer is employed as the server running as ROS node with the central part of the DECL algorithm. Each robot has some ROS nodes that include programs to propagate the filter using wheel-encoder measurements and update the filter using the relative-pose measurements obtained from the computer vision system. These ROS nodes communicate through a TCP protocol. The accuracy of the relative pose measurements based on computer vision is set to 0.03 m for position and 5 de-

grees for orientation. The e-puck2 robots communicate with the host computer via Bluetooth. Since the sampling rate of the e-puck2 sensors is 10Hz, we synchronize the sampling rate of the robots and ZED camera to the same frequency. Note that the communication graph between robots changes randomly over time.

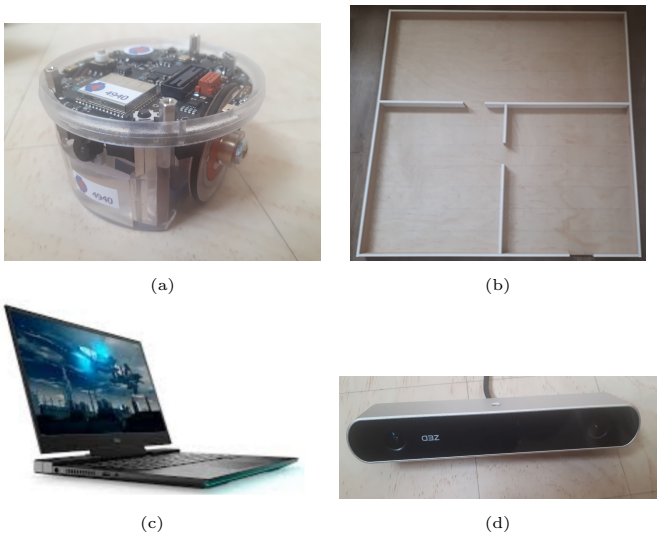

(a) (b)

(c) (d)

Figure 3.6: Experimental setup including (a) e-puck2 robot, (b) workspace, (c) gaming laptop (equipped with Nvidia GPU), (d) overhead ZED camera

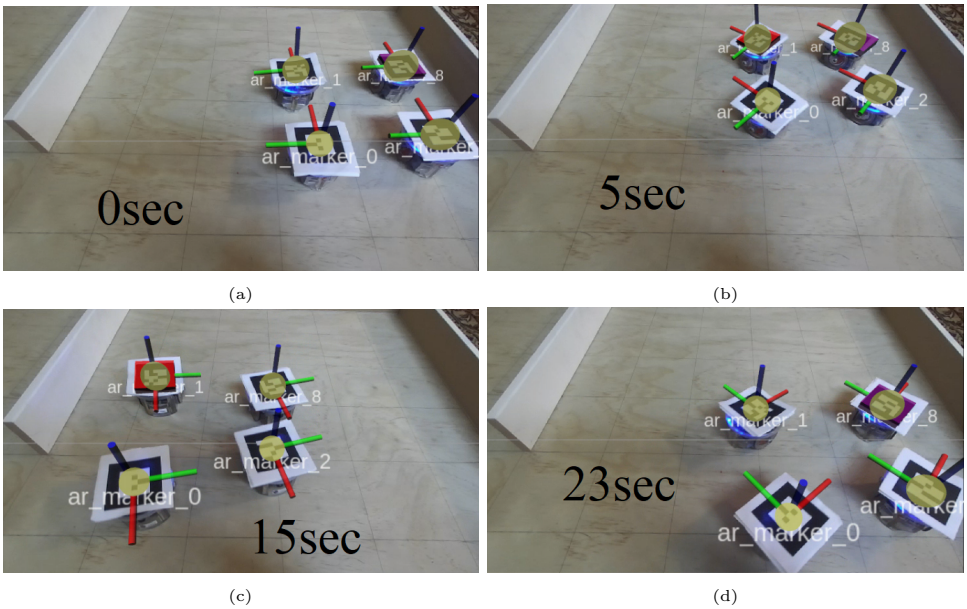

(a) (b)

(c) (d)

Figure 3.7: Each e-puck2 robot moves simultaneously along a circular trajectory. Also, Every robot is equipped with an ArUco tag that enables the overhead ZED camera to take a relative measurement.

The robots move counter-clockwise along a circular path with a radius of 0.13m (see Fig. 3.7). The system has an inherent time delay of between 0.15 and 0.195 s in the relative measurement due to camera latency, image processing, decision-making

process (event-triggered condition), and Bluetooth communication [36]. Our work ignores the effect of this delay in the estimation. This problem will be the scope of our future work. To evaluate the performance of our DECL algorithm, we use our experimental setup and consider the following methods:

1. **Pose estimates obtained using odometry sensors**: In this case, we consider the simple case in which the only information available to the robots to estimate pose is based on odometers. In this model, each robot estimates its own pose by integrating its measured velocity obtained from odometers and then propagates its estimates to its neighbors. This form of estimation is affected by the odometers' precision and suffers from wheel slippage. As a consequence, the estimation error tends to accumulate over time and pose estimates tend to deviate from actual values. Therefore, odometry sensors alone do not provide reliable estimates of the robot's position.

2. **Pose estimates using an overhead camera**: In this case, we use an overhead camera. In this model each robot is equipped with an Augmented Reality (AR) tag, thus allowing the overhead camera to obtain range and bearing relative measurements that are provided to the filters. This technique is based on computer vision and can provide more accurate pose estimates than wheel odometry. However, due to hardware limitations and real-time image processing, the position and orientation of each robot estimated by the camera are subject to delays [36].

3. **Pose estimates obtained using the proposed DECL algorithm 1**: In this case, we employ the proposed EKF to fuse the information obtained from the odometry sensors (filter propagation) along with the information from the overhead camera (filter updating) to improve localization accuracy. The combination of both odometry and camera sensors combines the advantages of each type of sensor. Indeed, although less precise than the overhead camera, odometry sensors have the benefit of being relatively unaffected by delay, thus the combination produces better results than either sensor type working alone. We compare the performance of the proposed EKF and communication rates of exteroceptive sensors (overhead camera) under *time-triggered* and *event-triggered* mechanisms.

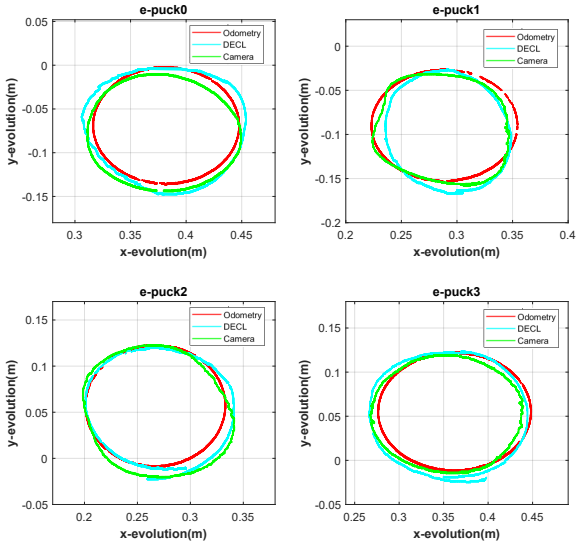

(a)

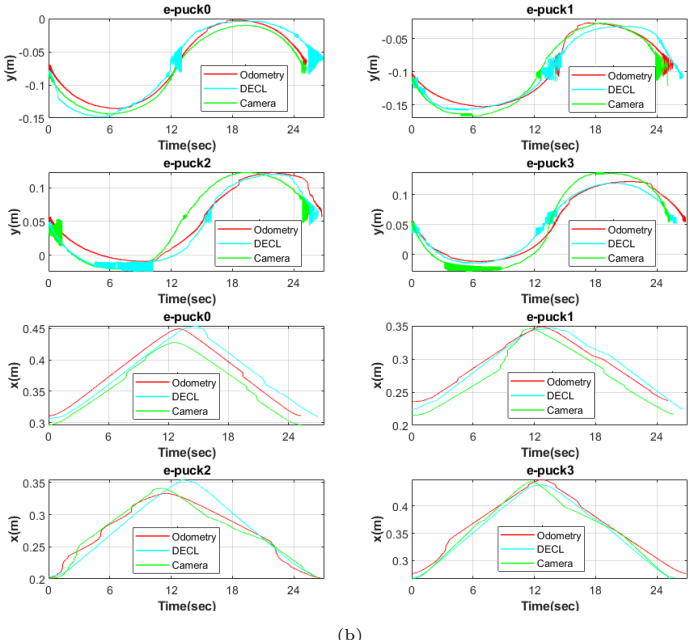

(b)

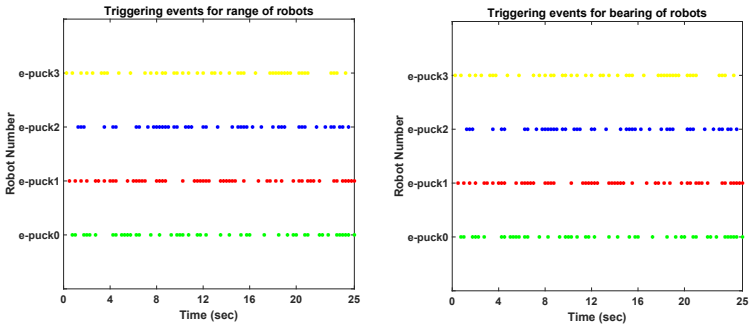

(c) (d)

Figure 3.8: (a)Trajectories of the e-puck2 robots under an experimental test generated by four simultaneously running ROS packages, one for the overhead camera location tracking (the curve indicated in green), one for the odometry estimate (the red curve), and the other one (the blue curve) to obtain location estimates by the DECL algorithm (Algorithm 1) under the time-triggered mechanism.; (b) camera, odometry and DECL trajectories of four robots respect to time in time-triggered mechanism; (c)-(d) the triggering times for range and bearing of the four robots in time-triggered mechanism

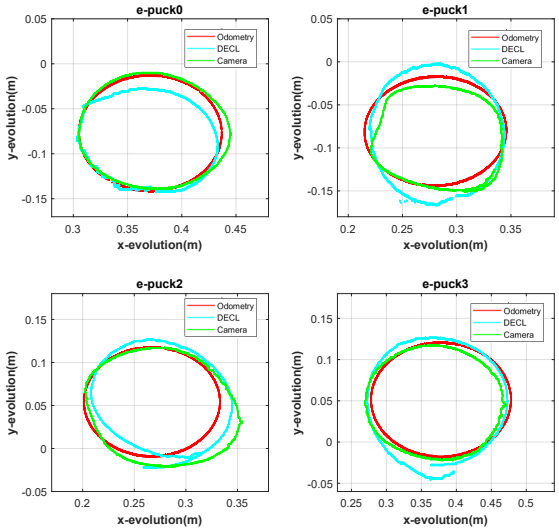

(a)

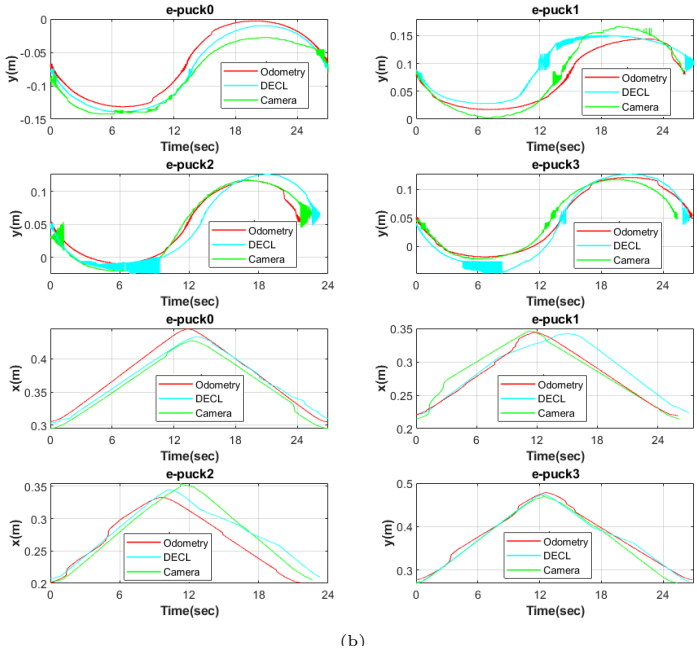

(b)

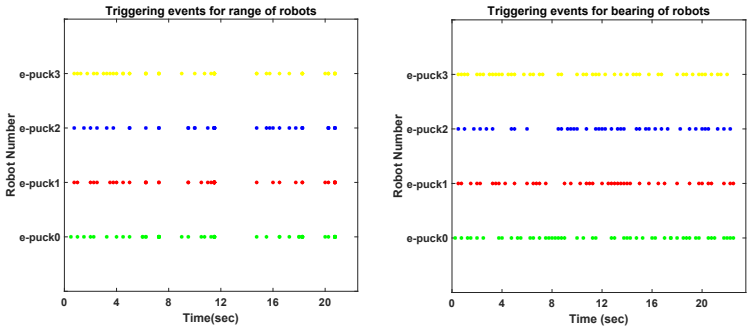

(c) (d)

Figure 3.9: (a)Trajectories of the e-puck2 robots under an experimental test generated by four simultaneously running ROS packages, one for the overhead camera location tracking (the curve indicated by green), one for the odometry estimate (the red curve), and the other one (the blue curve) to obtain location estimates by DECL algorithm (Algorithm 1) under event-triggered mechanism; (b)camera, odometry and DECL trajectories of four robots respect to time in event-triggered mechanism; (c)-(d) the triggering times for range and bearing of the four robots in event-triggered mechanism

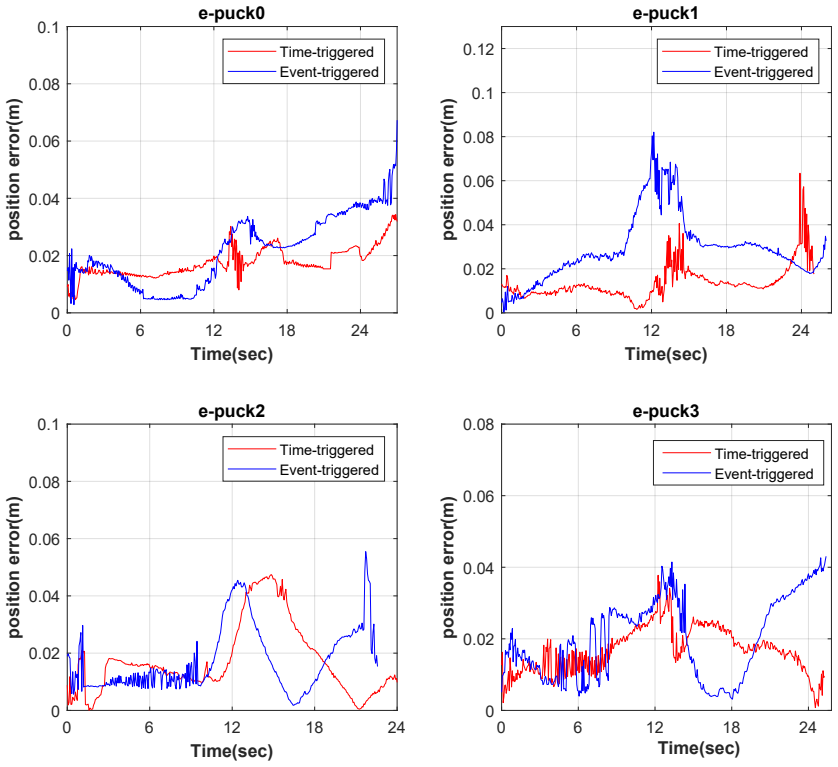

Figure 3.10: Experimental testing results: the estimated position error of each robot for time-triggered and event-triggered mechanism

Figs. 3.8 and Figs. 3.9 show the results of our experiments. In Fig. 3.8 we consider a *time-triggered* scenario in which each e-puck2 robot continuously receives relative measurements and estimates its pose. Fig. 3.8(a) shows the localization of four e-puck2 robots moving in a circular trajectory using the DECL algorithm, Fig. 3.8(b) indicates the localization of four e-puck2 robots using the DECL algorithm with respect to time, and Figs. 3.8(c) and Figs. 3.8(d) represents the triggering times for the range and bearing of four robots. Note that in the case of the time-triggered mechanism, the absence of triggering events in Fig. 3.8(c)-(d), indicates that the robot i performs as a stationary robot for the rest of the robots. As seen in Fig. 3.8, the pose estimation using DECL algorithm 1 (EKF) performs better since information is transferred at a regular rate with no losses. As Table 3.3 and Table 3.4 shows, the communication rate in the time-triggered mechanism is 1 for both range and bearing. Our main interest, however, is to obtain comparable results while reducing communication using the *event-triggered* mechanism. Thus, we study the effect of the triggering parameters on the overall DECL performance. In Fig. 3.9, we set $\delta^i = 0.05$ and $\xi^i = 0.05$ for range and $\delta^i = 0.01$ and

$\xi^i = 0.01$ for bearing of each robot. Notice that, in the case of the event-triggered mechanism, the absence of triggering instances in Figs. 3.9(c)-(d), indicates that the amount of transmitted exteroceptive sensor measurements is reduced due to an event-triggering mechanism and just a few intervals represent e-puck2 robot i performing as a stationary robot. As a result, the pose estimate from DECL algorithm 1 (EKF) provides acceptable localization quality with the reduced transmission of relative measurements (according to Table 3.3 and Table 3.4).

Fig. 3.10 shows the estimated position error of the four robots in the time-triggered and event-triggered cases. Comparing the estimated position error and average communication rate (Table 3.3 and Table 3.4) we conclude that the proposed *event-triggered* cooperative localization approach provides a sound tradeoff between communication resource savings and good localization performance.

Table 3.3: Average transmission rate for different triggering conditions considering the range of robot i relative to robot j (experiment)

Type of robot	e-puck0	e-puck1	e-puck2	e-puck3
Time-triggered	1	1	1	1
Event-triggered (δ^i, ξ^i)=(0.05,0.05)	0.6	0.47	0.53	0.65

Table 3.4: Average transmission rate for different triggering conditions considering the bearing of robot i relative to robot j (experiment)

Type of robot	e-puck0	e-puck1	e-puck2	e-puck3
Time-triggered	1	1	1	1
Event-triggered (δ^i, ξ^i)=(0.01,0.01)	0.97	0.81	0.93	0.98

Chapter 4

Decentralized Event-Triggered Cooperative Localization In Multi-Robot Systems Under Random Delays: With/Without Time Stamps Mechanism

I Introduction

In this chapter, we address the problem of decentralized event-triggered cooperative localization (DECL) for a group of mobile robots in the presence of time delays. First, we introduce a DECL algorithm for multi-robot systems under time delays. We consider two different scenarios (i) time-stamped (ii) non-time-stamped which leads to different DECL algorithms. Then, we provide the stochastic boundedness of filtering error considering bounded random delays. We show that if the delay due to multi-robot communication is sufficiently small, then by choosing proper event-triggering parameters, the filtering error and covariance remain bounded while reducing the transfer of information. Finally, simulation and experimental results using a team of four e-puck2 mobile robots demonstrate the effectiveness of the proposed algorithm.

The rest of this work is given as follows. In Section II, we describe the dynamics of the multi-robot system, define the problem statement, and introduce the event-triggering data-transferring mechanism. In section III we design the DECL for multi-robot systems with random delays considering the non-time-stamped mechanism. In section IV we consider the same problem solved in Section III but assuming a

time-stamped mechanism. In Section V, we present our simulation and experimental results. Finally, in Section VI we provide some final conclusions.

II Problem statement and Preliminaries

II.1 Notations

Given a matrix X, X^T, X^{-1} represent the transpose, and the inverse of X. $\mathbb{E}\{X\}$ or $\mathbb{E}[X]$ is the expectation of the random variable X. I represents the identity matrix with proper dimensions. The superscripts i and j are the identities of agent i and agent j. Superscripts $i-$, $j-$ and $ij-$ represent the propagation step of the filter. Superscripts $i+$, $j+$ and $ij+$ denote the updated step of the filter.

II.2 Dynamics of the multi-robot system

We consider a team of N mobile robots moving in a flat area and capable of sensing and communicating with the rest of the team. The general nonlinear system model for the motion of each robot $i \in \vartheta = \{1, 2, ..., N\}$ is described by [29]

$$\boldsymbol{x}_k^i = \boldsymbol{f}^i(\boldsymbol{x}_{k-1}^i, \boldsymbol{u}_{k-1}^i), \tag{4.1}$$

where the state vector $\boldsymbol{x}_k^i = [x^i(k), y^i(k), \phi^i(k)]^T$ represents the global pose (position and orientation) of robot i and $\boldsymbol{u}^i$ is the control input. We assume throughout that $\boldsymbol{u}^i = \boldsymbol{u}_a^i + \boldsymbol{\eta}^i$, is the velocity command of robot i measured from odometry or inertial sensors, where $\boldsymbol{u}_a^i$ represents the actual velocity and $\boldsymbol{\eta}^i$ is corresponding white-Gaussian process noise. The relative measurement is taken by robot i from robot j at a time k is described by the following equation [29]

$$\boldsymbol{z}_k^{ij} = \boldsymbol{h}_{ij}(\boldsymbol{x}_k^i, \boldsymbol{x}_k^j) + \boldsymbol{\nu}_k^{ij}, \tag{4.2}$$

where $\boldsymbol{h}_{ij}(x^i, x^j)$ is the measurement model and $\boldsymbol{\nu}^{ij}$ is measurement noise. The relative position measurements (range and bearing) are obtained via an overhead camera and augmented reality (AR) tags. The noises $\boldsymbol{\eta}^i$ and $\boldsymbol{\nu}^{ij}$ are independent zero-mean white Gaussian processes with known positive definite variances $\boldsymbol{Q}_k^i = \mathbb{E}[\boldsymbol{\eta}_k^i(\boldsymbol{\eta}_k^i)^T]$ and $\boldsymbol{R}_k^{ij} = \mathbb{E}[\boldsymbol{\nu}_k^{ij}(\boldsymbol{\nu}_k^{ij})^T]$. All noises are assumed to be mutually uncorrelated.

II.3 Problem Formulation

Fig. 4.1 shows the block diagram of DECL proposed in this work. This scheme is based on our previous work [62], but has been modified to include random delays. We consider a decentralized strategy in which robots work in a cooperative fashion;

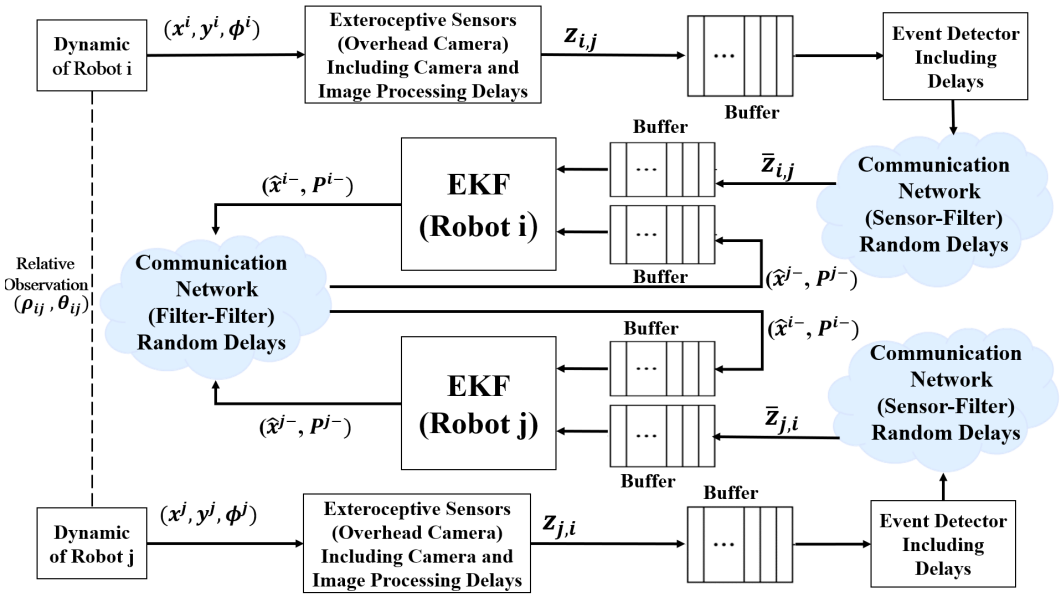

Figure 4.1: Block diagram of DECL algorithm under time delays

however, we do not assume all-to-all communication, thus significantly reducing the communications cost. We assume that each robot can share information with other robots only within a certain communication range. In this scenario, each robot i can detect a neighbor robot j only when they are within the reach of their exteroceptive sensors. When this is the case, we assume that robot i can share information with robot j. Consequently, the computation of the localization task is performed by one or more pairs of robots in the group. Here, the range-bearing measurements $\boldsymbol{z}_k^{ij}$ are sent to the event detector in a periodic manner and the event detector then decides whether or not the current sensor measurement is to be transmitted to the estimator over the unreliable communication network, based on a triggering rule. The range-bearing measurements $\bar{\boldsymbol{z}}_k^{ij}$ transmitted by the event detector to the corresponding filter is affected by time delays. This the time delay may represent the effect of the communication network, camera latency, image processing, and event-detector delays for the packets arriving at each robot. Since CL depends on agent-agent interaction via a network, communication delays have a significant impact on time delays [92]. Therefore in this work, we mainly focus on communication delays that occur due to limited bandwidth in the network. We assume that time delays occur randomly due to the unpredictable nature of stochastic factors such as latency, percentage of out-of-ordered packets in the communication channel, and re-transmitted packets. Considering the fact that packet $\bar{\boldsymbol{z}}_k^{ij}$ may be unavailable to the correspond-

ing filter in time, a D-length buffer is used to store delayed packets. Because of the limited buffer length, packet $\bar{\boldsymbol{z}}_{k-D}^{ij}$ will be discarded when the maximum number of random delays is more than D. The random delay occurring between the sensors and the filter, is denoted τ_k and takes value in $\mathcal{N} = \{1, ..., s\}$ where s is the largest delay. The probability distribution of the random delay is given as follows [92]:

$$\text{Prob}\Big\{\tau_k = i_s\Big\} = p_{i_s}, \qquad i_s \in \mathcal{N} \tag{4.3}$$

where $0 \leqslant p_{i_s} \leqslant 1$ and $\sum_{i_s \in \mathcal{N}} p_{i_s} = 1$ Because of the existence of the random delay during the data transmission, the actual measurement signal received by the filter is expressed as

$$\tilde{\boldsymbol{z}}_k^{ij} = \boldsymbol{z}_{k-\tau_k}^{ij} \tag{4.4}$$

Then, according to (4.1), (4.2) and (4.4) we have:

$$\begin{cases} \bar{\boldsymbol{x}}_k^i = \bar{\boldsymbol{f}}^i(\bar{\boldsymbol{x}}_{k-1}^i, \bar{\boldsymbol{u}}_{k-1}^i) \\ \tilde{\boldsymbol{z}}_k^{ij} = \boldsymbol{E}_{\tau_k} \bar{\boldsymbol{h}}_{ij}(\bar{\boldsymbol{x}}_k^i, \bar{\boldsymbol{x}}_k^j) + \boldsymbol{E}_{\tau_k} \bar{\boldsymbol{\nu}}_k^{ij}, \end{cases} \tag{4.5}$$

where

$$\begin{aligned}
&\bar{\boldsymbol{x}}_k^i = \begin{bmatrix} \boldsymbol{x}_k^i & \boldsymbol{x}_{k-1}^i & \cdots & \boldsymbol{x}_{k-s}^i \end{bmatrix}^T \\
&\bar{\boldsymbol{x}}_k^j = \begin{bmatrix} \boldsymbol{x}_k^j & \boldsymbol{x}_{k-1}^j & \cdots & \boldsymbol{x}_{k-s}^j \end{bmatrix}^T \\
&\bar{\boldsymbol{f}}(\bar{\boldsymbol{x}}_k^i, \bar{\boldsymbol{u}}_k^i) = \begin{bmatrix} \boldsymbol{f}(\boldsymbol{x}_k^i, \boldsymbol{u}_k^i) & \boldsymbol{f}(\boldsymbol{x}_{k-1}^i, \boldsymbol{u}_{k-1}^i) & \cdots & \boldsymbol{f}(\boldsymbol{x}_{k-s}^i, \boldsymbol{u}_{k-s}^i) \end{bmatrix}^T \\
&\bar{\boldsymbol{h}}_{ij}(\bar{\boldsymbol{x}}_k^i, \bar{\boldsymbol{x}}_k^j) = \begin{bmatrix} \boldsymbol{h}_{ij}(\boldsymbol{x}_k^i, \boldsymbol{x}_k^j) & \boldsymbol{h}_{ij}(\boldsymbol{x}_{k-1}^i, \boldsymbol{x}_{k-1}^j) & \cdots & \boldsymbol{h}_{ij}(\boldsymbol{x}_{k-s}^i, \boldsymbol{x}_{k-s}^j) \end{bmatrix}^T \\
&\bar{\boldsymbol{\nu}}_k^{ij} = \begin{bmatrix} \boldsymbol{\nu}_k^{ij} & \boldsymbol{\nu}_{k-1}^{ij} & \cdots & \boldsymbol{\nu}_{k-s}^{ij} \end{bmatrix}^T \\
&\boldsymbol{E}_{\tau_k} = \Big[\underbrace{\boldsymbol{0}_{m\times m} \quad \cdots \quad \boldsymbol{0}_{m\times m}}_{\tau_k} \quad \boldsymbol{I}_m \quad \underbrace{\boldsymbol{0}_{m\times m} \quad \cdots \quad \boldsymbol{0}_{m\times m}}_{s-\tau_k}\Big]^T
\end{aligned}$$

Note that the $\boldsymbol{E}_{\tau_k}$ is defined as an augmented matrix with zero entries, except the (τ_k+1)th element, which is the identity matrix. The recursive filter for the augment system (4.5) is defined as follows:

$$\begin{cases} \hat{\bar{\boldsymbol{x}}}_k^{i-} = \bar{\boldsymbol{f}}^i(\hat{\bar{\boldsymbol{x}}}_{k-1}^{i+}, \bar{\boldsymbol{u}}_{k-1}^i) \\ \hat{\bar{\boldsymbol{x}}}_k^{i+} = \hat{\bar{\boldsymbol{x}}}_k^{i-} + \boldsymbol{K}_k^i \Big[\tilde{\boldsymbol{z}}_k^{ij} - \boldsymbol{E}_d \hat{\boldsymbol{z}}_k^{ij}\Big] \end{cases} \tag{4.6}$$

where $\hat{\bar{\boldsymbol{x}}}_k^{i-}$ and $\hat{\bar{\boldsymbol{x}}}_k^{i+}$ denote, respectively, the prediction and estimate of $\bar{\boldsymbol{x}}_k^i$ at time instant k and $\boldsymbol{K}_k^i$ is the filter gain to be designed. $\hat{\boldsymbol{z}}_k^{ij}$ denote the predicted measurement. The matrix $\boldsymbol{E}_d$ is defined as follows:

$$\boldsymbol{E}_d = \Big[\underbrace{\boldsymbol{0}_{m\times m} \quad \cdots \quad \boldsymbol{0}_{m\times m}}_{d} \quad \boldsymbol{I}_m \quad \underbrace{\boldsymbol{0}_{m\times m} \quad \cdots \quad \boldsymbol{0}_{m\times m}}_{s-d}\Big]^T \tag{4.7}$$

where d is an integer satisfying:

$$d = \begin{cases} \lfloor \bar{\tau} \rfloor & \text{if } \ \bar{\tau} - \lfloor \bar{\tau} \rfloor < \frac{1}{2} \\ \lfloor \bar{\tau} \rfloor + 1, & \text{otherwise} \end{cases} \tag{4.8}$$

with $\bar{\tau} = \mathbb{E}[\tau_{k+1}] = \sum_{i \in \mathcal{N}} i p_i$ and $\lfloor \bar{\tau} \rfloor$ represents the biggest integer no bigger than $\bar{\tau}$. It is worth mentioning that the innovation of the proposed filter (4.6) contains the matrix $\boldsymbol{E}_d$ instead of $\boldsymbol{E}_{\tau_k}$. This is because the filter cannot include a random variable (e.g. τ_k). Therefore, we use the mathematical expectation $\bar{\tau}$ of the random variable $\boldsymbol{E}_{\tau_k}$ to construct the filter.

Furthermore, robots exchange estimated states and error covariance with each other in order to correct the estimation results. Therefore, we consider random transmission delays in the robot-to-robot communication channel, denoted as ξ_k, taking value in $\mathcal{M} = \{1, ..., n\}$, where n is largest delay. The probability distribution of the random delay is given by:

$$\text{Prob}\Big\{\xi_k = i_c\Big\} = p_{i_c}, \qquad i_c \in \mathcal{M} \tag{4.9}$$

where $0 \leqslant \boldsymbol{p}_{i_c} \leqslant 1$ and $\sum_{i_c \in \mathcal{M}} \boldsymbol{p}_{i_c} = 1$.

Also, because of the existence of random transmission delays during the data transmission, the actually predicted states and corresponding error covariance received by the filter can be expressed as follows:

$$\tilde{\hat{\boldsymbol{x}}}_k^{j-} = \hat{\boldsymbol{x}}_{k-\xi_k}^{j-} \tag{4.10}$$

$$\tilde{\boldsymbol{P}}_k^{j-} = \boldsymbol{P}_{k-\xi_k}^{j-} \tag{4.11}$$

We assume that the interaction (communication) topology of robots is modeled as an independent and identically distributed (i.i.d) random process.

Assumption 3. *We assume that the random variables for the communication channel between the sensor and filter of robots (τ_k) are independent of the communication channel between two filters (ξ_k) in i and k.*

Remark 5. *In this work, the random delay is modeled as a Bernoulli random variable with distribution [118]:*

$$\begin{aligned}
\tilde{\boldsymbol{z}}_k^{ij} &= \boldsymbol{\theta}_{0,k}\bar{\boldsymbol{z}}_k^{ij} + (\boldsymbol{I} - \boldsymbol{\theta}_{0,k})\boldsymbol{\theta}_{1,k}\bar{\boldsymbol{z}}_{k-1}^{ij} + \ldots + \prod_{i=0}^{s-1}(\boldsymbol{I} - \boldsymbol{\theta}_{i,k})\boldsymbol{\theta}_{s,k}\bar{\boldsymbol{z}}_{k-s}^{ij} \\
\tilde{\hat{\boldsymbol{x}}}_k^{j-} &= \boldsymbol{\lambda}_{0,k}\hat{\boldsymbol{x}}_k^{j-} + (\boldsymbol{I} - \boldsymbol{\lambda}_{0,k})\boldsymbol{\lambda}_{1,k}\hat{\boldsymbol{x}}_{k-1}^{j-} + \ldots + \prod_{i=0}^{n-1}(\boldsymbol{I} - \boldsymbol{\lambda}_{i,k})\boldsymbol{\lambda}_{n,k}\hat{\boldsymbol{x}}_{k-n}^{j-} \\
\tilde{\boldsymbol{P}}_k^{j-} &= \boldsymbol{\lambda}_{0,k}\boldsymbol{P}_k^{j-} + (\boldsymbol{I} - \boldsymbol{\lambda}_{0,k})\boldsymbol{\lambda}_{1,k}\boldsymbol{P}_{k-1}^{j-} + \ldots + \prod_{i=0}^{n-1}(\boldsymbol{I} - \boldsymbol{\lambda}_{i,k})\boldsymbol{\lambda}_{n,k}\boldsymbol{P}_{k-n}^{j-}
\end{aligned} \tag{4.12}$$

where $\theta_{i,k}$, $i = 0, 1, \ldots, s$ and $\lambda_{i,k}$, $i = 0, 1, \ldots, n$ are mutually uncorrelated scalar random variables having Bernoulli distribution taking values of 0 or 1 with the following probabilities:

$$\text{Prob}\{\boldsymbol{\theta}_{i,k} = 1\} = \bar{\boldsymbol{\theta}}_i \qquad \text{Prob}\{\boldsymbol{\theta}_{i,k} = 0\} = 1 - \bar{\boldsymbol{\theta}}_i \tag{4.13}$$

$$\text{Prob}\{\boldsymbol{\lambda}_{i,k} = 1\} = \bar{\boldsymbol{\lambda}}_i \qquad \text{Prob}\{\boldsymbol{\lambda}_{i,k} = 0\} = 1 - \bar{\boldsymbol{\lambda}}_i \tag{4.14}$$

From (4.3) and (4.9), the probability of random delays is:

$$\begin{aligned} \text{Prob}\{\tau_k = i_s\} &= \prod_{i=0}^{s-1} (1 - \bar{\boldsymbol{\theta}}_{i,k}) \bar{\boldsymbol{\theta}}_{s,k} \\ \text{Prob}\{\xi_k = i_c\} &= \prod_{i=0}^{s-1} (1 - \bar{\boldsymbol{\lambda}}_{i,k}) \bar{\boldsymbol{\lambda}}_{s,k} \end{aligned} \tag{4.15}$$

Remark 6. *It is important to notice that the size of the buffer D can impact the localization performance and computational load. Different buffer lengths can result in a different number of discarded packets and different delays.*

II.4 Event-Triggered Data Transferring Mechanism

In order to reduce the transmission rate of sensors and therefore extend battery life, the exteroceptive sensors (overhead camera) are equipped with an event-based scheduler that decides when range-bearing measurement transmission should take place. The event-detector works as follow: let $\boldsymbol{z}_k^{ij}$ denote the current sensor measurement and $\bar{\boldsymbol{z}}_k^{ij}$ the last measurement transmitted through a communication network. The triggering rule works as follows. Define now the binary decision variable $\boldsymbol{\gamma}_k^{ij}$:

$$\boldsymbol{\gamma}_k^{ij} = \begin{cases} \mathbf{1}, & \textbf{if} \quad \left\| \boldsymbol{e}_k^{ij} \right\| \geq \alpha_{ij} \left\| \boldsymbol{z}_k^{ij} \right\| + \beta_{ij} \\ \mathbf{0}, & \textbf{otherwise}. \end{cases} \tag{4.16}$$

where $\boldsymbol{e}_k^{ij} = \boldsymbol{z}_k^{ij} - \bar{\boldsymbol{z}}_{k-1}^{ij}$ is the error between transmitted measurement and the current measurement and α_{ij}, $\beta_{ij} > 0$ are the event-triggering parameters to be designed. Smaller event-triggering parameters α_{ij}, β_{ij}, result in more frequent triggering events. When the parameters α_{ij}, β_{ij} approach zero, the event-triggered system performs as a time-triggered system where transmission of information occurs at every sampling instant. This triggering condition is a discrete-time version of the so-called mixed-type triggering condition introduced in [91].

III Design of the CL with random delays (non-time-stamped mechanism)

III.1 Design of DECL without time stamps

In this section, we design the DECL algorithm via an extended Kalman filter (EKF) with the event-triggered mechanism (4.16) and random delays (Eqs. (4.4), (4.10), (4.11)). We assume that packets are transmitted without time-stamped technology, therefore the local filter does not have knowledge of delays except their probability at each time. First, we compute the covariances of the prediction and estimation errors. Second, we derive the upper bound for the estimation error covariance. Finally, we obtain the Kalman filter gain that minimizes the upper bound of the estimation error covariance. Our proof makes use of the following lemma and assumptions:

Lemma III.1. *For any two vectors a, $b \in \mathbb{R}^n$, one has [113]:*

$$ab^T + ba^T \leq \varepsilon aa^T + \varepsilon^{-1} bb^T. \tag{4.17}$$

where ε is positive constant.

Assumption 4. *The motion and measurement models for all robots in the group are identical.*

Assumption 5. *All robots in the team move in the sensing and communication range of each other.*

Theorem III.2. *Consider the nonlinear system (4.1) and (4.2) along with the event-triggered mechanism (4.16). Assume that the relative measurement $(\bar{\boldsymbol{z}}_k^{ij}, \bar{\boldsymbol{z}}_k^{ji})$ and the predicted belief $\boldsymbol{bel}_k^{i-} = (\hat{\bar{\boldsymbol{x}}}_k^{i-}, \bar{\boldsymbol{P}}_k^{i-})$, $\boldsymbol{bel}_k^{j-} = (\hat{\bar{\boldsymbol{x}}}_k^{j-}, \bar{\boldsymbol{P}}_k^{j-})$ are transmitted through non-time-stamped mechanism with random delays (4.4), (4.10) and (4.11) through the communication channels. For the DECL via the EKF, the upper bound of esti-*

mation error covariance $\bar{\boldsymbol{P}}_k^{i+}$ *can be obtained as follows:*

$$\begin{aligned}
\bar{\boldsymbol{\Sigma}}_k^{i+} &= \mathcal{C}_1\Big(\boldsymbol{I} - \boldsymbol{K}_k^i \boldsymbol{E}_d \bar{\mathcal{H}}_{i,k}^i\Big)\bar{\boldsymbol{P}}_k^{i-}\Big(\boldsymbol{I} - \boldsymbol{K}_k^i \boldsymbol{E}_d \bar{\mathcal{H}}_{i,k}^i\Big)^T \\
&- \sum_{i_c \in \mathcal{M}} \boldsymbol{p}_{i_c}\Big(\boldsymbol{I} - \boldsymbol{K}_k^i \boldsymbol{E}_d \bar{\mathcal{H}}_{i,k}^i\Big)\bar{\boldsymbol{P}}_k^{ij-}\Big(\boldsymbol{K}_k^i \boldsymbol{E}_d \boldsymbol{E}_{i_c} \bar{\mathcal{H}}_{j,k}^i\Big)^T \\
&- \sum_{i_c \in \mathcal{M}} \boldsymbol{p}_{i_c}\Big(\boldsymbol{K}_k^i \boldsymbol{E}_d \boldsymbol{E}_{i_c} \bar{\mathcal{H}}_{j,k}^i\Big)\bar{\boldsymbol{P}}_k^{ij-}\Big(\boldsymbol{I} - \boldsymbol{K}_k^i \boldsymbol{E}_d \bar{\mathcal{H}}_{i,k}^i\Big)^T \\
&+ \sum_{i_c \in \mathcal{M}} \boldsymbol{p}_{i_c}\mathcal{C}_2\Big(\boldsymbol{K}_k^i \boldsymbol{E}_d \boldsymbol{E}_{i_c} \bar{\mathcal{H}}_{j,k}^i\Big)\bar{\boldsymbol{P}}_k^{j-}\Big(\boldsymbol{K}_k^i \boldsymbol{E}_d \boldsymbol{E}_{i_c} \bar{\mathcal{H}}_{j,k}^i\Big)^T \\
&+ \sum_{i_s \in \mathcal{N}} \boldsymbol{p}_{i_s}\mathcal{C}_3\Big(\boldsymbol{K}_k^i(\boldsymbol{E}_{i_s} - \boldsymbol{E}_d)\Big)\boldsymbol{\Psi}_k^{ij}\Big(\boldsymbol{K}_k^i(\boldsymbol{E}_{i_s} - \boldsymbol{E}_d)\Big)^T \\
&+ \sum_{i_s \in \mathcal{N}} \boldsymbol{p}_{i_s}\mathcal{C}_4\Big(\boldsymbol{K}_k^i \boldsymbol{E}_{i_s}\Big)\boldsymbol{R}_k^{ij}\Big(\boldsymbol{K}_k^i \boldsymbol{E}_{i_s}\Big)^T \\
&+ \sum_{i_s \in \mathcal{M}} \boldsymbol{p}_{i_c}\mathcal{C}_6\Big(\boldsymbol{I} - \boldsymbol{E}_{i_c}\Big)\boldsymbol{\Pi}_k^j\Big(\boldsymbol{I} - \boldsymbol{E}_{i_c}\Big)^T \\
&+ \sum_{i_s \in \mathcal{N}} \boldsymbol{p}_{i_s}\mathcal{C}_5\Big(\boldsymbol{K}_k^i \boldsymbol{E}_{i_s}(\boldsymbol{I} - \boldsymbol{\gamma}_k^{ij})\Big)\boldsymbol{\delta}_k^{ij}\Big(\boldsymbol{K}_k^i \boldsymbol{E}_{i_s}(\boldsymbol{I} - \boldsymbol{\gamma}_k^{ij})\Big)^T,
\end{aligned} \tag{4.18}$$

where

$$\begin{aligned}
&\mathcal{C}_1 = (1 - \varepsilon_1 - \varepsilon_2 + \varepsilon_3), \quad \mathcal{C}_2 = (1 - \varepsilon_7), \quad \mathcal{C}_3 = (1 + \varepsilon_1^{-1} - \varepsilon_5^{-1}) \\
&\mathcal{C}_4 = (1 + \varepsilon_2^{-1} + \varepsilon_6^{-1}), \quad \mathcal{C}_5 = (1 + \varepsilon_3^{-1} - \varepsilon_5 - \varepsilon_6), \quad \mathcal{C}_6 = (1 - \varepsilon_7^{-1}) \\
&\mathbb{E}\Big[\boldsymbol{e}_k^{ij}(\boldsymbol{e}_k^{ij})^T\Big] = \boldsymbol{\delta}_k^{ij}, \quad \mathbb{E}\Big[\bar{\boldsymbol{x}}_k^j(\bar{\boldsymbol{x}}_k^j)^T\Big] = \boldsymbol{\Pi}_k^j, \quad \mathbb{E}\Big[\bar{\boldsymbol{h}}_{ij}(.)(\bar{\boldsymbol{h}}_{ij}(.))^T\Big] = \boldsymbol{\Psi}_k^{ij} \\
&\bar{\mathcal{A}}_k^i = \bar{\boldsymbol{A}}_k^i + \bar{\boldsymbol{B}}_k^i \bar{\boldsymbol{F}}_k^i \bar{\boldsymbol{M}}_k^i, \quad \bar{\mathcal{H}}_{i,k}^i = \bar{\boldsymbol{H}}_{i,k}^i + \bar{\boldsymbol{D}}_{i,k}^i \bar{\boldsymbol{C}}_{i,k}^i \boldsymbol{M}_{i,k}^i, \\
&\bar{\mathcal{H}}_{j,k}^i = \bar{\boldsymbol{H}}_{j,k}^i + \bar{\boldsymbol{D}}_{j,k}^i \bar{\boldsymbol{C}}_{j,k}^i \bar{\boldsymbol{M}}_{j,k}^i, \quad \bar{\boldsymbol{P}}_{k+1}^{i-} = \bar{\mathcal{A}}_k^i \bar{\boldsymbol{P}}_k^{i+}(\bar{\mathcal{A}}_k^i)^T + \bar{\boldsymbol{G}}_k^i \bar{\boldsymbol{Q}}_k^i(\bar{\boldsymbol{G}}_k^i)^T \\
&\bar{\boldsymbol{P}}_{k+1}^{ij-} = \bar{\mathcal{A}}_k^i \bar{\boldsymbol{P}}_k^{ij+}(\bar{\mathcal{A}}_k^j)^T.
\end{aligned}$$

Proof. The propagated state error of robot i for multi-robot dynamics system (4.1) at time instant $k+1$ can be defined by:

$$\tilde{\hat{\boldsymbol{x}}}_{k+1}^{i-} = \bar{\boldsymbol{x}}_{k+1}^i - \hat{\bar{\boldsymbol{x}}}_{k+1}^{i-} \tag{4.19}$$

where the propagated state of each robot $\hat{\bar{\boldsymbol{x}}}_{k+1}^{i-}$ is described by:

$$\hat{\bar{\boldsymbol{x}}}_{k+1}^{i-} = \boldsymbol{f}^i\Big(\hat{\bar{\boldsymbol{x}}}_k^{i+}, \bar{\boldsymbol{u}}_k^i\Big) \tag{4.20}$$

Expanding $\bar{\boldsymbol{f}}^i(\bar{\boldsymbol{x}}_k^i, \bar{\boldsymbol{u}}_k^i)$ using Taylor series around $\hat{\bar{\boldsymbol{x}}}_k^{i+}$, we have:

$$\bar{\boldsymbol{f}}^i\Big(\bar{\boldsymbol{x}}_k^i, \bar{\boldsymbol{u}}_k^i\Big) \approx \bar{\boldsymbol{f}}^i\Big(\hat{\bar{\boldsymbol{x}}}_k^{i+}, \bar{\boldsymbol{u}}_k^i\Big) + \bar{\boldsymbol{A}}_k^i\Big(\bar{\boldsymbol{x}}_k^i - \hat{\bar{\boldsymbol{x}}}_k^{i+}\Big) + o\Big(|\tilde{\bar{\boldsymbol{x}}}_k^{i+}|\Big) \tag{4.21}$$

where $\bar{\boldsymbol{A}}^i = \frac{\partial \bar{\boldsymbol{f}}^i(\hat{\bar{\boldsymbol{x}}}^{i+}, \bar{\boldsymbol{u}}^i)}{\partial \boldsymbol{x}^i}$ and $o\Big(|\tilde{\bar{\boldsymbol{x}}}_k^{i+}|\Big)$ represent the high-order terms of the Taylor series expansion. We introduce the unknown time-varying matrix $\bar{\boldsymbol{F}}_k^i$, and known scaling matrix $\bar{\boldsymbol{B}}_k^i$ to compensate the linearization error. We can write:

$$o\Big(|\tilde{\bar{\boldsymbol{x}}}_k^{i+}|\Big) = \bar{\boldsymbol{B}}_k^i \bar{\boldsymbol{F}}_k^i \bar{\boldsymbol{M}}_k^i \tilde{\bar{\boldsymbol{x}}}_k^{i+} \tag{4.22}$$

where $\bar{\boldsymbol{M}}_k^i$ is a known tuning matrix and assume that $\bar{\boldsymbol{F}}_k^i$ satisfies:

$$\bar{\boldsymbol{F}}_k^i(\bar{\boldsymbol{F}}_k^i)^T \leq \boldsymbol{I} \tag{4.23}$$

Defining $\bar{\mathcal{A}}_k^i = \left(\bar{\boldsymbol{A}}_k^i + \bar{\boldsymbol{B}}_k^i \bar{\boldsymbol{F}}_k^i \bar{\boldsymbol{M}}_k^i\right)$ and using (4.19)-(4.23), the propagated state error for robots i and j can be written as follows:

$$\tilde{\bar{\boldsymbol{x}}}_{k+1}^{i-} = \bar{\mathcal{A}}_k^i \tilde{\bar{\boldsymbol{x}}}_k^{i-} + \bar{\boldsymbol{G}}_k^i \bar{\boldsymbol{\eta}}_k^i \tag{4.24}$$

$$\tilde{\bar{\boldsymbol{x}}}_{k+1}^{j-} = \bar{\mathcal{A}}_k^j \tilde{\bar{\boldsymbol{x}}}_k^{j-} + \bar{\boldsymbol{G}}_k^j \bar{\boldsymbol{\eta}}_k^j \tag{4.25}$$

where $\bar{\boldsymbol{G}}^i = \frac{\partial \bar{\boldsymbol{f}}^i(\hat{\bar{\boldsymbol{x}}}^{i+}, \bar{\boldsymbol{u}}^i)}{\partial \bar{\boldsymbol{\eta}}^i}$, $\bar{\boldsymbol{G}}^j = \frac{\partial \bar{\boldsymbol{f}}^j(\hat{\bar{\boldsymbol{x}}}^{j+}, \bar{\boldsymbol{u}}^j)}{\partial \bar{\boldsymbol{\eta}}^j}$ and $\bar{\boldsymbol{A}}^j = \frac{\partial \bar{\boldsymbol{f}}^j(\hat{\bar{\boldsymbol{x}}}^{j+}, \bar{\boldsymbol{u}}^j)}{\partial \bar{\boldsymbol{x}}^j}$. Using Eqs. (4.24)-(4.25), the propagated state error covariance for robot i and cross-covariance between two robots (i and j) can be written by:

$$\bar{\boldsymbol{P}}_{k+1}^{i-} = \mathbb{E}\left[\left(\tilde{\bar{\boldsymbol{x}}}_{k+1}^{i-}\right)\left(\tilde{\bar{\boldsymbol{x}}}_{k+1}^{i-}\right)^T\right] = \bar{\mathcal{A}}_k^i \bar{\boldsymbol{P}}_k^{i+} (\bar{\mathcal{A}}_k^i)^T + \bar{\boldsymbol{G}}_k^i \bar{\boldsymbol{Q}}_k^i (\bar{\boldsymbol{G}}_k^i)^T \tag{4.26}$$

$$\bar{\boldsymbol{P}}_{k+1}^{ij-} = \mathbb{E}\left[\left(\tilde{\bar{\boldsymbol{x}}}_{k+1}^{i-}\right)\left(\tilde{\bar{\boldsymbol{x}}}_{k+1}^{j-}\right)^T\right] = \bar{\mathcal{A}}_k^i \bar{\boldsymbol{P}}_k^{ij+} (\bar{\mathcal{A}}_k^j)^T \tag{4.27}$$

The state estimates of each robot i for the augmented system (4.5) are defined as follows:

$$\hat{\bar{\boldsymbol{x}}}_{k+1}^{i+} = \hat{\bar{\boldsymbol{x}}}_{k+1}^{i-} + \boldsymbol{K}_{k+1}^i \left[\tilde{\boldsymbol{z}}_{k+1}^{ij} - \boldsymbol{E}_d \hat{\boldsymbol{z}}^{ij}(\hat{\bar{\boldsymbol{x}}}_{k+1}^{i-}, \hat{\bar{\boldsymbol{x}}}_{k+1}^{j-})\right] \tag{4.28}$$

where $\hat{\boldsymbol{z}}^{ij} = \bar{\boldsymbol{h}}_{ij}(\hat{\bar{\boldsymbol{x}}}^{i-}, \hat{\bar{\boldsymbol{x}}}^{j-})$ is the estimated measurement. Let the first-order expansion of $\bar{\boldsymbol{h}}_{ij}(\bar{\boldsymbol{x}}^i, \bar{\boldsymbol{x}}^j)$ around $(\hat{\bar{\boldsymbol{x}}}^{i-}, \hat{\bar{\boldsymbol{x}}}^{j-})$ be

$$\begin{aligned}\bar{\boldsymbol{h}}_{ij}(\bar{\boldsymbol{x}}^i, \bar{\boldsymbol{x}}^j) \approx \bar{\boldsymbol{h}}_{ij}(\hat{\bar{\boldsymbol{x}}}^{i-}, \hat{\bar{\boldsymbol{x}}}^{j-}) + \bar{\boldsymbol{H}}_i^i(\bar{\boldsymbol{x}}^i - \hat{\bar{\boldsymbol{x}}}^{i-}) + \bar{\boldsymbol{H}}_j^i(\bar{\boldsymbol{x}}^j - \hat{\bar{\boldsymbol{x}}}^{j-}) \\ + o\left(|\tilde{\bar{\boldsymbol{x}}}^{i-}|, |\tilde{\bar{\boldsymbol{x}}}^{j-}|\right)\end{aligned} \tag{4.29}$$

where $\bar{\boldsymbol{H}}_i^i = \frac{\partial \bar{\boldsymbol{h}}_{ij}(\hat{\bar{\boldsymbol{x}}}^{i-}, \hat{\bar{\boldsymbol{x}}}^{j-})}{\partial \bar{\boldsymbol{x}}^i}$, $\bar{\boldsymbol{H}}_j^i = \frac{\partial \bar{\boldsymbol{h}}_{ij}(\hat{\bar{\boldsymbol{x}}}^{i-}, \hat{\bar{\boldsymbol{x}}}^{j-})}{\partial \bar{\bar{\boldsymbol{x}}}^j}$ and $o\left(|\tilde{\bar{\boldsymbol{x}}}^{i-}|, |\tilde{\bar{\boldsymbol{x}}}^{j-}|\right)$ denote the high-order terms of the Taylor series expansion. We now introduce unknown time-varying matrices $\bar{\boldsymbol{C}}_{i,k}^i$ and $\bar{\boldsymbol{C}}_{j,k}^i$, and known scaling matrices $\bar{\boldsymbol{D}}_{i,k}^i$, $\bar{\boldsymbol{D}}_{j,k}^i$ accounting for the linearization errors of the measurement model:

$$o\left(|\tilde{\bar{\boldsymbol{x}}}_k^{i-}|, |\tilde{\bar{\boldsymbol{x}}}_k^{j-}|\right) = \bar{\boldsymbol{D}}_{i,k}^i \bar{\boldsymbol{C}}_{i,k}^i \bar{\boldsymbol{M}}_{i,k}^i \tilde{\bar{\boldsymbol{x}}}_k^{i-} + \bar{\boldsymbol{D}}_{j,k}^i \bar{\boldsymbol{C}}_{j,k}^i \bar{\boldsymbol{M}}_{j,k}^i \tilde{\bar{\boldsymbol{x}}}_k^{j-} \tag{4.30}$$

where $\bar{\boldsymbol{E}}_{i,k}^i$ and $\bar{\boldsymbol{E}}_{j,k}^i$ are known tuning matrices and assume that $\bar{\boldsymbol{C}}_{i,k}^i$ and $\bar{\boldsymbol{C}}_{j,k}^i$ satisfy:

$$\bar{\boldsymbol{C}}_{i,k}^i (\bar{\boldsymbol{C}}_{i,k}^i)^T \leq \boldsymbol{I} \tag{4.31}$$

$$\bar{\boldsymbol{C}}_{j,k}^i (\bar{\boldsymbol{C}}_{j,k}^i)^T \leq \boldsymbol{I} \tag{4.32}$$

Note that the matrices $\bar{\boldsymbol{D}}_{i,k}^i$, $\bar{\boldsymbol{D}}_{j,k}^i$, $\bar{\boldsymbol{M}}_{i,k}^i$, $\bar{\boldsymbol{M}}_{j,k}^i$, $\bar{\boldsymbol{B}}_k^i$ and $\bar{\boldsymbol{E}}_k^i$ should be designed appropriately. Considering the event-triggered mechanism (4.16) and random transmission delays which occurs in the channel from the sensor to the filter, the state

estimate for robot i is rewritten as follows:

$$\begin{array}{l}\hat{\boldsymbol{x}}^{i+}_{k+1} = \hat{\boldsymbol{x}}^{i-}_{k+1} + \boldsymbol{K}^{i}_{k+1}\Big[\boldsymbol{E}_{\tau_k}\bar{\boldsymbol{h}}_{ij}(\bar{\boldsymbol{x}}^{i}_{k+1}, \bar{\boldsymbol{x}}^{j}_{k+1}) + \boldsymbol{E}_{\tau_k}\bar{\boldsymbol{\nu}}^{ij}_{k+1} \\ -\boldsymbol{E}_{\tau_k}(\boldsymbol{I} - \boldsymbol{\gamma}^{ij}_{k+1})\boldsymbol{e}^{ij}_{k+1} - \boldsymbol{E}_{d}\hat{\boldsymbol{z}}^{ij}(\hat{\boldsymbol{x}}^{i-}_{k+1}, \hat{\boldsymbol{x}}^{j-}_{k+1})\Big]\end{array} \tag{4.33}$$

Using (4.29)-(4.33) and introducing $\bar{\mathcal{H}}^{i}_{i,k} = \bar{\boldsymbol{H}}^{i}_{i,k} + \bar{\boldsymbol{D}}^{i}_{i,k}\bar{\boldsymbol{C}}^{i}_{i,k}\boldsymbol{M}^{i}_{i,k}$, $\bar{\mathcal{H}}^{i}_{j,k} = \bar{\boldsymbol{H}}^{i}_{j,k} + \bar{\boldsymbol{D}}^{i}_{j,k}\bar{\boldsymbol{C}}^{i}_{j,k}\bar{\boldsymbol{M}}^{i}_{j,k}$, the estimation error for robot i can be written as follows:

$$\begin{array}{l}\tilde{\boldsymbol{\tilde{x}}}^{i+}_{k+1} = \Big(\boldsymbol{I} - \boldsymbol{K}^{i}_{k+1}\boldsymbol{E}_{d}\bar{\mathcal{H}}^{i}_{i,k+1}\Big)\tilde{\boldsymbol{\tilde{x}}}^{i-}_{k+1} - \boldsymbol{K}^{i}_{k+1}\boldsymbol{E}_{d}\boldsymbol{E}_{\xi_k}\bar{\mathcal{H}}^{i}_{j,k+1}\tilde{\boldsymbol{\tilde{x}}}^{j-}_{k+1} \\ -(\boldsymbol{I} - \boldsymbol{E}_{\xi_k})\bar{\boldsymbol{x}}^{j}_{k+1} - \boldsymbol{K}^{i}_{k+1}\boldsymbol{E}_{\tau_k}\bar{\boldsymbol{\nu}}^{ij}_{k+1} + \boldsymbol{K}^{i}_{k+1}\boldsymbol{E}_{\tau_k}(\boldsymbol{I} - \boldsymbol{\gamma}^{ij}_{k+1})\boldsymbol{e}^{ij}_{k+1} \\ -\boldsymbol{K}^{i}_{k+1}(\boldsymbol{E}_{\tau_k} - \boldsymbol{E}_{d})\bar{\boldsymbol{h}}_{ij}(\bar{\boldsymbol{x}}^{i}_{k+1}, \bar{\boldsymbol{x}}^{j}_{k+1})\end{array} \tag{4.34}$$

Using (4.34), the estimation error covariance matrix for robot i is written as follows:

$$\begin{array}{l}\bar{\boldsymbol{P}}^{i+}_{k+1} = \mathbb{E}\Big[\Big(\tilde{\boldsymbol{\tilde{x}}}^{i+}_{k+1}\Big)\Big(\tilde{\boldsymbol{\tilde{x}}}^{i+}_{k+1}\Big)^{T}\Big] = \\ \Big(\boldsymbol{I} - \boldsymbol{K}^{i}_{k+1}\boldsymbol{E}_{d}\bar{\mathcal{H}}^{i}_{i,k+1}\Big)\mathbb{E}\Big[\tilde{\boldsymbol{\tilde{x}}}^{i-}_{k+1}(\tilde{\boldsymbol{\tilde{x}}}^{i-}_{k+1})^{T}\Big]\Big(\boldsymbol{I} - \boldsymbol{K}^{i}_{k+1}\boldsymbol{E}_{d}\bar{\mathcal{H}}^{i}_{i,k+1}\Big)^{T} \\ -\sum_{i_c\in\mathcal{M}}\boldsymbol{p}_{i_c}\Big(\boldsymbol{I} - \boldsymbol{K}^{i}_{k+1}\boldsymbol{E}_{d}\bar{\mathcal{H}}^{i}_{i,k+1}\Big)\mathbb{E}\Big[\tilde{\boldsymbol{\tilde{x}}}^{i-}_{k+1}(\tilde{\boldsymbol{\tilde{x}}}^{j-}_{k+1})^{T}\Big]\Big(\boldsymbol{K}^{i}_{k+1}\boldsymbol{E}_{d}\boldsymbol{E}_{i_c}\bar{\mathcal{H}}^{i}_{j,k+1}\Big)^{T} \\ -\sum_{i_c\in\mathcal{M}}\boldsymbol{p}_{i_c}\Big(\boldsymbol{K}^{i}_{k+1}\boldsymbol{E}_{d}\boldsymbol{E}_{i_c}\bar{\mathcal{H}}^{i}_{j,k+1}\Big)\mathbb{E}\Big[\tilde{\boldsymbol{\tilde{x}}}^{j-}_{k+1}(\tilde{\boldsymbol{\tilde{x}}}^{i-}_{k+1})^{T}\Big]\Big(\boldsymbol{I} - \boldsymbol{K}^{i}_{k+1}\boldsymbol{E}_{d}\bar{\mathcal{H}}^{i}_{i,k+1}\Big)^{T} \\ -\sum_{i_s\in\mathcal{N}}\boldsymbol{p}_{i_s}\Big(\boldsymbol{I} - \boldsymbol{K}^{i}_{k+1}\boldsymbol{E}_{d}\bar{\mathcal{H}}^{i}_{i,k+1}\Big)\mathbb{E}\Big[\tilde{\boldsymbol{\tilde{x}}}^{i-}_{k+1}(\bar{\boldsymbol{\nu}}^{ij}_{k+1})^{T}\Big]\Big(\boldsymbol{K}^{i}_{k+1}\boldsymbol{E}_{i_s}\Big)^{T} \\ -\sum_{i_s\in\mathcal{N}}\boldsymbol{p}_{i_s}\Big(\boldsymbol{K}^{i}_{k+1}\boldsymbol{E}_{i_s}\Big)\mathbb{E}\Big[\bar{\boldsymbol{\nu}}^{ij}_{k+1}(\tilde{\boldsymbol{\tilde{x}}}^{i-}_{k+1})^{T}\Big]\Big(\boldsymbol{I} - \boldsymbol{K}^{i}_{k+1}\boldsymbol{E}_{d}\bar{\mathcal{H}}^{i}_{i,k+1}\Big)^{T} \\ +\sum_{i_s\in\mathcal{N}}\boldsymbol{p}_{i_s}\Big(\boldsymbol{I} - \boldsymbol{K}^{i}_{k+1}\boldsymbol{E}_{d}\bar{\mathcal{H}}^{i}_{i,k+1}\Big)\mathbb{E}\Big[\tilde{\boldsymbol{\tilde{x}}}^{i-}_{k+1}(\boldsymbol{e}^{ij}_{k+1})^{T}\Big]\Big(\boldsymbol{K}^{i}_{k+1}\boldsymbol{E}_{i_s}(\boldsymbol{I} - \boldsymbol{\gamma}^{ij}_{k+1})\Big)^{T} \\ +\sum_{i_s\in\mathcal{N}}\boldsymbol{p}_{i_s}\Big(\boldsymbol{K}^{i}_{k+1}\boldsymbol{E}_{i_s}(\boldsymbol{I} - \boldsymbol{\gamma}^{ij}_{k+1})\Big)\mathbb{E}\Big[\boldsymbol{e}^{ij}_{k+1}(\tilde{\boldsymbol{\tilde{x}}}^{i-}_{k+1})^{T}\Big]\Big(\boldsymbol{I} - \boldsymbol{K}^{i}_{k+1}\boldsymbol{E}_{d}\bar{\mathcal{H}}^{i}_{i,k+1}\Big)^{T} \\ -\sum_{i_s\in\mathcal{N}}\boldsymbol{p}_{i_s}\Big(\boldsymbol{I} - \boldsymbol{K}^{i}_{k+1}\boldsymbol{E}_{d}\bar{\mathcal{H}}^{i}_{i,k+1}\Big)\mathbb{E}\Big[\tilde{\boldsymbol{\tilde{x}}}^{i-}_{k+1}(\bar{\boldsymbol{h}}_{ij}(.,.))^{T}\Big]\Big(\boldsymbol{K}^{i}_{k+1}(\boldsymbol{E}_{i_s} - \boldsymbol{E}_{d})\Big)^{T} \\ -\sum_{i_s\in\mathcal{N}}\boldsymbol{p}_{i_s}\Big(\boldsymbol{K}^{i}_{k+1}(\boldsymbol{E}_{i_s} - \boldsymbol{E}_{d})\Big)\mathbb{E}\Big[\bar{\boldsymbol{h}}_{ij}(.,.)(\tilde{\boldsymbol{\tilde{x}}}^{i-}_{k+1})^{T}\Big]\Big(\boldsymbol{I} - \boldsymbol{K}^{i}_{k+1}\boldsymbol{E}_{d}\bar{\mathcal{H}}^{i}_{i,k+1}\Big)^{T} \\ -\sum_{i_s\in\mathcal{N}}\boldsymbol{p}_{i_s}\Big(\boldsymbol{K}^{i}_{k+1}\boldsymbol{E}_{i_s}(\boldsymbol{I} - \boldsymbol{\gamma}^{ij}_{k+1})\Big)\mathbb{E}\Big[\boldsymbol{e}^{ij}_{k+1}(\bar{\boldsymbol{\nu}}^{ij}_{k+1})^{T}\Big]\Big(\boldsymbol{K}^{i}_{k+1}\boldsymbol{E}_{i_s}\Big)^{T} \\ -\sum_{i_s\in\mathcal{N}}\boldsymbol{p}_{i_s}\Big(\boldsymbol{K}^{i}_{k+1}\boldsymbol{E}_{i_s}\Big)\mathbb{E}\Big[\bar{\boldsymbol{\nu}}^{ij}_{k+1}(\boldsymbol{e}^{ij}_{k+1})^{T}\Big]\Big(\boldsymbol{K}^{i}_{k+1}\boldsymbol{E}_{i_s}(\boldsymbol{I} - \boldsymbol{\gamma}^{ij}_{k+1})\Big)^{T} + \cdots\end{array} \tag{4.35}$$

We now look for an upper bound for the error covariance matrix. Defining positive scalars ε_1, ε_2, ε_3, ε_5, ε_6, $\varepsilon_7 > 0$ and applying Lemma III.1 we write for some terms:

$$\begin{array}{l}\sum_{i_s\in\mathcal{N}}\boldsymbol{p}_{i_s}\Big(\boldsymbol{I} - \boldsymbol{K}^{i}_{k+1}\boldsymbol{E}_{d}\bar{\mathcal{H}}^{i}_{i,k+1}\Big)\mathbb{E}\Big[\tilde{\boldsymbol{\tilde{x}}}^{i-}_{k+1}(\bar{\boldsymbol{\nu}}^{ij}_{k+1})^{T}\Big]\Big(\boldsymbol{K}^{i}_{k+1}\boldsymbol{E}_{i_s}\Big)^{T} \\ +\sum_{i_s\in\mathcal{N}}\boldsymbol{p}_{i_s}\Big(\boldsymbol{K}^{i}_{k+1}\boldsymbol{E}_{i_s}\Big)\mathbb{E}\Big[\bar{\boldsymbol{\nu}}^{ij}_{k+1}(\tilde{\boldsymbol{\tilde{x}}}^{i-}_{k+1})^{T}\Big]\Big(\boldsymbol{I} - \boldsymbol{K}^{i}_{k+1}\boldsymbol{E}_{d}\bar{\mathcal{H}}^{i}_{i,k+1}\Big)^{T} \leq \\ \varepsilon_2\Big(\boldsymbol{I} - \boldsymbol{K}^{i}_{k+1}\boldsymbol{E}_{d}\bar{\mathcal{H}}^{i}_{i,k+1}\Big)\bar{\boldsymbol{P}}^{i-}_{k+1}\Big(\boldsymbol{I} - \boldsymbol{K}^{i}_{k+1}\boldsymbol{E}_{d}\bar{\mathcal{H}}^{i}_{i,k+1}\Big)^{T} \\ +\varepsilon_2^{-1}\sum_{i_s\in\mathcal{N}}\boldsymbol{p}_{i_s}\Big(\boldsymbol{K}^{i}_{k+1}\boldsymbol{E}_{i_s}\Big)\bar{\boldsymbol{R}}^{ij}_{k+1}\Big(\boldsymbol{K}^{i}_{k+1}\boldsymbol{E}_{i_s}\Big)^{T}\end{array} \tag{4.36}$$

$$
\begin{aligned}
&\sum_{i_s\in\mathcal{N}}\boldsymbol{p}_{i_s}\Big(\boldsymbol{I}-\boldsymbol{K}^i_{k+1}\boldsymbol{E}_d\bar{\mathcal{H}}^i_{i,k+1}\Big)\mathbb{E}\Big[\tilde{\bar{\boldsymbol{x}}}^{i-}_{k+1}(\boldsymbol{e}^{ij}_{k+1})^T\Big]\Big(\boldsymbol{K}^i_{k+1}\boldsymbol{E}_{i_s}(\boldsymbol{I}-\boldsymbol{\gamma}^{ij}_{k+1})\Big)^T\\
&+\sum_{i_s\in\mathcal{N}}\boldsymbol{p}_{i_s}\Big(\boldsymbol{K}^i_{k+1}\boldsymbol{E}_{i_s}(\boldsymbol{I}-\boldsymbol{\gamma}^{ij}_{k+1})\Big)\mathbb{E}\Big[\boldsymbol{e}^{ij}_{k+1}(\tilde{\bar{\boldsymbol{x}}}^{i-}_{k+1})^T\Big]\Big(\boldsymbol{I}-\boldsymbol{K}^i_{k+1}\boldsymbol{E}_d\bar{\mathcal{H}}^i_{i,k+1}\Big)^T\\
&\leq\varepsilon_3\Big(\boldsymbol{I}-\boldsymbol{K}^i_{k+1}\boldsymbol{E}_d\bar{\mathcal{H}}^i_{i,k+1}\Big)\bar{\boldsymbol{P}}^{i-}_{k+1}\Big(\boldsymbol{I}-\boldsymbol{K}^i_{k+1}\boldsymbol{E}_d\bar{\mathcal{H}}^i_{i,k+1}\Big)^T\\
&+\varepsilon_3^{-1}\sum_{i_s\in\mathcal{N}}\boldsymbol{p}_{i_s}\Big(\boldsymbol{K}^i_{k+1}\boldsymbol{E}_{i_s}(\boldsymbol{I}-\boldsymbol{\gamma}^{ij}_{k+1})\Big)\boldsymbol{\delta}^{ij}_{k+1}\Big(\boldsymbol{K}^i_{k+1}\boldsymbol{E}_{i_s}(\boldsymbol{I}-\boldsymbol{\gamma}^{ij}_{k+1})\Big)^T
\end{aligned}
\tag{4.37}
$$

$$
\begin{aligned}
&\sum_{i_s\in\mathcal{N}}\boldsymbol{p}_{i_s}\Big(\boldsymbol{I}-\boldsymbol{K}^i_{k+1}\boldsymbol{E}_d\bar{\mathcal{H}}^i_{i,k+1}\Big)\mathbb{E}\Big[\tilde{\bar{\boldsymbol{x}}}^{i-}_{k+1}(\bar{\boldsymbol{h}}_{ij}(.,.))^T\Big]\Big(\boldsymbol{K}^i_{k+1}(\boldsymbol{E}_{i_s}-\boldsymbol{E}_d)\Big)^T\\
&+\sum_{i_s\in\mathcal{N}}\boldsymbol{p}_{i_s}\Big(\boldsymbol{K}^i_{k+1}(\boldsymbol{E}_{i_s}-\boldsymbol{E}_d)\Big)\mathbb{E}\Big[\bar{\boldsymbol{h}}_{ij}(.,.)(\tilde{\bar{\boldsymbol{x}}}^{i-}_{k+1})^T\Big]\Big(\boldsymbol{I}-\boldsymbol{K}^i_{k+1}\boldsymbol{E}_d\bar{\mathcal{H}}^i_{i,k+1}\Big)^T\\
&\varepsilon_1\Big(\boldsymbol{I}-\boldsymbol{K}^i_{k+1}\boldsymbol{E}_d\bar{\mathcal{H}}^i_{i,k+1}\Big)\bar{\boldsymbol{P}}^{i-}_{k+1}\Big(\boldsymbol{I}-\boldsymbol{K}^i_{k+1}\boldsymbol{E}_d\bar{\mathcal{H}}^i_{i,k+1}\Big)^T\\
&+\varepsilon_1^{-1}\sum_{i_s\in\mathcal{N}}\boldsymbol{p}_{i_s}\Big(\boldsymbol{K}^i_{k+1}(\boldsymbol{E}_{i_s}-\boldsymbol{E}_d)\Big)\boldsymbol{\Psi}^{ij}_{k+1}\Big(\boldsymbol{K}^i_{k+1}(\boldsymbol{E}_{i_s}-\boldsymbol{E}_d)\Big)^T
\end{aligned}
\tag{4.38}
$$

which leads to Eq. (4.18). Then, the proof is completed □

Remark 7. *It is important to notice that calculating the exact value of the estimation error covariance is impossible because of the terms* $\mathbb{E}[\tilde{\bar{\boldsymbol{x}}}^{i+}_k(\boldsymbol{e}^{ij}_k)^T]$, $\mathbb{E}[\tilde{\bar{\boldsymbol{x}}}^{i+}_k(\boldsymbol{\nu}^{ij}_k)^T]$, $\mathbb{E}[\boldsymbol{e}^{ij}_k(\boldsymbol{\nu}^{ij}_k)^T]$,... *which depend on the random delays, measurement noises and error of the event-triggered mechanism. Therefore, we compute the upper bound of the estimation error covariance (*$\bar{\boldsymbol{\Sigma}}^{i+}_k$*) with respect to random delay parameters (*$\boldsymbol{E}_{i_c}$, $\boldsymbol{E}_d$, $\boldsymbol{E}_{i_s}$*), event-triggering parameter (*$\boldsymbol{\delta}^{ij}_k$*), etc.*

Corollary III.2.1. Under the assumptions of Theorem III.2, the DECL gain is given by:

$$
\boldsymbol{K}^i_k=X(Y)^{-1} \tag{4.39}
$$

Where X and Y can be expressed as a follows:

$$
\begin{aligned}
X&=\mathcal{C}_1\bar{\boldsymbol{P}}^{i-}_k(\mathcal{H}^i_{i,k})^T\boldsymbol{E}_d^T+\sum_{i_c\in\mathcal{M}}\boldsymbol{p}_{i_c}\boldsymbol{E}_{i_c}\bar{\boldsymbol{P}}^{ij-}_k(\bar{\mathcal{H}}^i_{j,k})^T\boldsymbol{E}_{i_c}^T\boldsymbol{E}_d^T\\
Y&=\mathcal{C}_1\boldsymbol{E}_d\mathcal{H}^i_{i,k}\bar{\boldsymbol{P}}^{i-}_k(\bar{\mathcal{H}}^i_{i,k})^T\boldsymbol{E}_d^T+\mathcal{C}_4\sum_{i_s\in\mathcal{N}}\boldsymbol{p}_{i_s}\boldsymbol{E}_{i_s}\bar{\boldsymbol{R}}^{ij}_k\boldsymbol{E}_{i_s}^T\\
&\quad+\sum_{i_c\in\mathcal{M}}\boldsymbol{p}_{i_c}\boldsymbol{E}_d\bar{\mathcal{H}}^i_{i,k}\bar{\boldsymbol{P}}^{ij-}_k(\mathcal{H}^i_{j,k})^T\boldsymbol{E}_{i_c}^T\boldsymbol{E}_d^T\\
&\quad+\sum_{i_c\in\mathcal{M}}\boldsymbol{p}_{i_c}\boldsymbol{E}_d\boldsymbol{E}_{i_c}\bar{\mathcal{H}}^i_{j,k}\bar{\boldsymbol{P}}^{ij-}_k(\bar{\mathcal{H}}^i_{i,k})^T\boldsymbol{E}_d^T\\
&\quad+\mathcal{C}_2\sum_{i_c\in\mathcal{M}}\boldsymbol{p}_{i_c}\boldsymbol{E}_d\boldsymbol{E}_{i_c}\bar{\mathcal{H}}^i_{j,k}\bar{\boldsymbol{P}}^{j-}_k(\bar{\mathcal{H}}^i_{j,k})^T\boldsymbol{E}_{i_c}^T\boldsymbol{E}_d^T\\
&\quad+\mathcal{C}_3\sum_{i_s\in\mathcal{N}}\boldsymbol{p}_{i_s}(\boldsymbol{E}_{i_s}-\boldsymbol{E}_d)\boldsymbol{\Psi}^{ij}_k(\boldsymbol{E}_{i_s}-\boldsymbol{E}_d)^T\\
&\quad+\mathcal{C}_5\sum_{i_s\in\mathcal{N}}\boldsymbol{p}_{i_s}\boldsymbol{E}_{i_s}(I-\boldsymbol{\gamma}^{ij}_k)\boldsymbol{\delta}^{ij}_k(I-\boldsymbol{\gamma}^{ij}_k)^T\boldsymbol{E}_{i_s}^T
\end{aligned}
\tag{4.40}
$$

Remark 8. *Considering the structure of DECL gain in (4.39)-(4.40), the event-triggered mechanism and random delays (sensor-filter and filter-filter) introduce additional terms affecting the upper and the lower bounds of the filtering error and the covariance of filtering error, respectively. The optimal Kalman gain (4.39)-(4.40) can be obtained by minimizing the upper bound of the filtering error covariance with respect to Kalman gain, i.e.,* $\frac{\partial \bar{\boldsymbol{\Sigma}}_k^{i+}}{\partial \boldsymbol{K}_k^i} = 0$. *Also, note that the positive scalars* ε_1, ε_2, *etc, in Theorem III.2 can be tuned to minimize the upper bound of the error covariance and enhance the performance of the filter.*

III.2 Boundedness of estimation error for the DECL without time stamps

In this part, we analyze the stochastic stability of the event-triggered cooperative localization with random delays.

Lemma III.3. 36 *Suppose that there is a stochastic process* $\boldsymbol{V}_k(\boldsymbol{\zeta}_k)$ *as well as real constant numbers* $\underline{\boldsymbol{\kappa}}$, $\bar{\boldsymbol{\kappa}}$, $\boldsymbol{\mu} > 0$ *and* $\mathbf{0} < \boldsymbol{\sigma} \leq \mathbf{1}$ *such that*

$$\underline{\boldsymbol{\kappa}} \left\|\boldsymbol{\zeta}_k\right\|^2 \leq \boldsymbol{V}_k(\boldsymbol{\zeta}_k) \leq \bar{\boldsymbol{\kappa}} \left\|\boldsymbol{\zeta}_k\right\|^2 \tag{4.41}$$

$$\mathbb{E}\{\boldsymbol{V}_k(\boldsymbol{\zeta}_k)|\boldsymbol{\zeta}_{k-1}\} - \boldsymbol{V}_{k-1}(\boldsymbol{\zeta}_{k-1}) \leq \boldsymbol{\mu} - \boldsymbol{\sigma}\boldsymbol{V}_{k-1}(\boldsymbol{\zeta}_{k-1}) \tag{4.42}$$

are satisfied. Then the stochastic process is exponentially bounded in mean square, i.e., we have

$$\mathbb{E}\left\{\left\|\boldsymbol{\zeta}_k\right\|^2\right\} \leq \frac{\bar{\boldsymbol{\kappa}}}{\underline{\boldsymbol{\kappa}}}\mathbb{E}\left\{\left\|\boldsymbol{\zeta}_0\right\|^2\right\}(\mathbf{1}-\boldsymbol{\sigma})^k + \frac{\boldsymbol{\mu}}{\underline{\boldsymbol{\kappa}}}\sum_{i=1}^{k-1}(\mathbf{1}-\boldsymbol{\sigma})^i \tag{4.43}$$

and the stochastic process is bounded with probability one.

Assumption 6. *There exist real constants* $\underline{a}_i$, $\bar{a}_i$, $\underline{h}_i$, $\bar{h}_i$, $\underline{h}_{ij}$, $\bar{h}_{ij}$, $\underline{q}_i$, $\bar{q}_i$, $\underline{R}_{ij}$, $\bar{R}_{ij}$, $\underline{p}_{i_c}$, $\bar{p}_{i_c}$, $\underline{E}_d$, $\bar{E}_d$, $\underline{E}_{i_c}$, $\bar{E}_{i_c}$, $\bar{p}_i > 0$ *such that the following bounds on various matrices are satisfied for every* $k \geq 0$*:*

$$\begin{array}{lll} \underline{a}_i \leq \left\|\bar{\mathcal{A}}_k^i\right\| \leq \bar{a}_i, & \underline{h}_i \leq \left\|\bar{\mathcal{H}}_{i,k}^i\right\| \leq \bar{h}_i, & \underline{h}_{ij} \leq \left\|\bar{\mathcal{H}}_{j,k}^i\right\| \leq \bar{h}_{ij} \\ \underline{q}_i \leq \left\|\bar{\boldsymbol{Q}}_k^i\right\| \leq \bar{q}_i, & \underline{R}_{ij} \leq \left\|\bar{\boldsymbol{R}}_k^{ij}\right\| \leq \bar{R}_{ij}, & \underline{E}_{i_c} \leq \left\|\boldsymbol{E}_{i_c}\right\| \leq \bar{E}_{i_c} \\ \underline{E}_d \leq \left\|\boldsymbol{E}_d\right\| \leq \bar{E}_d, & \underline{p}_{i_c} \leq \left\|\boldsymbol{p}_{i_c}\right\| \leq \bar{p}_{i_c}, & \underline{g}_i \leq \left\|\bar{\boldsymbol{G}}_k^i\right\| \leq \bar{g}_i \end{array} \tag{4.44}$$

Theorem III.4. *Consider the nonlinear system (4.1) and (4.2) along with the event-triggered mechanism (4.16) and random delays (4.4), (4.10) and (4.11) and assume that Assumption 6 is satisfied. Given* $\underline{\boldsymbol{p}}_i \leq \bar{\boldsymbol{P}}^{i+}(0) \leq \bar{\boldsymbol{p}}_i$ *and* $\underline{\boldsymbol{p}}_{ij} \leq \bar{\boldsymbol{P}}^{ij+}(0) \leq$

$\bar{\boldsymbol{p}}_{ij}$ *where* $\bar{\boldsymbol{p}}_i$, $\underline{\boldsymbol{p}}_i$, $\bar{\boldsymbol{p}}_{ij}$ *and* $\underline{\boldsymbol{p}}_{ij}$ *are known positive values. If the following inequality is satisfied,*

$$\begin{aligned}\boldsymbol{P}^{i-}_{k+1} \leq \bar{a}_i^2\bar{p}_i + 2\bar{a}_i^2\Big(\mathcal{C}_1\bar{p}_i\bar{h}_i\bar{E}_d\Big)\Big[\boldsymbol{r}^{-1}_{i,\min} - \boldsymbol{r}^{-1}_{i,\max}\mathcal{C}_1\underline{E}_d\underline{h}_i\underline{p}_i\underline{h}_i^T\underline{E}_d^T\boldsymbol{r}^{-1}_{i,max}\Big]\\ \times\Big(\mathcal{C}_1\bar{p}_i\bar{h}_i\bar{E}_d\Big)^T + 2\bar{a}_i^2\Big(\sum_{i_c\in\mathcal{M}}\bar{p}_{i_c}\bar{E}_{i_c}\bar{p}_i\bar{h}_i^T\bar{E}_{i_c}^T\bar{E}_d^T\Big)\\ \times\Big[\boldsymbol{r}^{-1}_{i,\min} - \boldsymbol{r}^{-1}_{i,\max}\mathcal{C}_1\underline{E}_d\underline{h}_i\underline{p}_i\underline{h}_i^T\underline{E}_d^T\boldsymbol{r}^{-1}_{i,max}\Big]\\ \times\Big(\sum_{i_c\in\mathcal{M}}\bar{p}_{i_c}\bar{E}_{i_c}\bar{p}_{ij}\bar{h}_i^T\bar{E}_{i_c}^T\bar{E}_d^T\Big)^T \leq \bar{p}_i\end{aligned} \tag{4.45}$$

where

$$\begin{aligned}\boldsymbol{r}_{i,k} = \mathcal{C}_4\sum_{i_s\in\mathcal{N}}\boldsymbol{p}_{i_s}\boldsymbol{E}_{i_s}\bar{\boldsymbol{R}}_k^{ij}\boldsymbol{E}_{i_s}^T + \sum_{i_c\in\mathcal{M}}\boldsymbol{p}_{i_c}\boldsymbol{E}_d\bar{\mathcal{H}}^i_{i,k}\bar{\boldsymbol{P}}_k^{ij-}(\mathcal{H}^i_{j,k})^T\boldsymbol{E}_{i_c}^T\boldsymbol{E}_d^T\\ +\sum_{i_c\in\mathcal{M}}\boldsymbol{p}_{i_c}\boldsymbol{E}_d\boldsymbol{E}_{i_c}\bar{\mathcal{H}}^i_{j,k}\bar{\boldsymbol{P}}_k^{ij-}(\bar{\mathcal{H}}^i_{i,k})^T\boldsymbol{E}_d^T\\ +\mathcal{C}_2\sum_{i_c\in\mathcal{M}}\boldsymbol{p}_{i_c}\boldsymbol{E}_d\boldsymbol{E}_{i_c}\bar{\mathcal{H}}^i_{j,k}\bar{\boldsymbol{P}}_k^{j-}(\bar{\mathcal{H}}^i_{j,k})^T\boldsymbol{E}_{i_c}^T\boldsymbol{E}_d^T\\ +\mathcal{C}_3\sum_{i_s\in\mathcal{N}}\boldsymbol{p}_{i_s}(\boldsymbol{E}_{i_s}-\boldsymbol{E}_d)\boldsymbol{\Psi}_k^{ij}(\boldsymbol{E}_{i_s}-\boldsymbol{E}_d)^T\\ +\mathcal{C}_5\sum_{i_s\in\mathcal{N}}\boldsymbol{p}_{i_s}\boldsymbol{E}_{i_s}(I-\boldsymbol{\gamma}_k^{ij})\boldsymbol{\delta}_k^{ij}(I-\boldsymbol{\gamma}_k^{ij})^T\boldsymbol{E}_{i_s}^T\end{aligned}$$

then, the inequality $\underline{\boldsymbol{p}}_i \leq \boldsymbol{P}_k^{i+} \leq \boldsymbol{P}_k^{i-} \leq \bar{\boldsymbol{p}}_i$ *holds for any* $k \geq 1$.

Proof. It is obvious that the state estimation error and its error covariance are updated by receiving new relative measurements. The updated error covariance is written as follows:

$$\bar{\boldsymbol{P}}_k^{i+} = \bar{\boldsymbol{P}}_k^{i-} - \boldsymbol{K}_k^i\boldsymbol{S}_k^{ij}(\boldsymbol{K}_k^i)^T \tag{4.46}$$

$$\bar{\boldsymbol{P}}_k^{ij+} = \bar{\boldsymbol{P}}_k^{ij-} - \boldsymbol{K}_k^i\boldsymbol{S}_k^{ij}(\boldsymbol{K}_k^j)^T \tag{4.47}$$

Where $\boldsymbol{S}_k^{ij}$ is covariance of arriving innovation:

$$\begin{aligned}S_k^{ij} = \mathcal{C}_1\boldsymbol{E}_d\mathcal{H}^i_{i,k}\bar{\boldsymbol{P}}_k^{i-}(\bar{\mathcal{H}}^i_{i,k})^T\boldsymbol{E}_d^T + \mathcal{C}_4\sum_{i_s\in\mathcal{N}}\boldsymbol{p}_{i_s}\boldsymbol{E}_{i_s}\bar{\boldsymbol{R}}_k^{ij}\boldsymbol{E}_{i_s}^T\\ +\sum_{i_c\in\mathcal{M}}\boldsymbol{p}_{i_c}\boldsymbol{E}_d\bar{\mathcal{H}}^i_{i,k}\bar{\boldsymbol{P}}_k^{ij-}(\mathcal{H}^i_{j,k})^T\boldsymbol{E}_{i_c}^T\boldsymbol{E}_d^T\\ +\sum_{i_c\in\mathcal{M}}\boldsymbol{p}_{i_c}\boldsymbol{E}_d\boldsymbol{E}_{i_c}\bar{\mathcal{H}}^i_{j,k}\bar{\boldsymbol{P}}_k^{ij-}(\bar{\mathcal{H}}^i_{i,k})^T\boldsymbol{E}_d^T\\ +\mathcal{C}_2\sum_{i_c\in\mathcal{M}}\boldsymbol{p}_{i_c}\boldsymbol{E}_d\boldsymbol{E}_{i_c}\bar{\mathcal{H}}^i_{j,k}\bar{\boldsymbol{P}}_k^{j-}(\bar{\mathcal{H}}^i_{j,k})^T\boldsymbol{E}_{i_c}^T\boldsymbol{E}_d^T\\ +\mathcal{C}_3\sum_{i_s\in\mathcal{N}}\boldsymbol{p}_{i_s}(\boldsymbol{E}_{i_s}-\boldsymbol{E}_d)\boldsymbol{\Psi}_k^{ij}(\boldsymbol{E}_{i_s}-\boldsymbol{E}_d)^T\\ +\mathcal{C}_5\sum_{i_s\in\mathcal{N}}\boldsymbol{p}_{i_s}\boldsymbol{E}_{i_s}(I-\boldsymbol{\gamma}_k^{ij})\boldsymbol{\delta}_k^{ij}(I-\boldsymbol{\gamma}_k^{ij})^T\boldsymbol{E}_{i_s}^T\end{aligned}$$

So, we can show that $\bar{\boldsymbol{P}}_{k+1}^{i+} \leq \bar{\boldsymbol{P}}_{k+1}^{i-}$. Considering the propagated state error covari-

ance in (4.26) and substituting $\boldsymbol{K}_k^i$ in (4.39)-(4.40) we write:

$$\begin{aligned}
&\bar{\boldsymbol{P}}^{i-}(k+1) = \bar{\mathcal{A}}_k^i\Big[\bar{\boldsymbol{P}}_k^{i-} - \Big(\mathcal{C}_1\bar{\boldsymbol{P}}_k^{i-}(\mathcal{H}_{i,k}^i)^T\boldsymbol{E}_d^T + \sum_{i_c\in\mathcal{M}}\boldsymbol{p}_{i_c}\boldsymbol{E}_{i_c}\bar{\boldsymbol{P}}_k^{ij-}\\
&\times(\bar{\mathcal{H}}_{j,k}^i)^T\boldsymbol{E}_{i_c}^T\boldsymbol{E}_d^T\Big)(\boldsymbol{K}_k^i)^T\Big](\bar{\mathcal{A}}_k^i)^T + \bar{\boldsymbol{G}}_k^i\bar{\boldsymbol{Q}}_k^i(\bar{\boldsymbol{G}}_k^i)^T\\
&= \bar{\mathcal{A}}_k^i\Big[\bar{\boldsymbol{P}}^{i-}(k) - \Big(\mathcal{C}_1\bar{\boldsymbol{P}}_k^{i-}(\mathcal{H}_{i,k}^i)^T\boldsymbol{E}_d^T + \sum_{i_c\in\mathcal{M}}\boldsymbol{p}_{i_c}\boldsymbol{E}_{i_c}\bar{\boldsymbol{P}}_k^{ij-}(\bar{\mathcal{H}}_{j,k}^i)^T\boldsymbol{E}_{i_c}^T\boldsymbol{E}_d^T\Big)\\
&\times\Big\{\mathcal{C}_1\boldsymbol{E}_d\mathcal{H}_{i,k}^i\bar{\boldsymbol{P}}_k^{i-}(\bar{\mathcal{H}}_{i,k}^i)^T\boldsymbol{E}_d^T + r_k^i\Big\}^{-1}\Big(\mathcal{C}_1\bar{\boldsymbol{P}}_k^{i-}(\mathcal{H}_{i,k}^i)^T\boldsymbol{E}_d^T\\
&+\sum_{i_c\in\mathcal{M}}\boldsymbol{p}_{i_c}\boldsymbol{E}_{i_c}\bar{\boldsymbol{P}}_k^{ij-}(\bar{\mathcal{H}}_{j,k}^i)^T\boldsymbol{E}_{i_c}^T\boldsymbol{E}_d^T\Big)^T\Big](\bar{\mathcal{A}}_k^i)^T + \bar{\boldsymbol{G}}_k^i\bar{\boldsymbol{Q}}_k^i(\bar{\boldsymbol{G}}_k^i)^T
\end{aligned} \tag{4.48}$$

where

$$\begin{aligned}
\boldsymbol{r}_k^i = &\mathcal{C}_4\sum_{i_s\in\mathcal{N}}\boldsymbol{p}_{i_s}\boldsymbol{E}_{i_s}\bar{\boldsymbol{R}}_k^{ij}\boldsymbol{E}_{i_s}^T + \sum_{i_c\in\mathcal{M}}\boldsymbol{p}_{i_c}\boldsymbol{E}_d\bar{\mathcal{H}}_{i,k}^i\bar{\boldsymbol{P}}_k^{ij-}(\mathcal{H}_{j,k}^i)^T\boldsymbol{E}_{i_c}^T\boldsymbol{E}_d^T\\
&+\sum_{i_c\in\mathcal{M}}\boldsymbol{p}_{i_c}\boldsymbol{E}_d\boldsymbol{E}_{i_c}\bar{\mathcal{H}}_{j,k}^i\bar{\boldsymbol{P}}_k^{ij-}(\bar{\mathcal{H}}_{i,k}^i)^T\boldsymbol{E}_d^T\\
&+\mathcal{C}_2\sum_{i_c\in\mathcal{M}}\boldsymbol{p}_{i_c}\boldsymbol{E}_d\boldsymbol{E}_{i_c}\bar{\mathcal{H}}_{j,k}^i\bar{\boldsymbol{P}}_k^{j-}(\bar{\mathcal{H}}_{j,k}^i)^T\boldsymbol{E}_{i_c}^T\boldsymbol{E}_d^T\\
&+\mathcal{C}_3\sum_{i_s\in\mathcal{N}}\boldsymbol{p}_{i_s}(\boldsymbol{E}_{i_s}-\boldsymbol{E}_d)\boldsymbol{\Psi}_k^{ij}(\boldsymbol{E}_{i_s}-\boldsymbol{E}_d)^T\\
&+\mathcal{C}_5\sum_{i_s\in\mathcal{N}}\boldsymbol{p}_{i_s}\boldsymbol{E}_{i_s}(I-\boldsymbol{\gamma}_k^{ij})\boldsymbol{\delta}_k^{ij}(I-\boldsymbol{\gamma}_k^{ij})^T\boldsymbol{E}_{i_s}^T
\end{aligned} \tag{4.49}$$

Using the inequality $(A+B)^{-1} > A^{-1} - A^{-1}BA^{-1}$ we write:

$$\begin{aligned}
&\bar{\boldsymbol{P}}_{k+1}^{i-} \le \bar{\mathcal{A}}_k^i\bar{\boldsymbol{P}}_k^{i-}(\bar{\mathcal{A}}_k^i)^T + \bar{\mathcal{A}}_k^i\Big(\mathcal{C}_1\bar{\boldsymbol{P}}_k^{i-}(\mathcal{H}_{i,k}^i)^T\boldsymbol{E}_d^T\Big)\\
&\times\Big[(\boldsymbol{r}_k^i)^{-1} - (\boldsymbol{r}_k^i)^{-1}\Big(\mathcal{C}_1\boldsymbol{E}_d\mathcal{H}_{i,k}^i\bar{\boldsymbol{P}}_k^{i-}(\bar{\mathcal{H}}_{i,k}^i)^T\boldsymbol{E}_d^T\Big)(\boldsymbol{r}_k^i)^{-1}\Big]\\
&\times\Big(\mathcal{C}_1\bar{\boldsymbol{P}}_k^{i-}(\mathcal{H}_{i,k}^i)^T\boldsymbol{E}_d^T\Big)^T(\bar{\mathcal{A}}_k^i)^T + \bar{\mathcal{A}}_k^i\Big(\sum_{i_c\in\mathcal{M}}\boldsymbol{p}_{i_c}\boldsymbol{E}_{i_c}\bar{\boldsymbol{P}}_k^{ij-}(\bar{\mathcal{H}}_{j,k}^i)^T\boldsymbol{E}_{i_c}^T\boldsymbol{E}_d^T\Big)\\
&\times\Big[(\boldsymbol{r}_k^i)^{-1} - (\boldsymbol{r}_k^i)^{-1}\Big(\mathcal{C}_1\boldsymbol{E}_d\mathcal{H}_{i,k}^i\bar{\boldsymbol{P}}_k^{i-}(\bar{\mathcal{H}}_{i,k}^i)^T\boldsymbol{E}_d^T\Big)(\boldsymbol{r}_k^i)^{-1}\Big]\\
&\times\Big(\mathcal{C}_1\bar{\boldsymbol{P}}_k^{i-}(\mathcal{H}_{i,k}^i)^T\boldsymbol{E}_d^T\Big)^T(\bar{\mathcal{A}}_k^i)^T + \bar{\mathcal{A}}_k^i\Big(\sum_{i_c\in\mathcal{M}}\boldsymbol{p}_{i_c}\boldsymbol{E}_{i_c}\bar{\boldsymbol{P}}_k^{ij-}(\bar{\mathcal{H}}_{j,k}^i)^T\boldsymbol{E}_{i_c}^T\boldsymbol{E}_d^T\Big)\\
&\times\Big[(\boldsymbol{r}_k^i)^{-1} - (\boldsymbol{r}_k^i)^{-1}\Big(\mathcal{C}_1\boldsymbol{E}_d\mathcal{H}_{i,k}^i\bar{\boldsymbol{P}}_k^{i-}(\bar{\mathcal{H}}_{i,k}^i)^T\boldsymbol{E}_d^T\Big)(\boldsymbol{r}_k^i)^{-1}\Big]\\
&\times\Big(\sum_{i_c\in\mathcal{M}}\boldsymbol{p}_{i_c}\boldsymbol{E}_{i_c}\bar{\boldsymbol{P}}_k^{ij-}(\bar{\mathcal{H}}_{j,k}^i)^T\boldsymbol{E}_{i_c}^T\boldsymbol{E}_d^T\Big)^T(\bar{\mathcal{A}}_k^i)^T + \bar{\mathcal{A}}_k^i\Big(\mathcal{C}_1\bar{\boldsymbol{P}}_k^{i-}(\mathcal{H}_{i,k}^i)^T\boldsymbol{E}_d^T\Big)\\
&\times\Big[(\boldsymbol{r}_k^i)^{-1} - (\boldsymbol{r}_k^i)^{-1}\Big(\mathcal{C}_1\boldsymbol{E}_d\mathcal{H}_{i,k}^i\bar{\boldsymbol{P}}_k^{i-}(\bar{\mathcal{H}}_{i,k}^i)^T\boldsymbol{E}_d^T\Big)(\boldsymbol{r}_k^i)^{-1}\Big]\\
&\times\Big(\sum_{i_c\in\mathcal{M}}\boldsymbol{p}_{i_c}\boldsymbol{E}_{i_c}\bar{\boldsymbol{P}}_k^{ij-}(\bar{\mathcal{H}}_{j,k}^i)^T\boldsymbol{E}_{i_c}^T\boldsymbol{E}_d^T\Big)^T(\bar{\mathcal{A}}_k^i)^T \le 2\bar{\mathcal{A}}_k^i\Big(\mathcal{C}_1\bar{\boldsymbol{P}}_k^{i-}(\mathcal{H}_{i,k}^i)^T\boldsymbol{E}_d^T\Big)\\
&\times\Big[(\boldsymbol{r}_k^i)^{-1} - (\boldsymbol{r}_k^i)^{-1}\Big(\mathcal{C}_1\boldsymbol{E}_d\mathcal{H}_{i,k}^i\bar{\boldsymbol{P}}_k^{i-}(\bar{\mathcal{H}}_{i,k}^i)^T\boldsymbol{E}_d^T\Big)(\boldsymbol{r}_k^i)^{-1}\Big]\\
&\times\Big(\mathcal{C}_1\bar{\boldsymbol{P}}_k^{i-}(\mathcal{H}_{i,k}^i)^T\boldsymbol{E}_d^T\Big)^T(\bar{\mathcal{A}}_k^i)^T + 2\bar{\mathcal{A}}_k^i\Big(\sum_{i_c\in\mathcal{M}}\boldsymbol{p}_{i_c}\boldsymbol{E}_{i_c}\bar{\boldsymbol{P}}_k^{ij-}(\bar{\mathcal{H}}_{j,k}^i)^T\boldsymbol{E}_{i_c}^T\boldsymbol{E}_d^T\Big)\\
&\times\Big[(\boldsymbol{r}_k^i)^{-1} - (\boldsymbol{r}_k^i)^{-1}\Big(\mathcal{C}_1\boldsymbol{E}_d\mathcal{H}_{i,k}^i\bar{\boldsymbol{P}}_k^{i-}(\bar{\mathcal{H}}_{i,k}^i)^T\boldsymbol{E}_d^T\Big)(\boldsymbol{r}_k^i)^{-1}\Big]\\
&\times\Big(\sum_{i_c\in\mathcal{M}}\boldsymbol{p}_{i_c}\boldsymbol{E}_{i_c}\bar{\boldsymbol{P}}_k^{ij-}(\bar{\mathcal{H}}_{j,k}^i)^T\boldsymbol{E}_{i_c}^T\boldsymbol{E}_d^T\Big)^T(\bar{\mathcal{A}}_k^i)^T + \bar{\mathcal{A}}_k^i\bar{\boldsymbol{P}}_k^{i-}(\bar{\mathcal{A}}_k^i)^T
\end{aligned} \tag{4.50}$$

Now, in order to prove the boundedness of error covariance $\bar{\boldsymbol{P}}_{k+1}^{i-}$, we assume that $\underline{p}_i I \le \bar{\boldsymbol{P}}_k^{i-} \le \bar{p}_i I$ and $\underline{p}_{ij} I \le \bar{\boldsymbol{P}}_k^{ij-} \le \bar{p}_{ij} I$ holds at k, then we will show that it is true

in $k+1$.

$$\begin{aligned}\boldsymbol{P}_{k+1}^{i-} \leq\ & \bar{a}_i^2\bar{p}_i + 2\bar{a}_i^2\Big(\mathcal{C}_1\bar{p}_i\bar{h}_i\bar{E}_d\Big)\Big[\boldsymbol{r}_{i,\min}^{-1} - \boldsymbol{r}_{i,\max}^{-1}\mathcal{C}_1\underline{E}_d\underline{h}_i\underline{p}_i\underline{h}_i^T\underline{E}_d^T\boldsymbol{r}_{i,max}^{-1}\Big] \\ & \times\Big(\mathcal{C}_1\bar{p}_i\bar{h}_i\bar{E}_d\Big)^T + 2\bar{a}_i^2\Big(\sum_{i_c\in\mathcal{M}}\boldsymbol{p}_{i_c}\bar{E}_{i_c}\bar{p}_i\bar{h}_i^T\bar{E}_{i_c}^T\bar{E}_d^T\Big) \\ & \times\Big[\boldsymbol{r}_{i,\min}^{-1} - \boldsymbol{r}_{i,\max}^{-1}\mathcal{C}_1\underline{E}_d\underline{h}_i\underline{p}_i\underline{h}_i^T\underline{E}_d^T\boldsymbol{r}_{i,max}^{-1}\Big] \\ & \times\Big(\sum_{i_c\in\mathcal{M}}\boldsymbol{p}_{i_c}\bar{E}_{i_c}\bar{p}_{ij}\bar{h}_i^T\bar{E}_{i_c}^T\bar{E}_d^T\Big)^T \leq \bar{p}_i\end{aligned} \tag{4.51}$$

Therefore, we show that the error covariance matrix is bounded for $k \geq 1$ by mathematical induction, which completes the proof. □

Remark 9. *In Theorem III.4, we obtained sufficient conditions that ensure convergence and stochastic stability of the proposed filter. It is worth mentioning that all terms involving the dynamics of the multi-robot system, event-triggered scheme as well as random delays appear in condition (4.51). According to condition (4.51), if the upper bound of the input delay increases, then $\boldsymbol{r}_{i,\max}$ will increase, resulting in an increase of the upper bound of filtering error covariance. Also, the event-triggered parameters α_{ij}, $\beta_{ij} > 0$ in Eq. (4.16) have an impact on upper bound of the filtering error covariance. From Eq. (4.16), it can be seen that as the value of α_{ij}, β_{ij} increase, the average transmission rate of information ($\boldsymbol{\gamma}_k^{ij}$) is reduced. Moreover, based on condition (4.51), we can see that $\boldsymbol{r}_{i,\max}$ will increase as the value of α_{ij}, β_{ij} increase. Therefore, the upper bound of the filter error covariance increases with the value of α_{ij}, β_{ij}. Conversely, smaller values of α_{ij}, β_{ij} lead to a higher communication rate. In this scenario, the upper bound of the error covariance decreases resulting in better localization performance, at the cost of imposing a heavier burden on the communication network. These two scenarios lead to a tradeoff in the value of α_{ij}, β_{ij} to balance localization performance and reduced communication costs. When, both parameters of the event-triggered scheme (α_{ij}, β_{ij}) and the upper bound of input delays are large, the filtering error covariance might diverge. Convergence of the proposed filter is guaranteed provided that the maximum delays, event-triggered parameters, etc., satisfy inequality (4.51). If upper bound of the filtering error covariance converges asymptotically with k, then the filtering error covariance must converge as well.*

Note that the error covariance matrix in the developed CL does not represent the true estimation error exactly. Therefore, the result of Theorem III.4 can be used to analyze the performance of estimation error. This is done in our next Theorem.

Theorem III.5. *Consider the nonlinear system (4.1) and (4.2) along with the event-triggered mechanism (4.16) and random delays (4.4), (4.10) and (4.11). If*

$$\bar{\boldsymbol{P}}_k^{i+} \leq \bar{\boldsymbol{P}}_k^{i-} \leq \bar{\boldsymbol{p}}_i \tag{4.52}$$

and for some $\varepsilon^i > 0$, $\mathbb{E}\left\{\left\|\tilde{\tilde{\boldsymbol{x}}}^{i+}(0)\right\|^2\right\} \leq \varepsilon^i$, *then the filtering error* $\tilde{\tilde{\boldsymbol{x}}}_k^{i+} = \bar{\boldsymbol{x}}_k^i - \hat{\tilde{\boldsymbol{x}}}_k^{i+}$ *is exponentially bounded in mean square for any* $i \in \vartheta$.

Proof. First, we define the Lyapunov function as follows:

$$\boldsymbol{V}_k(\tilde{\tilde{\boldsymbol{x}}}_k^{i+}) = (\tilde{\tilde{\boldsymbol{x}}}_k^{i+})^T(\bar{\boldsymbol{P}}_k^{i+})^{-1}\tilde{\tilde{\boldsymbol{x}}}_k^{i+} \tag{4.53}$$

Using Theorem III.4 it is obtained that $\underline{\boldsymbol{p}}_i \boldsymbol{I} \leq \bar{\boldsymbol{P}}_k^{i+} \leq \bar{\boldsymbol{p}}_i \boldsymbol{I}$. The inequality constraint form of Eq. (4.53) is written as follows:

$$\tfrac{1}{\bar{\boldsymbol{p}}_i}\left\|\tilde{\tilde{\boldsymbol{x}}}_k^{i+}\right\|^2 \leq \boldsymbol{V}_k(\tilde{\tilde{\boldsymbol{x}}}_k^{i+}) \leq \tfrac{1}{\underline{\boldsymbol{p}}_i}\left\|\tilde{\tilde{\boldsymbol{x}}}_k^{i+}\right\|^2 \tag{4.54}$$

Next, we have to compute $\mathbb{E}\Big\{V_k(\tilde{\tilde{\boldsymbol{x}}}_k^{i+})|\tilde{\tilde{\boldsymbol{x}}}_{k-1}^{i+}\Big\}$ as follows:

$$\begin{aligned}\mathbb{E}\Big\{\boldsymbol{V}_k(\tilde{\tilde{\boldsymbol{x}}}_k^{i+})|\tilde{\tilde{\boldsymbol{x}}}_{k-1}^{i+}\Big\} &= \mathbb{E}\Big\{(\tilde{\tilde{\boldsymbol{x}}}_{k-1}^{i+})^T(\bar{\mathcal{A}}_{k-1}^i)^T\Big(\boldsymbol{I} - \boldsymbol{K}_{k+1}^i\boldsymbol{E}_d\bar{\mathcal{H}}_{i,k+1}^i\Big)^T \\ &\times(\bar{\boldsymbol{P}}_k^{i+})^{-1}\Big(\boldsymbol{I} - \boldsymbol{K}_{k+1}^i\boldsymbol{E}_d\bar{\mathcal{H}}_{i,k+1}^i\Big)\bar{\mathcal{A}}_{k-1}^i\tilde{\tilde{\boldsymbol{x}}}_{k-1}^{i+}\Big\} + \boldsymbol{\mu}_k^i\end{aligned} \tag{4.55}$$

Next, we have to ensure the boundary of $\mathbb{E}\Big\{V_k(\tilde{\tilde{\boldsymbol{x}}}_k^{i+})|\tilde{\tilde{\boldsymbol{x}}}_{k-1}^{i+}\Big\} - V_{k-1}(\tilde{\tilde{\boldsymbol{x}}}_{k-1}^{i+})$. Note that considering the property of conditional expectation that $\mathbb{E}\{\tilde{\tilde{\boldsymbol{x}}}_k^{i+}|\tilde{\tilde{\boldsymbol{x}}}_k^{i+}\} = \tilde{\tilde{\boldsymbol{x}}}_k^{i+}$.

$$\begin{aligned}&\mathbb{E}\Big\{V_k(\tilde{\tilde{\boldsymbol{x}}}_k^{i+})|\tilde{\tilde{\boldsymbol{x}}}_{k-1}^{i+}\Big\} - V_{k-1}(\tilde{\tilde{\boldsymbol{x}}}_{k-1}^{i+}) \leq \\ &(\tilde{\tilde{\boldsymbol{x}}}_{k-1}^{i+})^T\Bigg\{(\bar{\mathcal{A}}_{k-1}^i)^T\Big(\boldsymbol{I} - \boldsymbol{K}_{k+1}^i\boldsymbol{E}_d\bar{\mathcal{H}}_{i,k+1}^i\Big)^T\Bigg[\mathcal{C}_1\Big(\boldsymbol{I} - \boldsymbol{K}_k^i\boldsymbol{E}_d\bar{\mathcal{H}}_{i,k}^i\Big) \\ &\times\Big(\bar{\mathcal{A}}_{k-1}^i\bar{\boldsymbol{P}}_{k-1}^{i+}(\bar{\mathcal{A}}_{k-1}^i)^T + \bar{\boldsymbol{G}}_{k-1}^i\bar{\boldsymbol{Q}}_{k-1}^i(\bar{\boldsymbol{G}}_{k-1}^i)^T\Big)\Big(\boldsymbol{I} - \boldsymbol{K}_k^i\boldsymbol{E}_d\bar{\mathcal{H}}_{i,k}^i\Big)^T \\ &-\sum_{i_c\in\mathcal{M}}\boldsymbol{p}_{i_c}\Big(\boldsymbol{I} - \boldsymbol{K}_k^i\boldsymbol{E}_d\bar{\mathcal{H}}_{i,k}^i\Big)\Big(\bar{\mathcal{A}}_{k-1}^i\bar{\boldsymbol{P}}_{k-1}^{ij+}(\bar{\mathcal{A}}_{k-1}^j)^T\Big)\Big(\boldsymbol{K}_k^i\boldsymbol{E}_d\boldsymbol{E}_{i_c}\bar{\mathcal{H}}_{j,k}^i\Big)^T \\ &-\sum_{i_c\in\mathcal{M}}\boldsymbol{p}_{i_c}\Big(\boldsymbol{K}_k^i\boldsymbol{E}_d\boldsymbol{E}_{i_c}\bar{\mathcal{H}}_{j,k}^i\Big)\Big(\bar{\mathcal{A}}_{k-1}^i\bar{\boldsymbol{P}}_{k-1}^{ij+}(\bar{\mathcal{A}}_{k-1}^j)^T\Big)\Big(\boldsymbol{I} - \boldsymbol{K}_k^i\boldsymbol{E}_d\bar{\mathcal{H}}_{i,k}^i\Big)^T \\ &+\sum_{i_c\in\mathcal{M}}\boldsymbol{p}_{i_c}\mathcal{C}_2\Big(\boldsymbol{K}_k^i\boldsymbol{E}_d\boldsymbol{E}_{i_c}\bar{\mathcal{H}}_{j,k}^i\Big)\bar{\boldsymbol{P}}_k^{j-}\Big(\boldsymbol{K}_k^i\boldsymbol{E}_d\boldsymbol{E}_{i_c}\bar{\mathcal{H}}_{j,k}^i\Big)^T \\ &-\sum_{i_s\in\mathcal{N}}\boldsymbol{p}_{i_s}\mathcal{C}_3\Big(\boldsymbol{K}_k^i(\boldsymbol{E}_{i_s} - \boldsymbol{E}_d)\Big)\boldsymbol{\Psi}_k^{ij}\Big(\boldsymbol{K}_k^i(\boldsymbol{E}_{i_s} - \boldsymbol{E}_d)\Big)^T \\ &-\sum_{i_s\in\mathcal{N}}\boldsymbol{p}_{i_s}\mathcal{C}_4\Big(\boldsymbol{K}_k^i\boldsymbol{E}_{i_s}\Big)\boldsymbol{R}_k^{ij}\Big(\boldsymbol{K}_k^i\boldsymbol{E}_{i_s}\Big)^T + \sum_{i_s\in\mathcal{M}}\boldsymbol{p}_{i_c}\mathcal{C}_6\Big(\boldsymbol{I} - \boldsymbol{E}_{i_c}\Big)\boldsymbol{\Pi}_k^j\Big(\boldsymbol{I} - \boldsymbol{E}_{i_c}\Big)^T \\ &+\sum_{i_s\in\mathcal{N}}\boldsymbol{p}_{i_s}\mathcal{C}_5\Big(\boldsymbol{K}_k^i\boldsymbol{E}_{i_s}(\boldsymbol{I} - \boldsymbol{\gamma}_k^{ij})\Big)\boldsymbol{\delta}_k^{ij}\Big(\boldsymbol{K}_k^i\boldsymbol{E}_{i_s}(\boldsymbol{I} - \boldsymbol{\gamma}_k^{ij})\Big)^T\Bigg]^{-1} \\ &\times\bar{\mathcal{A}}_{k-1}^i\tilde{\tilde{\boldsymbol{x}}}_{k-1}^{i+} - \Big(\boldsymbol{P}_{k-1}^{i+}\Big)^{-1}\Bigg\}\tilde{\tilde{\boldsymbol{x}}}_{k-1}^{i+}\end{aligned} \tag{4.56}$$

Then, $\mathbb{E}\Big\{V_k(\tilde{\tilde{\boldsymbol{x}}}_k^{i+})|\tilde{\tilde{\boldsymbol{x}}}_{k-1}^{i+}\Big\} - V_{k-1}(\tilde{\tilde{\boldsymbol{x}}}_{k-1}^{i+})$ is written in the following form:

$$\mathbb{E}\Big\{V_k(\tilde{\tilde{\boldsymbol{x}}}_k^{i+})|\tilde{\tilde{\boldsymbol{x}}}_{k-1}^{i+}\Big\} - V_{k-1}(\tilde{\tilde{\boldsymbol{x}}}_{k-1}^{i+}) \leq \bar{\boldsymbol{\mu}}_k^i - \sigma_i \boldsymbol{V}_{k-1}(\tilde{\tilde{\boldsymbol{x}}}_{k-1}^{i+}) \tag{4.57}$$

We can show the following inequality:

$$0 < \sigma_i \leq 1 \tag{4.58}$$

According to Lemma IV.1, there is

$$\mathbb{E}\left\{\left\|\tilde{\tilde{\boldsymbol{x}}}_k^{i+}\right\|^2\right\} \leq \frac{\bar{\kappa}}{\underline{\kappa}}\mathbb{E}\left\{\left\|\tilde{\tilde{\boldsymbol{x}}}^{i+}(0)\right\|^2\right\}(1-\sigma_i)^{k+1} + \frac{\bar{\mu}^i}{\underline{\kappa}}\sum_{n=1}^{k-1}(1-\sigma_i)^i \tag{4.59}$$

The proof is completed. □

Remark 10. *According to (4.59) (see supplemental materials), the estimation error of the proposed filter decays exponentially provided that the initial estimation error is bounded and $0 < \sigma_i \leq 1$. Also, the upper bound of $\boldsymbol{\mu}_k^i$ depends on the event-triggering parameter, and the parameters of the random delays (sensor-filter and filter-filter communication channels), which affect the upper bound of $\mathbb{E}\left\{\left\|\tilde{\tilde{\boldsymbol{x}}}_k^{i+}\right\|^2\right\}$. Thus, by assuming bounded delays and choosing a proper event-triggered mechanism, one can limit the upper bound of the estimation error.*

IV Design of the CL Algorithm with random delays (a time-stamped mechanism)

IV.1 Design of DECL using non-time-stamped mechanism

In the preceding section, we derived an extended Kalman filter assuming that the data packets received by the filter were not time-stamped. In this section we revisit the previous result and derive an extended Kalman filter assuming time-stamped packets. In the time-stamp mechanism, the filter has perfect knowledge of the signal delay at each time. At time instant k, each measurement $\bar{\boldsymbol{z}}_k^{ij}$ with time-stamp has a delay of d_k^i time steps.

Theorem IV.1. *Consider the nonlinear system (4.1) and (4.2) along with the event-triggered mechanism (4.16). Assume that the relative measurement $(\bar{\boldsymbol{z}}_k^{ij}, \bar{\boldsymbol{z}}_k^{ji})$ and the predicted belief $\boldsymbol{bel}_k^{i-} = (\hat{\bar{\boldsymbol{x}}}_k^{i-}, \bar{\boldsymbol{P}}_k^{i-})$, $\boldsymbol{bel}_k^{j-} = (\hat{\bar{\boldsymbol{x}}}_k^{j-}, \bar{\boldsymbol{P}}_k^{j-})$ are transmitted through time-stamped mechanism with random delays (4.4), (4.10) and (4.11) through the*

communication channels. For the DECL via the EKF, the upper bound of estimation error covariance $\bar{\boldsymbol{P}}^{i-}_{ts,k}$ *can be obtained as follows:*

$$\begin{aligned}
\bar{\boldsymbol{\Sigma}}^{i+}_{ts,k} &= \mathcal{C}_1\Big(\boldsymbol{I}-\boldsymbol{K}^i_{ts,k}\boldsymbol{E}_{d,ts}\bar{\mathcal{H}}^i_{i,k}\Big)\bar{\boldsymbol{P}}^{i-}_{ts,k}\Big(\boldsymbol{I}-\boldsymbol{K}^i_{ts,k}\boldsymbol{E}_{d,ts}\bar{\mathcal{H}}^i_{i,k}\Big)^T\\
&-\Big(\boldsymbol{I}-\boldsymbol{K}^i_{ts,k}\boldsymbol{E}_{d,ts}\bar{\mathcal{H}}^i_{i,k}\Big)\bar{\boldsymbol{P}}^{ij-}_{ts,k}\Big(\boldsymbol{K}^i_{ts,k}\boldsymbol{E}_{d,ts}\boldsymbol{E}_{\xi_k,ts}\bar{\mathcal{H}}^i_{j,k}\Big)^T\\
&-\Big(\boldsymbol{K}^i_{ts,k}\boldsymbol{E}_{d,ts}\boldsymbol{E}_{\xi_k,ts}\bar{\mathcal{H}}^i_{j,k}\Big)\bar{\boldsymbol{P}}^{ij-}_{ts,k}\Big(\boldsymbol{I}-\boldsymbol{K}^i_{ts,k}\boldsymbol{E}_{d,ts}\bar{\mathcal{H}}^i_{i,k}\Big)^T\\
&+\mathcal{C}_2\Big(\boldsymbol{K}^i_{ts,k}\boldsymbol{E}_{d,ts}\boldsymbol{E}_{\xi_k,ts}\bar{\mathcal{H}}^i_{j,k}\Big)\bar{\boldsymbol{P}}^{j-}_{k}\Big(\boldsymbol{K}^i_{ts,k}\boldsymbol{E}_{d,ts}\boldsymbol{E}_{\xi_k,ts}\bar{\mathcal{H}}^i_{j,k}\Big)^T\\
&+\mathcal{C}_3\Big(\boldsymbol{K}^i_{ts,k}(\boldsymbol{E}_{\tau_k,ts}-\boldsymbol{E}_{d,ts})\Big)\boldsymbol{\Psi}^{ij}_{k}\Big(\boldsymbol{K}^i_{ts,k}(\boldsymbol{E}_{\tau_k,ts}-\boldsymbol{E}_{d,ts})\Big)^T\\
&+\mathcal{C}_4\Big(\boldsymbol{K}^i_{ts,k}\boldsymbol{E}_{\tau_k,ts}\Big)\boldsymbol{R}^{ij}_{k}\Big(\boldsymbol{K}^i_{ts,k}\boldsymbol{E}_{\tau_k,ts}\Big)^T\\
&+\mathcal{C}_6\Big(\boldsymbol{I}-\boldsymbol{E}_{\xi_k,ts}\Big)\boldsymbol{\Pi}^{j}_{k}\Big(\boldsymbol{I}-\boldsymbol{E}_{\xi_k,ts}\Big)^T\\
&+\mathcal{C}_5\Big(\boldsymbol{K}^i_{ts,k}\boldsymbol{E}_{\tau_k,ts}(\boldsymbol{I}-\boldsymbol{\gamma}^{ij}_{k})\Big)\boldsymbol{\delta}^{ij}_{k}\Big(\boldsymbol{K}^i_{ts,k}\boldsymbol{E}_{\tau_k,ts}(\boldsymbol{I}-\boldsymbol{\gamma}^{ij}_{k})\Big)^T
\end{aligned} \tag{4.60}$$

Proof. The proof is similar to the Theorem III.2 and is omitted. □

Corollary IV.1.1. Under the assumptions of Theorem IV.1, the DECL gain is given by:

$$\boldsymbol{K}^i_{ts,k} = X(Y)^{-1} \tag{4.61}$$

Where X and Y can be expressed as a follows:

$$\begin{aligned}
X &= \mathcal{C}_1\bar{\boldsymbol{P}}^{i-}_{ts,k}(\mathcal{H}^i_{i,k})^T\boldsymbol{E}^T_{d,ts}+\boldsymbol{E}_{\xi_k,ts}\bar{\boldsymbol{P}}^{ij-}_{ts,k}(\bar{\mathcal{H}}^i_{j,k})^T\boldsymbol{E}^T_{\xi_k,ts}\boldsymbol{E}^T_{d,ts}\\
Y &= \mathcal{C}_1\boldsymbol{E}_{d,ts}\mathcal{H}^i_{i,k}\bar{\boldsymbol{P}}^{i-}_{ts,k}(\bar{\mathcal{H}}^i_{i,k})^T\boldsymbol{E}^T_{d,ts}+\mathcal{C}_4\boldsymbol{E}_{\tau_k,ts}\bar{\boldsymbol{R}}^{ij}_{k}\boldsymbol{E}^T_{\tau_k,ts}\\
&\quad+\boldsymbol{E}_{d,ts}\bar{\mathcal{H}}^i_{i,k}\bar{\boldsymbol{P}}^{ij-}_{ts,k}(\mathcal{H}^i_{j,k})^T\boldsymbol{E}^T_{\xi_k,ts}\boldsymbol{E}^T_{d,ts}\\
&\quad+\boldsymbol{E}_{d,ts}\boldsymbol{E}_{\xi_k,ts}\bar{\mathcal{H}}^i_{j,k}\bar{\boldsymbol{P}}^{ij-}_{ts,k}(\bar{\mathcal{H}}^i_{i,k})^T\boldsymbol{E}^T_{d,ts}\\
&\quad+\mathcal{C}_2\boldsymbol{E}_{d,ts}\boldsymbol{E}_{\xi_k,ts}\bar{\mathcal{H}}^i_{j,k}\bar{\boldsymbol{P}}^{j-}_{ts,k}(\bar{\mathcal{H}}^i_{j,k})^T\boldsymbol{E}^T_{\xi_k,ts}\boldsymbol{E}^T_{d,ts}\\
&\quad+\mathcal{C}_3(\boldsymbol{E}_{\tau_k,ts}-\boldsymbol{E}_{d,ts})\boldsymbol{\Psi}^{ij}_{k}(\boldsymbol{E}_{\tau_k,ts}-\boldsymbol{E}_{d,ts})^T\\
&\quad+\mathcal{C}_5\boldsymbol{E}_{\tau_k,ts}(I-\boldsymbol{\gamma}^{ij}_{k})\boldsymbol{\delta}^{ij}_{k}(I-\boldsymbol{\gamma}^{ij}_{k})^T\boldsymbol{E}^T_{\tau_k,ts}
\end{aligned} \tag{4.62}$$

Remark 11. *It is important to notice that the main difference between localization of multi-robot systems with and without time-stamped mechanism is the nature of the matrices* $\boldsymbol{E}_{\tau_k}$, $\boldsymbol{E}_d$ *and* $\boldsymbol{E}_{\xi_k}$. *In the time-stamped case (see Theorem IV.1), the matrices* $\boldsymbol{E}_{\tau_k}$, $\boldsymbol{E}_d$ *and* $\boldsymbol{E}_{\xi_k}$ *are known at each time, whereas in the non-time-stamped case (see Theorem III.2), their expected values are employed. The filter with time-stamped technology provides better localization performance than without time-stamped technology in the presence of delayed measurements since it has the knowledge of delays involved. However, the non time-stamped mechanism may be an appropriate way to reduce communication costs in the case of limited bandwidth compared to the time-stamped mechanism.*

Algorithm 2 DECL Algorithm Under Random Delays

1: Initialize state estimation and error covariance as Robots $i \in \vartheta$ and $j \in \vartheta \backslash \{i\}$: $\hat{\bar{\mathbf{x}}}^{i+}(0) \in \mathbb{R}^{n^i}$, $\bar{\mathbf{P}}^{i+}(0) \in \mathbb{S}^{n^i}$, $\bar{\mathbf{P}}^{ij+}(0) = \mathbf{0}_{n^i \times n^j}$

2: **repeat**

3: **Propagation:** Compute the predicted state and error covariance for each robot:

$$\begin{aligned}
\hat{\bar{\boldsymbol{x}}}_{k+1}^{i-} &= \boldsymbol{f}^i\left(\hat{\bar{\boldsymbol{x}}}_k^{i+}, \bar{\boldsymbol{u}}_k^i\right) \\
\bar{\boldsymbol{P}}_{k+1}^{i-} &= \bar{\mathcal{A}}_k^i \bar{\boldsymbol{P}}_k^{i+} (\bar{\mathcal{A}}_k^i)^T + \bar{\boldsymbol{G}}_k^i \bar{\boldsymbol{Q}}_k^i (\bar{\boldsymbol{G}}_k^i)^T \\
\bar{\boldsymbol{P}}_{k+1}^{ij-} &= \bar{\mathcal{A}}_k^i \bar{\boldsymbol{P}}_k^{ij+} (\bar{\mathcal{A}}_k^j)^T
\end{aligned}$$

4: **Update:**

5: If robot i receive relative measurements $\mathbf{z}_k^{ij}$, then broadcast the predicted state and the corresponding error covariance to the other robots. The measurement residual and its covariance are:

$$\begin{aligned}
\Upsilon_k^{ij} &= \boldsymbol{E}_{\tau_k} \boldsymbol{z}_k^{ij} - \boldsymbol{E}_{\tau_k} (\boldsymbol{I} - \boldsymbol{\gamma}_{k+1}^i) \boldsymbol{e}_{k+1}^{ij} - \boldsymbol{E}_d \hat{\boldsymbol{z}}_k^{ij} \\
S_k^{ij} &= \mathcal{C}_1 \boldsymbol{E}_d \mathcal{H}_{i,k}^i \bar{\boldsymbol{P}}_k^{i-} (\bar{\mathcal{H}}_{i,k}^i)^T \boldsymbol{E}_d^T + \mathcal{C}_4 \sum_{i_s \in \mathcal{N}} \boldsymbol{p}_{i_s} \boldsymbol{E}_{i_s} \bar{\boldsymbol{R}}_k^{ij} \boldsymbol{E}_{i_s}^T \\
&\quad + \sum_{i_c \in \mathcal{M}} \boldsymbol{p}_{i_c} \boldsymbol{E}_d \bar{\mathcal{H}}_{i,k}^i \bar{\boldsymbol{P}}_k^{ij-} (\mathcal{H}_{j,k}^i)^T \boldsymbol{E}_{i_c}^T \boldsymbol{E}_d^T \\
&\quad + \sum_{i_c \in \mathcal{M}} \boldsymbol{p}_{i_c} \boldsymbol{E}_d \boldsymbol{E}_{i_c} \bar{\mathcal{H}}_{j,k}^i \bar{\boldsymbol{P}}_k^{ij-} (\bar{\mathcal{H}}_{i,k}^i)^T \boldsymbol{E}_d^T \\
&\quad + \mathcal{C}_2 \sum_{i_c \in \mathcal{M}} \boldsymbol{p}_{i_c} \boldsymbol{E}_d \boldsymbol{E}_{i_c} \bar{\mathcal{H}}_{j,k}^i \bar{\boldsymbol{P}}_k^{j-} (\bar{\mathcal{H}}_{j,k}^i)^T \boldsymbol{E}_{i_c}^T \boldsymbol{E}_d^T \\
&\quad + \mathcal{C}_3 \sum_{i_s \in \mathcal{N}} \boldsymbol{p}_{i_s} (\boldsymbol{E}_{i_s} - \boldsymbol{E}_d) \boldsymbol{\Psi}_k^{ij} (\boldsymbol{E}_{i_s} - \boldsymbol{E}_d)^T \\
&\quad + \mathcal{C}_5 \sum_{i_s \in \mathcal{N}} \boldsymbol{p}_{i_s} \boldsymbol{E}_{i_s} (I - \boldsymbol{\gamma}_k^{ij}) \boldsymbol{\delta}_k^{ij} (I - \boldsymbol{\gamma}_k^{ij})^T \boldsymbol{E}_{i_s}^T \\
S_{ts,k}^{ij} &= \mathcal{C}_1 \boldsymbol{E}_{d,ts} \mathcal{H}_{i,k}^i \bar{\boldsymbol{P}}_{ts,k}^{i-} (\bar{\mathcal{H}}_{i,k}^i)^T \boldsymbol{E}_{d,ts}^T + \mathcal{C}_4 \boldsymbol{E}_{\tau_k,ts} \bar{\boldsymbol{R}}_k^{ij} \boldsymbol{E}_{\tau_k,ts}^T \\
&\quad + \boldsymbol{E}_{d,ts} \bar{\mathcal{H}}_{i,k}^i \bar{\boldsymbol{P}}_{ts,k}^{ij-} (\mathcal{H}_{j,k}^i)^T \boldsymbol{E}_{\xi_k,ts}^T \boldsymbol{E}_{d,ts}^T \\
&\quad + \boldsymbol{E}_{d,ts} \boldsymbol{E}_{\xi_k,ts} \bar{\mathcal{H}}_{j,k}^i \bar{\boldsymbol{P}}_{ts,k}^{ij-} (\bar{\mathcal{H}}_{i,k}^i)^T \boldsymbol{E}_{d,ts}^T \\
&\quad + \mathcal{C}_2 \boldsymbol{E}_{d,ts} \boldsymbol{E}_{\xi_k,ts} \bar{\mathcal{H}}_{j,k}^i \bar{\boldsymbol{P}}_{ts,k}^{j-} (\bar{\mathcal{H}}_{j,k}^i)^T \boldsymbol{E}_{\xi_k,ts}^T \boldsymbol{E}_{d,ts}^T \\
&\quad + \mathcal{C}_3 (\boldsymbol{E}_{\tau_k,ts} - \boldsymbol{E}_{d,ts}) \boldsymbol{\Psi}_k^{ij} (\boldsymbol{E}_{\tau_k,ts} - \boldsymbol{E}_{d,ts})^T \\
&\quad + \mathcal{C}_5 \boldsymbol{E}_{\tau_k,ts} (I - \boldsymbol{\gamma}_k^{ij}) \boldsymbol{\delta}_k^{ij} (I - \boldsymbol{\gamma}_k^{ij})^T \boldsymbol{E}_{\tau_k,ts}^T
\end{aligned}$$

6: Compute optimal Kalman gain:

$$\begin{aligned}
\boldsymbol{K}_k^i &= \left[\mathcal{C}_1 \bar{\boldsymbol{P}}_k^{i-} (\mathcal{H}_{i,k}^i)^T \boldsymbol{E}_d^T + \sum_{i_c \in \mathcal{M}} \boldsymbol{p}_{i_c} \boldsymbol{E}_{i_c} \bar{\boldsymbol{P}}_k^{ij-} (\bar{\mathcal{H}}_{j,k}^i)^T \boldsymbol{E}_{i_c}^T \boldsymbol{E}_d^T \right] (S_k^{ij})^{-1} \\
\boldsymbol{K}_{ts,k}^i &= \left[\mathcal{C}_1 \bar{\boldsymbol{P}}_{ts,k}^{i-} (\mathcal{H}_{i,k}^i)^T \boldsymbol{E}_{d,ts}^T + \boldsymbol{E}_{\xi_k,ts} \bar{\boldsymbol{P}}_{ts,k}^{ij-} (\bar{\mathcal{H}}_{j,k}^i)^T \boldsymbol{E}_{\xi_k,ts}^T \boldsymbol{E}_{d,ts}^T \right] (S_{ts,k}^{ij})^{-1}
\end{aligned}$$

7: Update the filter with the current measurement:

$$\begin{aligned}
\hat{\bar{\boldsymbol{x}}}_k^{i+} &= \hat{\bar{\boldsymbol{x}}}_k^{i-} + \boldsymbol{K}_k^i \Upsilon_k^{ij} \\
\hat{\bar{\boldsymbol{x}}}_{ts,k}^{i+} &= \hat{\bar{\boldsymbol{x}}}_{ts,k}^{i-} + \boldsymbol{K}_{ts,k}^i \Upsilon_{ts,k}^{ij}
\end{aligned}$$

8: Update the error covariance:

$$\begin{aligned}
\bar{\boldsymbol{P}}_k^{i+} &= \bar{\boldsymbol{P}}_k^{i-} - \boldsymbol{K}_k^i S_k^{ij} (\boldsymbol{K}_k^i)^T \\
\bar{\boldsymbol{P}}_k^{ij+} &= \bar{\boldsymbol{P}}_k^{ij-} - \boldsymbol{K}_k^i S_k^{ij} (\boldsymbol{K}_k^j)^T \\
\bar{\boldsymbol{P}}_{ts,k}^{i+} &= \bar{\boldsymbol{P}}_{ts,k}^{i-} - \boldsymbol{K}_{ts,k}^i S_{ts,k}^{ij} (\boldsymbol{K}_{ts,k}^i)^T \\
\bar{\boldsymbol{P}}_{ts,k}^{ij+} &= \bar{\boldsymbol{P}}_{ts,k}^{ij-} - \boldsymbol{K}_{ts,k}^i S_{ts,k}^{ij} (\boldsymbol{K}_{ts,k}^j)^T
\end{aligned}$$

9: $k \leftarrow k + 1$

V Case study

V.1 Simulation Results

Simulations of the multi-robot cooperative localization are carried out to demonstrate the relation between the localization results and time delays and verify the performance of the proposed algorithms. Consider four mobile robots whose equations of motion are described by:

$$\begin{cases} x^i(t+1) = x^i(t) + \Delta t(v_m^i(t)\cos(\phi^i(t) + \Delta\phi^i(t)) \\ y^i(t+1) = y^i(t) + \Delta t(v_m^i(t)\sin(\phi^i(t) + \Delta\phi^i(t)) \\ \phi^i(t+1) = \phi^i(t) + \Delta t\omega^i(t) \qquad i \in \{1,2,3,4\} \end{cases} \tag{4.63}$$

where $[x^i(t), y^i(t), \phi^i(t)]^T$ represent the position and orientation of robots, $v_m^i(k)$ and $\omega^i(t)$ denote the linear and angular velocity, b is the distance between the wheels, $\Delta\phi^i(t)$ represent the uncertainty on the orientation. The control input of each robot i is the form of:

$$u^i(t) = \begin{bmatrix} \Delta L^i & \Delta R^i \end{bmatrix}^T \tag{4.64}$$

Where ΔL^i and ΔR^i are the distance moved by the left and the distance moved by the right wheels, respectively. ΔL^i and ΔR^i can be obtained by $\Delta t v_m^i(t) = \frac{\Delta R^i + \Delta L^i}{2}$ and $\Delta\phi^i(t) = \frac{\Delta R^i - \Delta L^i}{2b}$. Note that the control input $u^i(t)$ is measured from the odometry sensor. Also, relative pose measurements, i.e., range and bearing, of robot i relative to robot j are given by:

$$z^{ij}(t) = \begin{bmatrix} \rho_{ij}(t) \\ \theta_{ij}(t) \end{bmatrix} = \begin{bmatrix} \sqrt{(x^i(t) - x^j(t))^2 + (y^i(t) - y^j(t))^2} \\ \arctan(\frac{y^i(t) - y^j(t)}{x^i(t) - x^j(t)}) \end{bmatrix} \tag{4.65}$$

where:

$\rho_{ij}(t)$ is the range of the robot i relative to the robot j.

$\theta_{ij}(t)$ is the bearing of the robot i relative to the robot j.

We assume that additive white-Gaussian noise affects both the control input $u^i(t)$ and the relative pose measurements $z^{ij}(t)$. In mobile robots, these noises represent the impact of model uncertainties associated with the odometry sensor and camera. We will consider the following parameters in our simulations:

$$\begin{aligned} &u^i(t) = [\Delta L^i; \Delta R^i] = [0.25m; 0.25m], \\ &Q^i = \mathrm{diag}([(0.05\Delta L^i)^2; (0.05\Delta R^i)^2]), \\ &R^{ij} = \mathrm{diag}([0.1m^2; 0.1rad^2]) \end{aligned}$$

We assume that when robots $i \in \{1,2,3,4\}$ move in a random trajectory, the rest of the robots remain stationary. We choose a random control input for each of

the moving robots to show the robustness of the DECL algorithm to localize robots under random trajectories. In our simulations, we compare the following trajectories: 1) the actual pose of each robot; 2) pose estimation from the propagation of the filter; 3) pose estimation from the proposed DECL algorithm under random delays. We first examine the performance of the dead-reckoning method where each robot employs the wheel encoders to propagate the local filter independently and there is no exchange of range-bearing measurements between the four robots. As seen in Fig. 4.2 and Fig. 4.3, the position estimation for each robot using the dead-reckoning method does not accurately track the ground truth.

Non-Time-Stamped Mechanism

Fig. 4.2 shows the localization results of four mobile robots under time delays and event-triggered mechanisms. We consider a scenario in which packets are transmitted in a non-time-stamped technology, therefore the local filter for each robot does not have information on the delays incurred by each signal, and relies only on their probability at each time. In Fig. 4.2(a) and (b), we compare the performance of the proposed DECL algorithm (2) with the classical CL algorithm considering the one-step random delayed measurements as follows:

$$\tilde{\boldsymbol{z}}_k^{ij} = \boldsymbol{\theta}_{0,k}\bar{\boldsymbol{z}}_k^{ij} + (1-\boldsymbol{\theta}_{0,k})\boldsymbol{\theta}_{1,k}\bar{\boldsymbol{z}}_{k-1}^{ij} \tag{4.66}$$

where parameters $\theta_{0,k}$ and $\theta_{1,k}$ are Bernoulli-distributed with the rates of $\bar{\theta_0} = 0.1$ and $\bar{\theta_1} = 1$, respectively. As Fig. 4.2(a) and (b) show, the proposed filter has better accuracy than the classical filter. Then, we consider two-step random delayed measurements as follows:

$$\tilde{\boldsymbol{z}}_k^{ij} = \boldsymbol{\theta}_{0,k}\bar{z}_k^{ij} + (1-\boldsymbol{\theta}_{0,k})\boldsymbol{\theta}_{1,k}\bar{\boldsymbol{z}}_{k-1}^{ij} + (1-\boldsymbol{\theta}_{0,k})(1-\boldsymbol{\theta}_{1,k})\boldsymbol{\theta}_{2,k}\bar{\boldsymbol{z}}_{k-2}^{ij} \tag{4.67}$$

where parameters $\boldsymbol{\theta}_{0,k}$, $\boldsymbol{\theta}_{1,k}$ and $\boldsymbol{\theta}_{2,k}$ are Bernoulli-distributed with the rates of $\bar{\boldsymbol{\theta}_0} = 0.8$, $\bar{\boldsymbol{\theta}_1} = 0.99$ and $\bar{\boldsymbol{\theta}_2} = 1$ respectively. As Fig. 4.2(c) and (d) show, the proposed DECL algorithm 1 has better performance than the classical CL algorithm. To compare the performance of the proposed DECL with classical CL we use position error for each robot. The magnitude of position error for each robot at time k is given by $\mathrm{SE}_{\mathrm{k}}^{\mathrm{i}} = \sqrt{(x_k^i - \hat{x}_k^{i+})^2 + (y_k^i - \hat{y}_k^{i+})^2}$ where x_k^i and $\hat{x}_k^{i+}$ are the actual and estimated position in the x-axis, respectively, and y_k^i and $\hat{y}_k^{i+}$ are the actual and estimated position in the y-axis, respectively. According to Fig. 4.2(e), we conclude that our proposed algorithm (2) outperforms the classical CL under random

delays. We also evaluate the performance of the DECL algorithm with the proposed event-triggered mechanism in terms of the amount of information transmission and localization accuracy. Fig. 4.4(a)-(c) shows the localization of robots under different triggering conditions and considering the random delays. Also, Fig. 4.4(d)-(i) shows the triggering instance for the range and bearing of robots under different triggering conditions. Finally, we compare the position error of robots under different triggering conditions and consider the random delays in Fig. 4.4(j). Our analysis shows that as the parameters of the event-triggering mechanism increase, the average transmission rate of the relative measurements significantly reduces while localization error slightly increases. Therefore, it is important to tune the parameters of the event-triggered mechanism to achieve a balance between localization quality and communication rate.

Time-Stamped Mechanism

In this case, we consider a scenario in which communication packets are transmitted using time-stamped technology. In this case, the local filter has perfect knowledge of the delay at each time. Fig. 4.3(a)-(c) shows localization results without time delays, one-step, two-step, and three-step delayed measurements. Also, Fig. 4.3(e) shows that larger step delays cause a larger position error for each robot.

V.2 Experimental Validation

In this part, we validate our theoretical results by performing experiments on a real robotic system. The experimental setup (see Fig. 4.8) consists of a gaming laptop, a fleet of 4 e-puck2 mobile robots equipped with an ArUco tag, ZED stereo camera. We implement our algorithm on a robot operating system (ROS). The computer running ROS software can also handle the communication between the robots and the camera. Each e-puck2 robot in the team moves in a circular trajectory (see Fig. 4.7) and generates time-stamped odometry and inertial measurements used in the filter propagation step. The overhead ZED camera with the help of ArUco tags and the ArUco image processing library [117] generates the reference trajectory and also provides time-stamped range-bearing measurements. The accuracy of the range and bearing measurements based on computer vision is 0.05 m and 7 degrees, respectively. Using the ROS package [119] we synchronize timestamps to all odometry data, range and bearing measurements. Each e-puck2 robot runs several

ROS nodes simultaneously, including programs to propagate and update the local filter using time-stamped odometry and inertial and range-bearing measurements. These ROS nodes communicate through transmission control protocol (TCP). The robots communicate with the computer via Bluetooth. Since communication with robots via Bluetooth is done sequentially, the delays are different for each robot. Therefore, time delays are considered as an uncertainty term $\Delta d^i \in [0.15s, 0.195s]$ [36], $i \in \{1, 2, 3, 4\}$. Since the packets transmitted by the sensors are time-stamped, the filter has knowledge of the time delays. In our experiment, we compare the following trajectories: 1) Actual pose of each robot provided by overhead ZED camera; 2) pose estimation from odometry sensor; 3) pose estimation from the proposed DECL algorithm under random delays. Fig. 4.5 and Fig. 4.6 show the localization results of our experiments. The overhead camera provides the reference trajectory to examine the performance of the local filter. Note that the odometry sensor does not provide the reliable estimation of actual position of robots since odometry sensor translates the turn of the robot's wheels into the traveled distance and highly sensitive to the slippage. Fig. 4.5(a) show the estimated position of the robots (using DECL Algorithm) with time delays and a *time-triggered* mechanism which the range-bearing measurements improve the localization accuracy. In the implementation of the *event-triggering* mechanism, the overhead camera is equipped with an event-based scheduler which transmits the range and bearing measurements to each robot based on the triggering condition (4.16). Moreover, two triggering conditions are employed, one is for range and the other is for bearing. If the triggering condition for either the range or bearing is satisfied, then the robot receives the current range or bearing measurement from the overhead camera. Fig. 4.5(b)-(c) shows the results of the same algorithm but using the *event-triggered* mechanism proposed here. We also compare the position error of each robot for different triggering conditions considering inherent time delays in Fig. 4.6(a). Also, the triggering instances for the range and bearing of robots for different triggering conditions can be shown in Fig. 4.6(b)-(g). It can be seen that as the parameters of the event-triggered mechanism increase, the average communication rate of the range and bearing measurements are significantly reduced while slightly sacrificing localization accuracy. The event-triggering parameters were tuned such that the estimation error remains bounded despite time delays while the number of transmission packets between the sensor and filter is reduced.

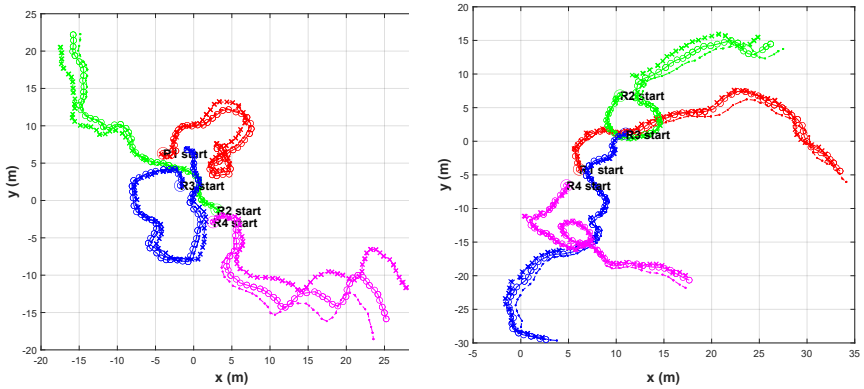

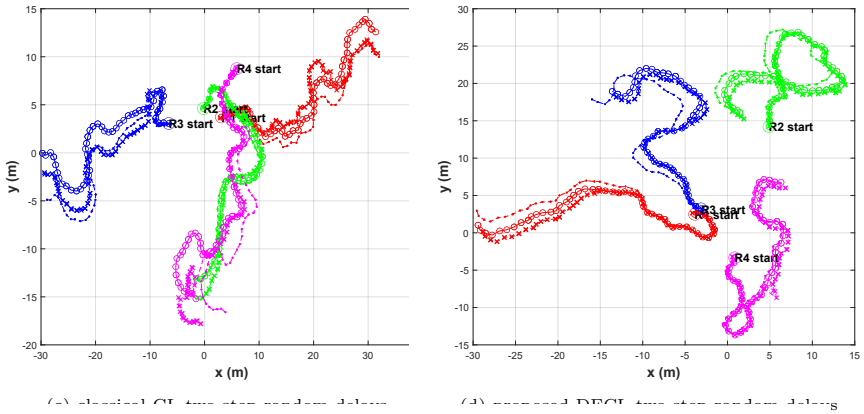

(c) classical CL two-step random delays (d) proposed DECL two-step random delays

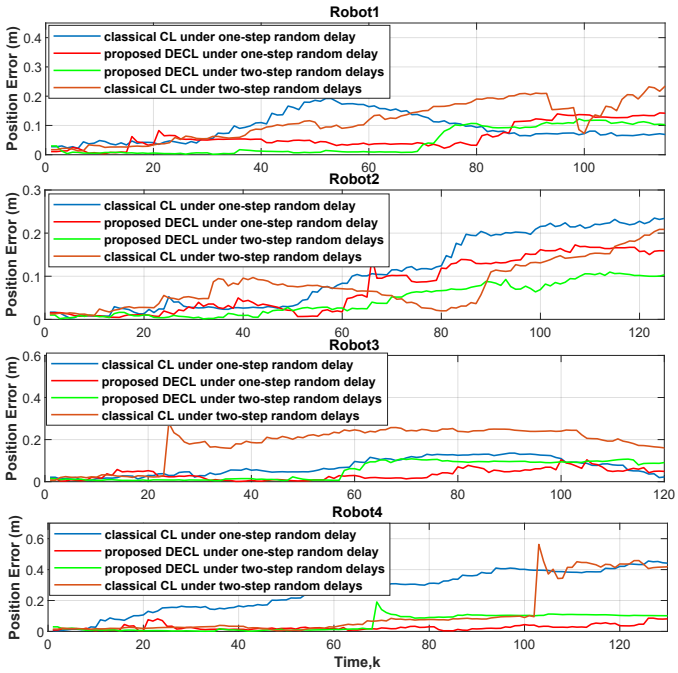

(e) position error under different scenarios

Figure 4.2: (a), (c). Localization of 4 robots by classical CL algorithm under the event-triggered mechanism and with time delays (non-time-stamped technology) (a) one-step random delay, (c) two-step random delays, (b), (d) Localization of 4 robots by proposed DECL algorithm (1) under the event-triggered mechanism and with time delays (b) one-step random delay, (d) two-step random delays, solid-o shows the ground truths, broken-dot shows the dead-reckoning and broken-x shows the EKF estimates of 4 robots, (e) the position error of each robot under different scenarios

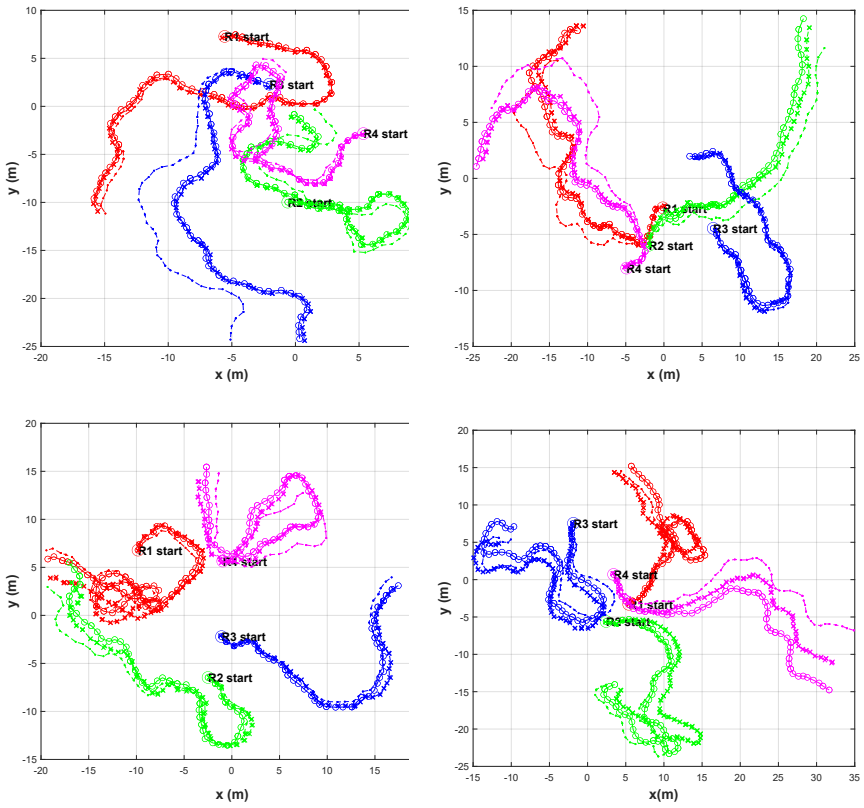

(c) proposed DECL two-step random delays

(d) proposed DECL three-step random delays

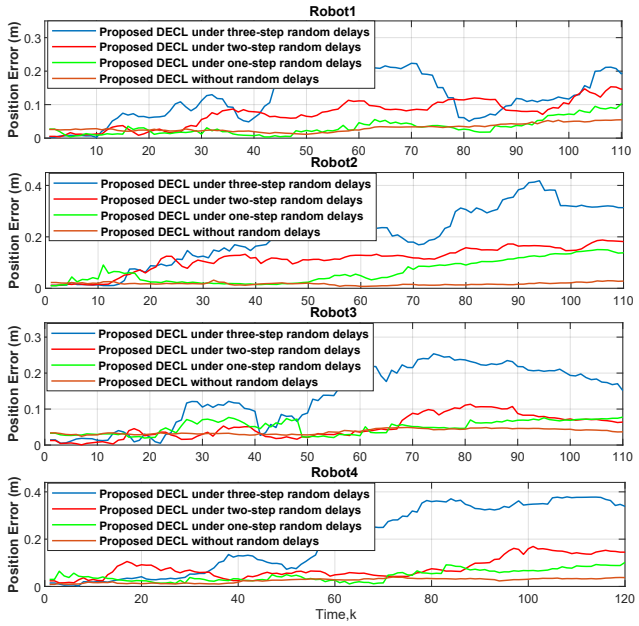

(e) position error under different scenarios

Figure 4.3: (a) Localization of 4 robots by proposed DECL algorithm under the event-triggered mechanism and without random delays (time-stamped technology); Localization of 4 robots by proposed DECL algorithm under the event-triggered mechanism and with time delays (time-stamped technology); (b) one-step random delay; (c) two-step random delays; (d) three-step random delays; solid-o shows the ground truths, broken-dot shows the dead-reckoning and broken-x shows the EKF estimates of 4 robots; (e) the position error of each robot using proposed DECL algorithm under different scenarios

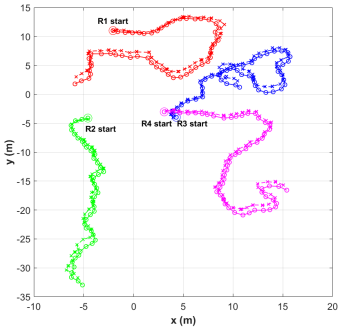

(a) localization of robots under time-triggered mechanism

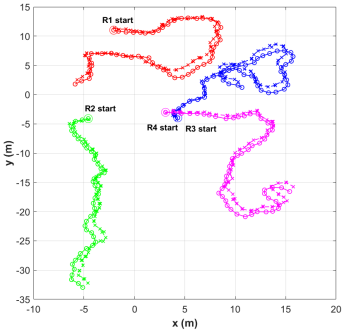

(b) localization of robots under event-triggered mechanism ($\alpha_{ij} = 0.05$ & $\beta_{ij} = 0.05$ for range and $\alpha_{ij} = 0.05$ & $\beta_{ij} = 0.05$ for bearing)

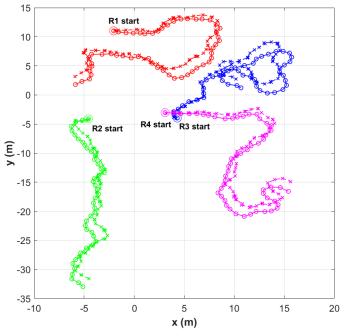

(c) localization of robots under event-triggered mechanism ($\alpha_{ij} = 0.07$ & $\beta_{ij} = 0.07$ for range and $\alpha_{ij} = 0.1$ & $\beta_{ij} = 0.1$ for bearing)

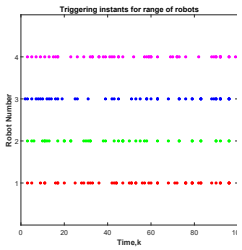

(d) triggering instances for a range of robots (case a)

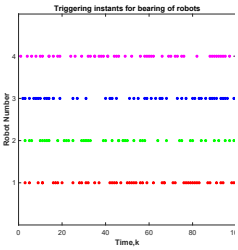

(e) triggering instances for the bearing of robots (case a)

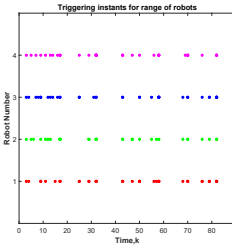

(f) triggering instances for a range of robots (case b)

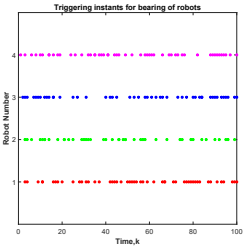

(g) triggering instances for bearing of robots (case b)

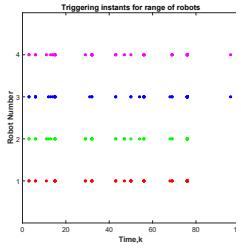

(h) triggering instances for a

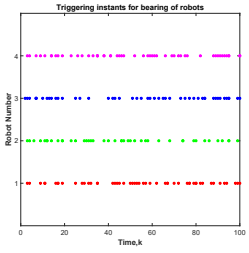

(i) triggering instances for

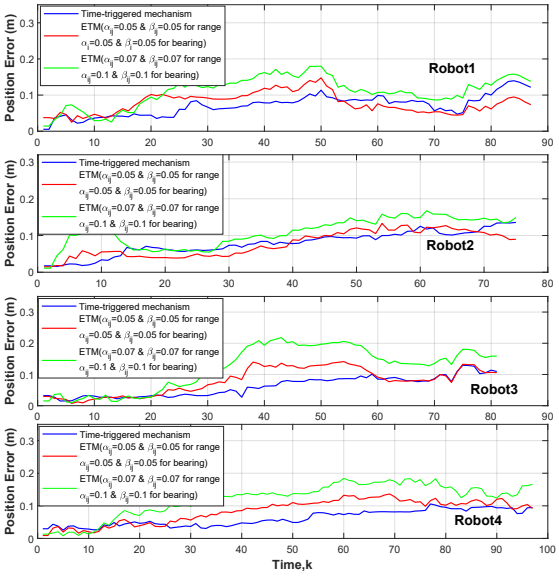

(j) The position error of each robot using the proposed DECL algorithm under different triggering mechanisms and considering random delays

Figure 4.4: Localization of 4 robots by proposed DECL algorithm under different triggering conditions considering random delays; solid-o shows the ground-truths and broken-x shows the EKF estimates of 4 robots.

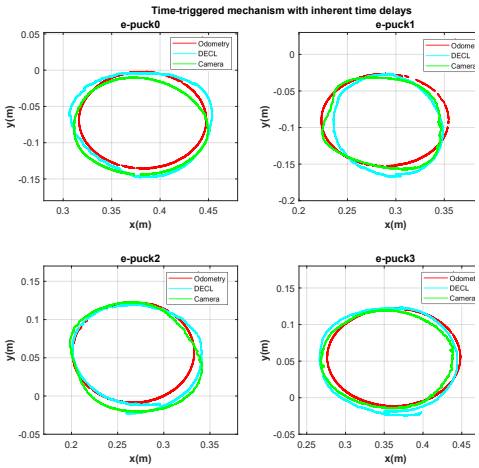

(a) localization of robots under time-triggered mechanism

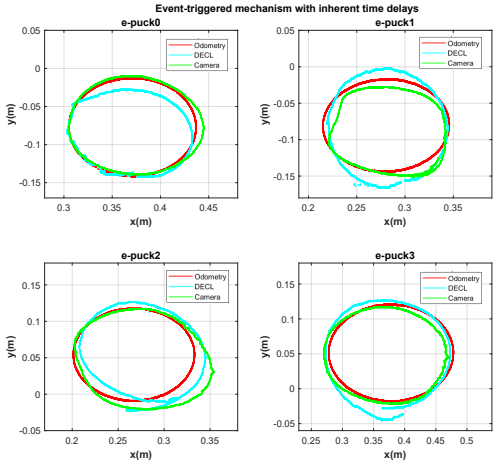

(b) localization of robots under event-triggered mechanism ($\alpha_{ij} = 0.05$ & $\beta_{ij} = 0.01$ for range and $\alpha_{ij} = 0.05$ & $\beta_{ij} = 0.01$ for bearing)

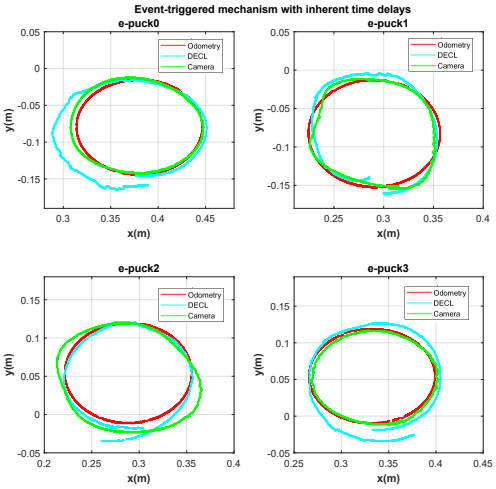

(c) localization of robots under event-triggered mechanism ($\alpha_{ij} = 0.1$ & $\beta_{ij} = 0.1$ for range and $\alpha_{ij} = 0.1$ & $\beta_{ij} = 0.1$ for bearing)

Figure 4.5: Trajectories of the e-puck2 mobile robots; the position estimated from overhead ZED camera (the curve indicated by green), the position estimated from odometry sensor (the red curve), and the position estimated by DECL Algorithm considering time-stamped information (the blue curve) under different triggering conditions and with inherent time delays

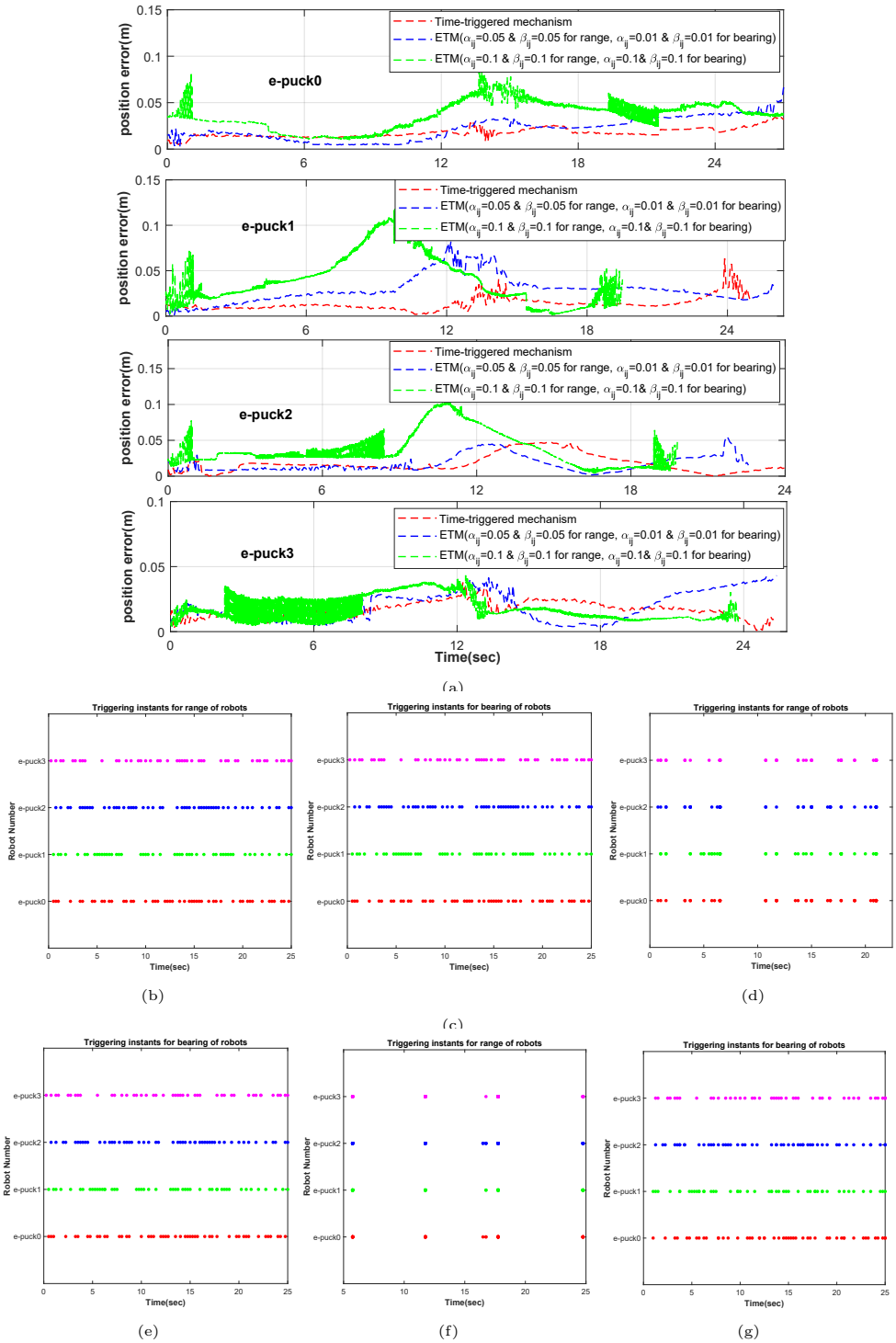

Figure 4.6: (a) The estimated position error of robots under different triggering conditions considering inherent time delays; (b)-(c) triggering instance for range and bearing of robots in time-triggered mechanism; (d)-(e) triggering instances for range and bearing of robots under event-triggered mechanism ($\alpha_{ij} = 0.05$ & $\beta_{ij} = 0.01$ for range and $\alpha_{ij} = 0.05$ & $\beta_{ij} = 0.01$ for bearing); (f)-(g) triggering instances for range and bearing of robots under event-triggered mechanism ($\alpha_{ij} = 0.1$ & $\beta_{ij} = 0.1$ for range and $\alpha_{ij} = 0.1$ & $\beta_{ij} = 0.1$ for bearing)

(a) (b) (c)

Figure 4.7: Experimental setup including (a) e-puck2 robot, (b) gaming laptop (equipped with Nvidia GPU), (c) overhead ZED camera,

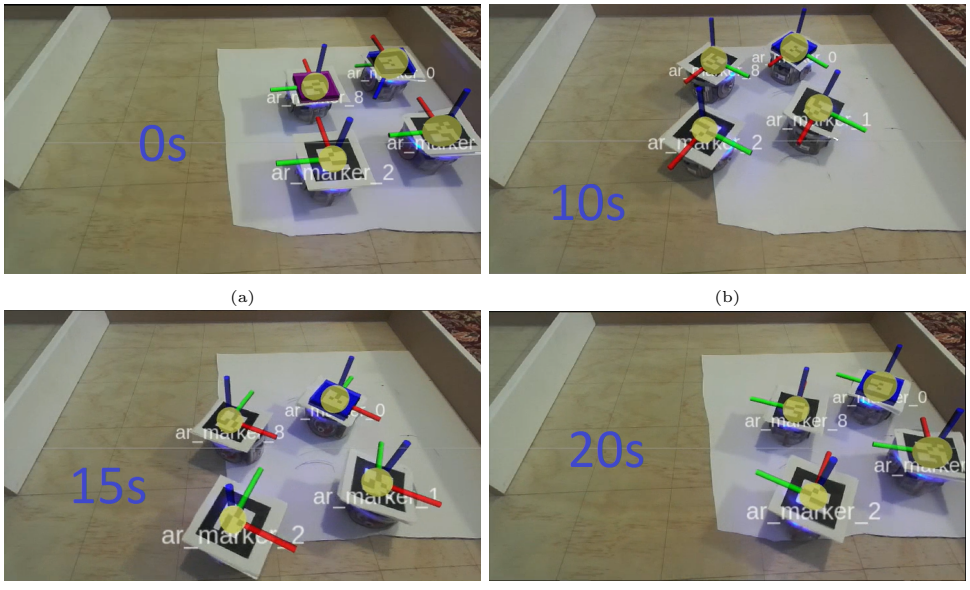

(a) (b) (c) (d)

Figure 4.8: Each e-puck2 robot move simultaneously in a counter clock-wise direction along a circle path. Also, the overhead ZED camera provide the relative measurement with the help of ArUco tags and image processing library.

Chapter 5

A Secure Decentralized Event-Triggered Cooperative Localization In Multi-Robot Systems Under Cyber Attack

I Introduction

In this chapter, we study the problem of a secure decentralized event-triggered cooperative localization (SDECL) for a team of mobile robots in an adversarial environment, where the objective is to perform localization in the presence of a malicious attacker. We consider a scenario in which the attacker is able to attack the communication channels between the exteroceptive sensors and filter of the robot and between two robots independently. First, we design a secure decentralized event-triggered cooperative localization in the multi-robot system against random Denial of Service (DoS) and False Data Injection (FDI) attacks. Then, we provide sufficient conditions that ensure the resilience and convergence of the proposed algorithm when the attacker signal rate is bounded. Simulation results show that by properly tuning the parameters of the event-triggered mechanism and considering the bounded attack rate, the proposed algorithm is resilient against cyber attacks. Also, experimental results using four e-puck2 mobile robots have demonstrated the effectiveness of the proposed method.

The rest of this work is organized as follows. Section II contains the dynamic of multi-robot systems, multi-robot interaction and attack strategy, problem statement, and event-triggered data transferring mechanism. In section III, we design an SDECL for multi-robot systems in the presence of a cyber attack. In Section IV, we

analyze the stochastic boundedness of the estimation error in the mean square for the SDECL algorithm under cyber attacks. In Section V we present the case study including the simulation and experimental results. Finally, Section VI contains some conclusions of the results.

Table 5.1: NOTATION

Notations	Description
$\mathbb{E}[.]$ or $\mathbb{E}\{.\}$	expectation of the random variable
$\mathrm{Tr}\{.\}$	trace of the matrix
diag(.)	block diagonal matrix
$\|.\|$	Euclidean norm of the vector
$\mathrm{Prob}\{X\}$	occurrence probability of event X
X^T	transpose of matrix X
X^{-1}	inverse of matrix X
$\mathbb{R}^{n^i}$	set of n^i-dimensional real vectors
$\mathbb{S}^{n^i}$	set of $n^i \times n^i$ real matrices
I	identity matrix of appropriate dimensions
i and j	identity of robot i and robot j
$\boldsymbol{x}^i(k)$	state vector of the robot i (position and orientation)
$\boldsymbol{u}^i_m(k)$	control input of robot i
$\boldsymbol{\eta}_i(k)$	process noise from control input of robot i
$\boldsymbol{\nu}_{ij}(k)$	measurement noise from exteroceptive sensors for pair (i,j)
$a_{ij}(k)$	indicator of interaction between robots
$\mathcal{N}_{ci}$	set of neighbors of robot i within certain range
$\boldsymbol{z}_{ij}(k)$	relative measurement taken by robot i from robot j
$\boldsymbol{Q}_i(k)$	covariance of $\boldsymbol{\eta}_i(k)$
$\boldsymbol{R}_{ij}(k)$	covariance of $\boldsymbol{\nu}_{ij}(k)$
$\boldsymbol{\mathcal{A}}_i(k)$, $\boldsymbol{G}_i(k)$	system matrix of robot i
$\boldsymbol{H}^i_i(k)$	sensor measurement matrix of robot i
$\boldsymbol{H}^i_j(k)$	sensor measurement matrix of pair (i,j)
l	l number of attacks launched to the communication links
$\boldsymbol{\alpha}^l_{ij}(k)$, $\boldsymbol{\beta}^l_{ij}(k)$	random variables are employed (for sensor measurement) to determine whether the (i,j)th communication channel (sensor-filter) is attacked by DoS and FDI at time k
$\boldsymbol{\zeta}^l_{ij}(k)$, $\boldsymbol{\lambda}^l_{ij}(k)$	random variables are employed (for propagated state) to determine whether the (i,j)th communication channel (filter-filter) is attacked by DoS and FDI at time k
$\boldsymbol{\sigma}^l_{ij}(k)$, $\boldsymbol{\tau}^l_{ij}(k)$	random variables are employed (for error covariance) to determine whether the (i,j)th communication channel (filter-filter) is attacked by DoS and FDI at time k
$\hat{\boldsymbol{x}}^{i-}(k)$	predicted state of robot i
$\tilde{\boldsymbol{x}}^{i-}(k)$	predicted state error of robot i
$\hat{\boldsymbol{x}}^{i+}(k)$	estimation of robot i
$\tilde{\boldsymbol{x}}^{i+}(k)$	estimation error of robot i
$\boldsymbol{P}^{i-}(k)$	predicted state error covariance of robot i
$\boldsymbol{P}^{i+}(k)$	estimation error covariance of robot i
$\boldsymbol{P}^{ij-}(k)$	predicted state error covariance between robots i and j
$\boldsymbol{P}^{ij+}(k)$	estimation error covariance between robots i and j
$\boldsymbol{K}_i(k)$	Kalman gain
Θ_{ij}, Λ_{ij}	event-triggered parameters for pair (i,j)
$\boldsymbol{\gamma}_{ij}(k)$	decision variable (event-detector) is used to decide whether or not the current relative measurement transmission occurs
ψ_{ij}	attack detector parameter for pair (i,j)
$\boldsymbol{d}_{ij}(k)$	decision variable (attack detector) is used to decide whether or not the packets transmit to the neighbors
$\boldsymbol{\xi}^l_{ij}(k)$	attacker signal for (i,j)th communication channel (sensor-filter)
$\boldsymbol{\varrho}^l_{ij}(k)$	attacker signal for (i,j)th communication channel (filter-filter)

II Problem statement and Preliminaries

II.1 Dynamic of Multi-Robot Systems

We consider a team of N mobile robots moving in the two-dimensional space. The general nonlinear motion of each robot, $i \in \vartheta = \{1, 2, ..., N\}$, is described as follows ([29]):

$$\boldsymbol{x}^i(k) = \boldsymbol{f}^i(\boldsymbol{x}^i(k-1), \boldsymbol{u}^i_m(k-1)), \tag{5.1}$$

where the state vector $\boldsymbol{x}^i(k) = [x^i(k), y^i(k), \theta^i(k)]^T$ contains the position and orientation of each robot with respect to global map and $\boldsymbol{u}^i_m$ is the control input. Each robot $i \in \vartheta$ uses odometry or inertial sensors to measure its linear velocity $\boldsymbol{u}^i_m = \boldsymbol{u}^i + \boldsymbol{\eta}_i$, where $\boldsymbol{u}^i$ represents the actual velocity and $\boldsymbol{\eta}_i$ is corresponding white-Gaussian noise. Each robot detects uniquely the other robots in the team using exteroceptive sensors and takes relative measurements with respect to them, including range or bearing or a combination of these measurements. The relative measurement is taken by robot i from robot j at a time k is described by ([29])

$$\boldsymbol{z}_{ij}(k) = \boldsymbol{h}_{ij}(\boldsymbol{x}^i(k), \boldsymbol{x}^j(k)) + \boldsymbol{\nu}_{ij}(k), \tag{5.2}$$

where $\boldsymbol{h}_{ij}(\boldsymbol{x}^i, \boldsymbol{x}^j)$ is the measurement model and $\boldsymbol{\nu}_{ij}$ is measurement noise. The noises $\boldsymbol{\eta}_i$ and $\boldsymbol{\nu}_{ij}$ are independent white-Gaussian processes with known positive definite variances $\boldsymbol{Q}_i(k) = \mathbb{E}[\boldsymbol{\eta}_i(k)\boldsymbol{\eta}_i(k)^T]$ and $\boldsymbol{R}_{ij}(k) = \mathbb{E}[\boldsymbol{\nu}_{ij}(k)\boldsymbol{\nu}_{ij}(k)^T]$. All noises are assumed to be mutually uncorrelated.

II.2 Multi-Robot Interaction and Attack Strategy

The interaction topology of robots is shown in Fig. 5.2. We assume that each robot can sense the other robots in the team and take relative measurements $\boldsymbol{z}_{ij}(k)$ and exchange information packets (propagated state and error covariance) with its neighboring robots residing within communication range. Since we have a set of N robots, we consider the interaction topology $\mathcal{G} = (\mathcal{V}, \mathcal{E}, \mathcal{L})$, where $\mathcal{V} = \{v_1, ..., v_N\}$ is the set of nodes in the graph. For each node v_i, the index $i \in \{1, 2, ..., N\}$ is the unique identifier of the agent i. $\mathcal{E}$ represents the set of information links of the propagated estimates (state and error covariance) exchange between robots. $\mathcal{L} = \lfloor a_{ij} \rfloor \in \mathbb{R}^{N \times N}$ is the adjacency matrix of the propagated estimates (state and error covariance) interaction topology. When $a_{ij} > 0$, robot i is able to receive information packets (propagated state and error covariance) from robot j, while $a_{ij} = 0$ indicates that there is no information flow from the robot j to robot i.

Notice that the resulting network topology is time-varying and reflects the practical scenario in a multi-robot system where robots can randomly sense the other robots in the team only within the reach of the exteroceptive sensors. Notice also that in this setup, measurement and communication links are identical. A robot j can exchange information packets with a neighbor robot i, only within a certain communication range with the robot i belongs to set $\mathcal{N}_{ci} = \{j \in \mathcal{V} : (i,j) \in \mathcal{E}\}$.

We consider that both DoS and FDI attacks can be randomly launched into the communication network and can arbitrarily block or manipulate sensor measurements and information exchange between robots. We assume that the number of attacks affecting the network is limited, in order to reflect real-world adversaries. As Fig. 5.2 shows the attacker launch randomly $l \in \Gamma = \{1, 2, .., M\}$ number of attacks at each time to the communication links (sensor measurements and estimates), where M is the maximum number of attacked links.

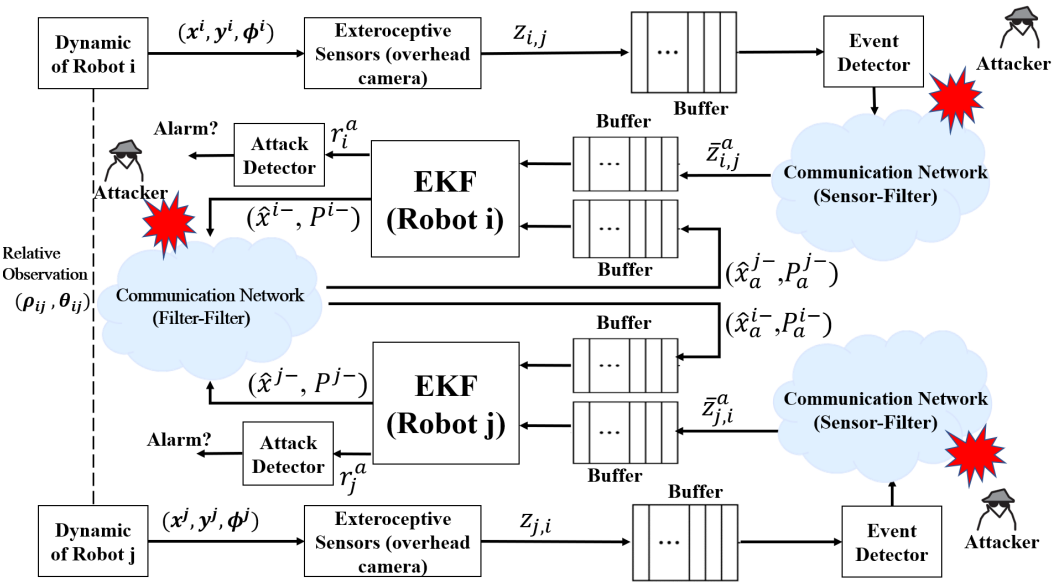

Figure 5.1: Block diagram of secure decentralized event-triggered cooperative localization (SDECL) algorithm under cyber attacks

II.3 Problem Statement

Fig. 5.1 shows the block diagram of the proposed SDECL algorithm. This scheme is based on our previous work [62] but has been modified to include cyber-attacks. Here, each robot i detects the other robots in the team using the exteroceptive sensors. The relative measurement $\boldsymbol{z}_{ij}(k)$ taken by each robot i are sent to the event detector which determines whether or not the current sensor measurement is to be

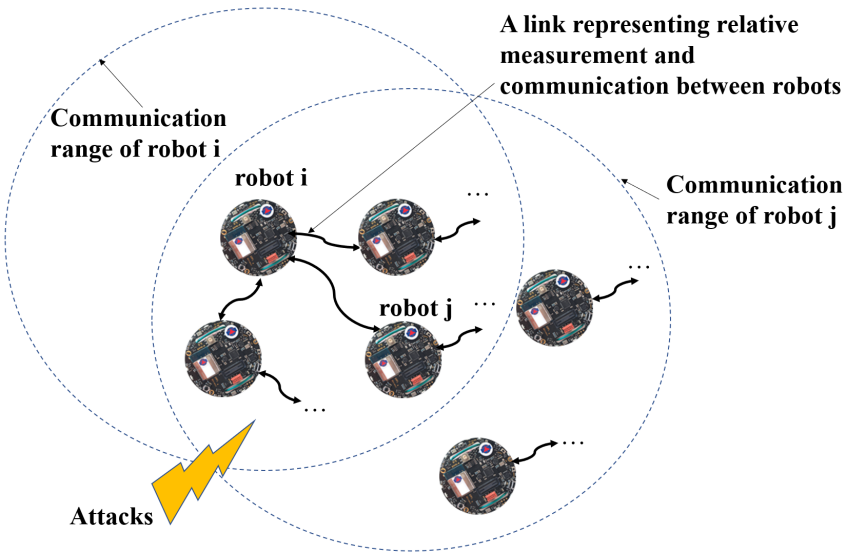

Figure 5.2: The interaction topology of robots under cyber attacks

transmitted to the filter over the unreliable communication network, based on a triggering rule. The relative measurement transmitted by the event detector to the corresponding filter may be tampered by malicious attackers. Both DoS and FDI attacks can block and contaminate the sensor measurements through the wireless networks which is described by [129]:

$$\bar{\boldsymbol{z}}^a_{ij}(k) = \boldsymbol{\alpha}^l_{ij}(k)\bar{\boldsymbol{z}}_{ij}(k) + (1 - \boldsymbol{\alpha}^l_{ij}(k))\boldsymbol{\beta}^l_{ij}(k)\boldsymbol{\xi}^l_{ij}(k) \tag{5.3}$$

where the random variables $\boldsymbol{\alpha}^l_{ij}(k)$ and $\boldsymbol{\beta}^l_{ij}(k)$ are mutual independent Bernoulli distributed white sequences taking values of 0 or 1 with the following probabilities:

$$\text{Prob}\{\boldsymbol{\alpha}^l_{ij}(k) = 1\} = \bar{\boldsymbol{\alpha}}^l_{ij}, \quad \text{Prob}\{\boldsymbol{\alpha}^l_{ij}(k) = 0\} = 1 - \bar{\boldsymbol{\alpha}}^l_{ij}$$

$$\text{Prob}\{\boldsymbol{\beta}^l_{ij}(k) = 1\} = \bar{\boldsymbol{\beta}}^l_{ij}, \quad \text{Prob}\{\boldsymbol{\beta}^l_{ij}(k) = 0\} = 1 - \bar{\boldsymbol{\beta}}^l_{ij}$$

Considering the different values of the random variables $\boldsymbol{\alpha}^l_{ij}(k)$ and $\boldsymbol{\beta}^l_{ij}(k)$ it is easy to see that the measurement model (5.3) comprises of three cases: (1) when $\boldsymbol{\alpha}^l_{ij}(k) = 1$, the filter receives the sensor signals; (2) when $\boldsymbol{\alpha}^l_{ij}(k) = 0$ and $\boldsymbol{\beta}^l_{ij}(k) = 1$, the system suffers from FDI attack; and (3) when $\boldsymbol{\alpha}^l_{ij}(k) = 0$ and $\boldsymbol{\beta}^l_{ij}(k) = 0$, the system is subject to DoS attack [129]. Note that the adversary signal $\boldsymbol{\xi}^l_{ij}(k)$ is bounded, e.g., $\mathbb{E}\{\boldsymbol{\xi}^l_{ij}(k)\boldsymbol{\xi}^l_{ij}(k)^T\} \leq \bar{\boldsymbol{\xi}}^l_{ij}$. Also, we assume that the random variables $\boldsymbol{\alpha}^l_{ij}(k)$ and $\boldsymbol{\beta}^l_{ij}(k)$ are independent of the system variables $\boldsymbol{x}^i(k)$, $\boldsymbol{u}^i_m(k)$, $\boldsymbol{\eta}_i(k)$ and $\boldsymbol{\nu}_{ij}(k)$.

Also, all robots exchange information regarding their propagated estimates (namely; states and error covariance) across the unprotected communication channel. The

exchanged information (propagated state and error covariance) between filters considering both DoS and FDI attacks is described by:

$$\hat{\boldsymbol{x}}_a^{j-}(k) = \boldsymbol{\zeta}_{ij}^l(k)\hat{\boldsymbol{x}}^{j-}(k) + (1 - \boldsymbol{\zeta}_{ij}^l(k))\boldsymbol{\lambda}_{ij}^l(k)\boldsymbol{\varrho}_{ij}^l(k) \tag{5.4}$$

$$\boldsymbol{P}_a^{j-}(k) = \boldsymbol{\sigma}_{ij}^l(k)\boldsymbol{P}^{j-}(k) + (1 - \boldsymbol{\sigma}_{ij}^l(k))\boldsymbol{\tau}_{ij}^l(k)\boldsymbol{\upsilon}_{ij}^l(k) \tag{5.5}$$

where the random variables $\boldsymbol{\zeta}_{ij}^l(k)$, $\boldsymbol{\lambda}_{ij}^l(k)$, $\boldsymbol{\sigma}_{ij}^l(k)$ and $\boldsymbol{\tau}_{ij}^l(k)$ are mutually independent Bernoulli distributed white sequences taking values of 0 or 1 with the following probabilities:

$$\text{Prob}\{\boldsymbol{\zeta}_{ij}^l(k) = 1\} = \bar{\boldsymbol{\zeta}}_{ij}^l, \quad \text{Prob}\{\boldsymbol{\zeta}_{ij}^l(k) = 0\} = 1 - \bar{\boldsymbol{\zeta}}_{ij}^l$$

$$\text{Prob}\{\boldsymbol{\lambda}_{ij}^l(k) = 1\} = \bar{\boldsymbol{\lambda}}_{ij}^l, \quad \text{Prob}\{\boldsymbol{\lambda}_{ij}^l(k) = 0\} = 1 - \bar{\boldsymbol{\lambda}}_{ij}^l$$

$$\text{Prob}\{\boldsymbol{\sigma}_{ij}^l(k) = 1\} = \bar{\boldsymbol{\sigma}}_{ij}^l, \quad \text{Prob}\{\boldsymbol{\sigma}_{ij}^l(k) = 0\} = 1 - \bar{\boldsymbol{\sigma}}_{ij}^l$$

$$\text{Prob}\{\boldsymbol{\tau}_{ij}^l(k) = 1\} = \bar{\boldsymbol{\tau}}_{ij}^l, \quad \text{Prob}\{\boldsymbol{\tau}_{ij}^l(k) = 0\} = 1 - \bar{\boldsymbol{\tau}}_{ij}^l$$

The same conclusion about the measurement model (5.3) can be applied to equations (5.4) and (5.5). Note that the adversaries signals $\boldsymbol{\varrho}_{ij}^l(k)$ and $\boldsymbol{\upsilon}_{ij}^l(k)$ are bounded, e.g., $\mathbb{E}\{\boldsymbol{\varrho}_{ij}^l(k)\boldsymbol{\varrho}_{ij}^l(k)^T\} \leq \bar{\boldsymbol{\varrho}}_{ij}^l$ and $\mathbb{E}\{\boldsymbol{\upsilon}_{ij}^l(k)\boldsymbol{\upsilon}_{ij}^l(k)^T\} \leq \bar{\boldsymbol{\upsilon}}_{ij}^l$. Also, the random variables $\boldsymbol{\zeta}_{ij}^l(k)$, $\boldsymbol{\lambda}_{ij}^l(k)$, $\boldsymbol{\sigma}_{ij}^l(k)$ and $\boldsymbol{\tau}_{ij}^l(k)$ are assumed to be independent from the system variables $\boldsymbol{x}^i(k)$, $\boldsymbol{u}_m^i(k)$, $\boldsymbol{\eta}_i(k)$ and $\boldsymbol{\nu}_{ij}(k)$.

The signals $\boldsymbol{\xi}_{ij}^l(k)$, $\boldsymbol{\varrho}_{ij}^l(k)$ and $\boldsymbol{\upsilon}_{ij}^l(k)$ are called the malicious inputs, and can be chosen as $\boldsymbol{h}_{ij}(\hat{\boldsymbol{x}}^{i-}(k), \hat{\boldsymbol{x}}_a^{j-}(k)) + \varpi_{ij}^l(k)$, $\hat{\boldsymbol{x}}_a^{j-}(k) + \chi_{ij}^l(k)$ and $\boldsymbol{P}^{j-} + \varsigma_{ij}^l(k)$ respectively, where $\varpi_{ij}^l(k)$, $\chi_{ij}^l(k)$ and $\varsigma_{ij}^l(k)$ are the bounded signals.

The attack detector at the estimator side monitors the filter behavior and detects possible cyber attacks by checking the statistical properties of the arriving *innovation*, i.e., $\Upsilon_{ij}^a(k) = \bar{\boldsymbol{z}}_{ij}^a(k) - \boldsymbol{h}_{ij}(\hat{\boldsymbol{x}}^{i-}(k), \hat{\boldsymbol{x}}_a^{j-}(k))$. This raises the challenge of how to use state estimates to detect possible attacks [121]. We now present a mechanism to detect the malicious attacks based on Euclidean norm [120] of *innovation* for each robot i:

$$\boldsymbol{d}_{ij}(k) = \begin{cases} \mathbf{1}, & \textbf{if} \quad \left\|\Upsilon_{ij}^a(k)\right\| \leq \psi_{ij} \\ \mathbf{0}, & \textbf{otherwise}. \end{cases} \tag{5.6}$$

where ψ_{ij} is the preset threshold. It can be seen in Fig. 1 that the detector decides whether to trigger the alarm for the robot i or not. The threshold ψ_{ij} should be appropriately chosen to balance the false alarm rate and the detection accuracy [121]. In order to minimize the false alarm rate caused by the relative measurement noise, we set the detector threshold ψ_{ij} to $3\boldsymbol{R}_{ij}$, where $\boldsymbol{R}_{ij}$ is the covariance of

the relative measurement noise. As a result, by setting the detector threshold to $3\boldsymbol{R}_{ij}$, the probability of a false alarm rate due to relative measurement noise can be reduced to 1%, the same value as in [120].

Remark 12. *Notice that, in practice, attacks can occur randomly. To protect the system against attacks, the defender can estimate the probability and intensity of the attack signal using statistical tests by monitoring the attacker's behavior online for a period of time. It is therefore reasonable to assume that the probability and the bound of the attack signal are statistically known to the defender. Similar assumptions can be found in references [122]-[124].*

Remark 13. *We assume that all stochastic variables regarding the communication channel between exteroceptive sensors and the robot's filter ($\alpha_{ij}^{l}(k)$, $\beta_{ij}^{l}(k)$) are independent with the communication channel between two filters ($\boldsymbol{\zeta}_{ij}^{l}(k)$, $\boldsymbol{\lambda}_{ij}^{l}(k)$, $\boldsymbol{\sigma}_{ij}^{l}(k)$, $\boldsymbol{\tau}_{ij}^{l}(k)$) in i, j and k.*

Remark 14. *In reality, an attacker can typically only launch a limited number of attacks on the communication links between agents due to limited energy resources. Denoting $\Xi_{ij} \subseteq \mathcal{N}_{ci}$ the set containing the measurement or communication links affected by attacks, then for l number of attacked measurement links $\{\boldsymbol{\alpha}_{ij}^{l}(k) = 0 \,|(i,j) \in \Xi_{ij}\}$ and attacked communication links $\{\boldsymbol{\zeta}_{ij}^{l}(k) = 0$ or $\boldsymbol{\sigma}_{ij}^{l}(k) = 0 | (i,j) \in \Xi_{ij}\}$.*

Remark 15. *In the FDI attack, it is assumed that the attacker knows the system model and employs a bounded signal to implement the attack. Notice that a bounded signal is preferred by the attacker due to resource constraints. Moreover, if the attack signal has a large amplitude then it can be easily detected by the detector. Thus, a sophisticated attacker prefers to transmit a bounded false signal to degrade localization performance. It is therefore reasonable to assume that the false signals transmitted by attackers are bounded. Similar assumptions can be found in [129], [125], [126]. Inspired by [129], [127], [128] we consider a scenario in which the attacker is able to filter the output relative measurements and corrupt them with the signal $\varpi_{ij}^{l}(k)$ to make the false signal $\boldsymbol{\xi}_{ij}^{l}(k)$ bounded, which is stealthier and difficult to detect.*

II.4 Event-Triggered Data Transferring Mechanism

In order to reduce the communication rate of sensors and therefore extend the battery life of mobile robots, the exteroceptive sensors are equipped with an event-

triggered scheduler that decides when relative measurement transmission should occur. The event detector mechanism (5.7) is based on mixed triggered mechanism [91] which works as follows. Define now the binary decision variable $\boldsymbol{\gamma}_{ij}(k)$:

$$\boldsymbol{\gamma}_{ij}(k) = \begin{cases} \mathbf{1}, & \textbf{if} \quad \|\boldsymbol{e}_{ij}(k)\| \geq \Theta_{ij}(k)\,\|\boldsymbol{z}_{ij}(k)\| + \Lambda_{ij}(k) \\ \mathbf{0}, & \textbf{otherwise}. \end{cases} \tag{5.7}$$

where $\boldsymbol{z}_{ij}(k)$ denotes the current sensor measurement, $\bar{\boldsymbol{z}}_{ij}(k)$ represents the last measurement transmitted through the channel and $\boldsymbol{e}_{ij}(k) = \boldsymbol{z}_{ij}(k) - \bar{\boldsymbol{z}}_{ij}(k)$ is the error between transmitted measurement (when triggered) and the current measurement at time k. $\Theta_{ij}(k)$, $\Lambda_{ij}(k) > 0$ are design parameters in the event-triggered mechanism. The smaller the value of Θ_{ij}, Λ_{ij}, the more events are triggered, which results in higher demands on communication resources and higher energy consumed by each robot. When the parameters $\Theta_{ij}(k)$, $\Lambda_{ij}(k) > 0$ are sufficiently small, the event-triggered mechanism performs as a time-triggered system. From Eq. (5.7), we see that, the measurement $\boldsymbol{z}_{ij}(k)$ will be sent to the estimator through an unreliable communication channel if and only if $\boldsymbol{\gamma}_{ij}(k) = 1$.

III Design of an SDECL under cyber attack

In this section, we design an SDECL algorithm via an extended Kalman filter (EKF) with an event-triggered mechanism (5.7) and consider cyber attacks (5.3)-(5.5). Firstly, we derive the prediction error and estimation error covariances. Then, we obtain the upper bound of the estimation error covariance by employing a stochastic analysis. Finally, we derive the Kalman gain for the proposed filter by minimizing the estimation error covariance. Before we proceed further, we introduce the following Lemma which will be used to obtain our results:

Lemma III.1. *For any two vectors x, $y \in \mathbb{R}^n$, there exists a scalar $\varepsilon \in \mathbb{R}$ such that the following inequality holds [113]:*

$$xy^T + yx^T \leq \varepsilon xx^T + \varepsilon^{-1} yy^T. \tag{5.8}$$

Theorem III.2. *Consider the nonlinear discrete-time system (5.1) and (5.2) with the event-triggered communication strategy (5.7). Assume that the relative measurement $(\bar{\boldsymbol{z}}_{ij}(k),\ \bar{\boldsymbol{z}}_{ji}(k))$ and the predicted belief $\boldsymbol{bel}^{i-}(k) = (\hat{\boldsymbol{x}}^{i-}, \boldsymbol{P}^{i-})$, $\boldsymbol{bel}^{j-}(k) = (\hat{\boldsymbol{x}}^{j-}, \boldsymbol{P}^{j-})$ are affected by DoS and FDI attacks (5.3)-(5.5) in the unreliable communication channels. For the secure CL via the EKF, the upper bound of estimation*

error covariance can be obtained as follows:

$$
\begin{aligned}
&\boldsymbol{P}^{i+}(k) \leq \mathcal{C}_1 \bar{\Phi}^1_{ij}(k)\boldsymbol{P}^{i-}(k)\bar{\Phi}^1_{ij}(k)^T \\
&-\Big\{\sum_{j\in\mathcal{N}_{ci}} \bar{\Phi}^1_{ij}(k)\boldsymbol{P}^{ij-}(k)\bar{\Phi}^2_{i}(k)^T\Big\}\boldsymbol{K}_i(k)^T \\
&-\boldsymbol{K}_i(k)\Big\{\sum_{j\in\mathcal{N}_{ci}} \bar{\Phi}^2_{ij}(k)\boldsymbol{P}^{ij-}(k)\bar{\Phi}^1_{ij}(k)^T\Big\} \\
&+\mathcal{C}_2\boldsymbol{K}_i(k)\Big\{\sum_{j,s\in\mathcal{N}_{ci},j\neq s} \bar{\Phi}^2_{ij}(k)\boldsymbol{P}^{js-}(k)\bar{\Phi}^2_{is}(k)^T\Big\}\boldsymbol{K}_i(k)^T \\
&+\mathcal{C}_2\boldsymbol{K}_i(k)\Big\{\sum_{j\in\mathcal{N}_{ci}} \bar{\Phi}^2_{ij}(k)\boldsymbol{P}^{j-}(k)\bar{\Phi}^2_{ij}(k)^T\Big\}\boldsymbol{K}_i(k)^T \\
&+\mathcal{C}_3\boldsymbol{K}_i(k)\Big\{\sum_{j\in\mathcal{N}_{ci}} \bar{\Phi}^3_{ij}(k)\boldsymbol{R}_{ij}(k)\bar{\Phi}^3_{ij}(k)^T\Big\}\boldsymbol{K}_i(k)^T \\
&+\mathcal{C}_4\boldsymbol{K}_i(k)\mathbb{E}\Big\{\sum_{j\in\mathcal{N}_{ci}} \bar{\Phi}^4_{ij}(k)\boldsymbol{h}_{ij}\big(\hat{\boldsymbol{x}}^{i-}(k),\hat{\boldsymbol{x}}^{j-}_a(k)\big) \\
&\qquad\qquad \times\boldsymbol{h}_{ij}\big(\hat{\boldsymbol{x}}^{i-}(k),\hat{\boldsymbol{x}}^{j-}_a(k)\big)^T\bar{\Phi}^4_{ij}(k)^T\Big\}\boldsymbol{K}_i(k)^T \\
&+\mathcal{C}_5\boldsymbol{K}_i(k)\Big\{\sum_{j\in\mathcal{N}_{ci}} \bar{\Phi}^5_{ij}(k)\bar{\boldsymbol{\xi}}^{-\ l}_{ij}(k)\bar{\Phi}^5_{ij}(k)^T\Big\}\boldsymbol{K}_i(k)^T \\
&+\mathcal{C}_6\boldsymbol{K}_i(k)\Big\{\sum_{j\in\mathcal{N}_{ci}} \bar{\Phi}^6_{ij}(k)\bar{\boldsymbol{\varrho}}^l_{ij}(k)\bar{\Phi}^6_{ij}(k)^T\Big\}\boldsymbol{K}_i(k)^T \\
&+\mathcal{C}_7\boldsymbol{K}_i(k)\Big\{\sum_{j\in\mathcal{N}_{ci}} \bar{\Phi}^7_{ij}(k)\boldsymbol{\delta}_{ij}(k)\bar{\Phi}^7_{ij}(k)^T\Big\}\boldsymbol{K}_i(k)^T \\
&+\boldsymbol{K}_i(k)\Big\{\sum_{j\in\mathcal{N}_{ci}} \bar{\Phi}^8_{ij}(k)X_j(k)\bar{\Phi}^8_{ij}(k)^T\Big\}\boldsymbol{K}_i(k)^T
\end{aligned}
\tag{5.9}
$$

where

$$\boldsymbol{P}^{i-}(k) = \mathcal{A}_i(k-1)\boldsymbol{P}^{i+}(k-1)\mathcal{A}_i(k-1)^T + \boldsymbol{G}_i(k-1)\boldsymbol{Q}_i(k-1)\boldsymbol{G}_i(k-1)^T$$
$$\boldsymbol{P}^{ij-}(k) = \mathcal{A}_i(k-1)\boldsymbol{P}^{ij+}(k-1)\mathcal{A}_j(k-1)^T$$

$$\bar{\Phi}^1_{ij}(k) = \Big(\boldsymbol{I} - \boldsymbol{K}_i(k)\sum_{j\in\mathcal{N}_{ci}} d_{ij}(k)\mathbb{E}\Big\{a_{ij}(k)\Big\}\bar{\boldsymbol{\alpha}}^l_{ij}\mathcal{H}^i_i(k)\Big)$$

$$\bar{\Phi}^2_{ij}(k) = d_{ij}(k)\mathbb{E}\Big\{a_{ij}(k)\Big\}\bar{\boldsymbol{\alpha}}^l_{ij}\mathcal{H}^i_j(k)\bar{\boldsymbol{\zeta}}^l_{ij}, \qquad \bar{\Phi}^3_{ij}(k) = d_{ij}(k)\mathbb{E}\Big\{a_{ij}(k)\Big\}\bar{\boldsymbol{\alpha}}^l_{ij}$$

$$\mathcal{A}_i(k) = \boldsymbol{A}_i(k) + \boldsymbol{B}_i(k)\boldsymbol{F}_i(k)\boldsymbol{E}_i(k), \quad \mathcal{H}^i_i(k) = \boldsymbol{H}^i_i(k) + \boldsymbol{D}^i_i(k)\boldsymbol{C}^i_i(k)\boldsymbol{E}^i_i(k)$$

$$\bar{\Phi}^4_{ij}(k) = d_{ij}(k)\mathbb{E}\Big\{a_{ij}(k)\Big\}(\bar{\boldsymbol{\alpha}}^l_{ij} - 1), \quad \mathcal{H}^i_j(k) = \boldsymbol{H}^i_j(k) + \boldsymbol{D}^i_j(k)\boldsymbol{C}^i_j(k)\boldsymbol{E}^i_j(k)$$

$$\bar{\Phi}^5_{ij}(k) = d_{ij}(k)\mathbb{E}\Big\{a_{ij}(k)\Big\}(1 - \bar{\boldsymbol{\alpha}}^l_{ij})\bar{\boldsymbol{\beta}}^l_{ij}$$

$$\bar{\Phi}^6_{ij}(k) = d_{ij}(k)\mathbb{E}\Big\{a_{ij}(k)\Big\}\boldsymbol{\alpha}^l_{ij}\mathcal{H}^i_j(k)(1 - \bar{\boldsymbol{\zeta}}^l_{ij})\bar{\boldsymbol{\lambda}}^l_{ij}$$

$$\bar{\Phi}^7_{ij}(k) = d_{ij}(k)\mathbb{E}\Big\{a_{ij}(k)\Big\}\bar{\boldsymbol{\alpha}}^l_{ij}(1 - \mathbb{E}\Big\{\boldsymbol{\gamma}_{ij}(k)\Big\})$$

$$\bar{\Phi}^8_{ij}(k) = d_{ij}(k)\mathbb{E}\Big\{a_{ij}(k)\Big\}\bar{\boldsymbol{\alpha}}^l_{ij}\mathcal{H}^i_j(k)(1 - \bar{\boldsymbol{\zeta}}^l_{ij})$$

$$\mathcal{C}_1 = (1 - \varepsilon_1 - \varepsilon_2 - \varepsilon_3 - \varepsilon_4 + \varepsilon_5 + \varepsilon_6), \qquad \mathcal{C}_2 = (1 + \varepsilon_7)$$

$$\mathcal{C}_3 = (1 - \varepsilon_2^{-1} - \varepsilon_8), \quad \mathcal{C}_4 = (1 - \varepsilon_3^{-1} + \varepsilon_8^{-1} - \varepsilon_9), \quad \mathcal{C}_5 = (1 - \varepsilon_4^{-1})$$

$$\mathcal{C}_6 = (1+\varepsilon_5^{-1}-\varepsilon_9^{-1}), \quad \mathcal{C}_7 = (1+\varepsilon_6^{-1}-\varepsilon_8^{-1}), \quad \mathbb{E}\Big\{\boldsymbol{\lambda}_{ij}^l(k)\Big\} = \bar{\boldsymbol{\lambda}}_{ij}^l$$

$$\mathbb{E}\Big\{\boldsymbol{\alpha}_{ij}^l(k)\Big\} = \bar{\boldsymbol{\alpha}}_{ij}^l, \quad \mathbb{E}\Big\{\boldsymbol{\beta}_{ij}^l(k)\Big\} = \bar{\boldsymbol{\beta}}_{ij}^l, \quad \mathbb{E}\Big\{\boldsymbol{\zeta}_{ij}^l(k)\Big\} = \bar{\boldsymbol{\zeta}}_{ij}^l$$

$$\mathbb{E}\Big\{\boldsymbol{x}^j(k)\boldsymbol{x}^j(k)^T\Big\} = X_j(k), \qquad \mathbb{E}\Big\{\boldsymbol{e}_{ij}(k)\boldsymbol{e}_{ij}(k)^T\Big\} = \boldsymbol{\delta}_{ij}(k)$$

$$\mathbb{E}\Big\{\boldsymbol{\xi}_{ij}^l(k)\boldsymbol{\xi}_{ij}^l(k)^T\Big\} = \bar{\boldsymbol{\xi}}_{ij}^l(k), \qquad \mathbb{E}\Big\{\boldsymbol{\varrho}_{ij}^l(k)\boldsymbol{\varrho}_{ij}^l(k)^T\Big\} = \bar{\boldsymbol{\varrho}}_{ij}^l(k)$$

Proof. The predicted state error of robot i for multi-robot system (5.1) at time instant $k+1$ can be described by:

$$\tilde{\boldsymbol{x}}^{i-}(k+1) = \boldsymbol{x}^i(k+1) - \hat{\boldsymbol{x}}^{i-}(k+1) \tag{5.10}$$

where the predicted state of each robot $\hat{\boldsymbol{x}}^{i-}(k+1)$ is defined by:

$$\hat{\boldsymbol{x}}^{i-}(k+1) = \boldsymbol{f}^i\Big(\hat{\boldsymbol{x}}^{i+}(k), \boldsymbol{u}_m^i(k)\Big) \tag{5.11}$$

Expanding $\boldsymbol{f}^i(\boldsymbol{x}^i(k), \boldsymbol{u}_m^i(k))$ using Taylor series around $\hat{\boldsymbol{x}}^{i+}(k)$, we have:

$$\begin{aligned}\boldsymbol{f}^i\Big(\boldsymbol{x}^i(k), \boldsymbol{u}_m^i(k)\Big) \approx \boldsymbol{f}^i\Big(\hat{\boldsymbol{x}}^{i+}(k), \boldsymbol{u}_m^i(k)\Big) \\ +\boldsymbol{A}_i(k)\Big(\boldsymbol{x}^i(k) - \hat{\boldsymbol{x}}^{i+}(k)\Big) + o\Big(|\tilde{\boldsymbol{x}}^{i+}(k)|\Big)\end{aligned} \tag{5.12}$$

where $\boldsymbol{A}_i = \frac{\partial \boldsymbol{f}^i(\hat{\boldsymbol{x}}^{i+}, \boldsymbol{u}_m^i)}{\partial \boldsymbol{x}^i}$ and $o\Big(|\tilde{\boldsymbol{x}}^{i+}(k)|\Big)$ denote the high-order terms of the Taylor series expansion. Following [129], [130], we introduce the unknown time-varying matrix $\boldsymbol{F}_i(k)$, and known scaling matrix $\boldsymbol{B}_i(k)$ to account for the linearization error. We can write:

$$o\Big(|\tilde{\boldsymbol{x}}^{i+}(k)|\Big) = \boldsymbol{B}_i(k)\boldsymbol{F}_i(k)\boldsymbol{E}_i(k)\tilde{\boldsymbol{x}}^{i+}(k) \tag{5.13}$$

where $\boldsymbol{E}_i(k)$ is a known tuning matrix and assume that $\boldsymbol{F}_i(k)$ satisfies:

$$\boldsymbol{F}_i(k)\boldsymbol{F}_i(k)^T \leq \boldsymbol{I} \tag{5.14}$$

Defining $\mathcal{A}_i(k) = \Big(\boldsymbol{A}_i(k) + \boldsymbol{B}_i(k)\boldsymbol{F}_i(k)\boldsymbol{E}_i(k)\Big)$ and using (5.10)-(5.13), the predicted state error for robots i and j can be computed as follows:

$$\tilde{\boldsymbol{x}}^{i-}(k+1) = \mathcal{A}_i(k)\tilde{\boldsymbol{x}}^{i-}(k) + \boldsymbol{G}_i(k)\boldsymbol{\eta}_i(k) \tag{5.15}$$

$$\tilde{\boldsymbol{x}}^{j-}(k+1) = \mathcal{A}_j(k)\tilde{\boldsymbol{x}}^{j-}(k) + \boldsymbol{G}_j(k)\boldsymbol{\eta}_j(k) \tag{5.16}$$

where $\boldsymbol{G}_i = \frac{\partial \boldsymbol{f}^i(\hat{\boldsymbol{x}}^{i+}, \boldsymbol{u}_m^i)}{\partial \boldsymbol{\eta}_i}$, $\boldsymbol{G}_j = \frac{\partial \boldsymbol{f}^j(\hat{\boldsymbol{x}}^{j+}, \boldsymbol{u}_m^j)}{\partial \boldsymbol{\eta}_j}$ and $\boldsymbol{A}_j = \frac{\partial \boldsymbol{f}^j(\hat{\boldsymbol{x}}^{j+}, \boldsymbol{u}_m^j)}{\partial \boldsymbol{x}^j}$. Using Eqs. (5.15)-(5.16), the predicted state error covariance for robot i and cross-covariance between two robots (i and j) are represented by:

$$\begin{aligned}\boldsymbol{P}^{i-}(k+1) = \mathbb{E}\Bigg[\Big(\tilde{\boldsymbol{x}}^{i-}(k+1)\Big)\Big(\tilde{\boldsymbol{x}}^{i-}(k+1)\Big)^T\Bigg] = \\ \mathcal{A}_i(k)\boldsymbol{P}^{i+}(k)\mathcal{A}_i(k)^T + \boldsymbol{G}_i(k)\boldsymbol{Q}_i(k)\boldsymbol{G}_i(k)^T\end{aligned} \tag{5.17}$$

$$\boldsymbol{P}^{ij-}(k+1) = \mathbb{E}\Big[\Big(\tilde{\boldsymbol{x}}^{i-}(k+1)\Big)\Big(\tilde{\boldsymbol{x}}^{j-}(k+1)\Big)^T\Big] = \mathcal{A}_i(k)\boldsymbol{P}^{ij+}(k)\mathcal{A}_j(k)^T \tag{5.18}$$

Considering the event-triggered mechanism (5.7) and random cyber attack (5.3), the current transmitted measurement is as follows (for simplicity of the notation we use time instant k instead of time instant $k+1$):

$$\begin{aligned}\bar{\boldsymbol{z}}^a_{ij}(k) = \boldsymbol{\alpha}^l_{ij}(k)\Big(\boldsymbol{z}_{ij}(k) - (1-\boldsymbol{\gamma}_{ij}(k))\boldsymbol{e}_{ij}(k)\Big) \\ +(1-\boldsymbol{\alpha}^l_{ij}(k))\boldsymbol{\beta}^l_{ij}(k)\boldsymbol{\xi}^l_{ij}(k)\end{aligned} \tag{5.19}$$

The arriving innovation can be computed as follows:

$$\begin{aligned}\Upsilon^a_{ij}(k) = \boldsymbol{\alpha}^l_{ij}(k)\Big(\boldsymbol{z}_{ij}(k) - (1-\boldsymbol{\gamma}_{ij}(k))\boldsymbol{e}_{ij}(k)\Big) \\ +(1-\boldsymbol{\alpha}^l_{ij}(k))\boldsymbol{\beta}^l_{ij}(k)\boldsymbol{\xi}^l_{ij}(k) - \boldsymbol{h}_{ij}\Big(\hat{\boldsymbol{x}}^{i-}(k), \hat{\boldsymbol{x}}^{j-}_a(k)\Big)\end{aligned} \tag{5.20}$$

The state estimates of each robot are corrected according to:

$$\begin{aligned}\hat{\boldsymbol{x}}^{i+}(k) = \hat{\boldsymbol{x}}^{i-}(k) + \boldsymbol{K}_i(k)\Big[\sum_{j\in\mathcal{N}_{ci}} d_{ij}(k)a_{ij}(k)\Big(\bar{\boldsymbol{z}}^a_{ij}(k) \\ -\boldsymbol{h}_{ij}(\hat{\boldsymbol{x}}^{i-}(k), \hat{\boldsymbol{x}}^{j-}_a(k))\Big)\Big]\end{aligned} \tag{5.21}$$

where $\boldsymbol{h}_{ij}(\hat{\boldsymbol{x}}^{i-}, \hat{\boldsymbol{x}}^{j-})$ is the predicted measurement. Let the first-order expansion of $\boldsymbol{h}_{ij}(\boldsymbol{x}^i, \boldsymbol{x}^j)$ around $(\hat{\boldsymbol{x}}^{i-}, \hat{\boldsymbol{x}}^{j-})$ be

$$\begin{aligned}\boldsymbol{h}_{ij}(\boldsymbol{x}^i, \boldsymbol{x}^j) \approx \boldsymbol{h}_{ij}(\hat{\boldsymbol{x}}^{i-}, \hat{\boldsymbol{x}}^{j-}) + \boldsymbol{H}^i_i(\boldsymbol{x}^i - \hat{\boldsymbol{x}}^{i-}) + \boldsymbol{H}^i_j(\boldsymbol{x}^j - \hat{\boldsymbol{x}}^{j-}) \\ +o\Big(|\tilde{\boldsymbol{x}}^{i-}(k)|, |\tilde{\boldsymbol{x}}^{j-}(k)|\Big)\end{aligned} \tag{5.22}$$

where $\boldsymbol{H}^i_i = \frac{\partial \boldsymbol{h}_{ij}(\hat{\boldsymbol{x}}^{i-}, \hat{\boldsymbol{x}}^{j-})}{\partial \boldsymbol{x}^i}$, $\boldsymbol{H}^i_j = \frac{\partial \boldsymbol{h}_{ij}(\hat{\boldsymbol{x}}^{i-}, \hat{\boldsymbol{x}}^{j-})}{\partial \boldsymbol{x}^j}$ and $o\Big(|\tilde{\boldsymbol{x}}^{i-}(k)|, |\tilde{\boldsymbol{x}}^{j-}(k)|\Big)$ represent the high-order terms of the Taylor series expansion. We now introduce unknown time-varying matrices $\boldsymbol{C}^i_i(k)$ and $\boldsymbol{C}^i_j(k)$, and known scaling matrices $\boldsymbol{D}^i_i(k)$, $\boldsymbol{D}^i_j(k)$ accounting for the linearization errors of the measurement model:

$$\begin{aligned}o\Big(|\tilde{\boldsymbol{x}}^{i-}(k)|, |\tilde{\boldsymbol{x}}^{j-}(k)|\Big) = \boldsymbol{D}^i_i(k)\boldsymbol{C}^i_i(k)\boldsymbol{E}^i_i(k)\tilde{\boldsymbol{x}}^{i-}(k) \\ +\boldsymbol{D}^i_j(k)\boldsymbol{C}^i_j(k)\boldsymbol{E}^i_j(k)\tilde{\boldsymbol{x}}^{j-}(k)\end{aligned} \tag{5.23}$$

where $\boldsymbol{E}^i_i(k)$ and $\boldsymbol{E}^i_j(k)$ are known tuning matrices and assume that $\boldsymbol{C}^i_i(k)$ and $\boldsymbol{C}^i_j(k)$ satisfy:

$$\boldsymbol{C}^i_i(k)\boldsymbol{C}^i_i(k)^T \leq \boldsymbol{I} \tag{5.24}$$

$$\boldsymbol{C}^i_j(k)\boldsymbol{C}^i_j(k)^T \leq \boldsymbol{I} \tag{5.25}$$

Note that the matrices $\boldsymbol{D}_i^i(k)$, $\boldsymbol{D}_j^i(k)$, $\boldsymbol{E}_i^i(k)$, $\boldsymbol{E}_j^i(k)$, $\boldsymbol{B}_i(k)$ and $\boldsymbol{E}_i(k)$ should be designed appropriately. Substituting (5.19) into (5.21), we have:

$$\begin{aligned}\hat{\boldsymbol{x}}^{i+}(k) = \hat{\boldsymbol{x}}^{i-}(k) + \boldsymbol{K}_i(k)\Bigg[\sum_{j\in\mathcal{N}_{ci}} d_{ij}(k)a_{ij}(k)\Bigg(\boldsymbol{\alpha}_{ij}^l(k)\Big(\boldsymbol{z}_{ij}(k) \\ -(1-\boldsymbol{\gamma}_{ij}(k))\boldsymbol{e}_{ij}(k)\Big) + (1-\boldsymbol{\alpha}_{ij}^l(k))\boldsymbol{\beta}_{ij}^l(k)\boldsymbol{\xi}_{ij}^l(k) \\ -\boldsymbol{h}_{ij}(\hat{\boldsymbol{x}}^{i-}(k), \hat{\boldsymbol{x}}_a^{j-}(k))\Bigg)\Bigg]\end{aligned} \tag{5.26}$$

Using (5.22)-(5.26) and introducing $\mathcal{H}_i^i(k) = \boldsymbol{H}_i^i(k) + \boldsymbol{D}_i^i(k)\boldsymbol{C}_i^i(k)\boldsymbol{E}_i^i(k)$, $\mathcal{H}_j^i(k) = \boldsymbol{H}_j^i(k) + \boldsymbol{D}_j^i(k)\boldsymbol{C}_j^i(k)\boldsymbol{E}_j^i(k)$ the estimation error can be computed as follows:

$$\begin{aligned}&\tilde{\boldsymbol{x}}^{i+}(k) = \boldsymbol{x}^i(k) - \hat{\boldsymbol{x}}^{i+}(k) = \Phi_{ij}^1(k)\tilde{\boldsymbol{x}}^{i-}(k) \\ &-\boldsymbol{K}_i(k)\sum_{j\in\mathcal{N}_{ci}}\Phi_{ij}^2(k)\tilde{\boldsymbol{x}}^{j-}(k) - \boldsymbol{K}_i(k)\sum_{j\in\mathcal{N}_{ci}}\Phi_{ij}^3(k)\boldsymbol{\nu}_{ij}(k) \\ &-\boldsymbol{K}_i(k)\sum_{j\in\mathcal{N}_{ci}}\Phi_{ij}^4(k)\boldsymbol{h}_{ij}\big(\hat{\boldsymbol{x}}^{i-}(k), \hat{\boldsymbol{x}}_a^{j-}(k)\big) \\ &-\boldsymbol{K}_i(k)\sum_{j\in\mathcal{N}_{ci}}\Phi_{ij}^5(k)\boldsymbol{\xi}_{ij}^l(k) + \boldsymbol{K}_i(k)\sum_{j\in\mathcal{N}_{ci}}\Phi_{ij}^6(k)\boldsymbol{\varrho}_{ij}^l(k) \\ &+\boldsymbol{K}_i(k)\sum_{j\in\mathcal{N}_{ci}}\Phi_{ij}^7(k)\boldsymbol{e}_{ij}(k) - \boldsymbol{K}_i(k)\sum_{j\in\mathcal{N}_{ci}}\Phi_{ij}^8(k)\boldsymbol{x}^j(k)\end{aligned} \tag{5.27}$$

where

$$\Phi_{ij}^1(k) = \Big(\boldsymbol{I} - \boldsymbol{K}_i(k)\sum_{j\in\mathcal{N}_{ci}} d_{ij}(k)a_{ij}(k)\boldsymbol{\alpha}_{ij}^l(k)\mathcal{H}_i^i(k)\Big)$$

$$\Phi_{ij}^2(k) = d_{ij}(k)a_{ij}(k)\boldsymbol{\alpha}_{ij}^l(k)\mathcal{H}_j^i(k)\boldsymbol{\zeta}_{ij}^l(k)$$

$$\Phi_{ij}^3(k) = d_{ij}(k)a_{ij}(k)\boldsymbol{\alpha}_{ij}^l(k),\ \Phi_{ij}^4(k) = d_{ij}(k)a_{ij}(k)(\boldsymbol{\alpha}_{ij}^l(k) - 1)$$

$$\Phi_{ij}^5(k) = d_{ij}(k)a_{ij}(k)(1-\boldsymbol{\alpha}_{ij}^l(k))\boldsymbol{\beta}_{ij}^l(k)$$

$$\Phi_{ij}^6(k) = d_{ij}(k)a_{ij}(k)\boldsymbol{\alpha}_{ij}^l(k)\mathcal{H}_j^i(k)(1-\boldsymbol{\zeta}_{ij}^l(k))\boldsymbol{\lambda}_{ij}^l(k)$$

$$\Phi_{ij}^7(k) = d_{ij}(k)a_{ij}(k)\boldsymbol{\alpha}_{ij}^l(k)(1-\boldsymbol{\gamma}_{ij}(k))$$

$$\Phi_{ij}^8(k) = d_{ij}(k)a_{ij}(k)\boldsymbol{\alpha}_{ij}^l(k)\mathcal{H}_j^i(k)(1-\boldsymbol{\zeta}_{ij}^l(k))$$

Using (5.27), the estimation error covariance matrix can be computed as follows:

$$
\begin{aligned}
&\boldsymbol{P}^{i+}(k) = \mathbb{E}\Big\{\tilde{\boldsymbol{x}}^{i+}(k)\tilde{\boldsymbol{x}}^{i+}(k)^T\Big\} = \mathbb{E}\Big\{\Phi^1_{ij}(k)\tilde{\boldsymbol{x}}^{i-}(k)\tilde{\boldsymbol{x}}^{i-}(k)^T\Phi^1_{ij}(k)^T\Big\}\\
&+\boldsymbol{K}_i(k)\mathbb{E}\Big\{\Big[\sum_{j\in\mathcal{N}_{ci}}\Phi^2_{ij}(k)\tilde{\boldsymbol{x}}^{j-}(k)\Big]\Big[\sum_{j\in\mathcal{N}_{ci}}\Phi^2_{ij}(k)\tilde{\boldsymbol{x}}^{j-}(k)\Big]^T\Big\}\boldsymbol{K}_i(k)^T + \boldsymbol{K}_i(k)\mathbb{E}\Big\{\Big[\sum_{j\in\mathcal{N}_{ci}}\Phi^3_{ij}(k)\boldsymbol{\nu}_{ij}(k)\Big]\Big[\sum_{j\in\mathcal{N}_{ci}}\Phi^3_{ij}(k)\boldsymbol{\nu}_{ij}(k)\Big]^T\Big\}\boldsymbol{K}_i(k)^T\\
&+\boldsymbol{K}_i(k)\mathbb{E}\Big\{\Big[\sum_{j\in\mathcal{N}_{ci}}\Phi^4_{ij}(k)\boldsymbol{h}_{ij}(.)\Big]\Big[\sum_{j\in\mathcal{N}_{ci}}\Phi^4_{ij}(k)\boldsymbol{h}_{ij}(.)\Big]^T\Big\}\boldsymbol{K}_i(k)^T + \boldsymbol{K}_i(k)\mathbb{E}\Big\{\Big[\sum_{j\in\mathcal{N}_{ci}}\Phi^5_{ij}(k)\boldsymbol{\xi}^l_{ij}(k)\Big]\Big[\sum_{j\in\mathcal{N}_{ci}}\Phi^5_{ij}(k)\boldsymbol{\xi}^l_{ij}(k)\Big]^T\Big\}\boldsymbol{K}_i(k)^T\\
&+\boldsymbol{K}_i(k)\mathbb{E}\Big\{\Big[\sum_{j\in\mathcal{N}_{ci}}\Phi^6_{ij}(k)\boldsymbol{\varrho}^l_{ij}(k)\Big]\Big[\sum_{j\in\mathcal{N}_{ci}}\Phi^6_{ij}(k)\boldsymbol{\varrho}^l_{ij}(k)\Big]^T\Big\}\boldsymbol{K}_i(k)^T + \boldsymbol{K}_i(k)\mathbb{E}\Big\{\Big[\sum_{j\in\mathcal{N}_{ci}}\Phi^7_{ij}(k)\boldsymbol{e}_{ij}(k)\Big]\Big[\sum_{j\in\mathcal{N}_{ci}}\Phi^7_{ij}(k)\boldsymbol{e}_{ij}(k)\Big]^T\Big\}\boldsymbol{K}_i(k)^T\\
&+\boldsymbol{K}_i(k)\mathbb{E}\Big\{\Big[\sum_{j\in\mathcal{N}_{ci}}\Phi^8_{ij}(k)\boldsymbol{x}^j(k)\Big]\Big[\sum_{j\in\mathcal{N}_{ci}}\Phi^8_{ij}(k)\boldsymbol{x}^j(k)\Big]^T\Big\}\boldsymbol{K}_i(k)^T - \mathbb{E}\Big\{\Phi^1_{ij}(k)\tilde{\boldsymbol{x}}^{i-}(k)\Big[\sum_{j\in\mathcal{N}_{ci}}\Phi^2_{ij}(k)\tilde{\boldsymbol{x}}^{j-}(k)\Big]^T\Big\}\boldsymbol{K}_i(k)^T\\
&-\boldsymbol{K}_i(k)\mathbb{E}\Big\{\Big[\sum_{j\in\mathcal{N}_{ci}}\Phi^2_{ij}(k)\tilde{\boldsymbol{x}}^{j-}(k)\Big]\tilde{\boldsymbol{x}}^{i-}(k)^T\Phi^1_{ij}(k)^T\Big\} - \mathbb{E}\Big\{\Phi^1_{ij}(k)\tilde{\boldsymbol{x}}^{i-}(k)\Big[\sum_{j\in\mathcal{N}_{ci}}\Phi^3_{ij}(k)\boldsymbol{\nu}_{ij}(k)\Big]^T\Big\}\boldsymbol{K}_i(k)^T\\
&-\boldsymbol{K}_i(k)\mathbb{E}\Big\{\Big[\sum_{j\in\mathcal{N}_{ci}}\Phi^3_{ij}(k)\boldsymbol{\nu}_{ij}(k)\Big]\tilde{\boldsymbol{x}}^{i-}(k)^T\Phi^1_{ij}(k)^T\Big\} - \mathbb{E}\Big\{\Phi^1_{ij}(k)\tilde{\boldsymbol{x}}^{i-}(k)\Big[\sum_{j\in\mathcal{N}_{ci}}\Phi^4_{ij}(k)\boldsymbol{h}_{ij}(.)\Big]^T\Big\}\boldsymbol{K}_i(k)^T\\
&-\boldsymbol{K}_i(k)\mathbb{E}\Big\{\Big[\sum_{j\in\mathcal{N}_{ci}}\Phi^4_{ij}(k)\boldsymbol{h}_{ij}(.)\Big]\tilde{\boldsymbol{x}}^{i-}(k)^T\Phi^1_{ij}(k)^T\Big\} - \mathbb{E}\Big\{\Phi^1_{ij}(k)\tilde{\boldsymbol{x}}^{i-}(k)\Big[\sum_{j\in\mathcal{N}_{ci}}\Phi^5_{ij}(k)\boldsymbol{\xi}^l_{ij}(k)\Big]^T\Big\}\boldsymbol{K}_i(k)^T\\
&-\boldsymbol{K}_i(k)\mathbb{E}\Big\{\Big[\sum_{j\in\mathcal{N}_{ci}}\Phi^5_{ij}(k)\boldsymbol{\xi}^l_{ij}(k)\Big]\tilde{\boldsymbol{x}}^{i-}(k)^T\Phi^1_{ij}(k)^T\Big\} + \mathbb{E}\Big\{\Phi^1_{ij}(k)\tilde{\boldsymbol{x}}^{i-}(k)\Big[\sum_{j\in\mathcal{N}_{ci}}\Phi^6_{ij}(k)\boldsymbol{\varrho}^l_{ij}(k)\Big]^T\Big\}\boldsymbol{K}_i(k)^T\\
&+\boldsymbol{K}_i(k)\mathbb{E}\Big\{\Big[\sum_{j\in\mathcal{N}_{ci}}\Phi^6_{ij}(k)\boldsymbol{\varrho}^l_{ij}(k)\Big]\tilde{\boldsymbol{x}}^{i-}(k)^T\Phi^1_{ij}(k)^T\Big\} + \mathbb{E}\Big\{\Phi^1_{ij}(k)\tilde{\boldsymbol{x}}^{i-}(k)\Big[\sum_{j\in\mathcal{N}_{ci}}\Phi^7_{ij}(k)\boldsymbol{e}_{ij}(k)\Big]^T\Big\}\boldsymbol{K}_i(k)^T\\
&+\boldsymbol{K}_i(k)\mathbb{E}\Big\{\Big[\sum_{j\in\mathcal{N}_{ci}}\Phi^7_{ij}(k)\boldsymbol{e}_{ij}(k)\Big]\tilde{\boldsymbol{x}}^{i-}(k)^T\Phi^1_{ij}(k)^T\Big\} - \boldsymbol{K}_i(k)\mathbb{E}\Big\{\Big[\sum_{j\in\mathcal{N}_{ci}}\Phi^3_{ij}(k)\boldsymbol{\nu}_{ij}(k)\Big]\Big[\sum_{j\in\mathcal{N}_{ci}}\Phi^7_{ij}(k)\boldsymbol{e}_{ij}(k)\Big]^T\Big\}\boldsymbol{K}_i(k)^T\\
&-\boldsymbol{K}_i(k)\mathbb{E}\Big\{\Big[\sum_{j\in\mathcal{N}_{ci}}\Phi^7_{ij}(k)\boldsymbol{e}_{ij}(k)\Big]\Big[\sum_{j\in\mathcal{N}_{ci}}\Phi^3_{ij}(k)\boldsymbol{\nu}_{ij}(k)\Big]^T\Big\}\boldsymbol{K}_i(k)^T + \boldsymbol{K}_i(k)\mathbb{E}\Big\{\Big[\sum_{j\in\mathcal{N}_{ci}}\Phi^2_{ij}(k)\tilde{\boldsymbol{x}}^{j-}(k)\Big]\Big[\sum_{j\in\mathcal{N}_{ci}}\Phi^4_{ij}(k)\boldsymbol{h}_{ij}(.)\Big]^T\Big\}\boldsymbol{K}_i(k)^T\\
&+\boldsymbol{K}_i(k)\mathbb{E}\Big\{\Big[\sum_{j\in\mathcal{N}_{ci}}\Phi^4_{ij}(k)\boldsymbol{h}_{ij}(.)\Big]\Big[\sum_{j\in\mathcal{N}_{ci}}\Phi^2_{ij}(k)\tilde{\boldsymbol{x}}^{j-}(k)\Big]^T\Big\}\boldsymbol{K}_i(k)^T - \boldsymbol{K}_i(k)\mathbb{E}\Big\{\Big[\sum_{j\in\mathcal{N}_{ci}}\Phi^6_{ij}(k)\boldsymbol{\varrho}^l_{ij}(k)\Big]\Big[\sum_{j\in\mathcal{N}_{ci}}\Phi^4_{ij}(k)\boldsymbol{h}_{ij}(.)\Big]^T\Big\}\boldsymbol{K}_i(k)^T\\
&-\boldsymbol{K}_i(k)\mathbb{E}\Big\{\Big[\sum_{j\in\mathcal{N}_{ci}}\Phi^4_{ij}(k)\boldsymbol{h}_{ij}(.)\Big]\Big[\sum_{j\in\mathcal{N}_{ci}}\Phi^6_{ij}(k)\boldsymbol{\varrho}^l_{ij}(k)\Big]^T\Big\}\boldsymbol{K}_i(k)^T
\end{aligned}
\tag{5.28}
$$

Defining constants ε_1, ε_2, ε_3, ε_4, ε_5, ε_6, ε_7, ε_8, $\varepsilon_9 > 0$ and applying Lemma III.1 we obtain an upper bound of the error covariance matrix (5.9), which completes the proof. □

Remark 16. *It is important to notice that it is impossible to compute the actual value of the estimation error covariance due to some terms* $\mathbb{E}\Big\{\Big[\sum_{j\in\mathcal{N}_{ci}}\Phi^5_i(k)\boldsymbol{\xi}^l_{ij}(k)\Big]\tilde{\boldsymbol{x}}^{i-}(k)^T\Phi^1_i(k)^T\Big\}$, $\mathbb{E}\Big\{\Big[\sum_{j\in\mathcal{N}_{ci}}\Phi^3_i(k)\boldsymbol{\nu}_{ij}(k)\Big]\tilde{\boldsymbol{x}}^{i-}(k)^T\Phi^1_i(k)^T\Big\}$, *... (see Eq. (5.28) for details) which depend on random cyber attacks, random measurement noise, event-triggering parameter and etc. Therefore, using Lemma III.1 we provide an upper bound for the estimation error covariance with respect to the parameters of random attacks, event-triggering parameter and etc.*

Corollary III.2.1. Under the result of Theorem III.2, the optimal Kalman filter gain that minimizes the upper bound of estimation error covariance $\bar{\boldsymbol{P}}^{i+}(k)$ is given

by:

$$\boldsymbol{K}_i(k) = X(Y)^{-1} \tag{5.29}$$

Where X and Y can be expressed as a follows:

$$X = \mathcal{C}_1 \boldsymbol{P}^{i-}(k)\bar{\mathcal{F}}_{ij}(k) + \sum_{j\in\mathcal{N}_{ci}} \boldsymbol{P}^{ij-}(k)\bar{\Phi}^2_{ij}(k)^T \tag{5.30}$$

$$\begin{aligned}
Y =& \mathcal{C}_1\bar{\mathcal{F}}_{ij}(k)\boldsymbol{P}^{i-}(k)\bar{\mathcal{F}}_{ij}(k)^T + \sum_{j\in\mathcal{N}_{ci}} \bar{\mathcal{F}}_{ij}(k)\boldsymbol{P}^{ij-}(k)\bar{\Phi}^2_{ij}(k)^T \\
&+ \sum_{j\in\mathcal{N}_{ci}} \bar{\Phi}^2_{ij}(k)\boldsymbol{P}^{ij-}(k)\bar{\mathcal{F}}_{ij}(k)^T + \mathcal{C}_2 \sum_{j,s\in\mathcal{N}_{ci}} \bar{\Phi}^2_{ij}(k)\boldsymbol{P}^{js-}(k)\bar{\Phi}^2_{is}(k)^T \\
&+\mathcal{C}_3 \sum_{j\in\mathcal{N}_{ci}} \bar{\Phi}^3_{ij}(k)\boldsymbol{R}_{ij}(k)\bar{\Phi}^3_{ij}(k)^T + \mathcal{C}_5 \sum_{j\in\mathcal{N}_{ci}} \bar{\Phi}^5_{ij}(k)\bar{\boldsymbol{\xi}}^{-\ l}_{ij}(k)\bar{\Phi}^5_{ij}(k)^T \\
&+\mathcal{C}_6 \sum_{j\in\mathcal{N}_{ci}} \bar{\Phi}^6_{ij}(k)\bar{\boldsymbol{\varrho}}^l_{ij}(k)\bar{\Phi}^6_{ij}(k)^T + \mathcal{C}_7 \sum_{j\in\mathcal{N}_{ci}} \bar{\Phi}^7_{ij}(k)\boldsymbol{\delta}_{ij}(k)\bar{\Phi}^7_{ij}(k)^T \\
&+\mathcal{C}_4\mathbb{E}\Big\{ \sum_{j\in\mathcal{N}_{ci}} \bar{\Phi}^4_{ij}(k)\boldsymbol{h}_{ij}(\hat{\boldsymbol{x}}^{i-}(k), \hat{\boldsymbol{x}}^{j-}_a(k))\boldsymbol{h}_{ij}(\hat{\boldsymbol{x}}^{i-}(k), \hat{\boldsymbol{x}}^{j-}_a(k))^T \\
&\times\bar{\Phi}^4_{ij}(k)^T\Big\} + \sum_{j\in\mathcal{N}_{ci}} \bar{\Phi}^8_{ij}(k)X_j(k)\bar{\Phi}^8_{ij}(k)^T
\end{aligned} \tag{5.31}$$

and also $\bar{\mathcal{F}}_{ij}(k)$ is defined as

$$\bar{\mathcal{F}}_{ij}(k) = \sum_{j\in\mathcal{N}_{ci}} d_{ij}(k)\mathbb{E}\Big\{a_{ij}(k)\Big\}\bar{\boldsymbol{\alpha}}^l_{ij}\mathcal{H}^i_i(k)$$

Remark 17. *In Corollary III.2.1, we obtain the optimal Kalman filter gain for the proposed filter by minimizing the trace of the upper bound of the estimation error covariance. Considering the structure of the optimal Kalman gain in (5.30)-(5.31), the event-triggered mechanism and cyber-attacks introduce additional parameters affecting the upper and the lower bounds of the estimation error and the estimation error covariance. Moreover, in the absence of the attack, the optimal gain in (5.30)-(5.31) is the same as the one in [62]. Also, note that the proposed filter is suboptimal due to the parameters of the cyber attacks, the event-triggered mechanism, and the topology of the interaction between robots. In order to improve the filter's performance, the parameters ε_1, ε_2,... can be tuned in a way that the upper bound of estimation error covariance is minimized further. Specifically, the parameters ε_1, ε_2,... can be obtained by an optimization algorithm (genetic algorithm) in the MATLAB code "$[x, f_{min}] = ga(f(x), n_x, \cdots)$", where $f(x)$ is the objective function (upper bound of error covariance) to be optimized and n_x is the dimension of $f(x)$. Note that a similar approach can be found in [56].*

IV Boundedness of estimation error for the proposed SDECL

In this section, we analyze the resilience of the proposed filter under cyber attacks. We derive sufficient conditions that ensure convergence and stochastic stability of the proposed filter.

Lemma IV.1. *([131]) Assume there is a stochastic process $\boldsymbol{V}_k(\boldsymbol{\pi}_k)$ as well as real numbers $\underline{\boldsymbol{\kappa}}$, $\bar{\boldsymbol{\kappa}}$, $\boldsymbol{\mu} > 0$ and $0 < \boldsymbol{\phi} \leq 1$ such that*

$$\underline{\boldsymbol{\kappa}} \left\|\boldsymbol{\pi}_k\right\|^2 \leq \boldsymbol{V}_k(\boldsymbol{\pi}_k) \leq \bar{\boldsymbol{\kappa}} \left\|\boldsymbol{\pi}_k\right\|^2 \tag{5.32}$$

and

$$\mathbb{E}\{\boldsymbol{V}_k(\boldsymbol{\pi}_k)|\boldsymbol{\pi}_{k-1}\} - \boldsymbol{V}_{k-1}(\boldsymbol{\pi}_{k-1}) \leq \boldsymbol{\mu} - \boldsymbol{\phi}\boldsymbol{V}_{k-1}(\boldsymbol{\pi}_{k-1}) \tag{5.33}$$

are satisfied. Then the stochastic process is exponentially bounded in mean square sense, i.e.,

$$\mathbb{E}\left\{\left\|\boldsymbol{\pi}_k\right\|^2\right\} \leq \frac{\bar{\boldsymbol{\kappa}}}{\underline{\boldsymbol{\kappa}}}\mathbb{E}\left\{\left\|\boldsymbol{\pi}_0\right\|^2\right\}(1-\boldsymbol{\phi})^k + \frac{\boldsymbol{\mu}}{\underline{\boldsymbol{\kappa}}}\sum_{n=1}^{k-1}(1-\boldsymbol{\phi})^n \tag{5.34}$$

and the stochastic process is bounded with probability one.

Assumption 7. *There exist real constants $\underline{a}_i$, $\bar{a}_i$, $\underline{h}_i$, $\bar{h}_i$, $\underline{h}_{ij}$, $\bar{h}_{ij}$, $\underline{q}_i$, $\bar{q}_i$, $\underline{R}_{ij}$, $\bar{R}_{ij}$, $\underline{g}_i$, $\bar{g}_i > 0$ such that the following bounds on various matrices are satisfied for every $k \geq 0$:*

$$\begin{array}{ll} \underline{a}_i \leq \|\mathcal{A}_i(k)\| \leq \bar{a}_i, & \underline{h}_i \leq \left\|\mathcal{H}_i^i(k)\right\| \leq \bar{h}_i, \\ \underline{h}_{ij} \leq \left\|\mathcal{H}_j^i(k)\right\| \leq \bar{h}_{ij}, & \underline{q}_i \leq \left\|\bar{\boldsymbol{Q}}_i(k)\right\| \leq \bar{q}_i, \\ \underline{R}_{ij} \leq \|\boldsymbol{R}_{ij}(k)\| \leq \bar{R}_{ij}, & \underline{g}_i \leq \|\boldsymbol{G}_i(k)\| \leq \bar{g}_i \end{array}$$

Theorem IV.2. *Assume that the nonlinear discrete-time system (5.1) and (5.2) with the event-triggered communication strategy (5.7) and random cyber attacks (5.3)-(5.5) satisfies Assumption 7. Given $\underline{\boldsymbol{p}}_i \leq \boldsymbol{P}^{i+}(0) \leq \bar{\boldsymbol{p}}_i$ and $\underline{\boldsymbol{p}}_{ij} \leq \boldsymbol{P}^{ij+}(0) \leq \bar{\boldsymbol{p}}_{ij}$ where $\bar{\boldsymbol{p}}_i$, $\underline{\boldsymbol{p}}_i$, $\bar{\boldsymbol{p}}_{ij}$ and $\underline{\boldsymbol{p}}_{ij}$ are known positive values. If the following inequality is satisfied,*

$$\begin{aligned} &\bar{a}_i^2\bar{p}_i + 2\bar{a}_i^2\Big(\mathcal{C}_1\bar{p}_i\bar{\mathcal{F}}_{ij,\max}\Big)\Big[\boldsymbol{r}_{ij,\min}^{-1} - \boldsymbol{r}_{ij,\max}^{-1}\mathcal{C}_1\bar{\mathcal{F}}_{ij,\min}\underline{p}_i\bar{\mathcal{F}}_{ij,\min}^T \\ &\times\boldsymbol{r}_{ij,max}^{-1}\Big]\Big(\mathcal{C}_1\bar{p}_i\bar{\mathcal{F}}_{ij,\max}\Big)^T + 2\bar{a}_i^2\Big(\sum_{j\in\mathcal{N}_{ci}}\bar{p}_{ij}\bar{\Phi}_{ij,\max}^{2^T}\Big)\Big[\boldsymbol{r}_{ij,\min}^{-1} - \\ &\boldsymbol{r}_{ij,\max}^{-1}\mathcal{C}_1\bar{\mathcal{F}}_{ij,\min}\underline{p}_i\bar{\mathcal{F}}_{ij,\min}^T\boldsymbol{r}_{ij,\max}^{-1}\Big]\Big(\sum_{j\in\mathcal{N}_{ci}}\bar{p}_{ij}\bar{\Phi}_{ij,\max}^{2^T}\Big)^T \leq \bar{p}_i \end{aligned} \tag{5.35}$$

where

$$\bar{d}_{ij} = \{d_{ij}|\max_{j\in\mathcal{N}_{ci}}(\psi_{ij})\}, \qquad \underline{d}_{ij} = \{d_{ij}|\min_{j\in\mathcal{N}_{ci}}(\psi_{ij})\}$$

$$\underline{\boldsymbol{\gamma}}_{ij} \leq \mathbb{E}\Big\{\boldsymbol{\gamma}_{ij}\Big\} \leq \bar{\boldsymbol{\gamma}}_{ij}$$

$$\bar{\mathcal{F}}_{ij,\max} = \sum_{j\in\mathcal{N}_{ci}} \bar{d}_{ij}\bar{a}_{ij}\bar{\boldsymbol{\alpha}}^l_{ij,\max}\bar{h}_{ij},\ \bar{\mathcal{F}}_{ij,\min} = \sum_{j\in\mathcal{N}_{ci}} \underline{d}_{ij}\bar{a}_{ij}\bar{\boldsymbol{\alpha}}^l_{ij,\min}\underline{h}_{ij}$$

$$\bar{\Phi}^2_{ij,\max} = \bar{d}_{ij}\bar{a}_{ij}\bar{\boldsymbol{\alpha}}^l_{ij,\max}\bar{h}_{ij}\bar{\boldsymbol{\zeta}}^l_{ij,\max},\quad \bar{\Phi}^2_{ij,\min} = \underline{d}_{ij}\bar{a}_{ij}\bar{\boldsymbol{\alpha}}^l_{ij,\min}\underline{h}_{ij}\underline{\boldsymbol{\zeta}}^l_{ij,\min}$$

$$\bar{\Phi}^3_{ij,\max} = \bar{d}_{ij}\bar{a}_{ij}\bar{\boldsymbol{\alpha}}^l_{ij,\max},\qquad \bar{\Phi}^3_{ij,\min} = \underline{d}_{ij}\bar{a}_{ij}\bar{\boldsymbol{\alpha}}^l_{ij,\min}$$

$$\bar{\Phi}^4_{ij,\max} = \bar{d}_{ij}\bar{a}_{ij}(\bar{\boldsymbol{\alpha}}^l_{ij,\min} - 1),\qquad \bar{\Phi}^4_{ij,\min} = \underline{d}_{ij}\bar{a}_{ij}(\bar{\boldsymbol{\alpha}}^l_{ij,\max} - 1)$$

$$\bar{\Phi}^5_{ij,\max} = \bar{d}_{ij}\bar{a}_{ij}(1-\bar{\boldsymbol{\alpha}}^l_{ij,\min})\bar{\boldsymbol{\beta}}^l_{ij,\max},\quad \bar{\Phi}^5_{ij,\min} = \underline{d}_{ij}\bar{a}_{ij}(1-\bar{\boldsymbol{\alpha}}^l_{ij,\max})\bar{\boldsymbol{\beta}}^l_{ij,\min}$$

$$\bar{\Phi}^7_{ij,\max} = \bar{d}_{ij}\bar{a}_{ij}\bar{\boldsymbol{\alpha}}^l_{ij,\max}(1-\underline{\boldsymbol{\gamma}}_{ij}),\quad \bar{\Phi}^7_{ij,\min} = \underline{d}_{ij}\bar{a}_{ij}\bar{\boldsymbol{\alpha}}^l_{ij,\min}(1-\bar{\boldsymbol{\gamma}}_{ij})$$

$$\bar{\Phi}^8_{ij,\max} = \bar{d}_{ij}\bar{a}_{ij}\bar{\boldsymbol{\alpha}}^l_{ij,\max}\bar{h}_{ij}(1-\bar{\boldsymbol{\zeta}}^l_{ij,\min})$$

$$\bar{\Phi}^8_{ij,\min} = \underline{d}_{ij}\bar{a}_{ij}\bar{\boldsymbol{\alpha}}^l_{ij,\min}\underline{h}_{ij}(1-\bar{\boldsymbol{\zeta}}^l_{ij,\max})$$

$$\bar{\Phi}^6_{ij,\max} = \bar{d}_{ij}\bar{a}_{ij}\boldsymbol{\alpha}^l_{ij,\max}\bar{h}_{ij}(1-\bar{\boldsymbol{\zeta}}^l_{ij,\min})\bar{\boldsymbol{\lambda}}^l_{ij,\max}$$

$$\bar{\Phi}^6_{ij,\min} = \underline{d}_{ij}\bar{a}_{ij}\boldsymbol{\alpha}^l_{ij,\min}\underline{h}_{ij}(1-\bar{\boldsymbol{\zeta}}^l_{ij,\max})\bar{\boldsymbol{\lambda}}^l_{ij,\min}$$

$$\begin{aligned}
\boldsymbol{r}_{ij,\max} =& \sum_{j\in\mathcal{N}_{ci}} \bar{\mathcal{F}}_{ij,\max}\bar{\boldsymbol{p}}_{ij}(\bar{\Phi}^2_{ij,\max})^T + \sum_{j\in\mathcal{N}_{ci}} \bar{\Phi}^2_{ij,\max}\bar{\boldsymbol{p}}_{ij}\bar{\mathcal{F}}^T_{ij,\max}\\
&+\mathcal{C}_2\sum_{j,s\in\mathcal{N}_{ci}} \bar{\Phi}^2_{ij,\max}\bar{\boldsymbol{p}}_{js}(\bar{\Phi}^2_{is,\max})^T + \mathcal{C}_3\sum_{j\in\mathcal{N}_{ci}} \bar{\Phi}^3_{ij,\max}\bar{\boldsymbol{R}}_{ij}(\bar{\Phi}^3_{ij,\max})^T\\
&+\mathcal{C}_5\sum_{j\in\mathcal{N}_{ci}} \bar{\Phi}^5_{ij,\max}\bar{\boldsymbol{\xi}_{ij}}^l(\bar{\Phi}^5_{ij,\max})^T + \mathcal{C}_6\sum_{j\in\mathcal{N}_{ci}} \bar{\Phi}^6_{ij,\max}\bar{\boldsymbol{\varrho}}^l_{ij}(\bar{\Phi}^6_{ij,\max})^T\\
&+\mathcal{C}_7\sum_{j\in\mathcal{N}_{ci}} \bar{\Phi}^7_{ij,\max}\bar{\boldsymbol{\delta}}_{ij}(\bar{\Phi}^7_{ij,\max})^T + \sum_{j\in\mathcal{N}_{ci}} \bar{\Phi}^8_{ij,\max}\bar{X}_j(\bar{\Phi}^8_{ij,\max})^T\\
&+\mathcal{C}_4\sum_{j\in\mathcal{N}_{ci}} \bar{\Phi}^4_{ij,\max}\bar{h}_{ij}(\bar{\Phi}^4_{ij,\max})^T
\end{aligned}$$

$$\begin{aligned}
\boldsymbol{r}_{ij,\min} =& \sum_{j\in\mathcal{N}_{ci}} \bar{\mathcal{F}}_{ij,\min}\underline{\boldsymbol{p}}_{ij}(\bar{\Phi}^2_{ij,\min})^T + \sum_{j\in\mathcal{N}_{ci}} \bar{\Phi}^2_{ij,\min}\underline{\boldsymbol{p}}_{ij}\bar{\mathcal{F}}^T_{ij,\min}\\
&+\mathcal{C}_2\sum_{j,s\in\mathcal{N}_{ci}} \bar{\Phi}^2_{ij,\min}\underline{\boldsymbol{p}}_{js}(\bar{\Phi}^2_{is,\min})^T + \mathcal{C}_3\sum_{j\in\mathcal{N}_{ci}} \bar{\Phi}^3_{ij,\min}\underline{\boldsymbol{R}}_{ij}(\bar{\Phi}^3_{ij,\min})^T\\
&+\mathcal{C}_5\sum_{j\in\mathcal{N}_{ci}} \bar{\Phi}^5_{ij,\min}\underline{\boldsymbol{\xi}_{ij}}^l(\bar{\Phi}^5_{ij,\min})^T + \mathcal{C}_6\sum_{j\in\mathcal{N}_{ci}} \bar{\Phi}^6_{ij,\min}\underline{\boldsymbol{\varrho}}^l_{ij}(\bar{\Phi}^6_{ij,\min})^T\\
&+\mathcal{C}_7\sum_{j\in\mathcal{N}_{ci}} \bar{\Phi}^7_{ij,\min}\underline{\boldsymbol{\delta}}_{ij}(\bar{\Phi}^7_{ij,\min})^T + \sum_{j\in\mathcal{N}_{ci}} \bar{\Phi}^8_{ij,\min}\underline{X}_j(\bar{\Phi}^8_{ij,\min})^T\\
&+\mathcal{C}_4\sum_{j\in\mathcal{N}_{ci}} \bar{\Phi}^4_{ij,\min}\underline{h}_{ij}(\bar{\Phi}^4_{ij,\min})^T
\end{aligned}$$

then, the inequality $\underline{\boldsymbol{p}}_i \leq \boldsymbol{P}^{i+}(k) \leq \boldsymbol{P}^{i-}(k) \leq \bar{\boldsymbol{p}}_i$ *holds for any* $k \geq 1$.

Proof. The proof is given in Appendix B. □

Remark 18. *In Theorem IV.2, we provide a sufficient condition for the convergence and resilience of the proposed filter using mathematical induction and matrix analysis. It is important to notice that condition (5.35) includes all terms involving the dynamics of the multi-robot system, event-triggered mechanism, cyber-attacks, communication topology as well as attack detector. In practice, the boundary of the multi-robot system in Assumption 1, the bound of the attacker signal and its probability, and the interaction of robots can be estimated by the defender using parameter identification. Note that if the bound of attack signals ($\boldsymbol{\xi}_{ij}^{l}$, $\boldsymbol{\varrho}_{ij}^{l}$, etc) increases according to condition (5.35), then $\boldsymbol{r}_{ij,\max}$ will increase, resulting in an increase of the upper bound of estimation error covariance. Also, the parameters Θ_{ij}, $\Lambda_{ij} > 0$ of the event-triggering mechanism in Eq. (5.7) affect the upper bound of the estimation error covariance. From (5.7), we can see that the average communication rate $\underline{\boldsymbol{\gamma}}_{ij}$ decreases as the value of Θ_{ij}, Λ_{ij} increase. Moreover, based on (5.35), we can see that $\boldsymbol{r}_{ij,\max}$ will increase as the value of Θ_{ij}, Λ_{ij} increase. Therefore, we conclude that the upper bound of error covariance increases with the value of Θ_{ij}, Λ_{ij}. Conversely, smaller values of Θ_{ij}, Λ_{ij} result in less data transmission. It follows from (5.35) that the upper bound of the error covariance would be decreased and better estimation performance would be expected at the cost of imposing a heavy burden on the communication channels. These two scenarios lead to a tradeoff in the value of Θ_{ij}, Λ_{ij} to balance between the estimation performance and reduced network transmission. When, both parameters of the event triggered mechanism (Θ_{ij}, Λ_{ij}) and those of the adversary signal ($\boldsymbol{\xi}_{ij}^{l}$, $\boldsymbol{\varrho}_{ij}^{l}$, etc) are large, the estimation error covariance might diverge. Convergence and resilience of the proposed filter are guaranteed provided that the attack signals, event-triggered parameters, etc., satisfy inequality (5.35). If the upper bound of the estimation error covariance converges asymptotically with k, then the error covariance must converge as well.*

Remark 19. *The parameter ψ_{ij} of the detection mechanism in Eq. (5.6) affects the performance of the proposed filter. When the sensor measurements of robot j are under malicious attack, the data received from robot j, namely, propagated state and error covariance, is suspicious and then the detector may trigger the alarm by setting $d_{ij}(k) = 0$ (representing a presence of attack) to avoid the transmission of the packets to other robots. As a result, the detection mechanism reduces the impact of malicious attack and improve the performance of the filter. Note that the defender may design the detector threshold (ψ_{ij}) in order to minimize the missing*

attack report rate, assuming knowledge of the boundary of the multi-robot system in Assumption 1, the bound of attacker signals and its probability, the interaction of robots, event-triggered parameters.

Note that the estimation error covariance in the SDECL algorithm does not represent the actual estimation error exactly. Therefore, the result of Theorem IV.2 can be employed to analyze the performance of the estimation error. This is done in our next Theorem.

Theorem IV.3. *Consider the nonlinear discrete-time system (5.1) and (5.2) with the event-triggered communication strategy (5.7) and random cyber attacks (5.3)-(5.5). If*

$$\hat{\boldsymbol{P}}^{i+}(k) \leq \hat{\boldsymbol{P}}^{i-}(k) \leq \bar{\boldsymbol{p}}_i \tag{5.36}$$

and for some $\epsilon_i > 0$, $\mathbb{E}\left\{\left\|\tilde{\boldsymbol{x}}^{i+}(0)\right\|^2\right\} \leq \epsilon_i$, *then the estimation error* $\tilde{\boldsymbol{x}}^{i+}(k) = \boldsymbol{x}^i(k) - \hat{\boldsymbol{x}}^{i+}(k)$ *is exponentially bounded in mean square for any* $i \in \vartheta$.

Proof. First, we choose the Lyapunov function as follows:

$$\boldsymbol{V}_k(\tilde{\boldsymbol{x}}^{i+}(k)) = \tilde{\boldsymbol{x}}^{i+}(k)^T\Big(\boldsymbol{P}^{i+}(k)\Big)^{-1}\tilde{\boldsymbol{x}}^{i+}(k) \tag{5.37}$$

Using Theorem IV.2 it is obtained that $\underline{\boldsymbol{p}}_i\boldsymbol{I} \leq \boldsymbol{P}^{i+}(k) \leq \bar{\boldsymbol{p}}_i\boldsymbol{I}$. According to the condition in (5.35), the Lyapunov function Eq. (5.37) is bounded according to the following inequality:

$$\tfrac{1}{\bar{\boldsymbol{p}}_i}\left\|\tilde{\boldsymbol{x}}^{i+}(k)\right\|^2 \leq \boldsymbol{V}_k(\tilde{\boldsymbol{x}}^{i+}(k)) \leq \tfrac{1}{\underline{\boldsymbol{p}}_i}\left\|\tilde{\boldsymbol{x}}^{i+}(k)\right\|^2 \tag{5.38}$$

Next, we will have to ensure the boundary of $\mathbb{E}\Big\{\boldsymbol{V}_k(\tilde{\boldsymbol{x}}^{i+}(k))|\tilde{\boldsymbol{x}}^{i+}(k-1)\Big\} - \boldsymbol{V}_{k-1}(\tilde{\boldsymbol{x}}^{i+}(k-1))$. On the basis of Eq. (5.37), the conditional expectation $\mathbb{E}\Big\{\boldsymbol{V}_k(\tilde{\boldsymbol{x}}^{i+}(k))|\tilde{\boldsymbol{x}}^{i+}(k-1)\Big\}$ is derived:

$$\begin{aligned}&\mathbb{E}\Big\{\boldsymbol{V}_k(\tilde{\boldsymbol{x}}^{i+}(k))|\tilde{\boldsymbol{x}}^{i+}(k-1)\Big\} = \mathbb{E}\Big\{\tilde{\boldsymbol{x}}^{i+}(k-1)^T\mathcal{A}_i(k-1)^T\bar{\Phi}^1_{ij}(k)^T\\ &\times\Big(\boldsymbol{P}^{i+}(k)\Big)^{-1}\bar{\Phi}^1_{ij}(k)\mathcal{A}_i(k-1)\tilde{\boldsymbol{x}}^{i+}(k-1)\Big\} + \boldsymbol{\mu}_{ij}(k)\end{aligned} \tag{5.39}$$

Considering the property of conditional expectation that $\mathbb{E}\Big\{\tilde{\boldsymbol{x}}^{i+}(k)|\tilde{\boldsymbol{x}}^{i+}(k)\Big\} = \tilde{\boldsymbol{x}}^{i+}(k)$,

the following equation is obtained by subtracting $\boldsymbol{V}_{k-1}(\tilde{\boldsymbol{x}}^{i+}(k-1))$ from Eq. (5.39):

$$
\begin{aligned}
&\mathbb{E}\Big\{\boldsymbol{V}_k(\tilde{\boldsymbol{x}}^{i+}(k))|\tilde{\boldsymbol{x}}^{i+}(k-1)\Big\} - \boldsymbol{V}_{k-1}(\tilde{\boldsymbol{x}}^{i+}(k-1)) \leq \tilde{\boldsymbol{x}}^{i+}(k-1)^T \\
&\times\Bigg\{\mathcal{A}_i(k-1)^T\bar{\Phi}^1_{ij}(k)^T\Big[\mathcal{C}_1\bar{\Phi}^1_{ij}(k)\Big(\mathcal{A}_i(k-1)\boldsymbol{P}^{i+}(k-1)\mathcal{A}_i(k-1)^T \\
&+\boldsymbol{G}_i(k-1)\boldsymbol{Q}_i(k-1)\boldsymbol{G}_i(k-1)^T\Big)\bar{\Phi}^1_{ij}(k)^T \\
&-\Big\{\sum_{j\in\mathcal{N}_{ci}}\bar{\Phi}^1_{ij}(k)\Big(\mathcal{A}_i(k-1)\boldsymbol{P}^{ij+}(k-1)\mathcal{A}_j(k-1)^T\Big)\bar{\Phi}^2_{ij}(k)^T\Big\}\boldsymbol{K}_i(k)^T \\
&-\boldsymbol{K}_i(k)\Big\{\sum_{j\in\mathcal{N}_{ci}}\bar{\Phi}^2_{ij}(k)\Big(\mathcal{A}_i(k-1)\boldsymbol{P}^{ij+}(k-1)\mathcal{A}_j(k-1)^T\Big)\bar{\Phi}^1_{ij}(k)^T\Big\} \\
&+\mathcal{C}_2\boldsymbol{K}_i(k)\Big\{\sum_{j,s\in\mathcal{N}_{ci}}\bar{\Phi}^2_{ij}(k)\boldsymbol{P}^{js-}(k)\bar{\Phi}^2_{is}(k)^T\Big\}\boldsymbol{K}_i(k)^T \\
&+\mathcal{C}_3\boldsymbol{K}_i(k)\Big\{\sum_{j\in\mathcal{N}_{ci}}\bar{\Phi}^3_{ij}(k)\boldsymbol{R}_{ij}(k)\bar{\Phi}^3_{ij}(k)^T\Big\}\boldsymbol{K}_i(k)^T \\
&+\mathcal{C}_4\boldsymbol{K}_i(k)\mathbb{E}\Big\{\sum_{j\in\mathcal{N}_{ci}}\bar{\Phi}^4_{ij}(k)\boldsymbol{h}_{ij}(\hat{\boldsymbol{x}}^{i-}(k),\hat{\boldsymbol{x}}^{j-}_a(k)) \\
&\qquad\times\boldsymbol{h}_{ij}(\hat{\boldsymbol{x}}^{i-}(k),\hat{\boldsymbol{x}}^{j-}_a(k))^T\bar{\Phi}^4_{ij}(k)^T\Big\}\boldsymbol{K}_i(k)^T \\
&+\mathcal{C}_5\boldsymbol{K}_i(k)\Big\{\sum_{j\in\mathcal{N}_{ci}}\bar{\Phi}^5_{ij}(k)\bar{\boldsymbol{\xi}}^{-\,l}_{ij}(k)\bar{\Phi}^5_{ij}(k)^T\Big\}\boldsymbol{K}_i(k)^T \\
&+\mathcal{C}_6\boldsymbol{K}_i(k)\Big\{\sum_{j\in\mathcal{N}_{ci}}\bar{\Phi}^6_{ij}(k)\bar{\boldsymbol{\varrho}}^l_{ij}(k)\bar{\Phi}^6_{ij}(k)^T\Big\}\boldsymbol{K}_i(k)^T \\
&+\mathcal{C}_7\boldsymbol{K}_i(k)\Big\{\sum_{j\in\mathcal{N}_{ci}}\bar{\Phi}^7_{ij}(k)\boldsymbol{\delta}_{ij}(k)\bar{\Phi}^7_{ij}(k)^T\Big\}\boldsymbol{K}_i(k)^T \\
&+\boldsymbol{K}_i(k)\Big\{\sum_{j\in\mathcal{N}_{ci}}\bar{\Phi}^8_{ij}(k)X_j(k)\bar{\Phi}^8_{ij}(k)^T\Big\}\boldsymbol{K}_i(k)^T\Big]^{-1} \\
&\times\bar{\Phi}^1_{ij}(k)\mathcal{A}_i(k-1) - \Big(\boldsymbol{P}^{i+}(k-1)\Big)^{-1}\Bigg\}\tilde{\boldsymbol{x}}^{i+}(k-1)
\end{aligned}
\tag{5.40}
$$

According to Eqs. (5.30)-(5.31), the following inequality for Kalman gain is given as:

$$
\begin{aligned}
&\|\boldsymbol{K}_i(k)\| \leq \Big(\mathcal{C}_1\bar{p}_i\bar{\mathcal{F}}_{ij,\max} + \sum_{j\in\mathcal{N}_{ci}}\bar{p}_{ij}\bar{\Phi}^{2^T}_{ij,\max}\Big) \\
&\times\Big(\mathcal{C}_1\bar{\mathcal{F}}_{ij,\min}\underline{p}_i\bar{\mathcal{F}}^T_{ij,\min} + \boldsymbol{r}_{ij,\min}\Big)^{-1} = \bar{\boldsymbol{K}}_i
\end{aligned}
\tag{5.41}
$$

Both sides of $\boldsymbol{\mu}_{ij}(k)$ are scalars. Using Lemma III.1 and computing the trace of

$\boldsymbol{\mu}_{ij}(k)$, we have:

$$\begin{aligned}
&\bar{\boldsymbol{\mu}}_{ij}(k) \leq \mathbf{Tr}\Big\{ \sum_{j\in\mathcal{N}_{ci}} \Big\{\mathcal{A}_j(k-1)^T \bar{\Phi}^2_{ij}(k)^T\Big\}\boldsymbol{K}_i(k)^T\Big(\boldsymbol{P}^{i+}(k)\Big)^{-1} \\
&\times \boldsymbol{K}_i(k) \sum_{j\in\mathcal{N}_{ci}} \Big\{\bar{\Phi}^2_{ij}(k)\mathcal{A}_j(k-1)\boldsymbol{P}^{js+}(k-1)\Big\}\Big\} \\
&-\mathbf{Tr}\Big\{ \mathcal{A}_i(k-1)^T \bar{\Phi}^1_{ij}(k)^T\Big(\boldsymbol{P}^{i+}(k)\Big)^{-1}\boldsymbol{K}_i(k) \\
&\times \sum_{j\in\mathcal{N}_{ci}} \Big\{\bar{\Phi}^2_{ij}(k)\mathcal{A}_j(k-1)\boldsymbol{P}^{ij+}(k-1)\Big\}\Big\} \\
&-\mathbf{Tr}\Big\{ \sum_{j\in\mathcal{N}_{ci}} \Big\{\mathcal{A}_j(k-1)^T \bar{\Phi}^2_{ij}(k)^T\Big\}\boldsymbol{K}_i(k)^T\Big(\boldsymbol{P}^{i+}(k)\Big)^{-1} \\
&\times \sum_{j\in\mathcal{N}_{ci}} \Big\{\bar{\Phi}^1_{ij}(k)\mathcal{A}_i(k-1)\boldsymbol{P}^{ij+}(k-1)\Big\}\Big\} \\
&+\mathbf{Tr}\Big\{ \sum_{j\in\mathcal{N}_{ci}} \Big\{\bar{\Phi}^2_{ij}(k)\Big\}\boldsymbol{K}_i(k)^T\Big(\boldsymbol{P}^{i+}(k)\Big)^{-1}\boldsymbol{K}_i(k)\bar{\Phi}^2_{ij}(k) \\
&\times \sum_{j\in\mathcal{N}_{ci}} \Big\{\boldsymbol{G}_j(k-1)\boldsymbol{Q}_j(k-1)\boldsymbol{G}_j(k-1)^T\Big\}\Big\} \\
&+\mathbf{Tr}\Big\{ \sum_{j\in\mathcal{N}_{ci}} \Big\{\bar{\Phi}^1_{ij}(k)^T\Big\}\Big(\boldsymbol{P}^{i+}(k)\Big)^{-1} \sum_{j\in\mathcal{N}_{ci}} \Big\{\bar{\Phi}^1_{ij}(k)\Big\}\boldsymbol{G}_i(k-1) \\
&\times \boldsymbol{Q}_i(k-1)\boldsymbol{G}_i(k-1)^T\Big\} + \mathbf{Tr}\Big\{ \sum_{j\in\mathcal{N}_{ci}} \Big\{\bar{\Phi}^7_{ij}(k)^T\Big\}\boldsymbol{K}_i(k)^T \\
&\times \Big(\boldsymbol{P}^{i+}(k)\Big)^{-1}\boldsymbol{K}_i(k) \sum_{j\in\mathcal{N}_{ci}} \Big\{\bar{\Phi}^7_{ij}(k)\boldsymbol{\delta}_{ij}(k)\Big\}\Big\} + ...
\end{aligned} \tag{5.42}$$

Then, $\mathbb{E}\Big\{\boldsymbol{V}_k(\tilde{\boldsymbol{x}}^{i+}(k))|\tilde{\boldsymbol{x}}^{i+}(k-1)\Big\} - \boldsymbol{V}_{k-1}(\tilde{\boldsymbol{x}}^{i+}(k-1))$ is written in the following form:

$$\begin{aligned}
&\mathbb{E}\Big\{\boldsymbol{V}_k(\tilde{\boldsymbol{x}}^{i+}(k))|\tilde{\boldsymbol{x}}^{i+}(k-1)\Big\} - \boldsymbol{V}_{k-1}(\tilde{\boldsymbol{x}}^{i+}(k-1)) \leq \bar{\boldsymbol{\mu}}_{ij} \\
&-\phi_i \boldsymbol{V}_{k-1}(\tilde{\boldsymbol{x}}^{i+}(k-1))
\end{aligned} \tag{5.43}$$

we can show the following inequality:

$$0 < \phi_i \leq 1 \tag{5.44}$$

According to Lemma IV.1, there is

$$\begin{aligned}
&\mathbb{E}\left\{\left\|\tilde{\boldsymbol{x}}^{i+}(k)\right\|^2\right\} \leq \tfrac{\bar{\kappa}}{\underline{\kappa}}\mathbb{E}\left\{\left\|\tilde{\boldsymbol{x}}^{i+}(0)\right\|^2\right\}(1-\boldsymbol{\phi}_i)^k \\
&+\tfrac{\boldsymbol{\mu}_i}{\underline{\boldsymbol{\kappa}}}\sum_{n=1}^{k-1}(1-\boldsymbol{\phi}_i)^n
\end{aligned} \tag{5.45}$$

This completes the proof. □

Remark 20. *According to Theorem IV.3, the upper bound of $\bar{\boldsymbol{\mu}}_{ij}(k)$ in (5.42) depends on the event-triggered threshold, parameters of cyber attack (sensor-filter and filter-filter communication channels) which affects on the upper bound of $\mathbb{E}\left\{\left\|\tilde{\boldsymbol{x}}^{i+}(k)\right\|^2\right\}$. Thus, by assuming bounded attacker signal (DoS and FDI) and choosing a proper event triggered condition, one can limit the upper bound of filtering error.*

Algorithm 3 A Secure Decentralized Cooperative Localization Algorithm Under Cyber Attack

1: Initialize state estimation and error covariance matrix as Robots $i \in \vartheta$ and $j \in \vartheta \backslash \{i\}$: $\hat{\mathbf{x}}^{i+}(0) \in \mathbb{R}^{n^i}$, $\mathbf{P}^{i+}(0) \in \mathbb{S}^{n^i}$, $\mathbf{P}^{ij+}(0) = \mathbf{0}_{n^i \times n^j}$

2: **repeat**

3: **Propagation:** Compute the predicted state and error covariance for each robot:

$$\begin{aligned}\hat{\mathbf{x}}^{i-}(k) &= \mathbf{f}^i(\hat{\mathbf{x}}^{i+}(k-1), \mathbf{u}_m^{i+}(k-1)) \\ \mathbf{P}^{i-}(k) &= \mathbf{A}_i(k-1)\mathbf{P}^{i+}(k-1)\mathbf{A}_i(k-1)^T \\ &\quad +\mathbf{G}_i(k-1)\mathbf{Q}_i(k-1)\mathbf{G}_i(k-1)^T\end{aligned}$$

4: **Update:**

5: if robot $i \in \vartheta$ detect the other robot in the team, the relative measurement $\mathbf{z}_{ij}(k)$ taken by each robot will sent to event-detector to judge whether to transmit the current measurement or not through unprotected communication network. Then, each robot exchange propagated state and error covariance with the other robot through unreliable communication network. The arriving *innovation* and its covariance considering cyber attacks are as follows:

$$\begin{aligned}&\boldsymbol{\Upsilon}_{ij}^a(k) = \boldsymbol{\alpha}_{ij}^l(k)\bar{\mathbf{z}}_{ij}(k) + (1 - \boldsymbol{\alpha}_{\boldsymbol{ij}}{}^l(k))\boldsymbol{\beta}_{ij}^l(k)\boldsymbol{\xi}_{ij}^l(k) \\ &-\mathbf{h}_{ij}(\hat{\mathbf{x}}^{i-}(k), \hat{\mathbf{x}}^{j-}(k))\end{aligned}$$

$$\begin{aligned}\mathbf{S}_{ij}^a(k) &= \mathcal{C}_1\bar{\mathcal{F}}_{ij}(k)\mathbf{P}^{i-}(k)\bar{\mathcal{F}}_{ij}(k)^T + \sum_{j\in\mathcal{N}_{ci}}\bar{\mathcal{F}}_{ij}(k)\mathbf{P}^{ij-}(k)\bar{\Phi}_{ij}^2(k)^T \\ &+\sum_{j\in\mathcal{N}_{ci}}\bar{\Phi}_{ij}^2(k)\mathbf{P}^{ij-}(k)\bar{\mathcal{F}}_{ij}(k)^T + \mathcal{C}_2\sum_{j,s\in\mathcal{N}_{ci}}\bar{\Phi}_{ij}^2(k)\mathbf{P}^{js-}(k)\bar{\Phi}_{is}^2(k)^T \\ &+\mathcal{C}_3\sum_{j\in\mathcal{N}_{ci}}\bar{\Phi}_{ij}^3(k)\mathbf{R}_{ij}(k)\bar{\Phi}_{ij}^3(k)^T + \mathcal{C}_5\sum_{j\in\mathcal{N}_{ci}}\bar{\Phi}_{ij}^5(k)\bar{\boldsymbol{\xi}}_{ij}^{\ l}(k)\bar{\Phi}_{ij}^5(k)^T \\ &+\mathcal{C}_6\sum_{j\in\mathcal{N}_{ci}}\bar{\Phi}_{ij}^6(k)\bar{\boldsymbol{\varrho}}_{ij}^l(k)\bar{\Phi}_{ij}^6(k)^T + \mathcal{C}_7\sum_{j\in\mathcal{N}_{ci}}\bar{\Phi}_{ij}^7(k)\boldsymbol{\delta}_{ij}(k)\bar{\Phi}_{ij}^7(k)^T \\ &+\mathcal{C}_4\mathbb{E}\Big\{\sum_{j\in\mathcal{N}_{ci}}\bar{\Phi}_{ij}^4(k)\mathbf{h}_{ij}(\hat{\mathbf{x}}^{i-}(k), \hat{\mathbf{x}}_a^{j-}(k))\mathbf{h}_{ij}(\hat{\mathbf{x}}^{i-}(k), \hat{\mathbf{x}}_a^{j-}(k))^T \\ &\times\bar{\Phi}_{ij}^4(k)^T\Big\} + \sum_{j\in\mathcal{N}_{ci}}\bar{\Phi}_{ij}^8(k)\mathrm{X}_j(k)\bar{\Phi}_{ij}^8(k)^T\end{aligned}$$

- If arriving *innovation* is greater than the threshold, i.e., $\left\|\boldsymbol{\Upsilon}_{ij}^a(k)\right\| \geq \psi^i \Longrightarrow$ attack detected $\Longrightarrow$ trigger the alarm
- If arriving *innovation* is less than the threshold, i.e., $\left\|\boldsymbol{\Upsilon}_{ij}^a(k)\right\| < \psi^i \Longrightarrow$ proposed filter is resilient against cyber attacks $\Longrightarrow$ follow steps 6-9

6: Compute optimal Kalman gain under cyber attacks:

$$\mathbf{K}_i^a(k) = \left[\mathcal{C}_1\mathbf{P}^{i-}(k)\bar{\mathcal{F}}_{ij}(k) + \sum_{j\in\mathcal{N}_{ci}}\mathbf{P}^{ij-}(k)\bar{\Phi}_{ij}^2(k)^T\right](\mathbf{S}_{ij}^a(k))^{-1}$$

7: Update state estimation with the current measurement:

$$\hat{\mathbf{x}}_a^{i+}(k) = \hat{\mathbf{x}}^{i-}(k) + \mathbf{K}_i^a(k)\sum_{j\in\mathcal{N}_{ci}}\boldsymbol{\Upsilon}_{ij}^a(k)$$

8: Update the error covariance:

$$\begin{aligned}\mathbf{P}_a^{i+}(k) &= \mathbf{P}^{i-}(k) - \mathbf{K}_i^a(k)\mathbf{S}_{ij,a}(k)\mathbf{K}_i^a(k)^T \\ \mathbf{P}_a^{ij+}(k) &= \mathbf{P}^{ij-}(k) - \mathbf{K}_i^a(k)\mathbf{S}_{ij,a}(k)\mathbf{K}_j^a(k)^T\end{aligned}$$

9: $k \leftarrow k+1$

V Case study

V.1 Simulation Results

Table 5.2: The value and description of the parameters in simulation

Parameters	Description	Value
b	Distance between wheels	0.5
N	Number of robots	4
Q_i	Standard deviation of control input	$(0.05)^2\text{diag}([(\Delta L^i)^2;(\Delta R^i)^2])$
R_{ij}	Standard deviation of relative measurements	$\text{diag}([0.1m^2;0.1rad^2])$
$P^{i+}(0)$, $P^{j+}(0)$	Initial covariance matrix	$\text{diag}([0.15^2;0.15^2;0.15^2])$

In this subsection the performance of the proposed SDECL algorithm (1) under cyber attacks is verified by simulation results. The motion equations of the ith robot is described by:

$$\begin{cases} x^i(t+1) = x^i(t) + \Delta t v^i(t)\cos(\theta^i(t) + \Delta\theta^i(t)) \\ y^i(t+1) = y^i(t) + \Delta t v^i(t)\sin(\theta^i(t) + \Delta\theta^i(t)) \\ \theta^i(t+1) = \theta^i(t) + \Delta t\omega^i(t) \qquad i \in \{1,2,3,4\} \end{cases} \tag{5.46}$$

where $x^i(t) \in \mathbb{R}^{n^i}$ and $y^i(t) \in \mathbb{R}^{n^i}$ are the Cartesian coordinates of robot i, $\theta^i(t) \in \mathbb{R}^{n^i}$ is the orientation, $v^i(t)$ and $\omega^i(t) \in \mathbb{R}^{n^i}$ are the linear velocity and angular velocity, respectively. Denote $u^i(t) = [\Delta L_i, \Delta R_i]^T$, where ΔL_i and ΔR_i are distance moved by wheels. Note that, the control input of each robot i is measured by odometry and inertial sensors. Also, the relative measurements taken by robot $i \in \{1,2,3,4\}$ from robot $j \in \{1,2,3,4\} \setminus \{i\}$ is described by:

$$z_{ij}(t) = \begin{bmatrix} \rho_{ij}(t) \\ \theta_{ij}(t) \end{bmatrix} = \begin{bmatrix} \sqrt{(x^i(t) - x^j(t))^2 + (y^i(t) - y^j(t))^2} \\ \arctan(\frac{y^i(t) - y^j(t)}{x^i(t) - x^j(t)}) \end{bmatrix} \tag{5.47}$$

where:

$\rho_{ij}(t)$ is the range of robot i relative to the robot j.

$\theta_{ij}(t)$ is the bearing of the robot i relative to the robot j.

We assume that additive white-Gaussian noise affects both the control input $u^i(t)$ and the relative measurements $z_{ij}(t)$. In a practical application, these noises may account for the effect of model uncertainties associated with the wheel encoders and an overhead camera. In our simulations, we compare the following: 1) the Ground truth of each robot; 2) Localization of robots using filter propagation; 3) Localization of robots using the SDECL algorithm 1 with/without cyber attacks.

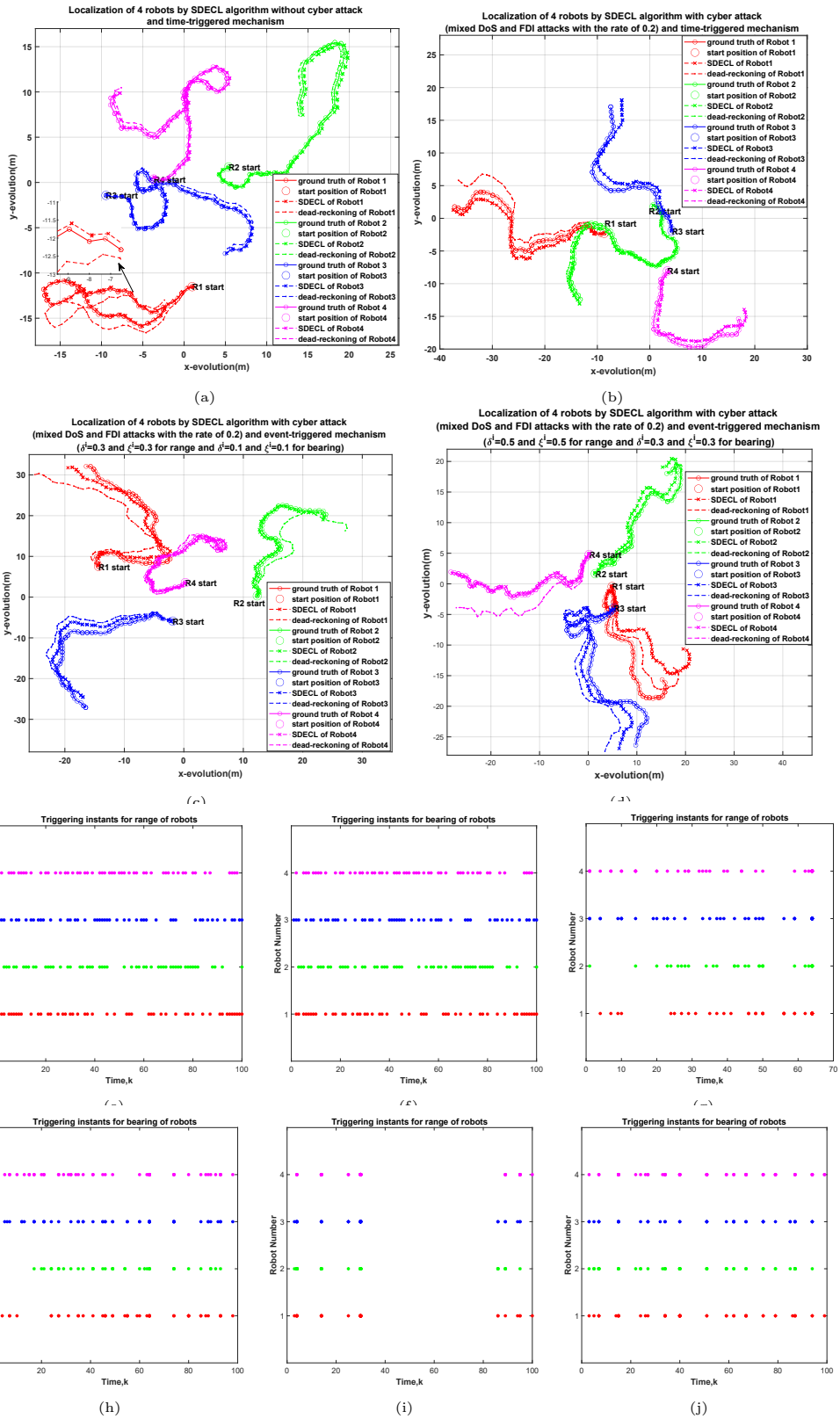

Figure 5.3: (a) Localization of 4 robots by the SDECL algorithm under event-triggered mechanism without cyber attack; (b)-(d) Localization of 4 robots by SDECL algorithm under different triggering conditions and with cyber attack; (e)-(j) the triggering instances for the range and bearing of the four robots; solid-o shows the ground truths, broken-dot shows the dead-reckoning and broken-x shows the EKF estimates of 4 robots.

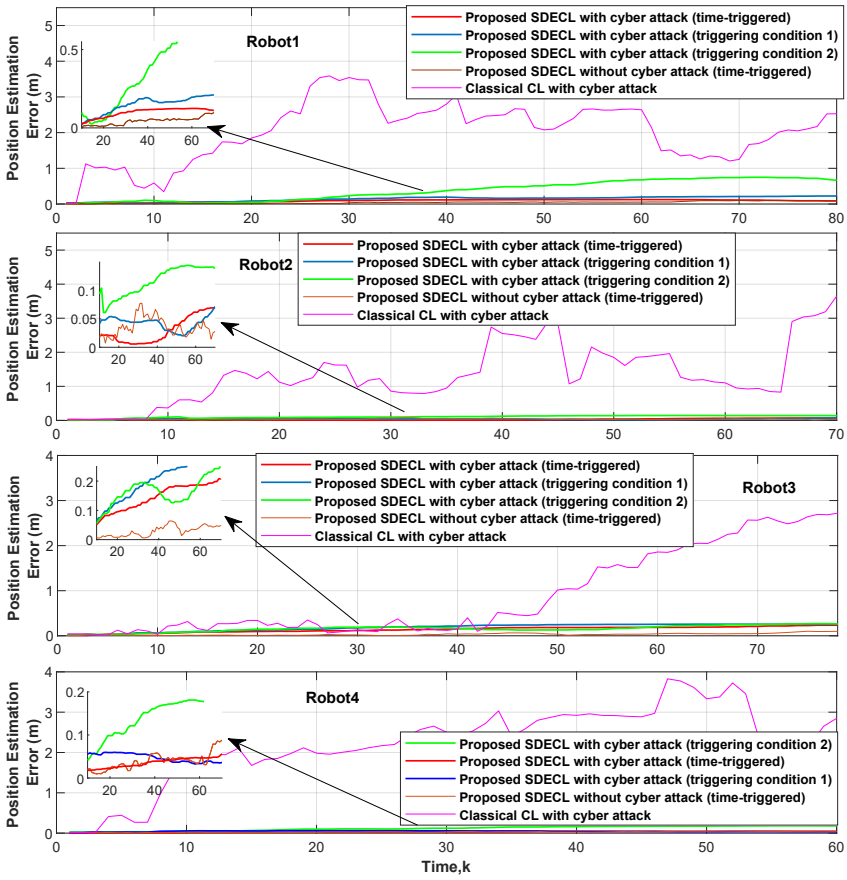

Figure 5.4: 1)The position estimation error of each robot using the SDECL algorithm for different scenarios; the brown curve shows under the event-triggered mechanism and without cyber attacks, the red, blue, and green curves show under different triggering conditions and with cyber attacks; 2)The pink color shows the position estimation error of each robot using classical CL algorithm under the event-triggered mechanism and with cyber attacks.

In our simulations, we assume that the mobile robots move in a random trajectory and at least one of them performs as a stationary robot. Robots then employ their exteroceptive sensors to observe the stationary robot and take relative measurements. We consider a scenario in which the filter corresponding to each robot receives information through an unreliable communication network. The moving robots then receive the predicted position and associated error covariance of each observed stationary robot over the unreliable communication network. An adversary can attempt to attack the communication between the sensor and filter of each robot and between two filters and degrade the localization quality. Fig. 5.3, Fig. 5.4, Fig. 5.5, and Fig. 5.6 show the outcome of our simulation results. We first evaluate the performance of the dead-reckoning method where each robot employs only the wheel encoders to estimate the pose (position and orientation) independently

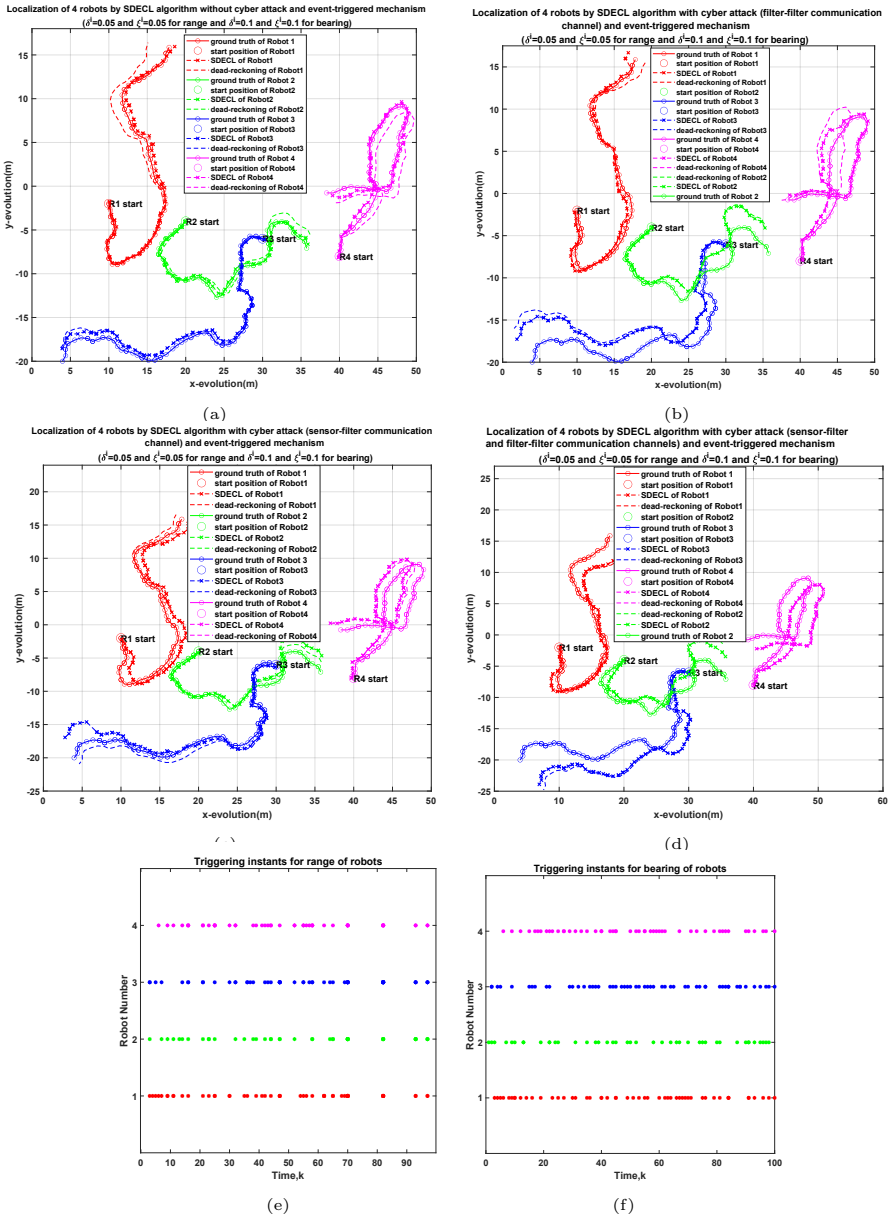

Figure 5.5: Localization of 4 robots by SDECL algorithm (a) under event-triggered mechanism without cyber attack; (b) with event-triggered mechanism and in the presence of malicious attacks on communication between the sensor measurements and the filter of the robot; (c) with event-triggered mechanism and in the presence of malicious attacks on communication between the filters; (d) with event-triggered mechanism and in the presence of malicious attacks on communication between the sensor measurements and the filter of robot and between the filters; (e)-(f) the triggering instances for range and bearing of the four robots

with no exchange of information (estimated states and error covariance) with other robots. As seen in Fig. 5.3 pose estimation error using the dead-reckoning method grow continuously for each robot, showing that using only local information (*i.e.* using only wheel-encoder information) is ineffective to determine the location of each robot in the team. Next, we consider the scenario in which each robot receives continuous (*i.e. time-triggered*) relative measurements through a reliable communi-

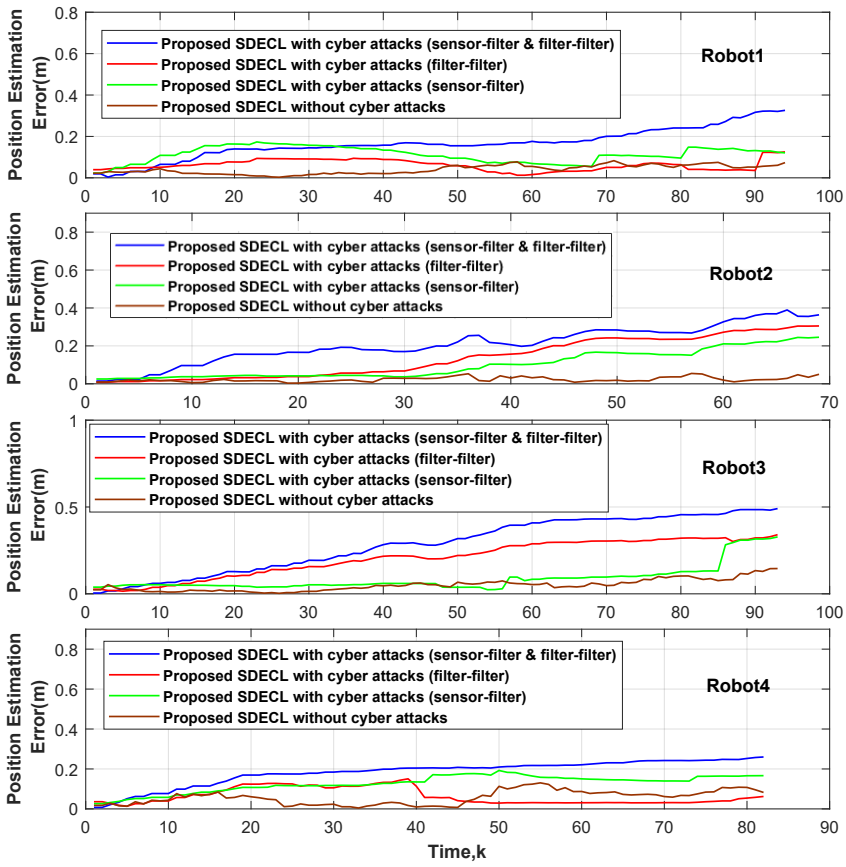

Figure 5.6: The position estimation error of each robot using SDECL algorithm for different scenarios.

cation network, without cyber attacks, and correct its pose estimation. As seen in Fig. 5.3(a), the pose estimation from the SDECL algorithm closely tracks the reference trajectory (ground truths). Fig. 5.3(e) and Fig. 5.3(f) indicate the triggering instances with respect to time for the range and bearing of each robot. Note that the absence of triggering times in the case of a time-triggered mechanism means that the robot i performs as a stationary robot for the rest of the robots.

Then, we simulate a scenario that includes mixed DoS and FDI attacks with a probability of 0.2 and 0.2 (both attacks) applied to the communication channel between the exteroceptive sensors and the corresponding estimator. In other words, we consider the case in which each robot receives relative measurement intermittently (with an event-triggered mechanism) in an unreliable communication network (with mixed DoS and FDI attacks) and correct its pose estimation using the proposed algorithm (1). Fig. 5.3(b), Fig. 5.3(c), and Fig. 5.3(d) show that when the event-triggering parameters increase for the same rate of DoS and FDI attacks,

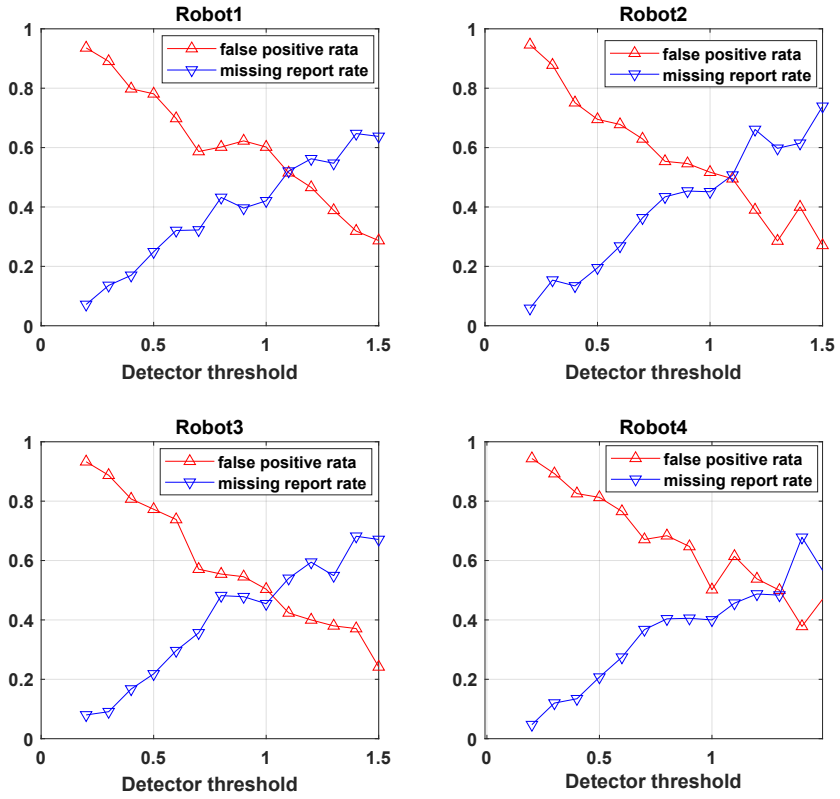

Figure 5.7: Relationship between detector threshold vs false positive rate and missing report rate

the quality of the tracking deteriorates slightly, however, the tracking error remains bounded. Fig. 5.3(g) and Fig. 5.3(h) display the triggering times corresponding to the event-triggering condition used in Fig. 5.3(c) and also Fig. 5.3(i) and Fig. 5.3(j) indicate the triggering instances corresponding to event-triggering condition used in Fig. 5.3(d). To compare the filter performance under different triggering conditions we use position error for each robot. According to Fig. 5.4, we conclude that our proposed algorithm (1) outperforms the classical CL under cyber attacks. Also, by properly tuning the triggering condition for the given attack rate, we can achieve good estimation while reducing the communication rate.

Then we consider the filter's performance under the following assumptions: (i) no attacks; when there is an attack affecting one of the following: (ii) communication between the sensor measurements and the robot's filter, (iii) communication between filters; (v) communication between the sensor measurements and the robot's filter, and between the filters. The results are shown in Fig. 5.5(a), Fig. 5.5(b), Fig. 5.5(c) and Fig. 5.5(d). We consider mixed DoS and FDI attacks with the probability of 0.1 and 0.1 applied in cases (ii), (iii) and (v). Also, the parameters of

the event-triggering conditions are the same in all cases. Fig. 5.5(e) and Fig. 5.5(f) show the triggering times corresponding to the event-triggering condition used in Fig. 5.5(a), Fig. 5.5(b), Fig. 5.5(c) and Fig. 5.5(d). Finally, we evaluate the performance of the filter by comparing the position error for all cases. We conclude that although the position error slightly increases in case (v) with respect to case (ii) and case (iii), the proposed filter still remains resilient against simultaneous attacks and considering the reduced amount of range-bearing measurements. Then we simulate the false alarm rate and missing report rate with different detector parameters. Fig. 5.7 shows the relationship between the false alarm rate and the missing report rate versus the detector parameter. It can be seen that the false alarm rate decreases when the detector threshold is increased, while the missing report rate increases when the detector threshold is increased. In other words, a small false alarm rate can be interpreted as the detector judging that normal relative measurements are untrustworthy, whereas a higher rate of the missing report can be interpreted that the detector judging that falsified relative measurements are credible.

V.2 Experimental Validation

In this subsection, we validate the performance of the SDECL algorithm by performing experiments on our robotic system. Our setup (see Fig. 5.8) consists of a Linux-based host computer equipped with Nvidia GPU, four e-puck2 mobile robots, an overhead ZED stereo camera, and a workspace of robots. The system is equipped with Robot Operating System (ROS) where each robot and the overhead camera correspond to a ROS node. Our computer vision system [117] tracks the pose of each robot with respect to the reference trajectory and also provides relative measurements. The accuracy of the computer vision-based positioning algorithm is 0.03m for range and 5 degrees for bearing. E-puck2 robots move along a circular trajectory simultaneously with a radius of 0.13 m (see Fig. 5.10). Each e-puck2 is equipped with an odometry sensor to propagate the filter. The host computer uses the ZED camera to collect data from the four e-puck2 robots and produce relative measurements (range and bearing) using computer vision software. The event detector uses the corresponding relative measurements to decide whether or not new information is to be transmitted to the robots. When a pair of robots receive new relative measurements, they exchange information (propagated state and error covariance) with each other to update the localization. The communication between e-puck2 robots

and the host computer is conducted through Bluetooth. There are inherent time delays in communication between two robots, the camera latency and image processing, and the event-detector. Also, the ROS package *message_filter* [119] is used to synchronize the time stamp of the odometry data and relative measurements. We perform two experiments as follows:

Localization of robots under cyber attacks

In this experiment, we compare the following: 1) A ground truth of each robot provided by the overhead ZED camera; 2) Localization of robots by odometry sensor; 3) Localization of robots using the SDECL algorithm 3 considering cyber attacks. Fig. 5.9 shows the results of our experiments. In our experiments, the trajectory generated by the overhead camera is employed as our reference trajectory. Note that the odometry sensor provides the pose estimates for the filter propagation. Each robot uses range-bearing measurements to improve localization accuracy. Fig. 5.9(a)-(d) and Fig. 5.9(e)-(h) show the performance of the SDECL algorithm under *time-triggered* and *event-triggered* mechanisms where packets transmitted in a reliable communication network. It can be seen that the *event-triggered* mechanism achieves a trade-off between localization accuracy and the number of transmitted packets. Fig. 5.9(i)-(l) shows the resiliency of the proposed SDECL algorithm in the presence of a bounded attack. We assume mixed DoS and FDI attacks with probabilities of 0.1 and 0.1 corrupting the sensor measurements in the sensor-filter communication channel. In this case, we assume that the attacker blocks and manipulates the relative measurement obtained from the camera in the communication channel between the exteroceptive sensors and the filter. It can be seen that the cyber attack deteriorates the localization accuracy slightly but still the proposed algorithm is resilient against bounded attacks. We also provide the position error of the four e-puck2 robots (see Fig. 5.11) by comparing (i) time-triggered mechanism without cyber attacks; (ii) event-triggered mechanism without cyber attacks; (iii) event-triggered mechanism with cyber attacks. We conclude that our algorithm provides satisfactory localization performance against cyber-attacks while reducing the amount of transmitted range-bearing measurements.

(a) (b) (c)

Figure 5.8: Experimental setup including (a) e-puck2 robot, (b) overhead ZED camera, (c) gaming laptop (equipped with Nvidia GPU)

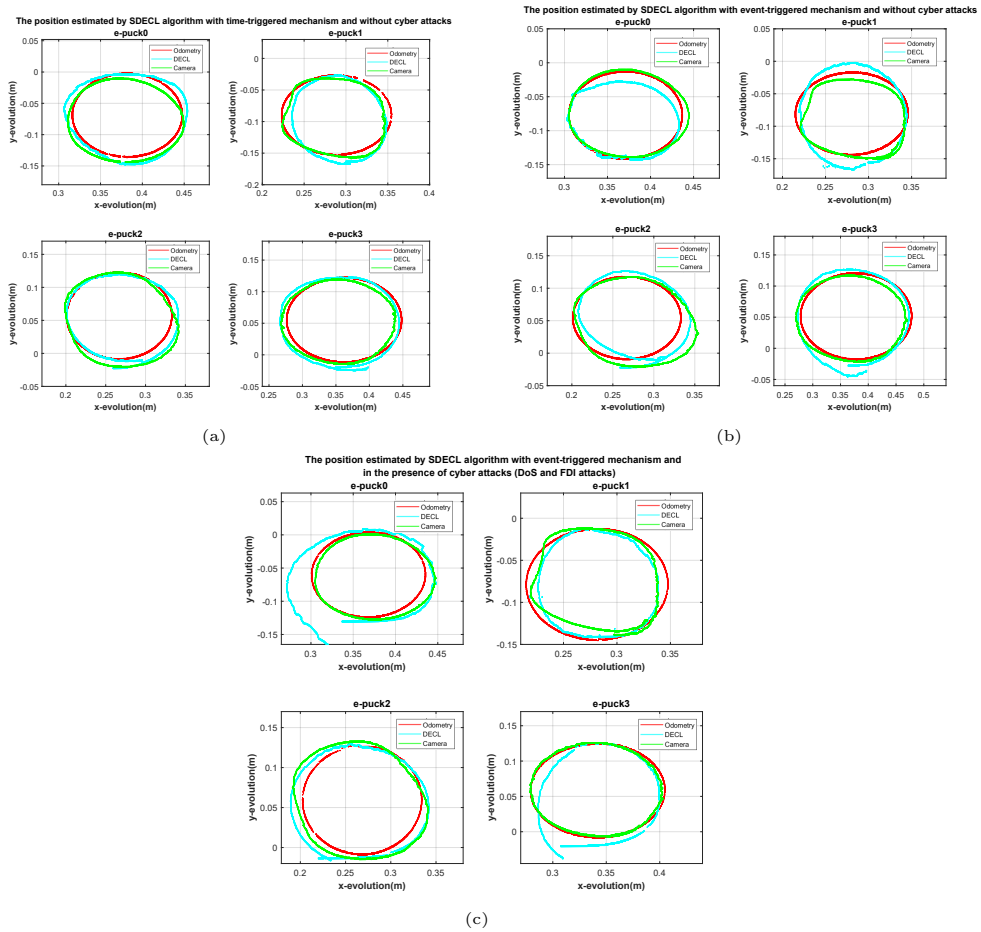

(a) (b)

(c)

Figure 5.9: Trajectories of the e-puck2 robots under an experimental test generated by four simultaneously running ROS packages, one for the camera location tracking (the green curve), one for the odometry estimate (the red curve), and the other one (the blue curve) to obtain location estimates by SDECL Algorithm (a)-(d) under the time-triggered mechanism and without cyber attacks; (e)-(h) under the event-triggered mechanism and without cyber attacks; (i)-(l) under the event-triggered mechanism and bounded cyber attacks

Cyber attack detection

In this experiment, we apply mixed DoS and FDI attacks to corrupt the transmitted relative measurement of e-puck0 under an unbounded attack signal. Since the attack

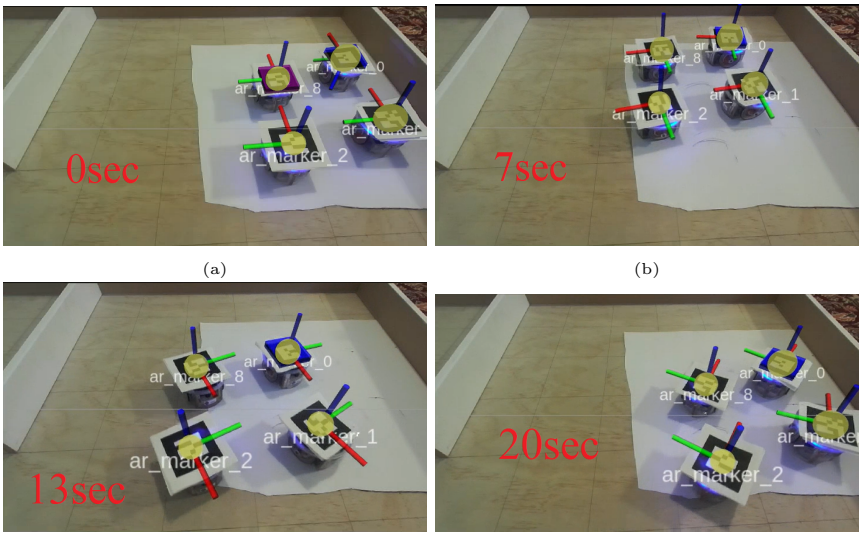

Figure 5.10: Status of robots under bounded attack rate; Proposed SDECL algorithm implemented on robots where robots moving simultaneously in circle trajectory.

detector monitors the filter by checking the arriving *innovation*, an alarm is triggered if the arriving *innovation* is greater than the threshold. Note that the LEDs of the e-pucks turn on when the alarm triggers, indicating the presence of a possible attack. Fig. 5.12(a)-(d) shows the status of e-pucks at $t = 0, 7, 13, 20$ s. According to the SDECL algorithm, all robots communicate with each other, in order to perform localization. When one of the robots receives corrupted sensor measurements, the corrupted packets (propagated state and error covariance) are transmitted to the other robots, thus increasing the norm of the arriving *innovation* and eventually triggering an alarm. It can be seen from Fig. 5.12(a)-(d) that the LEDs of all robots turned on as alarm since the corrupted packets (propagated state and error covariance) received from e-puck0 increase the arriving *innovation* of other robots and trigger the alarm indicating a possible attack. In Fig. 5.12(e)-(h) we consider the proposed attack detection mechanism. Here the alarm of e-puck0 is triggered indicating an attack, thus, the robot does not transmit the corrupted packets to the other robots. Therefore, we can see that the arriving *innovation* in the other robots is less than the threshold resulting in an improvement in the localization performance.

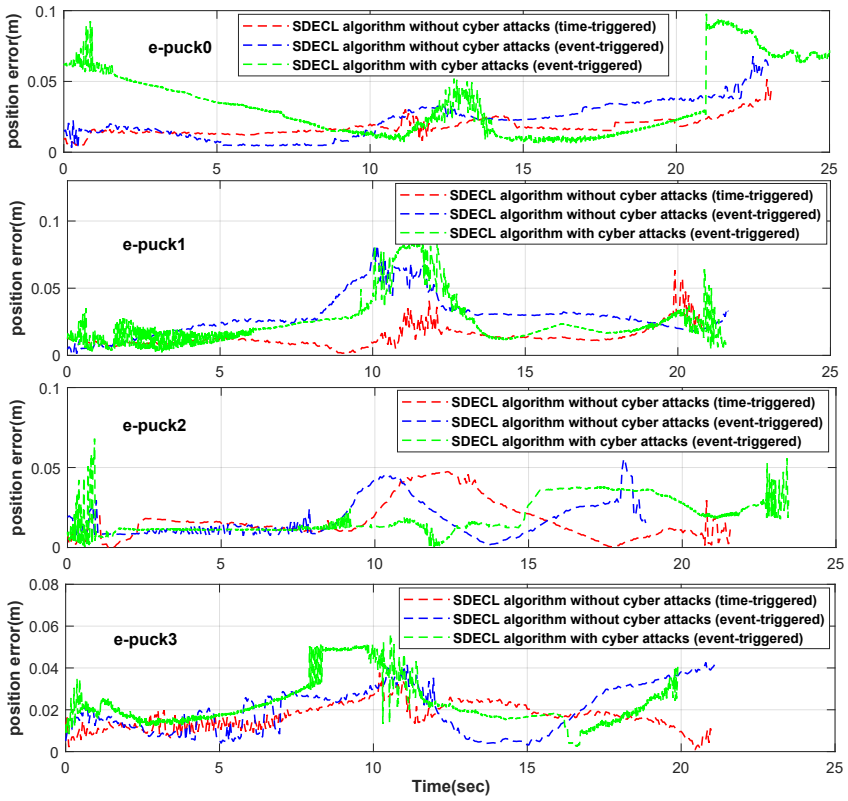

Figure 5.11: The estimated position error of each robot under (i) time-triggered mechanism and without cyber attacks; (ii) event-triggered mechanism and without cyber attacks; (iii) event-triggered mechanism and with cyber attacks

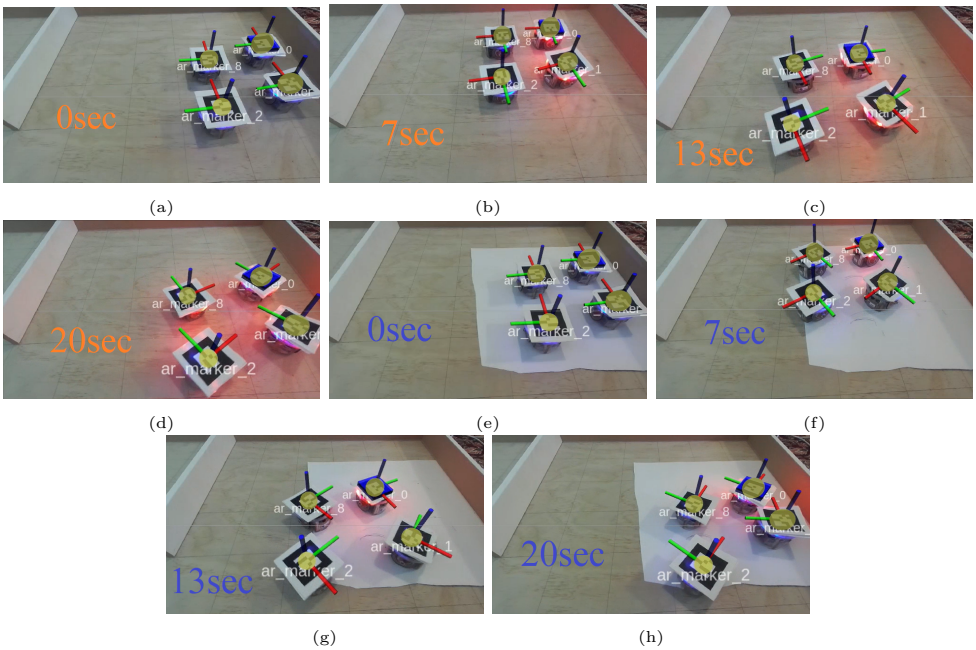

Figure 5.12: Status of robots under higher bound of attack signal; Proposed attack detector implemented on robots where robots moving simultaneously in circle trajectory.

Table 5.3: The value and description of the parameters in experiment

Parameters	Description	Value
b	Distance between wheels	0.053m
N	Number of robots	4
Q_i	Standard deviation of control input	$(0.05)^2\text{diag}([(\Delta L^i)^2; (\Delta R^i)^2])$
R_{ij}	Standard deviation of relative measurements	$\text{diag}([0.03m; 5^\circ])$
$P^{i+}(0)$, $P^{j+}(0)$	Initial covariance matrix of e-pucks	$\text{diag}([0.1^2; 0.1^2; 0.1^2])$
$\boldsymbol{x}^1(0)$	Initial pose of e-puck0	$[0.372, -0.129, 0]^T$
$\hat{\boldsymbol{x}}^{1+}(0)$	Initial estimated pose of e-puck0	$[0.372, -0.129, 0]^T$
$\boldsymbol{x}^2(0)$	Initial pose of e-puck1	$[0.305, -0.136, 0]^T$
$\hat{\boldsymbol{x}}^{2+}(0)$	Initial estimated pose of e-puck1	$[0.305, -0.136, 0]^T$
$\boldsymbol{x}^3(0)$	Initial pose of e-puck2	$[0.2679, -0.011, 0]^T$
$\hat{\boldsymbol{x}}^{3+}(0)$	Initial estimated pose of e-puck2	$[0.2679, -0.011, 0]^T$
$\boldsymbol{x}^4(0)$	Initial pose of e-puck3	$[0.339, -0.005, 0]^T$
$\hat{\boldsymbol{x}}^{4+}(0)$	Initial estimated pose of e-puck3	$[0.339, -0.005, 0]^T$

Chapter 6

Event-Triggered Consensus Control for Multi-Robot Systems with Cooperative Localization

I Introduction

In this chapter, we investigate the problem of event-triggered consensus control for a group of mobile robots based on cooperative localization (CL). In our framework, each robot employs the position estimates from CL to jointly achieve consensus. An event-triggered mechanism based on a mixed-type condition is adopted in order to reduce the frequency of control updates and unnecessary transmission of information between system components. Our goal is to design an event-triggered consensus controller based on CL such that the closed-loop system achieves the prescribed consensus in spite of inaccurate sensor measurements. We provide sufficient conditions that guarantee the desired consensus using eigenvalues and eigenvectors of the Laplacian matrix. We design the controller and filter gains as well as the parameters of the event-triggering mechanism simultaneously in terms of the solution for a linear matrix inequality (LMI). Finally, simulation and experimental results are used to demonstrate the effectiveness of the proposed approach.

The rest of this work is structured as follows. Section II introduces some preliminaries needed throughout the rest of the work. In Section III we derive sufficient conditions to ensure the desired consensus using a stochastic analysis combined with linear matrix inequalities. In Section IV, simulation and experiment results are conducted to show the effectiveness of the proposed method. Finally, the work presents

the conclusion in Section V.

Table 6.1: NOTATION

Notation List			
Notations	Description	Notations	Description
$\mathbb{E}\{.\}$	expectation of the random variable	diag(.)	block diagonal matrix
$\otimes$	Kronecker product	$\|.\|$	Euclidean norm of the vector
A^T	transpose of matrix A	A^{-1}	inverse of matrix A
I	identity matrix of appropriate dimensions	i and j	identity of robot i and robot j
$\boldsymbol{x}^i(k)$	state vector of the robot i	$\boldsymbol{u}^i(k)$	consensus control of robot i
$\boldsymbol{\eta}_i(k)$	process noise from control input of robot i	$\boldsymbol{\nu}_{ij}(k)$	measurement noise from exteroceptive sensors for pair (i,j)
$a_{ij}(k)$	indicator of interaction between robots	$\mathcal{N}_{ci}$	set of neighbors of robot i within communication range
$\boldsymbol{z}_{ij}(k)$	relative measurement taken by robot i from robot j	$\boldsymbol{Q}_i(k)$	covariance of $\boldsymbol{\eta}_i(k)$
$\boldsymbol{R}_{ij}(k)$	covariance of $\boldsymbol{\nu}_{ij}(k)$	$\boldsymbol{H}_i^i(k)$	sensor measurement matrix of robot i
$\boldsymbol{H}_j^i(k)$	sensor measurement matrix of pair (i,j)	$\hat{\boldsymbol{x}}^{i-}(k)$	propagated state of robot i
$\tilde{\boldsymbol{x}}^{i-}(k)$	propagated state error of robot i	$\hat{\boldsymbol{x}}^{i+}(k)$	estimation of robot i
$\tilde{\boldsymbol{x}}^{i+}(k)$	estimation error of robot i	$\boldsymbol{P}^{i-}(k)$	propagated state error covariance of robot i
$\boldsymbol{P}^{i+}(k)$	estimation error covariance of robot i	$\boldsymbol{P}^{ij-}(k)$	propagated state error covariance for the pair (i,j)
$\boldsymbol{P}^{ij+}(k)$	estimation error covariance for the pair (i,j)	$\boldsymbol{K}_i(k)$	Kalman gain of CL
$\boldsymbol{S}_{ij}$	covariance of innovation $\tilde{\boldsymbol{z}}_{ij}(k)$	α_i, β_i	event-triggered parameters of robot i
$\boldsymbol{\xi}_k$	consensus error (deviation of each state from the average state)	$G_i(k)$	consensus control gain
e_i	error of event-triggering sampling	δ	stepsize
$\mathcal{L}$	Laplacian matrix	$\lambda(A)$	eigenvalue of matrix A

II Problem Formulation and Preliminaries

II.1 Graph Theory

To work with a group of N robots we need some basic notions of graph theory. The interaction topology among N robots is modelled as a time-varying undirected graph $\mathcal{G}(k) = (\mathcal{V}, \mathcal{E}(k), \mathcal{A}(k))$. Let $\mathcal{V} = \{1, 2, ..., N\}$ represent an index set of N robots. An undirected edge of $\mathcal{G}(k)$ is represented by the ordered pair (i, j) which indicates that there is information flow from robot i to robot j. $\mathcal{A}(k) = \lfloor a_{ij}(k) \rfloor$

is the adjacency matrix where $a_{ij}(k) = 1$ if $(i, j) \in \mathcal{E}(k)$ otherwise $a_{ij}(k) = 0$. Also, $a_{ii}(k) = 0\ \forall i \in \{1, 2, ..., N\}$. The Laplacian matrix $\mathcal{L}(k) = [l_{ij}(k)]$ of the graph $\mathcal{G}$ is defined as $l_{ij}(k) = \sum_{i \neq j} a_{ij}(k)$ and $l_{ij}(k) = -a_{ij}(k)$ where $i \neq j$. The in-degree of robot i is defined as $\deg_{in}^{i}(k) = \sum_{j \in \mathcal{N}_{ci}} a_{ij}(k)$. Note that the variations of $\mathcal{G}(k)$ are driven by a random process, therefore the communication topology $\mathcal{G}(k)$ randomly switches s distinct graphs over the time, i.e., $\mathcal{G}_{un} = \{\mathcal{G}_1, \mathcal{G}_2, ..., \mathcal{G}_s\}$.

Assumption 8. *The interaction topologies $\mathcal{G}_1, \mathcal{G}_2, ..., \mathcal{G}_s$ among the N robots are undirected, and the union interaction topology $\mathcal{G}_{un} = \{\mathcal{G}_1, ..., \mathcal{G}_s\}$ has an undirected spanning tree [132].*

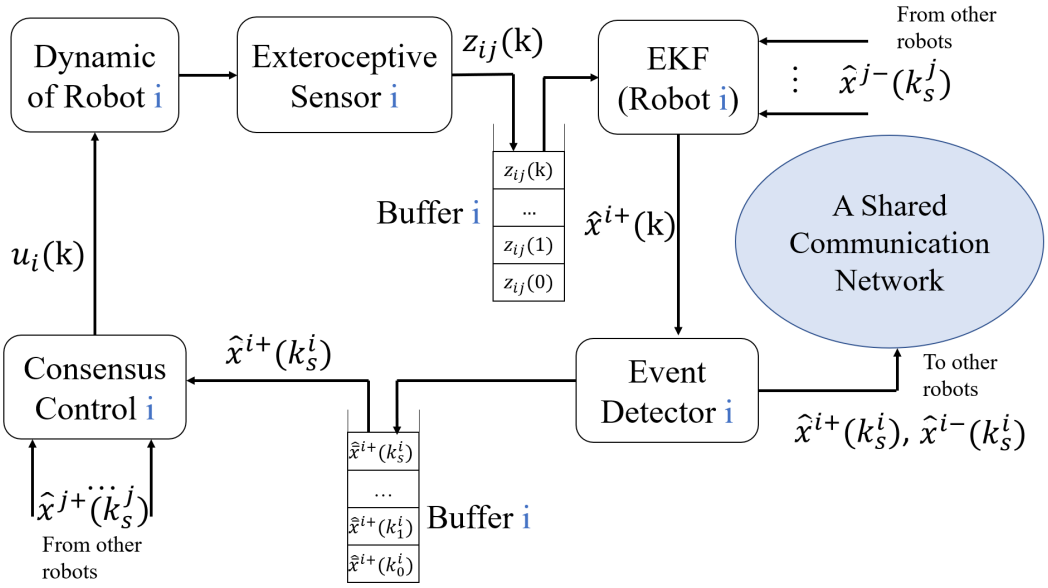

Figure 6.1: Block diagram of event-triggered consensus control for multi-robot systems with cooperative localization

II.2 Problem of Interest

We consider a group of N mobile robots working cooperatively to achieve a common objective. Each mobile robot employs position estimates obtained using cooperative localization (CL) to jointly achieve consensus. We assume a scenario in which each robot i is able to sense and take a relative measurement $\boldsymbol{z}_{ij}(k)$ with respect to its neighbours and also exchange information packets consistent with propagated and estimated position as well as error covariance with its neighbours residing within communication range. In other words, when performing consensus, robot j can exchange information with a neighbour robot i, only within certain communication

range defined as the set $\mathcal{N}_{ci} = \{j \in \mathcal{V} : (i,j) \in \mathcal{E}\}$. Notice also that the interaction topology of robots is time-varying representing the practical scenario in a multi-robot system where robots can randomly detect other robots in the group only within the reach of the exteroceptive sensors.

To reduce unnecessary communication between robots we use the event-triggered scheme as shown in Fig. 6.1 to decide whether or not the current position estimates are to be transmitted to neighbour robots through the communications network. For simplicity, we assume that the local clocks of all robots have been synchronized, which means that the event-checking instants of all robots are synchronized. Then based on transmitted position estimates, each robot generates the corresponding consensus control command. Also, the buffers in Fig. 6.1 store and retrieve information packets using a last-in-first-out protocol, which means that the filter and consensus control always receive the newest packets from the buffers.

Remark 21. *It is worth mentioning that when the robots are not residing within the communication range of each other, they may not able to maintain a connected communication topology. Therefore, in this work the communication topology at each time instant is not necessary to be connected which is more in line with the practical scenarios. Note also that, based on Assumption 1, our analysis only considers the connectivity of the union graph $\mathcal{G}_{un}$ rather than the exact graph at time k. According to the definition of the weighted adjacent matrix for $\mathcal{G}_{un}$, one can compute $\mathbb{E}\Big[\mathcal{L}(k)\Big] \triangleq \sum_{m=1}^{s} \pi_m \mathcal{L}_m$. Since $\mathcal{G}_{un}$ includes a spanning tree, zero is a simple eigenvalue of $\mathbb{E}\Big[\mathcal{L}(k)\Big]$, based on Assumption 8. A similar assumption can be found in references [132]-[133].*

II.3 Cooperative Localization

The motion equation of each robot i can be represented as follows [33]:

$$\begin{aligned} \boldsymbol{x}^i(k+1) &= \boldsymbol{f}^i(\boldsymbol{x}^i(k), v_m^i(k), \phi_m^i(k)) \\ &= \boldsymbol{x}^i(k) + \begin{bmatrix} \delta v_m^i(k)\cos(\phi_m^i(k)) \\ \delta v_m^i(k)\sin(\phi_m^i(k)) \end{bmatrix} \end{aligned} \tag{6.1}$$

where the vector state $\boldsymbol{x}^i(k) = [x^i(k), y^i(k)]^T$ represent the global position of robot i, v_m^i is the robot's linear velocity, ϕ_m^i is the robot's orientation, and δ is the sampling time. Each robot $i \in \mathcal{V}$ employs a wheel encoder to measure its linear velocity $v_m^i = v^i + \eta_v^i$ and to compute its absolute orientation $\phi_m^i = \phi^i + \eta_\phi^i$. The information

is used to compute the state propagation according to:

$$\begin{aligned}\hat{\boldsymbol{x}}^{i-}(k+1) &= \boldsymbol{f}^i(\hat{\boldsymbol{x}}^{i+}(k), v_m^i(k)) \\ &= \hat{\boldsymbol{x}}^{i+}(k) + \begin{bmatrix}\delta v^i(k)\cos(\phi^i(k))\\ \delta v^i(k)\sin(\phi^i(k))\end{bmatrix}\end{aligned} \tag{6.2}$$

where v^i is the actual linear velocity and ϕ^i is the actual orientation. Also, $\eta_v^i \sim N(0, \sigma_{\eta_v^i})$ and $\eta_\phi^i \sim N(0, \sigma_{\eta_\phi^i})$ are mutually uncorrelated zero-mean Gaussian white noises contaminating the linear velocity and orientation measurements, respectively. Defining the state propagation error $\tilde{\boldsymbol{x}}^{i-}(k) = \boldsymbol{x}^i(k) - \hat{\boldsymbol{x}}^{i-}(k)$, and taking equations (6.1) and (6.2) into account we can write:

$$\begin{aligned}\tilde{\boldsymbol{x}}^{i-}(k+1) = \tilde{\boldsymbol{x}}^{i+}(k) + \delta \begin{bmatrix}\cos(\phi^i(k)) & -v^i(k)\sin(\phi^i(k))\\ \sin(\phi^i(k)) & v^i(k)\sin(\phi^i(k))\end{bmatrix} \\ \times \begin{bmatrix}\eta_v^i(k)\\ \eta_\phi^i(k)\end{bmatrix} = \tilde{\boldsymbol{x}}^{i+}(k) + \delta \boldsymbol{C}_i(k)\eta_i(k)\end{aligned} \tag{6.3}$$

The propagated error covariance of the motion dynamics (6.1) is given by

$$\begin{aligned}\boldsymbol{P}^{i-}(k+1) &= \mathbb{E}\Big[\tilde{\boldsymbol{x}}^{i-}(k+1)\tilde{\boldsymbol{x}}^{i-}(k+1)^T\Big] = \boldsymbol{P}^{i+}(k) + \boldsymbol{Q}_i(k) \\ \boldsymbol{P}^{ij-}(k+1) &= \mathbb{E}\Big[\tilde{\boldsymbol{x}}^{i-}(k+1)\tilde{\boldsymbol{x}}^{j-}(k+1)^T\Big] = \boldsymbol{P}^{ij+}(k)\end{aligned} \tag{6.4}$$

where $\boldsymbol{Q}_i(k) = (\delta)^2 \boldsymbol{C}_i(k)\mathbb{E}\Big[\boldsymbol{\eta}_i(k)\boldsymbol{\eta}_i(k)^T\Big]\boldsymbol{C}_i(k)^T$. Next, whenever the robot i senses other robots in the team, it takes relative measurements from robot j using exteroceptive sensors, described as follows:

$$\boldsymbol{z}_{ij}(k) = \boldsymbol{h}_{ij}\big(\boldsymbol{x}^i(k), \boldsymbol{x}^j(k)\big) + \boldsymbol{\nu}_{ij}(k) \tag{6.5}$$

where $\boldsymbol{\nu}_{ij}$ is white-Gaussian measurement noise. The relative position measurement contains the range and bearing of robot i with respect to robot j. Considering relative measurements for each pair (i, j), the state estimation and covariance update for robot i can be obtained using extended Kalman filtering (EKF) as follows:

$$\begin{aligned}\hat{\boldsymbol{x}}^{i+}(k) &= \hat{\boldsymbol{x}}^{i-}(k) + \boldsymbol{K}_i(k)\Big[\sum_{j\in\mathcal{N}_{ci}} a_{ij}(k)\Big(\boldsymbol{z}_{ij}(k) - \boldsymbol{h}_{ij}(\hat{\boldsymbol{x}}^{i-}(k), \hat{\boldsymbol{x}}^{j-}(k))\Big)\Big] \\ \boldsymbol{P}^{i+}(k) &= \mathbb{E}\Big[\tilde{\boldsymbol{x}}^{i+}(k)\tilde{\boldsymbol{x}}^{i+}(k)^T\Big] = \boldsymbol{P}^{i-}(k) - \boldsymbol{K}_i(k)\boldsymbol{S}_{ij}(k)\boldsymbol{K}_i(k)^T \\ \boldsymbol{P}^{ij+}(k) &= \mathbb{E}\Big[\tilde{\boldsymbol{x}}^{i+}(k)\tilde{\boldsymbol{x}}^{j+}(k)^T\Big] = \boldsymbol{P}^{ij-}(k) - \boldsymbol{K}_i(k)\boldsymbol{S}_{ij}(k)\boldsymbol{K}_j(k)^T\end{aligned} \tag{6.6}$$

where $\boldsymbol{h}_{ij}(\hat{\boldsymbol{x}}^{i-}, \hat{\boldsymbol{x}}^{j-})$ is the propagated measurement. Let the first-order expansion of $\boldsymbol{h}_{ij}(\boldsymbol{x}^i, \boldsymbol{x}^j)$ around $(\hat{\boldsymbol{x}}^{i-}, \hat{\boldsymbol{x}}^{j-})$ be

$$\boldsymbol{h}_{ij}(\boldsymbol{x}^i, \boldsymbol{x}^j) \approx \boldsymbol{h}_{ij}(\hat{\boldsymbol{x}}^{i-}, \hat{\boldsymbol{x}}^{j-}) + \boldsymbol{H}_i^i(\boldsymbol{x}^i - \hat{\boldsymbol{x}}^{i-}) + \boldsymbol{H}_j^i(\boldsymbol{x}^j - \hat{\boldsymbol{x}}^{j-}) \tag{6.7}$$

where $\boldsymbol{H}_i^i = \frac{\partial \boldsymbol{h}_{ij}(\hat{\boldsymbol{x}}^{i-}, \hat{\boldsymbol{x}}^{j-})}{\partial \boldsymbol{x}^i}$ and $\boldsymbol{H}_j^i = \frac{\partial \boldsymbol{h}_{ij}(\hat{\boldsymbol{x}}^{i-}, \hat{\boldsymbol{x}}^{j-})}{\partial \boldsymbol{x}^j}$. Also, $\boldsymbol{K}_i$ and $\boldsymbol{K}_j$ are the Kalman gain for robot i and robot j and also $\boldsymbol{S}_{ij}$ is the covariance of the innovation $\tilde{\boldsymbol{z}}_{ij}(k) = \boldsymbol{z}_{ij}(k) - \boldsymbol{h}_{ij}(\hat{\boldsymbol{x}}^{i-}(k), \hat{\boldsymbol{x}}^{j-}(k))$ for pair (i, j).

II.4 Event-Triggered Consensus Control

Considering the nonlinear dynamics of N robots, we discretize (6.1) using the forward Euler approach as

$$\boldsymbol{x}^i(k+1) = \boldsymbol{x}^i(k) + \delta \boldsymbol{u}_i(k) + \delta \boldsymbol{C}_i(k)\boldsymbol{\eta}_i(k) \tag{6.8}$$

where

$$\boldsymbol{u}_i(k) = \begin{bmatrix} \boldsymbol{u}_i^x(k) \\ \boldsymbol{u}_i^y(k) \end{bmatrix} = \begin{bmatrix} v^i(k)\cos(\phi^i(k)) \\ v^i(k)\sin(\phi^i(k)) \end{bmatrix}$$

Without loss of generality, we assume that the error between desired orientation and the actual orientation of the robot is bounded. The consensus control based on estimated states obtained from the CL algorithm can be designed as follows:

$$\boldsymbol{u}_i(k) = \boldsymbol{G}_i(k) \sum_{j \in \mathcal{N}_{ci}} a_{ij}(k) \Big(\hat{\boldsymbol{x}}^{i+}(k) - \hat{\boldsymbol{x}}^{j+}(k) \Big) \tag{6.9}$$

where $\boldsymbol{G}_i(k)$ is the consensus control gain to be determined.

We now introduce the event-triggered scheme according to Fig. 6.1. In order to characterize such a scheme, let the triggering instances of robot i be $0 \leq k_0^i < k_1^i < k_2^i < \cdots < k_s^i$. The event-generator functions $\Upsilon_i(.,.,.) : \mathbb{R}^q \times \mathbb{R} \longrightarrow \mathbb{R}$ $(i = 1, 2, ..., N)$ are selected as follows:

$$\Upsilon_i\Big(\boldsymbol{e}_i(k), \alpha_i, \beta_i\Big) = \|\boldsymbol{e}_i(k)\|^2 - \alpha_i^2 \left\|\hat{\boldsymbol{x}}^{i+}(k)\right\|^2 - \beta_i^2 \tag{6.10}$$

Here, $\boldsymbol{e}_i(k) = \hat{\boldsymbol{x}}^{i+}(k) - \hat{\boldsymbol{x}}^{i+}(k_s^i)$ is the error between the local estimated state at the current time k and the latest triggering instance k_s^i and α_i, β_i are the design parameters of the event-triggering scheme. We treat the coordinate directions as a vector $(\hat{\boldsymbol{x}}^i(k) = [\hat{x}^i(k), \hat{y}^i(k)]^T)$ and use a single triggering condition. The triggering rule used in (6.10) is a discrete-time version of the so-called *mixed-type* triggering condition introduced in [91] which includes both *send-on-delta type* and *relative type* triggering conditions as special cases. Indeed, setting $\alpha_i = 0$ we obtain a *send-on-delta type* condition, whereas setting $\beta_i = 0$ we obtain a *relative-type* condition. Note that the parameter α_i is chosen such that $0 \leq \alpha_i < 1$, and usually it takes values close to zero. Also, the parameter β_i is chosen such that $\beta_i > 0$, [91]. The control executions are triggered whenever the following condition is satisfied:

$$\Upsilon_i(\boldsymbol{e}_i(k), \alpha_i, \beta_i) > 0. \tag{6.11}$$

Therefore, the sequence of triggering instances can be determined as follows:

$$k_{s+1}^i = \inf\{k \in \mathbb{N} | k > k_s^i, \Upsilon_i(\boldsymbol{e}_i(k), \alpha_i, \beta_i) > 0\}. \tag{6.12}$$

Considering the event-triggered setup for the consensus control, the closed-loop system can be written as follows:

$$\begin{cases} \hat{\boldsymbol{x}}^{i+}(k) = \hat{\boldsymbol{x}}^{i-}(k_s^i) + \boldsymbol{K}_i(k)\Big[\sum_{j\in\mathcal{N}_{ci}} a_{ij}(k)\Big(\boldsymbol{z}_{ij}(k) - \boldsymbol{h}_{ij}(\hat{\boldsymbol{x}}^{i-}(k_s^i), \hat{\boldsymbol{x}}^{j-}(k_s^j))\Big)\Big] \\ = \hat{\boldsymbol{x}}^{i-}(k) - e_i(k) + \boldsymbol{K}_i(k)\Big[\sum_{j\in\mathcal{N}_{ci}} a_{ij}(k)\Big(\boldsymbol{H}_i^i(k)\tilde{\boldsymbol{x}}^{i-}(k) + \boldsymbol{H}_j^i(k)\tilde{\boldsymbol{x}}^{j-}(k) \\ +\boldsymbol{\nu}_{ij}(k)\Big)\Big] - \boldsymbol{K}_i(k)\Big[\sum_{j\in\mathcal{N}_{ci}} a_{ij}(k)\Big(\boldsymbol{H}_i^i(k)e_i(k) + \boldsymbol{H}_j^i(k)e_j(k)\Big)\Big] \\ \boldsymbol{x}^i(k+1) = \boldsymbol{x}^i(k) + \delta\boldsymbol{G}_i(k)\Big[\sum_{j\in\mathcal{N}_{ci}} a_{ij}(k)\Big(\hat{\boldsymbol{x}}^{i+}(k) - \hat{\boldsymbol{x}}^{j+}(k)\Big)\Big] \\ \qquad +\delta\boldsymbol{G}_i(k)\Big[\sum_{j\in\mathcal{N}_{ci}} a_{ij}(k)\Big(e_j(k) - e_i(k)\Big)\Big] + \delta\boldsymbol{C}_i(k)\boldsymbol{\eta}_i(k) \end{cases} \tag{6.13}$$

Computing the estimation error $\tilde{\boldsymbol{x}}^{i+}(k) = \boldsymbol{x}^i(k) - \hat{\boldsymbol{x}}^{i+}(k)$, the closed-loop system (6.13) can be transformed into:

$$\begin{cases} \tilde{\boldsymbol{x}}^{i+}(k+1) = \tilde{\boldsymbol{x}}^{i+}(k) - e_i(k) + \delta\boldsymbol{C}_i(k)\boldsymbol{\eta}_i(k) \\ \qquad +\boldsymbol{K}_i(k)\Big[\sum_{j\in\mathcal{N}_{ci}} a_{ij}(k)\Big(\boldsymbol{H}_i(k)\big(\tilde{\boldsymbol{x}}^{i+}(k) - \tilde{\boldsymbol{x}}^{j+}(k)\big) + \boldsymbol{\nu}_{ij}(k)\Big)\Big] \\ \qquad -\boldsymbol{K}_i(k)\Big[\sum_{j\in\mathcal{N}_{ci}} a_{ij}(k)\Big(\boldsymbol{H}_i(k)\big(e_j(k) - e_i(k)\big)\Big)\Big] \\ \qquad +\boldsymbol{K}_i(k)\Big[\sum_{j\in\mathcal{N}_{ci}} a_{ij}(k)\Big(\delta\boldsymbol{H}_i(k)\big(\boldsymbol{C}_j(k)\eta_j(k) - \boldsymbol{C}_i(k)\eta_i(k)\big)\Big)\Big] \\ \boldsymbol{x}^i(k+1) = \boldsymbol{x}^i(k) + \delta\boldsymbol{G}_i(k)\Big[\sum_{j\in\mathcal{N}_{ci}} a_{ij}(k)\Big(\boldsymbol{x}^i(k) - \boldsymbol{x}^j(k)\Big)\Big] \\ \qquad -\delta\boldsymbol{G}_i(k)\Big[\sum_{j\in\mathcal{N}_{ci}} a_{ij}(k)\Big(\tilde{\boldsymbol{x}}^{i+}(k) - \tilde{\boldsymbol{x}}^{j+}(k)\Big)\Big] \\ \qquad +\delta\boldsymbol{G}_i(k)\Big[\sum_{j\in\mathcal{N}_{ci}} a_{ij}(k)\Big(e_j(k) - e_i(k)\Big)\Big] + \delta\boldsymbol{C}_i(k)\boldsymbol{\eta}_i(k) \end{cases} \tag{6.14}$$

In order to facilitate the discussion, the closed-loop system (6.14) can be written in compact form as follows:

$$\begin{cases} \boldsymbol{x}_{k+1} = \Big[I + \delta(\mathcal{L}_k \otimes G_k)\Big]\boldsymbol{x}_k - \delta(\mathcal{L}_k \otimes G_k)\tilde{\boldsymbol{x}}_k \\ \qquad -\delta(\mathcal{L}_k \otimes G_k)\boldsymbol{e}_k + \delta C_k\boldsymbol{\eta}_k \\ \tilde{\boldsymbol{x}}_{k+1} = \Big[I + \delta(\mathcal{L}_k \otimes K_k H_k)\Big]\tilde{\boldsymbol{x}}_k + \Big[I + (\mathcal{L}_k \otimes K_k H_k)\Big]\boldsymbol{e}_k \\ \qquad \delta\Big[I + (\mathcal{L}_k \otimes K_k H_k)\Big]C_k\boldsymbol{\eta}_k - (\mathcal{L}_k \otimes K_k)\boldsymbol{\nu}_k \end{cases} \tag{6.15}$$

where

$$\begin{aligned} &\boldsymbol{x}_k = \Big[\boldsymbol{x}^1(k)^T \;\; \boldsymbol{x}^2(k)^T \;...\; \boldsymbol{x}^N(k)^T\Big]^T, && \tilde{\boldsymbol{x}}_k = \Big[\tilde{\boldsymbol{x}}^{1+}(k)^T \;\; \tilde{\boldsymbol{x}}^{2+}(k)^T \;...\; \tilde{\boldsymbol{x}}^{N+}(k)^T\Big]^T \\ &\boldsymbol{e}_k = \Big[e_1(k)^T \;\; e_2(k)^T \;...\; e_N(k)^T\Big]^T, && \boldsymbol{\eta}_k = \Big[\boldsymbol{\eta}_1(k)^T \;\; \boldsymbol{\eta}_2(k)^T \;...\; \boldsymbol{\eta}_N(k)^T\Big]^T \\ &\boldsymbol{\nu}_k = \Big[\boldsymbol{\nu}_1(k)^T \;\; \boldsymbol{\nu}_2(k)^T \;...\; \boldsymbol{\nu}_N(k)^T\Big]^T, && \boldsymbol{K}_k = \Big[\boldsymbol{K}_1(k)^T \;\; \boldsymbol{K}_2(k)^T \;...\; \boldsymbol{K}_N(k)^T\Big]^T \\ &\boldsymbol{H}_k = \Big[\boldsymbol{H}_1(k)^T \;\; \boldsymbol{H}_2(k)^T \;...\; \boldsymbol{H}_N(k)^T\Big]^T, && \boldsymbol{G}_k = \Big[\boldsymbol{G}_1(k)^T \;\; \boldsymbol{G}_2(k)^T \;...\; \boldsymbol{G}_N(k)^T\Big]^T \\ &\boldsymbol{C}_k = \Big[\boldsymbol{C}_1(k)^T \;\; \boldsymbol{C}_2(k)^T \;...\; \boldsymbol{C}_N(k)^T\Big]^T, \end{aligned}$$

$$\mathcal{L}_k = \begin{bmatrix} -\deg_{in}^1 & a_{12} & a_{13} & \cdots & a_{1N} \\ a_{21} & -\deg_{in}^2 & a_{23} & \cdots & a_{2N} \\ \vdots & \vdots & \vdots & \ddots & \vdots \\ a_{N1} & a_{N2} & a_{N3} & \cdots & -\deg_{in}^N \end{bmatrix}.$$

We now define the average state of all agents as follows:

$$\bar{\boldsymbol{x}}_k = \frac{1}{N}\sum_{j=1}^{N}\boldsymbol{x}^i(k) = \frac{1}{N}(\mathbf{1}^T \otimes I)\boldsymbol{x}_k \tag{6.16}$$

Considering the interaction topology of agents, it is easy to obtain $\bar{\boldsymbol{x}}_{k+1}$:

$$\begin{aligned}
&\bar{\boldsymbol{x}}_{k+1} = \frac{1}{N}(\mathbf{1}^T \otimes I)\boldsymbol{x}_{k+1} = \frac{1}{N}(\mathbf{1}^T \otimes I)\Big\{\Big[I + \delta(\mathcal{L}_k \otimes G_k)\Big]\boldsymbol{x}_k \\
&-\delta(\mathcal{L}_k \otimes G_k)\tilde{\boldsymbol{x}}_k - \delta(\mathcal{L}_k \otimes G_k)\boldsymbol{e}_k + \delta C_k\boldsymbol{\eta}_k\Big\} = \\
&\Big[I + \delta(\mathcal{L}_k \otimes G_k)\Big]\bar{\boldsymbol{x}}_k - \frac{\delta}{N}(\mathbf{1}^T\mathcal{L}_k \otimes G_k)\tilde{\boldsymbol{x}}_k - \frac{\delta}{N}(\mathbf{1}^T\mathcal{L}_k \otimes G_k)\boldsymbol{e}_k.
\end{aligned} \tag{6.17}$$

The deviation of each state from the average state can be obtained as follows:

$$\begin{aligned}
&\boldsymbol{\xi}_{k+1} = \boldsymbol{x}_{k+1} - \bar{\boldsymbol{x}}_{k+1} = \Big\{\Big[I + \delta(\mathcal{L}_k \otimes G_k)\Big]\boldsymbol{x}_k - \delta(\mathcal{L}_k \otimes G_k)\tilde{\boldsymbol{x}}_k \\
&-\delta(\mathcal{L}_k \otimes G_k)\boldsymbol{e}_k + \delta C_k\boldsymbol{\eta}_k\Big\} - \Big\{\Big[I + \delta(\mathcal{L}_k \otimes G_k)\Big]\bar{\boldsymbol{x}}_k \\
&-\frac{\delta}{N}(\mathbf{1}^T\mathcal{L}_k \otimes G_k)\tilde{\boldsymbol{x}}_k - \frac{\delta}{N}(\mathbf{1}^T\mathcal{L}_k \otimes G_k)\boldsymbol{e}_k\Big\} = \Big[I + \delta(\mathcal{L}_k \otimes G_k)\Big]\boldsymbol{\xi}_k \\
&+\delta\Big((\mathscr{N}\mathcal{L}_k) \otimes G_k\Big)\tilde{\boldsymbol{x}}_k + \delta\Big((\mathscr{N}\mathcal{L}_k) \otimes G_k\Big)\boldsymbol{e}_k + \delta C_k\boldsymbol{\eta}_k,
\end{aligned} \tag{6.18}$$

where $\mathscr{N} = [n_{ij}]_{N\times N}$ with $n_{ij} = \dfrac{N-1}{N}$ for $i = j$ and $n_{ij} = \dfrac{-1}{N}$ for $i \neq j$. Given the coupling nature of MASs, we select $\phi_i \in \mathbb{R}^n$ with $\phi_i^T\mathcal{L} = \lambda_i\phi_i^T$ $(i = 2, 3, ..., N)$ to form a unitary matrix $M = [\dfrac{1}{\sqrt{N}}\phi_2 \ ... \ \phi_N]$ and then transform $\mathcal{L}_k$ to diagonal form as follows:

$$\text{diag}\{0, \lambda_2, ..., \lambda_N\} = M^T\mathcal{L}M \tag{6.19}$$

where each ϕ_i and λ_i is a pair of eigenvectors and eigenvalue of the Laplacian matrix $\mathcal{L}_k$. Then closed-loop system (6.15) can be written as follows:

$$\begin{cases}
\boldsymbol{\xi}_{k+1} = \Big[I + \delta(\mathcal{L}_k \otimes G_k)\Big]\boldsymbol{\xi}_k + \delta\Big((\mathscr{M}^T\mathscr{N}\mathcal{L}_k) \otimes G_k\Big)\tilde{\boldsymbol{x}}_k \\
\qquad +\delta\Big((\mathscr{M}^T\mathscr{N}\mathcal{L}_k) \otimes G_k\Big)\boldsymbol{e}_k + \delta C_k\boldsymbol{\eta}_k \\
\tilde{\boldsymbol{x}}_{k+1} = \Big[I + \delta(\Xi_k \otimes K_kH_k)\Big]\tilde{\boldsymbol{x}}_k + \Big[I + (\Xi_k \otimes K_kH_k)\Big]\boldsymbol{e}_k \\
\qquad \delta\Big[I + (\Xi_k \otimes K_kH_k)\Big]C_k\boldsymbol{\eta}_k - (\Xi_k \otimes K_k)\boldsymbol{\nu}_k
\end{cases} \tag{6.20}$$

where $\Xi_k = \text{diag}\{\lambda_2, ..., \lambda_N\}$ and $\mathscr{M} = [\phi_2^T \ ... \ \phi_N^T]^T$. We now introduce the following definition:

Definition II.1. Let the communication graph $\mathcal{G}$ and bounded function U be given. Assume that the initial position of the robots satisfy $\sum_{i=1}^{N}\left\|x^i(0) - (\frac{1}{N})\sum_{j=1}^{N}x^j(0)\right\| \leq \mathcal{X}_0$. The multi-robot system (6.8) with communication graph $\mathcal{G}$ is consensusable with bound U if the following condition satisfy [134]:

$$\mathbb{E}\Big\{\left\|x^i(k) - x^j(k)\right\|^2\Big\} \leq U, \quad i, j \in \mathcal{V}, k \geq 0 \tag{6.21}$$

Remark 22. *The distributed event-based control protocol* $\boldsymbol{u}_i(k) = \boldsymbol{G}_i(k) \sum_{j \in \mathcal{N}_{ci}} a_{ij}(k) \Big(\hat{\boldsymbol{x}}^{i+}(k_s^i) - \hat{\boldsymbol{x}}^{j+}(k_s^j) \Big)$ *is designed for robot i where the control protocol of robot i needs to be updated immediately not only at its own event-triggered times* k_0^i, k_1^i,... *but also at the event-triggered times of its neighbors* k_0^j, k_1^j,..., $j \in \mathcal{N}_{ci}$. *In other words, each robot i takes into account the last update value of each of its neighbors in its control protocol which is different from [135].*

Remark 23. *In this work, we adopt an event-based consensus control scheme in order to reduce the exchange of information between robots and reduce energy consumption. It is well established that a relative type triggering condition typically causes too many unnecessary events. On the other hand, an absolute type triggering condition can reduce the transmission of information between robots at the cost of consensus performance degradation. In this work, we use a mixed-type triggering condition which includes both absolute and relative type conditions as special cases and leads to a tradeoff between the convergence rate of the consensus error and a reduced number of events. See reference [136] for further details. Also, our proposed event-triggering scheme depends only on the state estimates of each robot and is independent of the state estimates of the neighboring robots as is the case in references [74], [93]-[95]. Therefore, with the proposed triggering condition, unnecessary communication is significantly reduced.*

Remark 24. *It is worth mentioning that the boundary of the orientation error must be small to ensure convergence of the EKF filter. This condition is satisfied whenever the orientation of the robots changes slowly. In this case, we can ignore the higher-order terms in the Taylor series expansion during the filter design. Moreover, under these conditions, our design is based on the linear part in the presence of sensor noise and the proposed event-triggered mechanism.*

III Main Result

In this section, we consider the consensus problem for the multi-robot system (6.15) using a mixed-type event-triggering condition (6.10). We provide sufficient conditions that guarantee consensus of the multi-robot system (6.15) in the mean square sense using the Lyapunov stability theorem and stochastic analysis.

III.1 Consensus Analysis

Theorem III.1. *Consider the multi-robot system (6.15) with communication graph $\mathcal{G}$ and event-triggering condition (6.10). Bounded consensus in a mean-square sense for a group of robots is achieved provided that the following matrix inequality and consensus bound are satisfied:*

$$\begin{bmatrix} -\mathcal{P}+\gamma I & \epsilon\mathcal{A} & \bar{\mathcal{B}} \\ \epsilon\mathcal{A}^T & -\mathcal{P}^{-1} & 0 \\ \bar{\mathcal{B}}^T & 0 & -\mathcal{P}^{-1} \end{bmatrix} < 0 \tag{6.22}$$

$$U(\mathcal{X}_0,\beta,Q,R) = \max\left\{\frac{\lambda_{\max}(\mathcal{P})}{\lambda_{\min}(\mathcal{P})}\mathcal{X}_0^2, \frac{\rho}{\rho-1}\Phi\right\} \tag{6.23}$$

where

$$\mathcal{A} = \begin{bmatrix} \Big(I+\delta(\mathcal{L}_k\otimes G_k)\Big) & -\delta\Big((\mathscr{M}^T\mathscr{N}\mathcal{L}_k)\otimes G_k\Big) \\ 0 & \Big(I+\delta(\Xi_k\otimes K_kH_k)\Big) \end{bmatrix}$$

$$\mathcal{B} = \begin{bmatrix} \delta\Big((\mathscr{M}^T\mathscr{N}\mathcal{L}_k)\otimes G_k\Big) \\ \Big(I+(\Xi_k\otimes K_kH_k)\Big) \end{bmatrix},\ \bar{\mathcal{B}} = \begin{bmatrix} \delta\Big((\mathscr{M}^T\mathscr{N}\mathcal{L}_k)\otimes \alpha G_k\Big) \\ \Big(\alpha+(\Xi_k\otimes \alpha K_kH_k)\Big) \end{bmatrix}$$

$$\mathcal{C} = \begin{bmatrix} \delta C_k \\ \delta\Big(I+(\Xi_k\otimes K_kH_k)\Big)C_k \end{bmatrix},\ \mathcal{D} = \begin{bmatrix} 0 \\ -(\Xi_k\otimes K_k) \end{bmatrix},$$

$$\mathcal{P} = \begin{bmatrix} I\otimes P_1 & I\otimes P_2 \\ I\otimes P_2 & I\otimes P_3 \end{bmatrix},\ \Phi = \lambda_{\max}(\Psi)\sum_{i=1}^{N}(\beta_i^2+Q_i^2+R_{ij}^2),$$

$$\rho = \frac{\lambda_{\max}(\mathcal{P})}{\lambda_{\min}(\mathcal{P})-\gamma},\quad \epsilon = \sqrt{(1+\varepsilon_1+\varepsilon_2+\varepsilon_3)},\quad \alpha = \mathrm{diag}\{\alpha_1,\alpha_2,...,\alpha_N\}$$

Proof. First, we construct the following Lyapunov function:

$$\boldsymbol{V}_k = \boldsymbol{X}_k^T\mathcal{P}\boldsymbol{X}_k \tag{6.24}$$

where $\boldsymbol{X}_k = [\boldsymbol{\xi}_k^T, \tilde{\boldsymbol{x}}_k^T]^T$. Computing the difference of $\boldsymbol{V}_k$ along the trajectory (7.24) and taking the mathematical expectation:

$$\begin{aligned} &\mathbb{E}\{\Delta\boldsymbol{V}_k|\boldsymbol{X}_k\} = \mathbb{E}\{\boldsymbol{V}_{k+1}|\boldsymbol{X}_k\} - \boldsymbol{V}_k = \mathbb{E}\Big\{\Big(\mathcal{A}\boldsymbol{X}_k+\mathcal{B}\boldsymbol{e}_k+\mathcal{C}\boldsymbol{\eta}_k+\mathcal{D}\boldsymbol{\nu}_k\Big)^T \\ &\times\mathcal{P}(\mathcal{A}\boldsymbol{X}_k+\mathcal{B}\boldsymbol{e}_k+\mathcal{C}\boldsymbol{\eta}_k+\mathcal{D}\boldsymbol{\nu}_k)\Big\} = \boldsymbol{X}_k^T\Big(\mathcal{A}^T\mathcal{P}\mathcal{A}-\mathcal{P}\Big)\boldsymbol{X}_k \\ &+2\boldsymbol{X}_k^T\mathcal{A}^T\mathcal{P}\mathcal{B}\boldsymbol{e}_k + 2\boldsymbol{X}_k^T\mathcal{A}^T\mathcal{P}\mathcal{C}\boldsymbol{\eta}_k + 2\boldsymbol{X}_k^T\mathcal{A}^T\mathcal{P}\mathcal{D}\boldsymbol{\nu}_k + 2\boldsymbol{\nu}_k^T\mathcal{D}^T\mathcal{P}\mathcal{B}\boldsymbol{e}_k \\ &+\boldsymbol{e}_k^T\mathcal{B}^T\mathcal{P}\mathcal{B}\boldsymbol{e}_k + \boldsymbol{\nu}_k^T\mathcal{D}^T\mathcal{P}\mathcal{D}\boldsymbol{\nu}_k + \boldsymbol{\eta}_k^T\mathcal{C}^T\mathcal{P}\mathcal{C}\boldsymbol{\eta}_k. \end{aligned} \tag{6.25}$$

Using the inequality $2a^Tb \le \varepsilon a^Ta + \varepsilon^{-1}b^Tb$ we obtain:

$$2\boldsymbol{X}_k^T\mathcal{A}^T\mathcal{P}\mathcal{B}\boldsymbol{e}_k \le \varepsilon_1\boldsymbol{X}_k^T\mathcal{A}^T\mathcal{P}\mathcal{A}\boldsymbol{X}_k + \varepsilon_1^{-1}\boldsymbol{e}_k^T\mathcal{B}^T\mathcal{P}\mathcal{B}\boldsymbol{e}_k \tag{6.26}$$

$$2\boldsymbol{X}_k^T\mathcal{A}^T\mathcal{P}\mathcal{C}\boldsymbol{\eta}_k \le \varepsilon_2\boldsymbol{X}_k^T\mathcal{A}^T\mathcal{P}\mathcal{A}\boldsymbol{X}_k + \varepsilon_2^{-1}\boldsymbol{\nu}_k^T\mathcal{D}^T\mathcal{P}\mathcal{D}\boldsymbol{\nu}_k \tag{6.27}$$

$$2\boldsymbol{X}_k^T\mathcal{A}^T\mathcal{P}\mathcal{D}\boldsymbol{\nu}_k \le \varepsilon_3\boldsymbol{X}_k^T\mathcal{A}^T\mathcal{P}\mathcal{A}\boldsymbol{X}_k + \varepsilon_3^{-1}\boldsymbol{\eta}_k^T\mathcal{C}^T\mathcal{P}\mathcal{C}\boldsymbol{\eta}_k \tag{6.28}$$

$$2\boldsymbol{\nu}_k^T\mathcal{D}^T\mathcal{P}\mathcal{B}\boldsymbol{e}_k \leq \varepsilon_4\boldsymbol{\nu}_k^T\mathcal{D}^T\mathcal{P}\mathcal{D}\boldsymbol{\nu}_k + \varepsilon_4^{-1}\boldsymbol{e}_k^T\mathcal{B}^T\mathcal{P}\mathcal{B}\boldsymbol{e}_k. \tag{6.29}$$

Substituting Equations (6.26)-(6.29) into (6.25) we obtain:

$$\begin{array}{l}\mathbb{E}\{\Delta\boldsymbol{V}_k|\boldsymbol{X}_k\} = \boldsymbol{X}_k^T\Big((1+\varepsilon_1+\varepsilon_2+\varepsilon_3)\mathcal{A}^T\mathcal{P}\mathcal{A} - \mathcal{P}\Big)\boldsymbol{X}_k \\ +(1+\varepsilon_1^{-1}+\varepsilon_4^{-1})\boldsymbol{e}_k^T\mathcal{B}^T\mathcal{P}\mathcal{B}\boldsymbol{e}_k + (1+\varepsilon_2^{-1}+\varepsilon_4^{-1})\boldsymbol{\nu}_k^T\mathcal{D}^T\mathcal{P}\mathcal{D}\boldsymbol{\nu}_k \\ +(1+\varepsilon_3^{-1})\boldsymbol{\eta}_k^T\mathcal{C}^T\mathcal{P}\mathcal{C}\boldsymbol{\eta}_k.\end{array} \tag{6.30}$$

Using the event-triggering condition (6.10) we have:

$$\begin{array}{rl}\boldsymbol{e}_k^T\mathcal{B}^T\mathcal{P}\mathcal{B}\boldsymbol{e}_k \leq \lambda_{\max}(\mathcal{B}^T\mathcal{P}\mathcal{B})\boldsymbol{e}_k^T\boldsymbol{e}_k \leq \lambda_{\max}(\mathcal{B}^T\mathcal{P}\mathcal{B})\sum_{i=1}^{N}\boldsymbol{e}_i^2(k) & \\ \leq \lambda_{\max}(\mathcal{B}^T\mathcal{P}\mathcal{B})\Big[\sum_{i=1}^{N}\alpha_i^2\hat{\boldsymbol{x}}^{i+}(k)^T\hat{\boldsymbol{x}}^{i+}(k) + \beta_i^2\Big] & \\ \leq \lambda_{\max}(\mathcal{B}^T\mathcal{P}\mathcal{B})\Big[\sum_{i=1}^{N}\alpha_i^2\boldsymbol{\xi}^i(k)^T\boldsymbol{\xi}^i(k) + \beta_i^2\Big] & \\ \leq X_k^T\bar{\mathcal{B}}^T\mathcal{P}\bar{\mathcal{B}}X_k + \lambda_{\max}(\mathcal{B}^T\mathcal{P}\mathcal{B})\sum_{i=1}^{N}\beta_i^2. & \end{array} \tag{6.31}$$

Substituting inequality (6.31) into equation (6.30), we obtain the following expression:

$$\begin{array}{l}\mathbb{E}\{\Delta\boldsymbol{V}_k|\boldsymbol{X}_k\} = \boldsymbol{X}_k^T\Big((1+\varepsilon_1+\varepsilon_2+\varepsilon_3)\mathcal{A}^T\mathcal{P}\mathcal{A} + \alpha^T\mathcal{B}^T\mathcal{P}\mathcal{B}\alpha - \mathcal{P}\Big)\boldsymbol{X}_k \\ +(1+\varepsilon_1^{-1}+\varepsilon_4^{-1})\boldsymbol{e}_k^T\mathcal{B}^T\mathcal{P}\mathcal{B}\boldsymbol{e}_k + (1+\varepsilon_2^{-1}+\varepsilon_4^{-1})\boldsymbol{\nu}_k^T\mathcal{D}^T\mathcal{P}\mathcal{D}\boldsymbol{\nu}_k \\ +(1+\varepsilon_3^{-1})\boldsymbol{\eta}_k^T\mathcal{C}^T\mathcal{P}\mathcal{C}\boldsymbol{\eta}_k \leq -\gamma\boldsymbol{X}_k^T\boldsymbol{X}_k + \Phi,\end{array} \tag{6.32}$$

where

$$\begin{array}{l}\Psi = (1+\varepsilon_1^{-1}+\varepsilon_4^{-1})\mathcal{B}^T\mathcal{P}\mathcal{B} + (1+\varepsilon_2^{-1}+\varepsilon_4^{-1})\mathcal{D}^T\mathcal{P}\mathcal{D} \\ \quad +(1+\varepsilon_3^{-1})\mathcal{C}^T\mathcal{P}\mathcal{C} \\ \Phi = \lambda_{\max}(\Psi)\sum_{i=1}^{N}(\beta_i^2 + Q_i^2 + R_{ij}^2).\end{array}$$

From (6.32) we find the condition for bounded consensus of MASs:

$$(1+\varepsilon_1+\varepsilon_2+\varepsilon_3)\mathcal{A}^T\mathcal{P}\mathcal{A} + \bar{\mathcal{B}}^T\mathcal{P}\bar{\mathcal{B}}\alpha - \mathcal{P} + \gamma I < 0. \tag{6.33}$$

Now we look for the boundary U of consensus. According to (6.33) for any $\rho > 1$ we have:

$$\begin{array}{l}\rho^{k+1}\mathbb{E}\{V_{k+1}\} - \rho^k\mathbb{E}\{V_k\} \leq \rho^{k+1}\mathbb{E}\{\Delta V_k\} + \rho^k(\rho-1)\mathbb{E}\{V_k\} \\ \leq \rho^{k+1}\Big[-\gamma\mathbb{E}\Big\{\|\boldsymbol{X}_k\|^2\Big\} + \Phi\Big] + \rho^k(\rho-1)\mathbb{E}\Big\{\|\boldsymbol{X}_k\|^2\Big\} \\ \leq \Big(\lambda_{\max}(\mathcal{P})(\rho-1) - \gamma\rho\Big)\rho^k\mathbb{E}\Big\{\|\boldsymbol{X}_k\|^2\Big\} + \rho^{k+1}\Phi.\end{array} \tag{6.34}$$

Selecting a proper positive scalar ρ satisfying $\lambda_{\max}(\mathcal{P})(\rho-1) - \gamma\rho = 0$, we can write:

$$\rho^k\mathbb{E}\{V_k\} - \mathbb{E}\{V_0\} \leq \sum_{n=1}^{k}\rho^n\Phi. \tag{6.35}$$

Thus,

$$\begin{array}{l}\mathbb{E}\{V_k\} \leq \rho^{-k}\mathbb{E}\{V_0\} + \sum_{n=1}^{k}\rho^{n-k}\Phi = \rho^{-k}\mathbb{E}\{V_0\} + \dfrac{(1-\rho^{-k})\Phi}{1-\rho^{-1}} \\ = \rho^{-k}\Big(\mathbb{E}\{V_0\} - \dfrac{\rho\Phi}{\rho-1}\Big) + \dfrac{\rho\Phi}{\rho-1} \leq \max\Big\{\mathbb{E}\{V_0\}, \dfrac{\rho\Phi}{\rho-1}\Big\}.\end{array} \tag{6.36}$$

We know that

$$\mathbb{E}\{V_0\} = X_0^T \mathcal{P} X_0 \leq \lambda_{\max}(\mathcal{P}) \mathbb{E}\Big\{ \|\boldsymbol{X}_{0\cdot}\|^2 \Big\} \tag{6.37}$$

From Definition III.1 we have:

$$\mathbb{E}\Big\{ \|\boldsymbol{X}_0\|^2 \Big\} = \sum_{i=1}^{N} \left\| x^i(0) - (\frac{1}{N}) \sum_{j=1}^{N} x^j(0) \right\|^2 \leq \mathcal{X}_0^2. \tag{6.38}$$

Then, we can show that:

$$U(\mathcal{X}_0, \beta, Q, R) = \max \left\{ \frac{\lambda_{\max}(\mathcal{P})}{\lambda_{\min}(\mathcal{P})} \mathcal{X}_0^2, \frac{\rho}{\rho - 1} \Phi \right\} \tag{6.39}$$

Finally, using the Schur complement lemma, inequality (6.33) can be converted into the following condition (6.22) which complete the proof. □

Remark 25. *In the proof of theorem III.1, we employ the inequality* $2a^T b \leq \varepsilon a^T a + \varepsilon^{-1} b^T b$ *to deal with the cross terms* e_k, η_k, ν_k *and design the distributed consensus control. Note that due to cross terms (such as* $2\boldsymbol{X}_k^T \mathcal{A}^T \mathcal{P} \mathcal{B} \boldsymbol{e}_k$, $2\boldsymbol{X}_k^T \mathcal{A}^T \mathcal{P} \mathcal{C} \boldsymbol{\eta}_k$,*...) the matrix inequality (6.22) includes the parameters* ε_1, ε_2,*... which can be optimized further to minimize the consensus bound.*

Remark 26. *In this work, we assume that each agent checks the triggering condition (6.10) periodically using the same sampling period and that all agents are synchronized. For simplicity, our analysis neglects a small delay* $\Delta T_i > 0$ *that accounts for the effect of the communication delays between agents. This delay is inevitable due to the unpredictable nature of the network and can be accounted for using the same analysis presented in [90]. When the number of agents is small, this delay is typically negligible. However, as the number of agents increases, the delay* ΔT_i *might result in asynchronous behaviour that requires a more detailed analysis. The number of robots that can be tolerated under the presents assumptions, depends on the characteristics of the robots and the network. Future research will elaborate on this problem. See also the experimental results is Section IV for further details.*

III.2 Distributed Event-Triggered Controller Design

Theorem III.1 in the previous subsection provides sufficient conditions that guarantee bounded consensus for the multi-robot system. However the controller and Kalman gain and also the event-triggering parameters are difficult to obtain directly from the matrix inequality (6.22) due to the nonlinear terms αG_k, αK_k as well as

the terms $\mathcal{P}^{-1}$ and $\mathcal{P}$. In this section we present an LMI based approach to the design of suitable control and Kalman gains as well as event-triggered parameters.

Theorem III.2. *Consider the multi-robot system (6.15) with communication graph $\mathcal{G}$ and event-triggering condition (6.10). Bounded consensus for the multi-robot system (6.15) is achieved if there exist matrix sequences $\bar{K}_k$, $\bar{G}_k$, $\mathcal{P}$ and α satisfying the following linear matrix inequality:*

$$\begin{bmatrix} -\mathcal{P}+\gamma I & \epsilon\mathcal{A} & \bar{\mathcal{B}} \\ \epsilon\mathcal{A}^T & \mathcal{P}-\Omega-\Omega^T & 0 \\ \bar{\mathcal{B}}^T & 0 & \mathcal{P}-2I \end{bmatrix} < 0 \tag{6.40}$$

$$\mathcal{A} = \begin{bmatrix} \Big(\alpha+\delta(\mathcal{L}_k\otimes\bar{G}_k)\Big) & -\delta\Big((\mathscr{M}^T\mathscr{N}\mathcal{L}_k)\otimes\bar{G}_k\Big) \\ 0 & \Big(\alpha+\delta(\Xi_k\otimes\bar{K}_kH_k)\Big) \end{bmatrix}$$

$$\bar{\mathcal{B}} = \begin{bmatrix} \delta\Big((\mathscr{M}^T\mathscr{N}\mathcal{L}_k)\otimes\bar{G}_k\Big) \\ \Big(\alpha+(\Xi_k\otimes\bar{K}_kH_k)\Big) \end{bmatrix},\ \Omega = \begin{bmatrix} \alpha & 0 \\ 0 & \alpha \end{bmatrix},\ \alpha = \mathrm{diag}\{\alpha_1,\alpha_2,...,\alpha_N\}$$

with consensus bound given by:

$$U(\mathcal{X}_0,\beta,Q,R) = \max\left\{\frac{\lambda_{\max}(\mathcal{P})}{\lambda_{\min}(\mathcal{P})}\mathcal{X}_0^2, \frac{\rho}{\rho-1}\Phi\right\}. \tag{6.41}$$

Moreover, the gains are given by $K_k = \bar{K}_k\alpha^{-1}$ and $G_k = \bar{G}_k\alpha^{-1}$.

Proof. Pre- and post-multiplying inequality (6.22) by $\mathrm{diag}(I,\Omega,I)$ and $\mathrm{diag}(I,\Omega^T,I)$ and taking into account that

$$\begin{cases} (\Omega-\mathcal{P})\mathcal{P}^{-1}(\Omega-\mathcal{P})^T \geq 0 \\ (I-\mathcal{P})\mathcal{P}^{-1}(I-\mathcal{P})^T \geq 0 \end{cases} \tag{6.42}$$

We can write

$$\begin{cases} -\Omega\mathcal{P}^{-1}\Omega^T \leq \mathcal{P}-\Omega-\Omega^T \\ -\mathcal{P}^{-1} \leq \mathcal{P}-2I \end{cases} \tag{6.43}$$

which implies the LMI condition (6.40). This completes the proof. □

Remark 27. *Theorem III.2 is written in the form of the LMI condition (6.40) whose solution determines the consensus control gain. We design the controller, filter gains, as well as the parameters of the event-triggered mechanism simultaneously thus guaranteeing that the desire consensus performance is achieved along with reduced frequency update of the controllers. Notice also that the consensus bound U is a function of initial position of the robots ($\mathcal{X}_0$), threshold term of event-triggered mechanism (β), the covariance of process noise (Q) and the covariance of the relative measurement noise (R). In summary, a suitable consensus bound can be obtained by optimizing the controller parameters and filter gains as well as the parameters*

of the event-triggering mechanism. In other words, the design can be carried out as an optimization problem that maximizes the consensus bound while satisfying the stability condition (6.40), i.e.

$$\begin{aligned} &\max_{\bar{K}_k,\bar{G}_k,\mathcal{P},\alpha,\beta} && U(\mathcal{X}_0,\beta,Q,R) \\ &s.t. && \text{LMI condition (6.40)} \end{aligned} \tag{6.44}$$

Remark 28. *It is worth mentioning that the terms $\mathcal{L}_k$, K_k, etc, in the LMI (6.40) are time-varying and therefore the LMI condition must be solved online. Moreover, since (6.40) depends on the Kalman gain K_k, the error covariance $\boldsymbol{P}^{i+}(k)$, $\boldsymbol{P}^{ij+}(k)$ (in the CL algorithm) must be bounded in order to ensure a feasible solution. It is also worth noting that our main results can be easily extended to the case when the Lyapunov matrix $\mathcal{P}$ is time-varying. With our established framework, the consensus bound can be obtained analogously as $U(\mathcal{X}_0,\beta,Q,R) = \max\left\{\frac{\lambda_{\max}(\mathcal{P}_0)}{\lambda_{\min}(\mathcal{P}_k)}\mathcal{X}_0^2 + \frac{1}{\lambda_{\min}(\mathcal{P}_k)}\bar{\rho}_k\bar{\Phi}_k\right\}$ where $\bar{\rho}_k = \begin{bmatrix}\rho_1^1 & \rho_2^2 & \cdots & \rho_k^k\end{bmatrix}$ and $\bar{\Phi}_k = \begin{bmatrix}\Phi_1 & \Phi_2 & \cdots & \Phi_k\end{bmatrix}^T$ for the time-varying Lyapunov matrix by making some minor modifications in Eqs. (6.34)-(6.39).*

In the next section we provide an algorithm to implement the controller in a practical setting.

Algorithm 4 Distributed event-based consensus control for a group of mobile robots with cooperative localization

1: **Input**:Initialize position, estimated position and error covariance matrix of robots $i \in \{1,2,...,N\}$ and $j \in \vartheta\backslash\{i\}$: $\mathrm{x}^i(0) \in \mathbb{R}^{n^i}$, $\mathrm{x}^j(0) \in \mathbb{R}^{n^j}$, $\mathrm{y}^i(0) \in \mathbb{R}^{n^i}$, $\mathrm{y}^j(0) \in \mathbb{R}^{n^j}$, $\hat{\mathrm{x}}^{i+}(0) \in \mathbb{R}^{n^i}$, $\hat{\mathrm{y}}^{i+}(0) \in \mathbb{R}^{n^i}$, $\hat{\mathrm{x}}^{j+}(0) \in \mathbb{R}^{n^j}$, $\hat{\mathrm{y}}^{j+}(0) \in \mathbb{R}^{n^j}$, $\mathbf{P}^{i+}(0) \in \mathbb{S}^{n^i}$, $\mathbf{P}^{ij+}(0) = \mathbf{0}_{n^i\times n^j}$, $\mathbf{P}^{j+}(0) \in \mathbb{S}^{n^i}$, and choose a small tolerance parameter $\boldsymbol{\epsilon} \ll 0.05$
2: **Output**:Velocity comments $\mathbf{u}_i^x(k)$, $\mathbf{u}_i^y(k)$; position information $\mathrm{x}^i(k)$, $\mathrm{y}^i(k)$; performance index $\mathscr{D}_i$
3: **while** $\left\|\mathrm{x}^i(k) - \mathrm{x}^j(k)\right\| \leq \boldsymbol{\epsilon}$ & $\left\|\mathrm{y}^i(k) - \mathrm{y}^j(k)\right\| \leq \boldsymbol{\epsilon}$ **do**
4: Given sensor measurements (Odometry and IMU) predict the position and error covariance of robots using Eqs. (2) and (4).
5: Whenever robot i detects the other robots in the team, it takes a relative measurement $\boldsymbol{z}_{ij}(k)$ respect to its neighbors and also exchange information packets consisting of propagated and estimated position as well as error covariance with its neighbors residing within communication range. The estimated position and error covariance of robots can be computed using Eq. (6)
6: Robot i broadcast the current estimated position $\hat{\mathrm{x}}^{i+}(k_s^i)$ and $\hat{\mathrm{y}}^{i+}(k_s^i)$ to the neighbors by checking its triggering conditions in (10). If the condition in (10) is satisfied, the robot i broadcasts the current estimated position to the network.
7: The speed comments is computed for robot i in x and y coordinates using Eq. (9); then the desired orientation $\theta_i = \arctan\left(\mathbf{u}_i^x(k), \mathbf{u}_i^y(k)\right)$, and the desired velocity $v^i = \sqrt{\left(\mathbf{u}_i^x(k)\right)^2 + \left(\mathbf{u}_i^y(k)\right)^2}$ is computed for robot i.
8: Robot i rotates in place until its heading reach to the desired orientation θ_i and the length of rotating time is recorded as ΔT_i
9: Robot i moves forward/backward if its heading reach to the desired orientation θ_i, at the velocity $v^i + (\frac{v^i}{\tau})$ for the time period $\tau\Delta T_i$.
10: Robot i keeps moving forward/backward at v^i until it receives the updates information from other robots.
11: **end while**

IV CASE STUDY

IV.1 Simulation Results

In this section, we consider a multi-robot systems and verify our event-triggered consensus control based on cooperative localization (CL) via simulation. We consider a scenario in which a group of mobile robots $i \in \{1, 2, 3, 4\}$ are in motion and at least one of them performs as a stationary robot. Then, robots use their extroceptive sensors to take relative measurements and receive the predicted position and associated error covariance with respect to the observed stationary robot. Meanwhile, the moving robots updates position estimates using cooperative localization (CL) and perform consensus. We assume the initial position of the robots is $\boldsymbol{x}^1(0) = [20, -10]^T$, $\boldsymbol{x}^2(0) = [-20, -10]^T$, $\boldsymbol{x}^3(0) = [-20, 10]^T$, and $\boldsymbol{x}^4(0) = [20, 10]^T$. The covariance of the control input is $Q_i = (0.05)^2\text{diag}([(\Delta L^i)^2; (\Delta R^i)^2])$ and the covariance of the sensor measurements is $R_{ij} = \text{diag}([0.001m^2; 0.001rad^2])$. In our simulations, we consider the position $\bar{\boldsymbol{x}}_{des} = [0, 0]^T$ as consensus of robots. Note that the communication graph is considered as time-varying. In our simulations, we consider four different communication strategies to compare the consensus performance and the amount of information transmitted by each robot. We first design time-triggered consensus control where each robot transmits position estimates to their neighbours continuously. Fig. 6.2(a)-(b) shows the trajectory of the four robots. As shown in the figure, all robots approach the origin thus reaching bounded consensus in mean-square sense. Note that the position estimates from CL can track the actual position precisely. Also, the triggering instances for the motion of robots are illustrated in Fig. 6.2(c)-(f). Next, we consider the event-triggered consensus control, where robots transmit position estimates based on the triggering condition (6.10). We compare the following three event-triggering mechanisms (i) absolute type with parameters $\alpha_i = 0$, $\beta_i = 0.04$; (ii) relative type with parameters $\alpha_i = 0.04$, $\beta_i = 0.0$ and (iii) mixed type with parameters $\alpha_i = 0.04$, $\beta_i = 0.04$. It can be seen from Fig. 6.2, that the mixed-type triggering condition generally yields the most desirable consensus performance with much reduced transmitted information. Also, the CL has comparable performance in estimating the position of robots. However, the relative type triggering condition generated many events and the absolute type triggering condition reduced the unnecessary communications at the cost of consensus performance degradation.

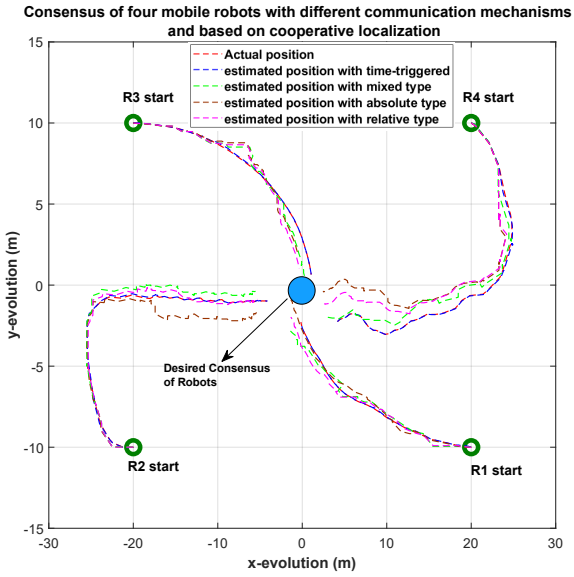

(a) actual position and estimated position (CL) trajectories of four robots on the xy-plane

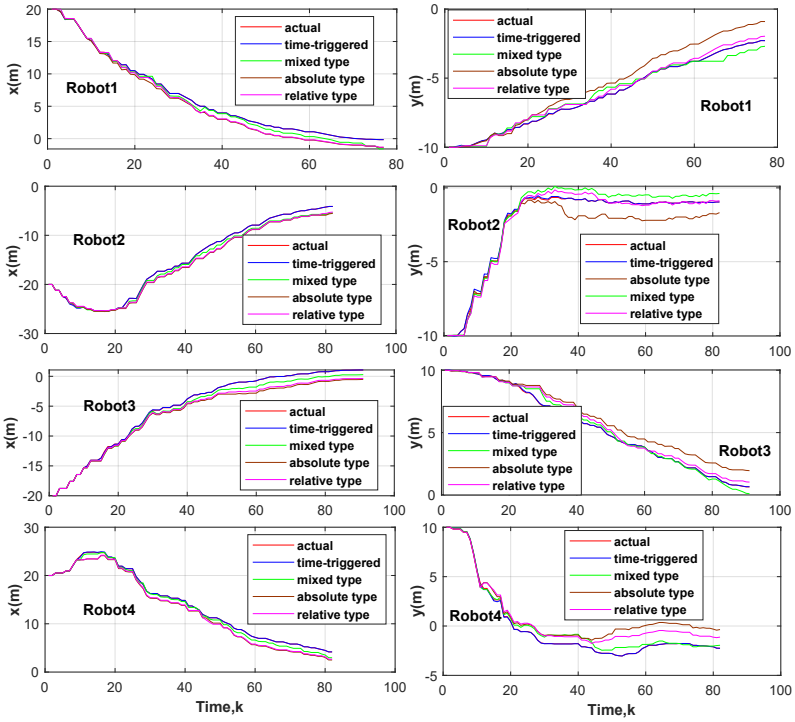

(b) actual position and estimated position (CL) trajectories of four robots with respect to time

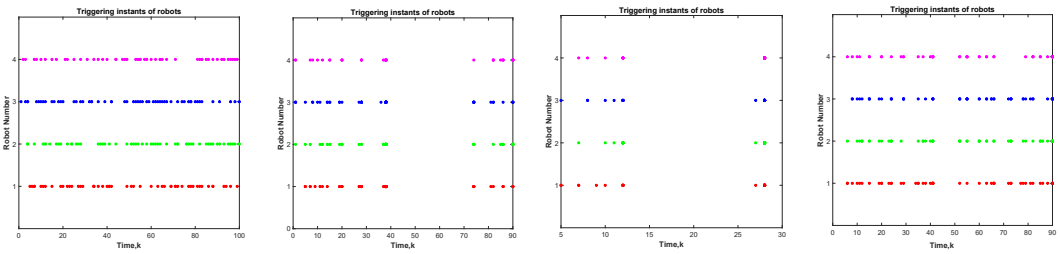

(c) triggering times of robots in time-triggered scheme

(d) triggering times of robots in mixed type condition

(e) triggering times of robots in absolute type condition

(f) triggering times of robots in relative type condition

Figure 6.2: Simulation testing results: Consensus of four mobile robots based on CL with different communication mechanisms

IV.2 Experimental Validation

In this part, we experimentally validate our proposed event-triggered consensus control mechanism. Our experimental setup consists of four e-puck2 robots, a ZED camera, and a host computer, referred to as the *base station* (see Fig. 6.3). We use the open-source Robot Operating System (ROS) as the middleware. The base station processes acquired camera images from the four e-puck2 robots using computer vision to obtain position estimates of the robots using the CL algorithm. The velocity feedback control signal is computed at the base station and transmitted to each robot through Bluetooth, to steer robots to the agreement position. Note that the transmission of information packets to other robots is decided by the event detector (6.10). The localization algorithm fuses the position estimate obtained from the computer vision with odometry sensor readings to get a more accurate position estimate for the consensus control. More details about cooperative localization can be found in [62]. The communication topology between robots in this work is considered as time-varying. The initial position of the e-puck2 robots are set to $x_{\text{epuck0}}(0) = 0.2, y_{\text{epuck0}}(0) = -0.1$, $x_{\text{epuck1}}(0) = -0.2, y_{\text{epuck1}}(0) = -0.1$, $x_{\text{epuck2}}(0) = -0.2, x_{\text{epuck2}}(0) = 0.1$ and $x_{\text{epuck3}}(0) = 0.2, x_{\text{epuck3}}(0) = 0.1$. In this experiment, we set the position $\bar{\boldsymbol{x}}_{des} = [0, 0]^T$ as consensus of e-puck2 robots. Our goal is to design and implement the event-triggered consensus control to ensure each e-puck2 robot converges to the desired consensus position with a minimum amount of transmitted information between robots. More specifically, we provide the trajectory of positions and velocities as well as performance indexes for four different communication mechanisms (i) time-triggered mechanism; (ii) absolute type with parameters $\alpha_i = 0$, $\beta_i = 0.1$; (iii) relative type with parameters $\alpha_i = 0.1$, $\beta_i = 0.0$ and (iv) mixed type with parameters $\alpha_i = 0.1$, $\beta_i = 0.1$. Fig. 6.4(a)-(b) shows the consensus results of the position and velocities of all four robots implemented with different communication strategies. Note that in the experiment the position of robots is measured by the odometry sensor in order to show the update process (or inter-event times) in the position of robots under different triggering conditions. Also, we define the consensus performance of each robot by $\mathscr{D}_i = \sum_{k=1}^{M} \Big[(x_k^i - \bar{x}_k)^2 + (y_k^i - \bar{y}_k)^2 \Big]$ where x_k^i and y_k^i are the position of robot i in the x and y direction, respectively and $\bar{x}_k$ and $\bar{y}_k$ are the consensus position in the x and y direction. Table 6.2 represents the performance index of each robot for different

triggering conditions. Figure 6.4(c)-(j) shows the triggering instances for the control inputs (linear velocity and angular velocity) of each robot in the implementation of different communication mechanisms. Based on our analysis (1) the relative type triggering condition leads to much unnecessary communication between robots (see Fig. 6.4(g)-(h)); (2) the absolute type triggering condition reduces the unnecessary communication between robots at the cost of consensus performance degradation (see Table 6.2 and Fig. 6.4(e)-(f)); (3) the mixed-type triggering condition provide the satisfactory consensus performance with the much-reduced transmission of information (see Table 6.2 and Fig. 6.4(i)-(j)).

(a) (b) (c)

Figure 6.3: Experimental setup including (a) four e-puck2 robots equipped with ArUco tags, (b) overhead ZED camera, (c) e-puck2 robot

Table 6.2: The performance index of mean-square consensus for different event-triggered conditions

Type of e-puck robot	e-puck0	e-puck1	e-puck2	e-puck3
Time-triggered	2.5589	3.3523	3.8946	2.1537
Relative-type	3.8233	3.7573	7.2534	6.2312
Mixed-type	3.2373	4.6100	5.6915	4.8050
Absolute-type	3.9601	5.9048	9.2555	7.3006

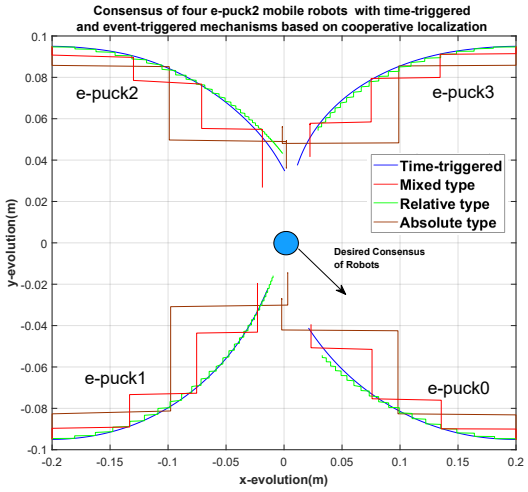

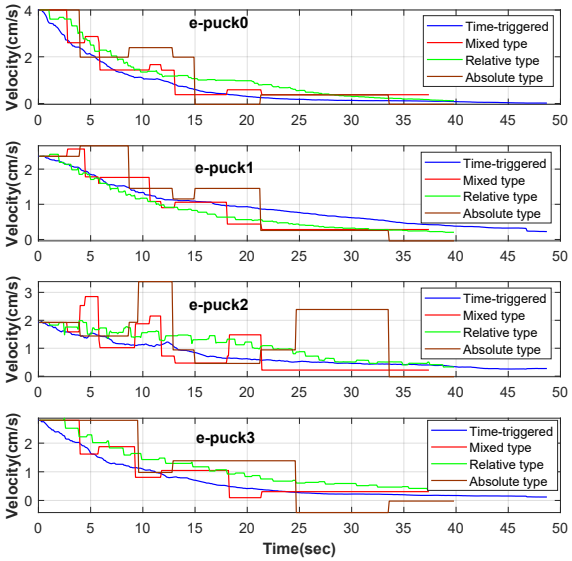

(b) velocities of four robots respect to time

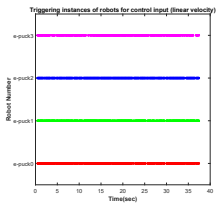

(c) triggering times of robots for linear velocity in time-triggered scheme

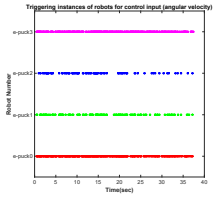

(d) triggering times of robots for angular velocity in time-triggered scheme

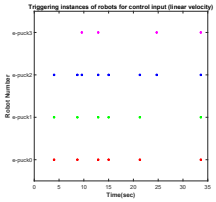

(e) triggering times of robots for linear velocity in absolute-type condition

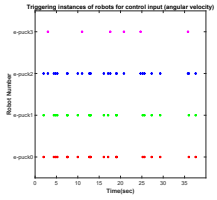

(f) triggering times of robots for angular velocity in absolute-type condition

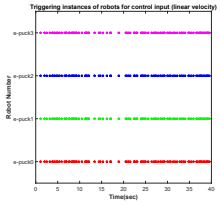

(g) triggering times of robots for linear velocity in relative-type condition

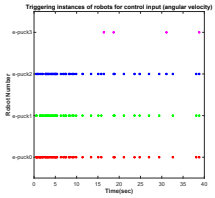

(h) triggering times of robots for angular velocity in relative-type condition

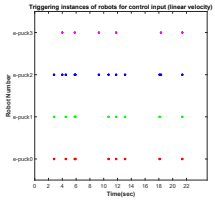

(i) triggering times of robots for linear velocity in mixed-type condition

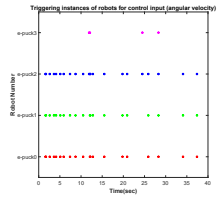

(j) triggering times of robots for angular velocity in mixed-type condition

Figure 6.4: Experimental testing results: Consensus of e-puck2 robots with CL under different communication mechanisms

Chapter 7

Event-Based Secure Consensus Control for Multi-Robot Systems with Cooperative Localization Against DoS Attacks

I Introduction

In this chapter, we investigate the secure consensus control problem for multi-robot systems with event-triggered communication strategy under aperiodic energy-limited denial-of-service (DoS) attacks, where DoS attacks prevent the transmission of information between robots. Each robot is equipped with onboard sensors to estimate its position cooperatively by taking relative measurements and exchanging the local positioning information with other robots through the unreliable communication network. In the meantime, each robot determines its consensus control based on transmitted position estimates and steers the robot to the desired consensus position. Therefore, our goal is to design a secure control scheme for each robot based on cooperative localization (CL) with an event-triggered mechanism and obtain a sufficient condition for the upper bound of duration and the maximum number of attacks such that N robots can move to the desired secure consensus position in the presence of DoS attacks. Finally, simulation and experimental results are presented to show the effectiveness of obtained theoretical results.

The remaining of this chapter is organized as follows. In Section II we introduce some related preliminary results and formulate the problem to be solved. In Section

III, we derive sufficient conditions such that the MARs reach secure consensus. In Section IV, we conduct simulations and experiments to show the effectiveness of proposed method. Finally, in Section V we present some conclusions.

Table 7.1: NOTATION

Notations	Description
$\mathbb{E}\{.\}$	expectation of the random variable
diag(.)	block diagonal matrix
$\otimes$	Kronecker product
$\circ$	Hadamard product
$\|.\|$	Euclidean norm of the vector
A^T	transpose of matrix A
A^{-1}	inverse of matrix A
I	identity matrix of appropriate dimensions
i and j	identity of robot i and robot j
$\boldsymbol{x}^i(k)$	state vector of the robot i
$\boldsymbol{u}^i(k)$	consensus control of robot i
$\boldsymbol{\eta}_i(k)$	process noise from control input of robot i
$\boldsymbol{\nu}_{ij}(k)$	measurement noise from exteroceptive sensors for pair (i,j)
$a_{ij}(k)$	indicator of interaction between robots
$\mathcal{N}_{ci}$	set of neighbors of robot i within communication range
$\boldsymbol{z}_{ij}(k)$	relative measurement taken by robot i from robot j
$\boldsymbol{Q}_i(k)$	covariance of $\boldsymbol{\eta}_i(k)$
$\boldsymbol{R}_{ij}(k)$	covariance of $\boldsymbol{\nu}_{ij}(k)$
$\boldsymbol{H}_i^i(k)$	sensor measurement matrix of robot i
$\boldsymbol{H}_j^i(k)$	sensor measurement matrix of pair (i,j)
$\hat{\boldsymbol{x}}^{i-}(k)$	propagated state of robot i
$\tilde{\boldsymbol{x}}^{i-}(k)$	propagated state error of robot i
$\hat{\boldsymbol{x}}^{i+}(k)$	estimation of robot i
$\tilde{\boldsymbol{x}}^{i+}(k)$	estimation error of robot i
$\boldsymbol{P}^{i-}(k)$	propagated state error covariance of robot i
$\boldsymbol{P}^{i+}(k)$	estimation error covariance of robot i
$\boldsymbol{P}^{ij-}(k)$	propagated state error covariance for the pair (i,j)
$\boldsymbol{P}^{ij+}(k)$	estimation error covariance for the pair (i,j)
$\boldsymbol{K}_i(k)$	Kalman gain of CL
$\boldsymbol{S}_{ij}$	covariance of innovation $\tilde{\boldsymbol{z}}_{ij}(k)$
α_i, β_i	event-triggered parameters of robot i
$\boldsymbol{\xi}_k$	consensus error (deviation of each state from the average state)
$G_i(k)$	consensus control gain
e_i	error of event-triggering sampling
δ	stepsize
$\mathcal{L}$	Laplacian matrix
$\lambda_{\min}(A)$	the minimum eigenvalue of the matrix A
$\lambda_{\max}(A)$	the maximum eigenvalue of the matrix A

II Problem Formulation and Preliminaries

II.1 Graph Theory

We consider a MRSs with N robots which communicate with each other according to the interaction topology denoted by graph $\mathcal{G} = (\mathcal{V}, \mathcal{E}, \mathcal{A})$. Here $\mathcal{V} = \{v_1, ..., v_N\}$

is the set of nodes in the graph. For a node v_i, the robot index $i \in \{1, 2, ..., N\}$ is the unique identifier of the robot i. $\mathcal{E}$ represents the edge set, *i.e.* $v_{ij} = (v_i, v_j) \in \mathcal{E}$ if there is a line of communication between robots i and j. $\mathcal{A} = \lfloor a_{ij} \rfloor \in \mathbb{R}^{N \times N}$ is the adjacency matrix where $a_{ij} = 1$ if $v_{ij} \in \mathcal{E}$ otherwise $a_{ij} = 0$. Also, $a_{ii} = 0$ $\forall i \in \{1, 2, ..., N\}$. The graph Laplacian $\mathcal{L} = [l_{ij}] \in \mathbb{R}^{n_i \times n_i}$ is defined as $l_{ij} = \sum_{i \neq j} a_{ij}$ and $l_{ij} = -a_{ij}$ where $i \neq j$.

II.2 Problem Statement

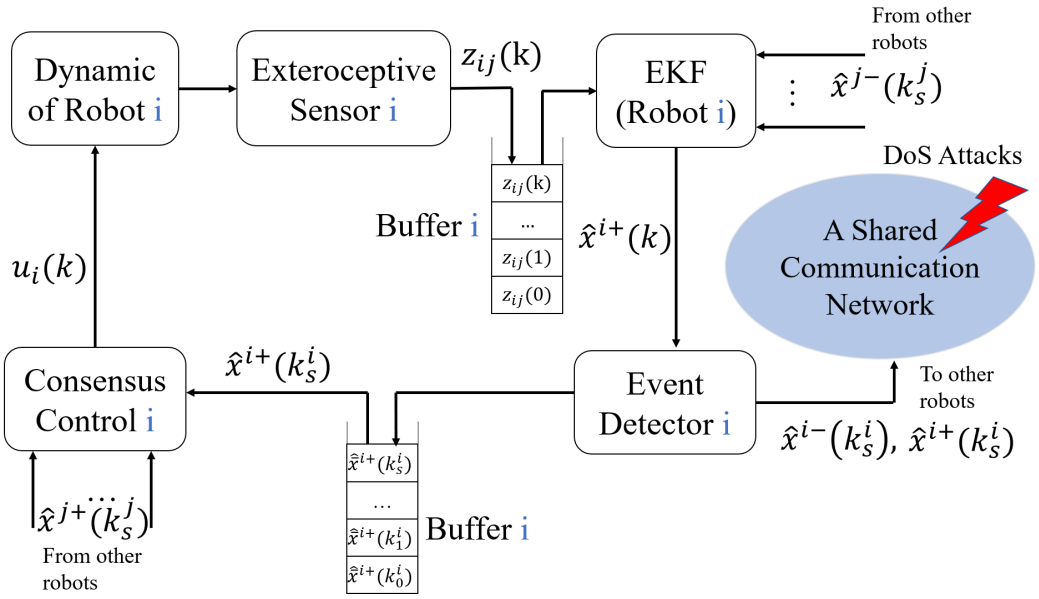

Figure 7.1: Block diagram of event-based secure consensus control for multi-robot systems with cooperative localization under DoS attacks

We consider a team of N mobile robots equipped with onboard sensors where each robot localize itself cooperatively in a global coordinate system and aims to reach consensus (see Fig. 7.1). More specifically, each mobile robot use its exteroceptive sensors to observe neighbouring robots and take relative measurements $\boldsymbol{z}_{ij}(k)$. The information collected, namely propagated and estimated position and error covariance, is then shared with the neighbouring robots. Note that each robot i can only communicate with neighbouring robots within certain range, defined as the set $\mathcal{N}_{ci}$, satisfying: $\mathcal{N}_{ci} = \{j \in \mathcal{V} : a_{ij} = 1\}$. To construct the neighbouring set we assume that each robot, equipped with a set of exteroceptive sensors (camera, etc), randomly observes the other robots in the team, whenever they are within range. Therefore, the resulting communication graph is time-varying and can be considered as a practical scenario for the multi-robot system. The position estimate

of each robot is sent to the event-detector which decides whether or not the information is to be transmitted based on a triggering condition. The consensus control in each robot determines the velocity feedback control signal based on the transmitted position estimates and steer the robot to the desired agreement position.

In this work, we consider an scenario in which the adversary can block some communication channels between robots by launching DoS attacks for a period of time so that the information exchange among robots is not possible. Based on above discussion, we aim to design a resilient control scheme based on cooperative localization (CL) with event-triggered mechanism and investigate under what conditions the N robots can move cooperatively to the desired consensus position despite the presence of DoS attacks.

Remark 29. *The buffers used in Fig. 7.1 store and retrieve information packets, namely, relative measurements and position estimates, based on a last-in-first-out rule which can improve the performance of the localization and secure consensus of MRSs in the presence of DoS attacks.*

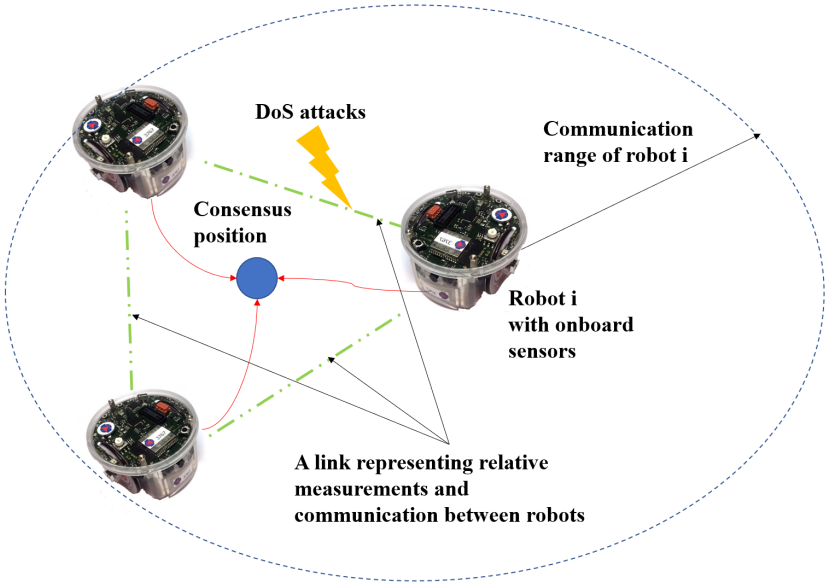

Figure 7.2: Illustration of consensus of multi-robot systems under DoS attacks.

II.3 DoS Attack Model

Consider now the DoS attacks. We consider an scenario in which the attacker has the limited energy. Therefore the DoS attacks appear on a time-sequence which can be described as in Fig. 7.3. The entire sequence can be divided into two areas. The

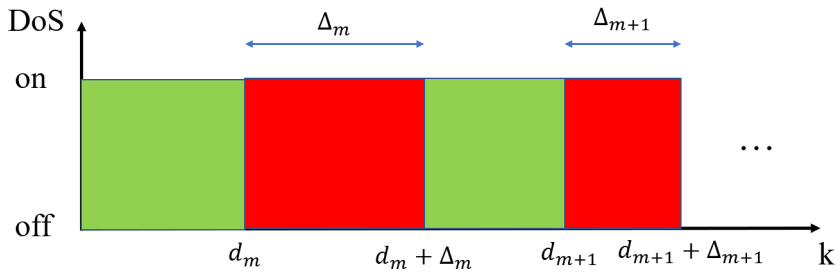

Figure 7.3: DoS attacks based on time-sequence

green area Π_s represents the communication area without attacks. The red area Π_a represents the time sections where the DoS attacks are active and transmission of information between some robots is interrupted. The mth attack interval is denoted as $D_m = \{d_m\} \cup [d_m, d_m + \Delta_m]$, where $\{d_m\}$, $d_m \in \mathbb{N}$ is the DoS attack occurring instants and Δ_m is the duration of attack. The indicator variable of the DoS attack for pair (i, j) is defined as follows:

$$\rho_{ij}(k) = \begin{cases} 0, & k \in \Pi_s(k_1, k_2) \\ \\ 1, & k \in \Pi_a(k_1, k_2) \end{cases} \tag{7.1}$$

which shows the status of the communication channel for the pair (i, j). We now introduce the following assumptions regarding the duration and frequency of the DoS attacks:

Assumption 9. *For $k_2 > k_1 \geq 0$, denoting $n(k_1, k_2)$ the total number of DoS attacks over the interval $[k_1, k_2]$, there exist scalars $\tau_D \in \mathbb{R}$ and $c \in \mathbb{R}$ such that [137]*

$$n(k_1, k_2) \leq c + \frac{k_2 - k_1}{\tau_D} \tag{7.2}$$

Assumption 10. *For $k_2 > k_1 \geq 0$, denoting $\Xi_a(k_1, k_2)$ the total duration of the DoS attacks over the interval $[k_1, k_2]$, there exist scalars $T_D \in \mathbb{R}$ and $\varsigma \in \mathbb{R}$ such that [137]:*

$$|\Xi_a(k_1, k_2)| \leq \varsigma + \frac{k_2 - k_1}{T_D} \tag{7.3}$$

Remark 30. *Assumptions 1 and 2 convey practical restrictions consistent with an attacker whose energy to produce the attack is limited. Notice that a DoS attack of unlimited duration and frequency requires continuous supply of energy, which is impractical. Also, different from [76]-[80] which assume that the adversary can launch the attack signals to block all the communication transmissions in each interval, we relax this assumption and consider a practical scenario in which given constraints*

on energies and resources, the adversary can attack a limited number of communication links. Furthermore, compared with the periodic DoS attack employed in [79], we assume that attacks occur randomly and each attack can have different duration.

Assumption 11. *The packets transmitted by the robots are time-stamped.*

II.4 Dynamics of Multi-Robot Systems and Cooperative Localization

We consider a group of N mobile robots with unique identity $i \in \mathcal{V} = \{1, 2, ..., N\}$. The motion equation for robot i is given by [33]:

$$\begin{aligned} \boldsymbol{x}^i(k+1) &= \boldsymbol{f}^i(\boldsymbol{x}^i(k), v_m^i(k), \phi^i(k)) \\ &= \boldsymbol{x}^i(k) + \begin{bmatrix} \delta v_m^i(k)\cos(\phi^i(k)) \\ \delta v_m^i(k)\sin(\phi^i(k)) \end{bmatrix} \end{aligned} \tag{7.4}$$

where the state vector $\boldsymbol{x}^i(k) = [x^i(k), y^i(k)]$ is the position of robot i respect to global coordinates, v^i is the velocity command, ϕ^i is the orientation of robot i and δ is the sampling time. Note that the velocity command $v_m^i = v^i + \eta_i$ can be obtained from odometry or inertial measurement unit (IMU), where v^i is the actual linear velocity and η_i is the self-motion measurement noise modelled as white, zero-mean Gaussian noise. Each robot i performs self-localization by propagating state as follows:

$$\begin{aligned} \hat{\boldsymbol{x}}^{i-}(k+1) &= \boldsymbol{f}^i(\hat{\boldsymbol{x}}^{i+}(k), v_m^i(k)) \\ &= \hat{\boldsymbol{x}}^{i+}(k) + \begin{bmatrix} \delta v^i(k)\cos(\phi^i(k)) \\ \delta v^i(k)\sin(\phi^i(k)). \end{bmatrix} \end{aligned} \tag{7.5}$$

Define the propagated error as follows: $\tilde{\boldsymbol{x}}^{i-}(k) = \boldsymbol{x}^i(k) - \hat{\boldsymbol{x}}^{i-}(k)$. Then, using the motion equation (7.4) and propagated state (7.5) the propagated state error is given by:

$$\begin{aligned} \tilde{\boldsymbol{x}}^{i-}(k+1) &= \tilde{\boldsymbol{x}}^{i+}(k) + \delta \begin{bmatrix} \eta_i(k)\cos(\phi^i(k)) \\ \eta_i(k)\sin(\phi^i(k)) \end{bmatrix} \\ &= \tilde{\boldsymbol{x}}^{i+}(k) + \delta \begin{bmatrix} \eta_i^x(k) \\ \eta_i^y(k) \end{bmatrix} \\ &= \tilde{\boldsymbol{x}}^{i+}(k) + \delta\eta_i(k). \end{aligned} \tag{7.6}$$

The propagated error covariance for the motion equation (7.4) can be computed as follows:

$$\boldsymbol{P}^{i-}(k+1) = \mathbb{E}\Big[\tilde{\boldsymbol{x}}^{i-}(k+1)\tilde{\boldsymbol{x}}^{i-}(k+1)^T\Big] = \boldsymbol{P}^{i+}(k) + \boldsymbol{Q}_i(k) \tag{7.7}$$

$$\boldsymbol{P}^{ij-}(k+1) = \mathbb{E}\Big[\tilde{\boldsymbol{x}}^{i-}(k+1)\tilde{\boldsymbol{x}}^{j-}(k+1)^T\Big] = \boldsymbol{P}^{ij+}(k) \tag{7.8}$$

where $\boldsymbol{Q}_i(k) = (\delta)^2\mathbb{E}[\boldsymbol{\eta}_i(k)\boldsymbol{\eta}_i(k)^T]$. Since, each robot i only propagates the motion dynamics (7.4) to perform self-localization, the propagated state error (7.6) can increase due to the noise term $\eta_i(k)$. In order to reduce the estimation error, we employ

a CL algorithm based on extended Kalman filter (EKF). Each robot i equipped with exteroceptive sensors to observe uniquely the other robots in the team and takes relative measurements described as follows [33]:

$$\boldsymbol{z}_{ij}(k) = \boldsymbol{h}_{ij}\big(\boldsymbol{x}^i(k), \boldsymbol{x}^j(k)\big) + \boldsymbol{\nu}_{ij}(k) \tag{7.9}$$

where $\boldsymbol{\nu}_{ij}$ is white-Gaussian measurement noise and $\boldsymbol{h}_{ij}\big(\boldsymbol{x}^i(k), \boldsymbol{x}^j(k)\big)$ is the measurement model. The relative measurements includes range and bearing of robot i respect to robot j. Considering an scenario in which each robot i is able to take relative measurements form multiple robots can significantly improve the localization accuracy, especially in the presence of DoS attacks. The updated position estimate and covariance update for robot i can be represented as follows:

$$\begin{aligned}\hat{\boldsymbol{x}}^{i+}(k) = \hat{\boldsymbol{x}}^{i-}(k) + \boldsymbol{K}_i(k)\Big[\sum_{j\in\mathcal{N}_{ci}} a_{ij}(k)\Big(\boldsymbol{z}_{ij}(k) \\ -\boldsymbol{h}_{ij}(\hat{\boldsymbol{x}}^{i-}(k), \hat{\boldsymbol{x}}^{j-}(k))\Big)\Big]\end{aligned} \tag{7.10}$$

$$\boldsymbol{P}^{i+}(k) = \boldsymbol{P}^{i-}(k) - \boldsymbol{K}_i(k)\boldsymbol{S}_{ij}(k)\boldsymbol{K}_i(k)^T \tag{7.11}$$

$$\boldsymbol{P}^{ij+}(k) = \boldsymbol{P}^{ij-}(k) - \boldsymbol{K}_i(k)\boldsymbol{S}_{ij}(k)\boldsymbol{K}_j(k)^T \tag{7.12}$$

where $\boldsymbol{h}_{ij}(\hat{\boldsymbol{x}}^{i-}, \hat{\boldsymbol{x}}^{j-})$ is the propagated measurement. Expanding $\boldsymbol{h}_{ij}(\boldsymbol{x}^i, \boldsymbol{x}^j)$ using a series Taylor around $(\hat{\boldsymbol{x}}^{i-}, \hat{\boldsymbol{x}}^{j-})$ we have:

$$\boldsymbol{h}_{ij}(\boldsymbol{x}^i, \boldsymbol{x}^j) \approx \boldsymbol{h}_{ij}(\hat{\boldsymbol{x}}^{i-}, \hat{\boldsymbol{x}}^{j-}) + \boldsymbol{H}_i^i(\boldsymbol{x}^i - \hat{\boldsymbol{x}}^{i-}) + \boldsymbol{H}_j^i(\boldsymbol{x}^j - \hat{\boldsymbol{x}}^{j-}) \tag{7.13}$$

where $\boldsymbol{H}_i^i = \frac{\partial \boldsymbol{h}_{ij}(\hat{\boldsymbol{x}}^{i-}, \hat{\boldsymbol{x}}^{j-})}{\partial \boldsymbol{x}^i}$ and $\boldsymbol{H}_j^i = \frac{\partial \boldsymbol{h}_{ij}(\hat{\boldsymbol{x}}^{i-}, \hat{\boldsymbol{x}}^{j-})}{\partial \boldsymbol{x}^j}$. Also, $\boldsymbol{K}_i$ and $\boldsymbol{K}_j$ are the Kalman gains for robot i and robot j and $\boldsymbol{S}_{ij}$ is the covariance of the innovation $\tilde{\boldsymbol{z}}_{ij}(k) = \boldsymbol{z}_{ij}(k) - \boldsymbol{h}_{ij}(\hat{\boldsymbol{x}}^{i-}(k), \hat{\boldsymbol{x}}^{j-}(k))$ for pair (i, j).

III Event-triggered Secure Consensus Control

To reach secure consensus of the multi-robot system, we develop a secure control scheme with event-triggered mechanism in the presence of DoS attacks. Then, we analyze the closed-loop stability under DoS attacks. Finally, we provide a sufficient conditions for the upper bound of the duration of attacks and the maximum number of attacks that the group of N robots can tolerate while reaching to the desired secure consensus.

III.1 Secure Control Scheme Design

The linearized, discrete-time motion model for robot i can be represented as follows:

$$\boldsymbol{x}^i(k+1) = \boldsymbol{x}^i(k) + \delta \boldsymbol{u}_i(k) + \delta \boldsymbol{\eta}_i(k) \tag{7.14}$$

where the control input vector (speed command) and self-motion measurement noise are given by

$$\boldsymbol{u}_i(k) = \begin{bmatrix} \boldsymbol{u}_i^x(k) \\ \boldsymbol{u}_i^y(k) \end{bmatrix} = \begin{bmatrix} v^i(k)\cos(\phi^i(k)) \\ v^i(k)\sin(\phi^i(k)) \end{bmatrix}$$

$$\boldsymbol{\eta}_i(k) = \begin{bmatrix} \boldsymbol{\eta}_i^x(k) \\ \boldsymbol{\eta}_i^y(k) \end{bmatrix} = \begin{bmatrix} \eta_i(k)\cos(\phi^i(k)) \\ \eta_i(k)\sin(\phi^i(k)) \end{bmatrix}.$$

Using the position estimates, the consensus control for each robot i can be written as follows:

$$\boldsymbol{u}_i(k) = \boldsymbol{G}_i(k)\Big[\sum_{j\in\mathcal{N}_{ci}} a_{ij}(k)\Big(\hat{\boldsymbol{x}}^{i+}(k) - \hat{\boldsymbol{x}}^{j+}(k)\Big)\Big] \tag{7.15}$$

where $\boldsymbol{G}_i(k)$ is the consensus gain to be designed.

We now consider the event-triggered mechanism to reduce the update frequency of controllers (see Fig. 7.1). In order to characterize such mechanism, let the triggering instances of robot i be $0 \le k_0^i < k_1^i < k_2^i < ... < k_s^i$ and event-generator functions $\Upsilon_i(.,.,.) : \mathbb{R}^q \times \mathbb{R} \longrightarrow \mathbb{R}$ $(i = 1, 2, ..., N)$ be chosen as follows:

$$\Upsilon_i\Big(e_i(k), \alpha_i, \beta_i\Big) = e_i(k)^T e_i(k) - \alpha_i \hat{\boldsymbol{x}}^{i+}(k)^T \hat{\boldsymbol{x}}^{i+}(k) - \beta_i \ . \tag{7.16}$$

Here, $e_i(k) = \hat{\boldsymbol{x}}^{i+}(k) - \hat{\boldsymbol{x}}^{i+}(k_s^i)$, where $\hat{\boldsymbol{x}}^{i+}(k_s^i)$ is the local state estimate at the latest transmitting instant k_s^i and α_i, β_i are the parameters event-triggered mechanism to be designed. The controller can be updated only when the given triggering condition satisfy:

$$\Upsilon_i(e_i(k), \alpha_i, \beta_i) > 0 \tag{7.17}$$

Therefore, sequence of transmission instants for robot i can be determined as follows:

$$k_{s+1}^i = \inf\{k \in \mathbb{N} | k > k_s^i, \Upsilon_i(e_i(k), \alpha_i, \beta_i) > 0\} \ . \tag{7.18}$$

Considering the DoS attacks and event-triggering mechanism, we propose the following resilient consensus control scheme for each robot i:

$$\begin{aligned} \boldsymbol{u}_i(k) = &\Big(1 - \rho_{ij}(k)\Big)\delta \boldsymbol{G}_{i,1}(k)\Big[\sum_{j\in\mathcal{N}_{ci}} a_{ij}(k)\Big(\hat{\boldsymbol{x}}^{i+}(k) - \hat{\boldsymbol{x}}^{j+}(k)\Big)\Big] \\ &+\Big(1 - \rho_{ij}(k)\Big)\delta \boldsymbol{G}_{i,1}(k)\Big[\sum_{j\in\mathcal{N}_{ci}} a_{ij}(k)\Big(e_j(k) - e_i(k)\Big)\Big] \\ &+\rho_{ij}(k)\delta \boldsymbol{G}_{i,2}(k)\Big[\sum_{j\in\mathcal{N}_{ci}} a_{ij}(k)\Big(\hat{\boldsymbol{q}}^{i+}(k) - \hat{\boldsymbol{q}}^{j+}(k)\Big)\Big]. \end{aligned} \tag{7.19}$$

The closed-loop equations for the MRSs under DoS attacks, including the event-triggered mechanism for the consensus control, can bewritten as follows:

$$\begin{aligned}
&\hat{\boldsymbol{x}}^{i+}(k) = \hat{\boldsymbol{x}}^{i-}(k) - e_i(k) + \Big(1-\rho_{ij}(k)\Big)\boldsymbol{K}_{i,1}(k)\Big[\sum_{j\in\mathcal{N}_{ci}} a_{ij}(k) \\
&\times\Big(\boldsymbol{H}_i^i(k)\tilde{\boldsymbol{x}}^{i-}(k) + \boldsymbol{H}_j^i(k)\tilde{\boldsymbol{x}}^{j-}(k) + \boldsymbol{\nu}_{ij}(k)\Big)\Big] - \Big(1-\rho_{ij}(k)\Big) \\
&\times\boldsymbol{K}_{i,1}(k)\Big[\sum_{j\in\mathcal{N}_{ci}} a_{ij}(k)\Big(\boldsymbol{H}_i^i(k)e_i(k) + \boldsymbol{H}_j^i(k)e_j(k)\Big)\Big] \\
&+\rho_{ij}(k)\boldsymbol{K}_{i,2}(k)\Big[\sum_{j\in\mathcal{N}_{ci}} a_{ij}(k)\Big(\boldsymbol{H}_i^i(k)\tilde{\boldsymbol{q}}^{i-}(k) + \boldsymbol{H}_j^i(k)\tilde{\boldsymbol{q}}^{j-}(k) \\
&+\boldsymbol{\nu}_{ij}(k)\Big)\Big]
\end{aligned} \tag{7.20}$$

$$\begin{aligned}
&\boldsymbol{x}^i(k+1) = \boldsymbol{x}^i(k) \\
&+\Big(1-\rho_{ij}(k)\Big)\delta\boldsymbol{G}_{i,1}(k)\Big[\sum_{j\in\mathcal{N}_{ci}} a_{ij}(k)\Big(\hat{\boldsymbol{x}}^{i+}(k) - \hat{\boldsymbol{x}}^{j+}(k)\Big)\Big] \\
&+\Big(1-\rho_{ij}(k)\Big)\delta\boldsymbol{G}_{i,1}(k)\Big[\sum_{j\in\mathcal{N}_{ci}} a_{ij}(k)\Big(e_j(k) - e_i(k)\Big)\Big] \\
&+\delta\boldsymbol{\eta}_i(k) + \rho_{ij}(k)\delta\boldsymbol{G}_{i,2}(k)\Big[\sum_{j\in\mathcal{N}_{ci}} a_{ij}(k)\Big(\hat{\boldsymbol{q}}^{i+}(k) - \hat{\boldsymbol{q}}^{j+}(k)\Big)\Big].
\end{aligned} \tag{7.21}$$

Remark 31. *Notice that we have divided the transmission of information into two parts: (i)* $\Big(1-\rho_{ij}(k)\Big)$ *is used for communication links free of DoS attacks; (ii)* $\rho_{ij}(k)$ *is used for communication links under DoS attacks. Instead of assuming the position estimates received from attacked communication channels as zero and some constants, we consider the position estimates from neighbouring robots as* $\hat{\boldsymbol{q}}^{j+}(k)$ *which can be predicted based on the motion dynamic of robot* j*. Also, the last state estimates of robot* j *are stored in a buffer until the communication channel returns from an attack period to normal. This approach improves the resilience and secure consensus during DoS attack intervals. Note that since robot* i *can sense and communicate with multiple robots, the position estimate from CL can be reconstructed in the presence of DoS attacks.*

Computing the estimation error $\tilde{\boldsymbol{x}}^{i+}(k) = \boldsymbol{x}^i(k) - \hat{\boldsymbol{x}}^{i+}(k)$, the closed-loop system

(7.20) and (7.21) can be written as follows:

$$
\begin{aligned}
&\tilde{\boldsymbol{x}}^{i+}(k+1) = \tilde{\boldsymbol{x}}^{i+}(k) - e_i(k) + \delta\boldsymbol{\eta}_i(k) + \Big(1-\rho_{ij}(k)\Big)\\
&\times\boldsymbol{K}_{i,1}(k)\Big[\sum_{j\in\mathcal{N}_{ci}} a_{ij}(k)\Big(\boldsymbol{H}_i(k)\big(\tilde{\boldsymbol{x}}^{i+}(k)-\tilde{\boldsymbol{x}}^{j+}(k)\big)+\boldsymbol{\nu}_{ij}(k)\Big)\Big]\\
&-\Big(1-\rho_{ij}(k)\Big)\boldsymbol{K}_{i,1}(k)\Big[\sum_{j\in\mathcal{N}_{ci}} a_{ij}(k)\Big(\boldsymbol{H}_i(k)\big(e_j(k)-e_i(k)\big)\Big)\Big]\\
&+\Big(1-\rho_{ij}(k)\Big)\boldsymbol{K}_{i,1}(k)\Big[\sum_{j\in\mathcal{N}_{ci}} a_{ij}(k)\Big(\delta\boldsymbol{H}_i(k)\big(\eta_j(k)-\eta_i(k)\big)\Big)\Big]\\
&+\rho_{ij}(k)\boldsymbol{K}_{i,2}(k)\Big[\sum_{j\in\mathcal{N}_{ci}} a_{ij}(k)\Big(\boldsymbol{H}_i(k)\big(\tilde{\boldsymbol{q}}^{i+}(k)-\tilde{\boldsymbol{q}}^{j+}(k)\big)\\
&+\boldsymbol{\nu}_{ij}(k)\Big)\Big] + \rho_{ij}(k)\boldsymbol{K}_{i,2}(k)\Big[\sum_{j\in\mathcal{N}_{ci}} a_{ij}(k)\Big(\delta\boldsymbol{H}_i(k)\big(\eta_j(k)\\
&-\eta_i(k)\big)\Big)\Big]
\end{aligned}
\tag{7.22}
$$

$$
\begin{aligned}
&\boldsymbol{x}^i(k+1) =\\
&\boldsymbol{x}^i(k) + \Big(1-\rho_{ij}(k)\Big)\delta\boldsymbol{G}_{i,1}(k)\Big[\sum_{j\in\mathcal{N}_{ci}} a_{ij}(k)\Big(\boldsymbol{x}^i(k)-\boldsymbol{x}^j(k)\Big)\Big]\\
&+\Big(1-\rho_{ij}(k)\Big)\delta\boldsymbol{G}_{i,1}(k)\Big[\sum_{j\in\mathcal{N}_{ci}} a_{ij}(k)\Big(e_j(k)-e_i(k)\Big)\Big] + \delta\boldsymbol{\eta}_i(k)\\
&+\rho_{ij}(k)\delta\boldsymbol{G}_{i,2}(k)\Big[\sum_{j\in\mathcal{N}_{ci}} a_{ij}(k)\Big(\boldsymbol{x}^i(k)-\boldsymbol{x}^j(k)\Big)\Big] + \delta\boldsymbol{\eta}_i(k)\\
&-\rho_{ij}(k)\delta\boldsymbol{G}_{i,2}(k)\Big[\sum_{j\in\mathcal{N}_{ci}} a_{ij}(k)\Big(\tilde{\boldsymbol{q}}^{i+}(k)-\tilde{\boldsymbol{q}}^{j}(k)\Big)\Big]\\
&-\Big(1-\rho_{ij}(k)\Big)\delta\boldsymbol{G}_{i,1}(k)\Big[\sum_{j\in\mathcal{N}_{ci}} a_{ij}(k)\Big(\tilde{\boldsymbol{x}}^{i+}(k)-\tilde{\boldsymbol{x}}^{j}(k)\Big)\Big]
\end{aligned}
\tag{7.23}
$$

In order to facilitate the discussion, the closed-loop system (7.20) and (7.21) can be written as following form:

$$
\begin{cases}
\boldsymbol{x}_{k+1} = \Big[I+\delta\Big(\big((\mathbf{1}-\rho_k)\circ\mathcal{L}\big)\otimes G_1 + \big(\rho_k\circ\mathcal{L}\big)\otimes G_2\Big)\Big]\boldsymbol{x}_k\\
\quad -\delta\Big(\big((\mathbf{1}-\rho_k)\circ\mathcal{L}\big)\otimes G_1\Big)\tilde{\boldsymbol{x}}_k - \delta\Big(\big((\mathbf{1}-\rho_k)\circ\mathcal{L}\big)\otimes G_1\Big)\boldsymbol{e}_k\\
\quad -\delta\Big(\big(\rho_k\circ\mathcal{L}\big)\otimes G_2\Big)\tilde{\boldsymbol{q}}_k + \delta\boldsymbol{\eta}_k\\
\tilde{\boldsymbol{x}}_{k+1} = \Big[I+\delta\Big(\big((\mathbf{1}-\rho_k)\circ\mathcal{L}\big)\otimes K_1H\Big)\Big]\tilde{\boldsymbol{x}}_k\\
\quad +\Big[I+\Big(\big((\mathbf{1}-\rho_k)\circ\mathcal{L}\big)\otimes K_1H\Big)\Big]\boldsymbol{e}_k\\
\quad +\delta\Big[I+\Big(\big((\mathbf{1}-\rho_k)\circ\mathcal{L}\big)\otimes K_1H\Big)\Big]\boldsymbol{\eta}_k\\
\quad -\Big(\big((\mathbf{1}-\rho_k)\circ\mathcal{L}\big)\otimes K_1\Big)\boldsymbol{\nu}_k - \Big(\big(\rho_k\circ\mathcal{L}\big)\otimes K_2\Big)\boldsymbol{\nu}_k\\
\quad +\delta\Big(\big(\rho_k\circ\mathcal{L}\big)\otimes K_2H\Big)\tilde{\boldsymbol{q}}_k + \delta\Big(\big(\rho_k\circ\mathcal{L}\big)\otimes K_2H\Big)\boldsymbol{\eta}_k\\
\tilde{\boldsymbol{q}}_{k+1} = \Big[I+\delta(\mathcal{L}\otimes K_2H)\Big]\tilde{\boldsymbol{q}}_k + \delta\Big[I+(\mathcal{L}\otimes K_2H)\Big]\boldsymbol{\eta}_k\\
\quad -(\mathcal{L}\otimes K_2)\boldsymbol{\nu}_k
\end{cases}
\tag{7.24}
$$

where

$$
\begin{aligned}
\boldsymbol{x}_k &= \Big[\boldsymbol{x}^1(k)^T \;\; \boldsymbol{x}^2(k)^T \;\; ... \;\; \boldsymbol{x}^N(k)^T\Big]^T \\
\tilde{\boldsymbol{x}}_k &= \Big[\tilde{\boldsymbol{x}}^{1+}(k)^T \;\; \tilde{\boldsymbol{x}}^{2+}(k)^T \;\; ... \;\; \tilde{\boldsymbol{x}}^{N+}(k)^T\Big]^T \\
\boldsymbol{e}_k &= \Big[\boldsymbol{e}_1(k)^T \;\; \boldsymbol{e}_2(k)^T \;\; ... \;\; \boldsymbol{e}_N(k)^T\Big]^T \\
\boldsymbol{\eta}_k &= \Big[\boldsymbol{\eta}_1(k)^T \;\; \boldsymbol{\eta}_2(k)^T \;\; ... \;\; \boldsymbol{\eta}_N(k)^T\Big]^T \\
\boldsymbol{\nu}_k &= \Big[\boldsymbol{\nu}_1(k)^T \;\; \boldsymbol{\nu}_2(k)^T \;\; ... \;\; \boldsymbol{\nu}_N(k)^T\Big]^T \\
\boldsymbol{K}_1 &= \Big[\boldsymbol{K}_{1,1}(k)^T \;\; \boldsymbol{K}_{2,1}(k)^T \;\; ... \;\; \boldsymbol{K}_{N,1}(k)^T\Big]^T \\
\boldsymbol{\nu}_k &= \Big[\boldsymbol{\nu}_1(k)^T \;\; \boldsymbol{\nu}_2(k)^T \;\; ... \;\; \boldsymbol{\nu}_N(k)^T\Big]^T \\
\boldsymbol{K}_2 &= \Big[\boldsymbol{K}_{1,2}(k)^T \;\; \boldsymbol{K}_{2,2}(k)^T \;\; ... \;\; \boldsymbol{K}_{N,2}(k)^T\Big]^T \\
\boldsymbol{H}_k &= \Big[\boldsymbol{H}_1(k)^T \;\; \boldsymbol{H}_2(k)^T \;\; ... \;\; \boldsymbol{H}_N(k)^T\Big]^T \\
\boldsymbol{G}_1 &= \Big[\boldsymbol{G}_{1,1}(k)^T \;\; \boldsymbol{G}_{2,1}(k)^T \;\; ... \;\; \boldsymbol{G}_{N,1}(k)^T\Big]^T \\
\boldsymbol{G}_2 &= \Big[\boldsymbol{G}_{1,2}(k)^T \;\; \boldsymbol{G}_{2,2}(k)^T \;\; ... \;\; \boldsymbol{G}_{N,2}(k)^T\Big]^T \\
\mathcal{L} &= \begin{bmatrix} -\deg_{in}^1 & a_{12} & a_{13} & ... & a_{1N} \\ a_{21} & -\deg_{in}^2 & a_{23} & ... & a_{2N} \\ \vdots & \vdots & \vdots & \ddots & \vdots \\ a_{N1} & a_{N2} & a_{N3} & ... & -\deg_{in}^N \end{bmatrix}.
\end{aligned}
$$

We now define the average state of all robots as follows:

$$\bar{\boldsymbol{x}}_k = \tfrac{1}{N}\sum_{j=1}^{N} \boldsymbol{x}^i(k) = \tfrac{1}{N}(\mathbf{1}^T \otimes I)\boldsymbol{x}_k \tag{7.25}$$

Considering $\mathbf{1}\mathcal{L} = 0$, the deviation of each state from the average state can be computed as follows:

$$
\begin{aligned}
\boldsymbol{\xi}_{k+1} &= \boldsymbol{x}_{k+1} - (\mathbf{1}^T \otimes I)\bar{\boldsymbol{x}}_{k+1} = \Big[I + \delta\Big(\big((\mathbf{1} - \rho_k) \circ \mathcal{L}\big) \otimes G_1 \\
&+ \big(\rho_k \circ \mathcal{L}\big) \otimes G_2\Big)\Big]\boldsymbol{\xi}_k - \delta\Big(\big((\mathbf{1} - \rho_k) \circ \mathcal{L}\big) \otimes G_1\Big)\tilde{\boldsymbol{x}}_k \\
&- \delta\Big(\big((\mathbf{1} - \rho_k) \circ \mathcal{L}\big) \otimes G_1\Big)\boldsymbol{e}_k - \delta\Big(\big(\rho_k \circ \mathcal{L}\big) \otimes G_2\Big)\tilde{\boldsymbol{q}}_k + \delta\boldsymbol{\eta}_k.
\end{aligned} \tag{7.26}
$$

Considering the coupling nature of MRSs, we select $\phi_i \in \mathbb{R}^n$ with $\phi_i^T\mathcal{L} = \lambda_i\phi_i^T$ $(i = 2, 3, ..., N)$ to form a unitary matrix $M = [\frac{1}{\sqrt{N}}\phi_2 \;\; ... \;\; \phi_N]$ and then transform $\mathcal{L}$ to diagonal form as follows:

$$\text{diag}\{0, \lambda_2, ..., \lambda_N\} = M^T\mathcal{L}M \tag{7.27}$$

where for each i, ϕ_i and λ_i are a pair of eigenvector-eigenvalue of the Laplacian

matrix $\mathcal{L}$. Then closed-loop system (7.24) can be written as follows:

$$\begin{cases} \boldsymbol{\xi}_{k+1} = \Big[I + \delta\Big(\big((\mathbf{1}-\rho_k)\circ\mathcal{F}\big)\otimes G_1 + \big(\rho_k\circ\mathcal{F}\big)\otimes G_2\Big)\Big]\boldsymbol{\xi}_k \\ \quad -\delta\Big(\big((\mathbf{1}-\rho_k)\circ\mathcal{F}\big)\otimes G_1\Big)\tilde{\boldsymbol{x}}_k - \delta\Big(\big((\mathbf{1}-\rho_k)\circ\mathcal{F}\big)\otimes G_1\Big)\boldsymbol{e}_k \\ \quad -\delta\Big(\big(\rho_k\circ\mathcal{F}\big)\otimes G_2\Big)\tilde{\boldsymbol{q}}_k + \delta\boldsymbol{\eta}_k \\ \tilde{\boldsymbol{x}}_{k+1} = \Big[I + \delta\Big(\big((\mathbf{1}-\rho_k)\circ\mathcal{F}\big)\otimes K_1H\Big)\Big]\tilde{\boldsymbol{x}}_k \\ \quad +\Big[I + \Big(\big((\mathbf{1}-\rho_k)\circ\mathcal{F}\big)\otimes K_1H\Big)\Big]\boldsymbol{e}_k \\ \quad +\delta\Big[I + \Big(\big((\mathbf{1}-\rho_k)\circ\mathcal{F}\big)\otimes K_1H\Big)\Big]\boldsymbol{\eta}_k \\ \quad -\Big(\big((\mathbf{1}-\rho_k)\circ\mathcal{F}\big)\otimes K_1\Big)\boldsymbol{\nu}_k - \Big(\big(\rho_k\circ\mathcal{F}\big)\otimes K_2\Big)\boldsymbol{\nu}_k \\ \quad +\delta\Big(\big(\rho_k\circ\mathcal{F}\big)\otimes K_2H\Big)\tilde{\boldsymbol{q}}_k + \delta\Big(\big(\rho_k\circ\mathcal{F}\big)\otimes K_2H\Big)\boldsymbol{\eta}_k \\ \tilde{\boldsymbol{q}}_{k+1} = \Big[I + \delta(\mathcal{F}\otimes K_2H)\Big]\tilde{\boldsymbol{q}}_k + \delta\Big[I + (\mathcal{F}\otimes K_2H)\Big]\boldsymbol{\eta}_k \\ \quad -(\mathcal{F}\otimes K_2)\boldsymbol{\nu}_k \end{cases} \tag{7.28}$$

where $\mathcal{F} = \text{diag}\{\lambda_2, ..., \lambda_N\}$. Note that the above closed-loop system is defined in the period of DoS attacks where some partial communication channels are blocked. We can define the closed-loop system in the normal period, where communication is established without DoS attacks, as follows:

$$\begin{cases} \boldsymbol{\xi}_{k+1} = \Big[I + \delta(\mathcal{F}\otimes G)\Big]\boldsymbol{\xi}_k - \delta(\mathcal{F}\otimes G)\tilde{\boldsymbol{x}}_k \\ \quad -\delta(\mathcal{F}\otimes G)\boldsymbol{e}_k + \delta\boldsymbol{\eta}_k \\ \tilde{\boldsymbol{x}}_{k+1} = \Big[I + \delta(\mathcal{F}\otimes KH)\Big]\tilde{\boldsymbol{x}}_k + \Big[I + (\mathcal{F}\otimes KH)\Big]\boldsymbol{e}_k \\ \quad \delta\Big[I + (\mathcal{F}\otimes KH)\Big]\boldsymbol{\eta}_k - (\mathcal{F}\otimes K)\boldsymbol{\nu}_k. \end{cases} \tag{7.29}$$

We now introduce the following definition:

Definition III.1. Let the communication topology $\mathcal{G}$ of robots and consensus bound function U be given. Assume that the initial position of robots is such that $\sum_{i=1}^{N}\left\|x^i(0) - (\frac{1}{N})\sum_{j=1}^{N}x^j(0)\right\| \leq \mathcal{X}_0$. Then, the multi-robot system (7.14) with the proposed event-triggered control scheme (7.19) is secure consensusable under DoS attacks with bound U if the following condition is satisfied:

$$\mathbb{E}\Big\{\ \big\|x^i(k) - x^j(k)\big\|^2\ \Big\} \leq U, \quad i,j \in \mathcal{V}, k \geq 0 \tag{7.30}$$

Remark 32. *In this work, we considered a secure event-based consensus control scheme to reduce the adverse effect of DoS attacks on the consensus performance. Also, using this scheme we are able to reduce the usage of communication resources and save the energy consumed by each mobile robot. Different from the event-triggering mechanisms proposed in [76], [83]-[84] we employ a mixed-type triggering*

condition which contains both the absolute type and relative type conditions as special cases. Also, in contrast to [76], [78], [83]-[84], our proposed event-triggered scheme relies only on the state estimates of each robot itself and does not require state estimates from other robots. This is important since avoids continuous communication between robots to check the triggering condition.

III.2 Consensus Analysis

Theorem III.1. *Consider the MRSs (7.14) with communication topology $\mathcal{G}$ and event-triggering condition (7.17). A secure consensus in mean-square sense for a team of robots under DoS attacks is reached if the parameters τ_D and T_D satisfy*

$$\frac{1}{T_D}+\frac{\tau_d}{\tau_D}<\frac{(\tau_d-1)\ln(\gamma_1)-\ln(\mu)}{\ln(\gamma_2)-\ln(\gamma_1)}. \tag{7.31}$$

The parameters γ_1 and γ_2 can be obtained by solving the following linear matrix inequality (LMI) conditions:

$$\begin{bmatrix}-\mathcal{P}+\gamma_1 I & \mathcal{A}_s & \mathcal{B}_s\\ \mathcal{A}_s^T & -\epsilon^{-1}\mathcal{P}^{-1} & 0\\ \mathcal{B}_s^T & 0 & -\alpha^{-1}\mathcal{P}^{-1}\end{bmatrix}<0 \tag{7.32}$$

$$\begin{bmatrix}-\mathcal{S}+\gamma_2 I & \mathcal{A}_a & \mathcal{B}_a\\ \mathcal{A}_a^T & -\epsilon^{-1}\mathcal{S}^{-1} & 0\\ \mathcal{B}_a^T & 0 & -\alpha^{-1}\mathcal{S}^{-1}\end{bmatrix}<0. \tag{7.33}$$

Moreover, under these conditions, the following consensus bound is obtained:

$$U(\mathcal{X}_0,\beta,Q,R)=\max\left\{\tfrac{\sigma_{max}}{\sigma_{min}}\mathcal{X}_0^2,\tfrac{\rho}{\rho-1}\Phi\right\} \tag{7.34}$$

where

$$\mathcal{A}_s=\begin{bmatrix}I+\delta(\mathcal{F}\otimes G_1) & -\delta(\mathcal{F}\otimes G_1)\\ 0 & I+\delta(\mathcal{F}\otimes K_1H)\end{bmatrix},$$

$$\mathcal{B}_s=\begin{bmatrix}-\delta(\mathcal{F}\otimes G_1)\\ I+(\mathcal{F}\otimes K_1H)\end{bmatrix},\quad \mathcal{C}_s=\begin{bmatrix}\delta\\ I+(\mathcal{F}\otimes K_1H)\end{bmatrix},$$

$$\mathcal{D}_s=\begin{bmatrix}0\\ -(\mathcal{F}\otimes K_1)\end{bmatrix},\qquad \mathcal{P}=\begin{bmatrix}I\otimes P_1 & I\otimes P_2\\ I\otimes P_2 & I\otimes P_3\end{bmatrix},$$

$$\mathcal{A}_a=\begin{bmatrix}\Omega_1 & \Omega_2 & \Omega_3\\ 0 & \Omega_4 & \Omega_5\\ 0 & 0 & \Omega_6\end{bmatrix},\qquad \mathcal{B}_a=\begin{bmatrix}\Omega_7\\ \Omega_8\\ 0\end{bmatrix},$$

$$\mathcal{C}_a=\begin{bmatrix}\Omega_9\\ \Omega_{10}\\ 0\end{bmatrix},\qquad \mathcal{D}_a=\begin{bmatrix}0\\ \Omega_{11}\\ \Omega_{12}\end{bmatrix},\qquad \mathcal{S}=\begin{bmatrix}I\otimes S_1 & I\otimes S_2\\ I\otimes S_2 & I\otimes S_3\end{bmatrix}$$

$$
\begin{aligned}
\Omega_1 &= I + \delta\Big(\big((\mathbf{1}-\rho_k)\circ\mathcal{F}\big)\otimes G_1 + \big(\rho_k\circ\mathcal{F}\big)\otimes G_2\Big)\\
\Omega_2 &= -\delta\Big(\big((\mathbf{1}-\rho_k)\circ\mathcal{F}\big)\otimes G_1\Big)\\
\Omega_3 &= -\delta\Big(\big(\rho_k\circ\mathcal{F}\big)\otimes G_2\Big)\\
\Omega_4 &= I + \delta\Big(\big((\mathbf{1}-\rho_k)\circ\mathcal{F}\big)\otimes K_1H\Big)\\
\Omega_5 &= \delta\Big(\big(\rho_k\circ\mathcal{F}\big)\otimes K_2H\Big)\\
\Omega_6 &= I + \delta(\mathcal{F}\otimes K_2H)\\
\Omega_7 &= -\delta\Big(\big((\mathbf{1}-\rho_k)\circ\mathcal{F}\big)\otimes G_1\Big)\\
\Omega_8 &= I + \Big(\big((\mathbf{1}-\rho_k)\circ\mathcal{F}\big)\otimes K_1H\Big)\\
\Omega_9 &= \delta\\
\Omega_{10} &= \delta\Big[I + \Big(\big((\mathbf{1}-\rho_k)\circ\mathcal{F}\big)\otimes K_1H\Big)\Big]\\
&\quad +\delta\Big(\big(\rho_k\circ\mathcal{F}\big)\otimes K_2H\Big)\\
\Omega_{11} &= -\Big(\big((\mathbf{1}-\rho_k)\circ\mathcal{F}\big)\otimes K_1\Big) - \Big(\big(\rho_k\circ\mathcal{F}\big)\otimes K_2\Big)\\
\Omega_{12} &= -(\mathcal{F}\otimes K_2)\\
\Phi &= \lambda_{\max}(\Psi)\sum_{i=1}^{N}(\beta_i^2 + Q_i^2 + R_{ij}^2)\\
\sigma_{\max} &= \lambda_{\max}(\mathcal{P}),\quad \sigma_{\min} = \lambda_{\min}(\mathcal{P})\\
\zeta &= \tfrac{\sigma_{max}}{\sigma_{max}-\gamma}\\
\epsilon &= (1+\varepsilon_1+\varepsilon_2+\varepsilon_3).
\end{aligned}
$$

Proof. Consider the following Lyapunov function:

$$
\boldsymbol{V}_k = (1-\rho_k)\boldsymbol{V}_{1,k} + \rho_k\boldsymbol{V}_{2,k} \tag{7.35}
$$

where $\boldsymbol{V}_{1,k} = \boldsymbol{X}_{s,k}^T\mathcal{P}\boldsymbol{X}_{s,k}$, $\boldsymbol{V}_{2,k} = \boldsymbol{X}_{a,k}^T\mathcal{S}\boldsymbol{X}_{a,k}$, $\boldsymbol{X}_{s,k} = [\boldsymbol{\xi}_k^T, \tilde{\boldsymbol{x}}_k^T]^T$ and $\boldsymbol{X}_{a,k} = [\boldsymbol{\xi}_k^T, \tilde{\boldsymbol{x}}_k^T, \tilde{\boldsymbol{q}}_k^T]^T$. Dividing the time sequence in two parts, depending on whether or not an attack is present, we have: $k \in \Pi_s(k_1,k_2)$ and $k \in \Pi_a(k_1,k_2)$. Note that the matrices $\mathcal{P}$ and $\mathcal{S}$ are both positive definite. Also, the subscripts s and a are used for the period of without DoS attacks and under DoS attacks.

First, we consider the area $\Pi_s(k_1,k_2)$ without DoS attack, in which communication can be established among the robots. Computing the difference of $\boldsymbol{V}_{1,k}$ along the trajectories (7.29) and taking mathematical expectation we obtain:

$$
\begin{aligned}
&\mathbb{E}\{\Delta\boldsymbol{V}_{1,k}|\boldsymbol{X}_{s,k}\} = \mathbb{E}\{\boldsymbol{V}_{1,k+1}|\boldsymbol{X}_{s,k}\} - \boldsymbol{V}_{1,k}\\
&= \mathbb{E}\Big\{\Big(\mathcal{A}_s\boldsymbol{X}_{s,k} + \mathcal{B}_s\boldsymbol{e}_{s,k} + \mathcal{C}_s\boldsymbol{\eta}_{s,k} + \mathcal{D}_s\boldsymbol{\nu}_{s,k}\Big)^T\mathcal{P}\\
&\times(\mathcal{A}_s\boldsymbol{X}_{s,k} + \mathcal{B}_s\boldsymbol{e}_{s,k} + \mathcal{C}_s\boldsymbol{\eta}_{s,k} + \mathcal{D}_s\boldsymbol{\nu}_{s,k})\Big)\Big\}\\
&= \boldsymbol{X}_{s,k}^T\Big(\mathcal{A}_s^T\mathcal{P}\mathcal{A}_s - \mathcal{P}\Big)\boldsymbol{X}_{s,k} + 2\boldsymbol{X}_{s,k}^T\mathcal{A}_s^T\mathcal{P}\mathcal{B}_s\boldsymbol{e}_{s,k}\\
&+2\boldsymbol{X}_{s,k}^T\mathcal{A}_s^T\mathcal{P}\mathcal{C}_s\boldsymbol{\eta}_{s,k} + 2\boldsymbol{X}_{s,k}^T\mathcal{A}_s^T\mathcal{P}\mathcal{D}_s\boldsymbol{\nu}_{s,k} + 2\boldsymbol{\nu}_{s,k}^T\mathcal{D}_s^T\mathcal{P}\mathcal{B}_s\boldsymbol{e}_{s,k}\\
&+\boldsymbol{e}_{s,k}^T\mathcal{B}_s^T\mathcal{P}\mathcal{B}_s\boldsymbol{e}_{s,k} + \boldsymbol{\nu}_{s,k}^T\mathcal{D}_s^T\mathcal{P}\mathcal{D}_s\boldsymbol{\nu}_{s,k} + \boldsymbol{\eta}_{s,k}^T\mathcal{C}_s^T\mathcal{P}\mathcal{C}_s\boldsymbol{\eta}_{s,k}.
\end{aligned} \tag{7.36}
$$

Using Young's inequality: $2a^Tb \leq \varepsilon a^Ta + \varepsilon^{-1}b^Tb$, we obtain:

$$2\boldsymbol{X}_{s,k}^T\mathcal{A}_s^T\mathcal{P}\mathcal{B}_s\boldsymbol{e}_{s,k} \leq \varepsilon_1\boldsymbol{X}_{s,k}^T\mathcal{A}_s^T\mathcal{P}\mathcal{A}_s\boldsymbol{X}_{s,k} + \varepsilon_1^{-1}\boldsymbol{e}_{s,k}^T\mathcal{B}_s^T\mathcal{P}\mathcal{B}_s\boldsymbol{e}_{s,k} \tag{7.37}$$

$$2\boldsymbol{X}_{s,k}^T\mathcal{A}_s^T\mathcal{P}\mathcal{C}_s\boldsymbol{\eta}_{s,k} \leq \varepsilon_2\boldsymbol{X}_{s,k}^T\mathcal{A}_s^T\mathcal{P}\mathcal{A}_s\boldsymbol{X}_{s,k} + \varepsilon_2^{-1}\boldsymbol{\nu}_{s,k}^T\mathcal{D}_s^T\mathcal{P}\mathcal{D}_s\boldsymbol{\nu}_{s,k} \tag{7.38}$$

$$2\boldsymbol{X}_{s,k}^T\mathcal{A}_s^T\mathcal{P}\mathcal{D}_s\boldsymbol{\nu}_{s,k} \leq \varepsilon_3\boldsymbol{X}_{s,k}^T\mathcal{A}_s^T\mathcal{P}\mathcal{A}_s\boldsymbol{X}_{s,k} + \varepsilon_3^{-1}\boldsymbol{\eta}_{s,k}^T\mathcal{C}_s^T\mathcal{P}\mathcal{C}_s\boldsymbol{\eta}_{s,k} \tag{7.39}$$

$$2\boldsymbol{\nu}_{s,k}^T\mathcal{D}_s^T\mathcal{P}\mathcal{B}_s\boldsymbol{e}_{s,k} \leq \varepsilon_4\boldsymbol{\nu}_{s,k}^T\mathcal{D}_s^T\mathcal{P}\mathcal{D}_s\boldsymbol{\nu}_{s,k} + \varepsilon_4^{-1}\boldsymbol{e}_{s,k}^T\mathcal{B}_s^T\mathcal{P}\mathcal{B}_s\boldsymbol{e}_{s,k}. \tag{7.40}$$

Substituting Equations (7.37)-(7.40) into (7.36) we obtain:

$$\begin{aligned}&\mathbb{E}\{\Delta\boldsymbol{V}_{s,k}|\boldsymbol{X}_{s,k}\} = \boldsymbol{X}_{s,k}^T\Big((1+\varepsilon_1+\varepsilon_2+\varepsilon_3)\mathcal{A}_s^T\mathcal{P}\mathcal{A}_s - \mathcal{P}\Big)\boldsymbol{X}_{s,k}\\ &+(1+\varepsilon_1^{-1}+\varepsilon_4^{-1})\boldsymbol{e}_{s,k}^T\mathcal{B}_s^T\mathcal{P}\mathcal{B}_s\boldsymbol{e}_{s,k} + (1+\varepsilon_2^{-1}+\varepsilon_4^{-1})\boldsymbol{\nu}_{s,k}^T\mathcal{D}_s^T\mathcal{P}\mathcal{D}_s\boldsymbol{\nu}_{s,k}\\ &+(1+\varepsilon_3^{-1})\boldsymbol{\eta}_{s,k}^T\mathcal{C}_s^T\mathcal{P}\mathcal{C}_s\boldsymbol{\eta}_{s,k}.\end{aligned} \tag{7.41}$$

Using the event-triggering condition (7.17) we have:

$$\begin{aligned}&\boldsymbol{e}_{s,k}^T\mathcal{B}_s^T\mathcal{P}\mathcal{B}_s\boldsymbol{e}_{s,k} \leq \lambda_{\max}(\mathcal{B}_s^T\mathcal{P}\mathcal{B}_s)\boldsymbol{e}_{s,k}^T\boldsymbol{e}_{s,k}\\ &\leq \lambda_{\max}(\mathcal{B}_s^T\mathcal{P}\mathcal{B}_s)\sum_{i=1}^{N}\boldsymbol{e}_{i,s}^2(k)\\ &\leq \lambda_{\max}(\mathcal{B}_s^T\mathcal{P}\mathcal{B}_s)\Big[\alpha_i\sum_{i=1}^{N}\hat{\boldsymbol{x}}_s^{i+}(k)^T\hat{\boldsymbol{x}}_s^{i+}(k) + \beta_i\Big]\\ &\leq \lambda_{\max}(\mathcal{B}_s^T\mathcal{P}\mathcal{B}_s)\Big[\alpha_i\sum_{i=1}^{N}\boldsymbol{\xi}_s^i(k)^T\boldsymbol{\xi}_s^i(k) + \beta_i\Big]\\ &\leq \alpha X_{s,k}^T\mathcal{B}_s^T\mathcal{P}\mathcal{B}_sX_{s,k} + \lambda_{\max}(\mathcal{B}_s^T\mathcal{P}\mathcal{B}_s)\Big[\sum_{i=1}^{N}\beta_i\Big].\end{aligned} \tag{7.42}$$

Substituting inequality (7.42) in equation (7.41), the following expression is obtained:

$$\begin{aligned}&\mathbb{E}\{\Delta\boldsymbol{V}_{1,k}|\boldsymbol{X}_{s,k}\} =\\ &\boldsymbol{X}_k^T\Big((1+\varepsilon_1+\varepsilon_2+\varepsilon_3)\mathcal{A}_s^T\mathcal{P}\mathcal{A}_s + \alpha\mathcal{B}_s^T\mathcal{P}\mathcal{B}_s - \mathcal{P}\Big)\boldsymbol{X}_{s,k}\\ &+(1+\varepsilon_1^{-1}+\varepsilon_4^{-1})\boldsymbol{e}_{s,k}^T\mathcal{B}_s^T\mathcal{P}\mathcal{B}_s\boldsymbol{e}_{s,k} + (1+\varepsilon_2^{-1}+\varepsilon_4^{-1})\boldsymbol{\nu}_{s,k}^T\mathcal{D}_s^T\mathcal{P}\mathcal{D}_s\boldsymbol{\nu}_{s,k}\\ &+(1+\varepsilon_3^{-1})\boldsymbol{\eta}_{s,k}^T\mathcal{C}_s^T\mathcal{P}\mathcal{C}_s\boldsymbol{\eta}_{s,k} \leq -\gamma_1\boldsymbol{X}_{s,k}^T\boldsymbol{X}_{s,k} + \Phi_s,\end{aligned} \tag{7.43}$$

where

$$\begin{aligned}\Psi_s = &(1+\varepsilon_1^{-1}+\varepsilon_4^{-1})\mathcal{B}_s^T\mathcal{P}\mathcal{B}_s + (1+\varepsilon_2^{-1}+\varepsilon_4^{-1})\mathcal{D}_s^T\mathcal{P}\mathcal{D}_s\\ &+(1+\varepsilon_3^{-1})\mathcal{C}_s^T\mathcal{P}\mathcal{C}_s\end{aligned}$$

$$\Phi_s = \lambda_{\max}(\Psi_s)\sum_{i=1}^{N}(\beta_i + Q_i + R_{ij}).$$

From (7.43) we find a sufficient condition for the bounded consensus of MRSs during the normal period without DoS attacks:

$$(1+\varepsilon_1+\varepsilon_2+\varepsilon_3)\mathcal{A}_s^T\mathcal{P}\mathcal{A}_s + \alpha\mathcal{B}_s^T\mathcal{P}\mathcal{B}_s - \mathcal{P} + \gamma_1 I < 0. \tag{7.44}$$

Now we look for the boundary of consensus U. According to (7.43) for any $\zeta > 1$ we write:

$$\begin{aligned}
&\zeta^{k+1}\mathbb{E}\{V_{1,k+1}\} - \zeta^{k}\mathbb{E}\{V_{1,k}\} \\
&\leq \zeta^{k+1}\mathbb{E}\{\Delta V_{1,k}\} + \zeta^{k}(\zeta-1)\mathbb{E}\{V_{1,k}\} \\
&\leq \zeta^{k+1}[-\gamma_1 \mathbb{E}\Big\{ \|\boldsymbol{X}_{s,k}\|^2 \Big\} + \Phi_s] + \zeta^{k}(\zeta-1)\mathbb{E}\Big\{ \|\boldsymbol{X}_{s,k}\|^2 \Big\} \\
&\leq \Big(\sigma_{\max}(\zeta-1) - \gamma_1\zeta\Big)\rho^{k}\mathbb{E}\Big\{ \|\boldsymbol{X}_{s,k}\|^2 \Big\} + \zeta^{k+1}\Phi_s.
\end{aligned} \tag{7.45}$$

Selecting a proper positive scalar ζ satisfying $\sigma_{\max}(\zeta-1) - \gamma_1\zeta = 0$, we can write:

$$\zeta^{k}\mathbb{E}\{V_{1,k}\} - \mathbb{E}\{V_{1,0}\} \leq \sum_{n=1}^{k}\zeta^{n}\Phi_s, \tag{7.46}$$

which implies that:

$$\begin{aligned}
&\mathbb{E}\{V_{1,k}\} \leq \zeta^{-k}\mathbb{E}\{V_{1,0}\} + \sum_{n=1}^{k}\zeta^{n-k}\Phi_s \\
&= \zeta^{-k}\mathbb{E}\{V_{1,0}\} + \tfrac{(1-\zeta^{-k})\Phi_s}{1-\zeta^{-1}} \\
&= \zeta^{-k}\Big(\mathbb{E}\{V_{1,0}\} - \tfrac{\zeta\Phi_s}{\zeta-1}\Big) + \tfrac{\zeta\Phi_s}{\zeta-1} \\
&\leq \max\Big\{\mathbb{E}\{V_{1,0}\}, \tfrac{\zeta\Phi_s}{\zeta-1}\Big\}.
\end{aligned} \tag{7.47}$$

We know that

$$\mathbb{E}\{V_{1,0}\} = X_0^T\mathcal{P}X_0 \leq \lambda_{\max}(\mathcal{P})\mathbb{E}\Big\{ \|\boldsymbol{X}_0\|^2 \Big\}. \tag{7.48}$$

From Definition III.1 we have:

$$\mathbb{E}\Big\{ \|\boldsymbol{X}_0\|^2 \Big\} = \sum_{i=1}^{N}\left\| x^i(0) - (\tfrac{1}{N})\sum_{j=1}^{N}x^j(0) \right\|^2 \leq \mathcal{X}_0^2. \tag{7.49}$$

Finally, we can show that:

$$U(\mathcal{X}_0, \beta, Q, R) = \max\left\{ \tfrac{\sigma_{max}}{\sigma_{min}}\mathcal{X}_0^2, \tfrac{\zeta}{\zeta-1}\Phi_s \right\}. \tag{7.50}$$

Using the Schur complement lemma, inequality (7.44) can be transformed into the following LMI condition:

$$\begin{bmatrix} -\mathcal{P} + \gamma_1 I & \mathcal{A}_s & \mathcal{B}_s \\ \mathcal{A}_s^T & -\epsilon^{-1}\mathcal{P}^{-1} & 0 \\ \mathcal{B}_s^T & 0 & -\alpha^{-1}\mathcal{P}^{-1} \end{bmatrix} < 0. \tag{7.51}$$

We now consider the stability of the MRSs when $k \in \Pi_a(k_1, k_2)$, *i.e.* when some communication channels between robots are affected by DoS attacks. During this interval, if $\rho_{ij}(k) = 1$ the packets exchanged between robots are lost, and if $\rho_{ij}(k) = 0$

then robots can transmit the packets without DoS attacks. Considering the Lyapunov function $\boldsymbol{V}_{2,k} = \boldsymbol{X}_{a,k}^T \mathcal{S} \boldsymbol{X}_{a,k}$ along the trajectory (7.29) provides the following sufficient condition for the stability:

$$(1+\varepsilon_1+\varepsilon_2+\varepsilon_3)\mathcal{A}_a^T\mathcal{S}\mathcal{A}_a + \alpha\mathcal{B}_a^T\mathcal{S}\mathcal{B}_a - \mathcal{S} + \gamma_2 I < 0. \tag{7.52}$$

Using the Schur complement lemma, the inequality (7.52) can be transformed into the following LMI condition:

$$\begin{bmatrix} -\mathcal{S}+\gamma_2 I & \mathcal{A}_a & \mathcal{B}_a \\ \mathcal{A}_a^T & -\epsilon^{-1}\mathcal{S}^{-1} & 0 \\ \mathcal{B}_a^T & 0 & -\alpha^{-1}\mathcal{S}^{-1} \end{bmatrix} < 0. \tag{7.53}$$

Based on above analysis, we can combine the two scenarios with/without DoS attacks, to obtain the following relation:

$$\mathbb{E}\{\boldsymbol{V}_{k+1}\} = \begin{cases} -\gamma_1\mathbb{E}\{\boldsymbol{V}_k\} + \Phi_s, & k \in \Pi_s(k_1,k_2) \\ \\ -\gamma_2\mathbb{E}\{\boldsymbol{V}_k\} + \Phi_a, & k \in \Pi_a(k_1,k_2). \end{cases} \tag{7.54}$$

Consider the uncertainty on the duration of DoS attack, we can write:

$$\begin{array}{l} |\bar{\Xi}_a(k_1,k_2)| \leq |\Xi_a(k_1,k_2)| + n(0,k)\tau_d \\ \leq (\vartheta + c\tau_d) + \frac{1}{T_D} + \frac{\tau_d}{\tau_D} \\ = \vartheta^* + \frac{k}{T^*} \end{array} \tag{7.55}$$

where $\vartheta^* = (\vartheta + c\tau_d)$ and $T^* = \frac{\tau_D T_D}{\tau_D + \tau_d T_D}$. Then,

$$\begin{array}{rl} \mathbb{E}\{\boldsymbol{V}_{k+1}\} \leq & \mu^{n(0,k)}\gamma_1^{T_1(0,k)-|\bar{\Xi}_a(0,k)|}\gamma_2^{|\bar{\Xi}_a(0,k)|}\mathbb{E}\{\boldsymbol{V}_0\} \\ & + \max\left\{\frac{\sigma_{max}}{\sigma_{min}}\mathcal{X}_0^2, \frac{\zeta}{\zeta-1}\Phi\right\} \\ \leq & \mu^{N_0}\gamma_1^{-\tau_d N_0 - \vartheta^*}\gamma_2^{\vartheta^*}\left(\mu\gamma_1^{1-\tau_d-\frac{1}{T^*}}\gamma_2^{\frac{1}{T^*}}\right)^k\mathbb{E}\{\boldsymbol{V}_0\} \\ & + \max\left\{\frac{\sigma_{max}}{\sigma_{min}}\mathcal{X}_0^2, \frac{\zeta}{\zeta-1}\Phi\right\}. \end{array} \tag{7.56}$$

The condition for convergence is as follows:

$$\mu\gamma_1^{1-\tau_d-\frac{1}{T^*}}\gamma_2^{\frac{1}{T^*}} < 1 \tag{7.57}$$

which leads to the following condition for the duration of DoS attack:

$$\frac{1}{T^*} \leq \frac{(\tau_d-1)\ln(\gamma_1)-\ln(\mu)}{\ln(\gamma_2)-\ln(\gamma_1)}. \tag{7.58}$$

This completes the proof. □

Remark 33. *Theorem III.1 provides an upper bound for the DoS attack duty cycle in order to achieve secure consensus. Therefore, resilience and secure consensus*

is guaranteed if the duration of DoS attack is smaller than $\frac{(\tau_d-1)\ln(\gamma_1)-\ln(\mu)}{\ln(\gamma_2)-\ln(\gamma_1)}$. *However, a larger upper bound for the attack duration would provide stronger robustness against Dos attacks. The following optimization problem can formulated for this purpose:*

$$\begin{aligned} &\max_{K_1,K_2,G_1,G_2,\alpha,\gamma_1,\gamma_2} && \frac{(\tau_d-1)\ln(\gamma_1)-\ln(\mu)}{\ln(\gamma_2)-\ln(\gamma_1)} \\ &s.t. && \text{LMI conditions (7.32)} - \text{(7.33)} \end{aligned} \tag{7.59}$$

Remark 34. *In Theorem III.1, the consensus bound* U *depends upon the initial position of robots* ($\mathcal{X}_0$)*, covariance of process noise* (Q)*, covariance of relative measurement noise* (R)*, and parameter of event-triggered mechanism* (β)*. However, the duration of the DoS attacks can affect the convergence and secure consensus of the multi-robot system. Therefore, we consider the uncertainty term* τ_d *in the attack duration and co-design a controller and filter as well as the event-triggered mechanisms using LMI conditions (7.32)-(7.33) such that the the robustness of the system against DoS attacks is improved.*

Remark 35. *It is worth mentioning that Young's inequality* $2a^Tb \leq \varepsilon a^Ta+\varepsilon^{-1}b^Tb$ *is used to deal with some of the cross terms* e_k, η_k, ν_k *and design the secure consensus control. Note that parameters* ε_1, ε_2,... *in the LMIs (7.32)-(7.33) can be tuned further to minimize the consensus bound.*

IV Case Study

IV.1 Simulation Results

In this section, we verify the performance of the proposed secure consensus control with event-triggered mechanism in the presence of DoS attacks via simulation. We consider a group of four mobile robots equipped with on borad sensors to detect the neighbouring robots and measure range-bearing. We assume that the communication graph between robots can change over the time. We consider a scenario that each mobile robot localize itself cooperatively and perform secure consensus under the Dos attack strategy described in Fig. 7.4. We assume that the initial position of robots is $\boldsymbol{x}^1(0) = [20,-10]^T$, $\boldsymbol{x}^2(0) = [-20,-10]^T$, $\boldsymbol{x}^3(0) = [-20,10]^T$, $\boldsymbol{x}^4(0) = [20,10]^T$, the covariance of the control input $Q_i = (0.05)^2\text{diag}([(\Delta L^i)^2;(\Delta R^i)^2])$ and covariance of the sensor measurements $R_{ij} = \text{diag}([0.001m^2;0.001rad^2])$. In our simulations, the position $\bar{\boldsymbol{x}}_{des} = [0,0]^T$ is the desired consensus position. We first

consider a classical consensus control where position estimates received from the attacked communication links are set to zero when the DoS attacks occurs. Based on the trajectory of robots in Fig. 7.5(a) we can see that the robots fail to reach the desire consensus position. However, our proposed secure consensus control safely steers the robots to the desire consensus position despite the DoS attacks, thanks to the fact that a predictor estimates the position of neighbouring robots used in the control scheme during the attacks interval. Also, comparison of the localization error between the Fig. 7.5(b)-(c) and Fig. 7.6(b)-(c) shows that the localization results in our approach have better performance than the classical approach. Finally, using event-triggered mechanism we significantly reduce transmission between robots as can be seen in Fig. 7.6(d)-(e)

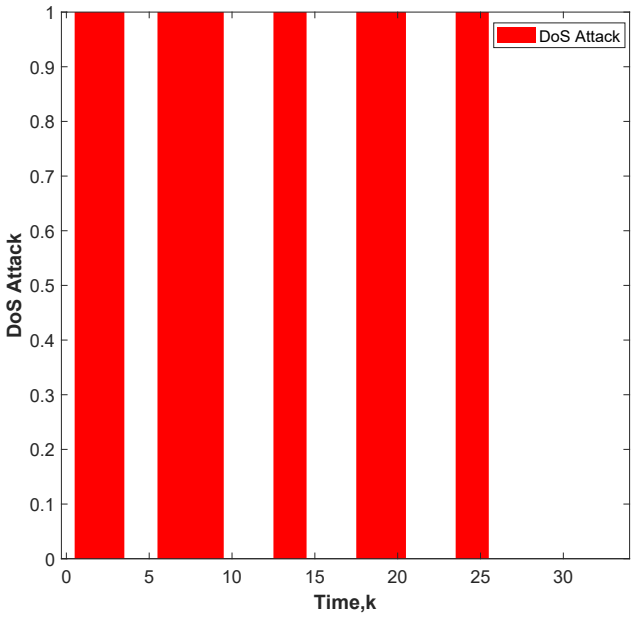

Figure 7.4: Time sequence of DoS attacks

IV.2 Experimental Validation

In this part, we implement and verify the performance of the proposed event-triggered secure consensus control experimentally. The experimental testbed (see Fig. 7.7) consist of four e-puck2 robots (equipped with ArUco tags), ZED camera and a Linux-based host computer (equipped with Robot Operating Systems). The e-puck2 robots can communicate with the host computer through Bluetooth. The host computer works as external processor collecting the camera images from the robots and processing them using computer vision library [117]. The information collected

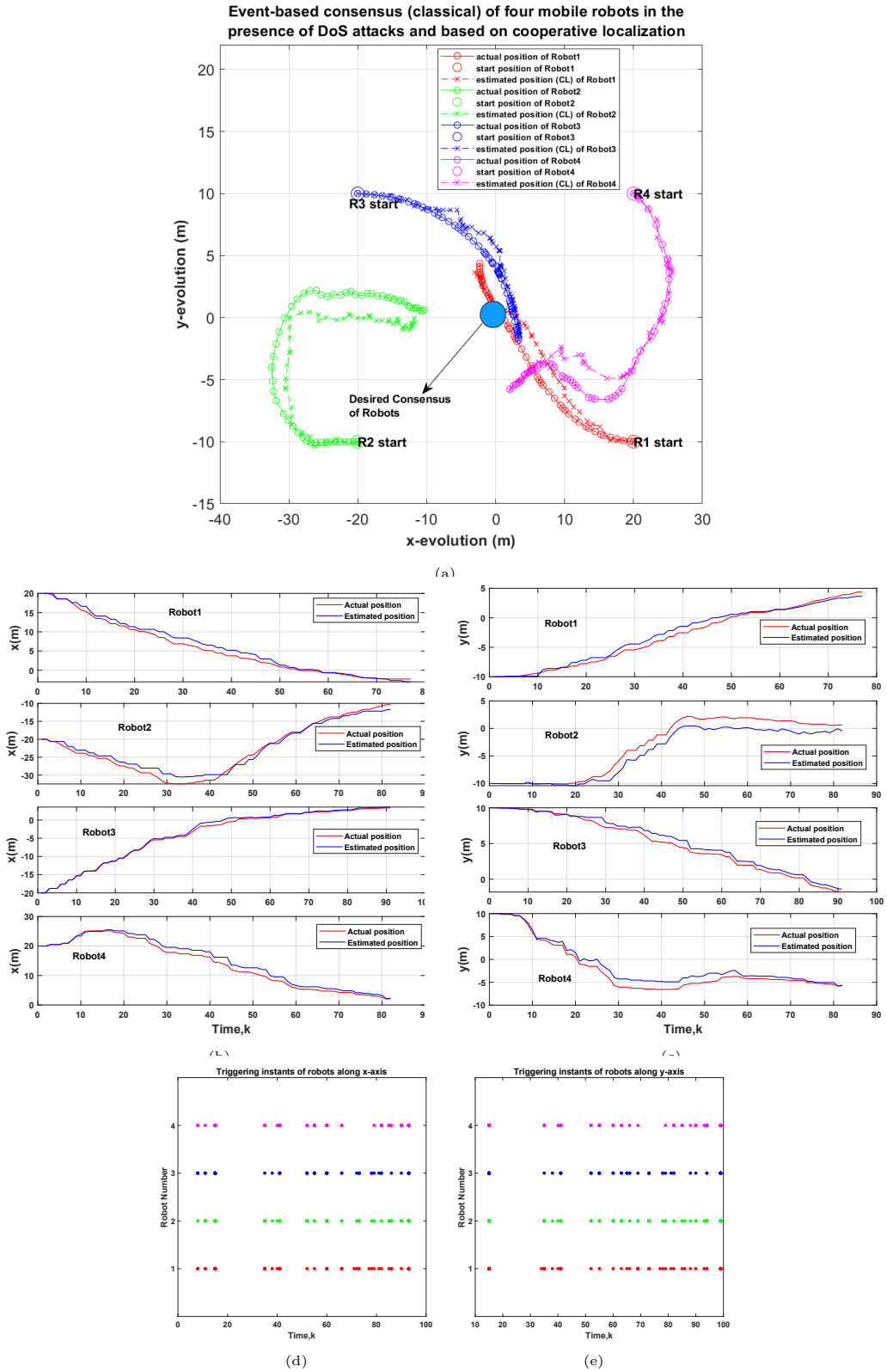

Figure 7.5: (a) Event-based secure consensus (classical) of four mobile robots based on cooperative localization (a) actual position and estimated position (CL) trajectories of four robots on the xy-plane (b),(c) actual position and estimated position (CL) trajectories of four robots respect to time (d), (e) triggering times of robots along x-axis and y-axis

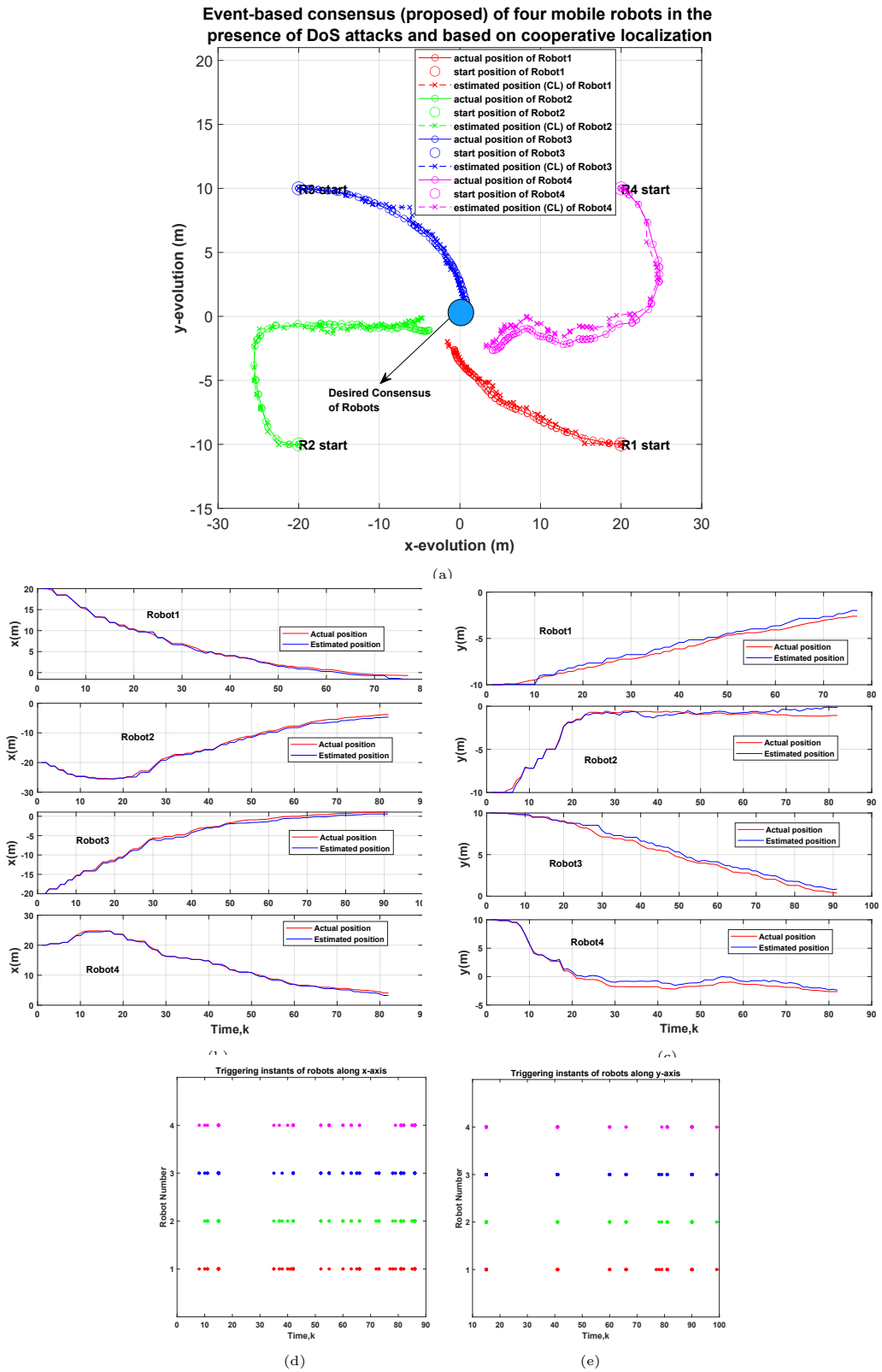

Figure 7.6: (a) Event-based secure consensus (proposed) of four mobile robots based on cooperative localization (a) actual position and estimated position (CL) trajectories of four robots on the xy-plane (b),(c) actual position and estimated position (CL) trajectories of four robots respect to time (d), (e) triggering times of robots along x-axis and y-axis

(a) (b) (c)

Figure 7.7: Experimental setup including (a) four e-puck2 robots equipped with ArUco tags, (b) overhead ZED camera, (c) e-puck2 robot

is used to calculate an estimate of the position of the e-puck2 robots by implementing the CL algorithm. In the meantime, the controller determines the velocity feedback control signal based on position estimates. The signal is then transmitted to each e-puck2 robots through Bluetooth to steer the robot to the desired consensus position. Note that each robot randomly observes the neighbouring robots and exchange position information over the unreliable network. The velocity control signal of each robot is implemented based on the event-triggered scheme where the positioning information of neighbouring robots is transmitted according to the decision made by the triggering condition (7.17). The e-puck2 robots begin their motion with initial positions $x_{\text{epuck0}}(0) = 0.2, y_{\text{epuck0}}(0) = -0.1$, $x_{\text{epuck1}}(0) = -0.2, y_{\text{epuck1}}(0) = -0.1$, $x_{\text{epuck2}}(0) = -0.2, x_{\text{epuck2}}(0) = 0.1$ and $x_{\text{epuck3}}(0) = 0.2, x_{\text{epuck3}}(0) = 0.1$. We consider a DoS attack with duration of 8s. Our goal is to design a resilient consensus control scheme in the presence of DoS attacks such that robots move to the desired consensus position with minimum amount of positioning transmitted between robots. According to Fig. 7.8 we see that: (1) Using a classical consensus control scheme where the velocity feedback control signal is maintained constant during the DoS attack interval, the robots cannot reach the desire consensus position; (2) The proposed secure consensus control scheme is able to compensate the adverse impact caused by the DoS attacks and achieve the desire consensus position with minimum amount of communication between robots. Clearly our proposed control scheme can improve the resiliency and tolerance of multi-robot system against DoS attacks.

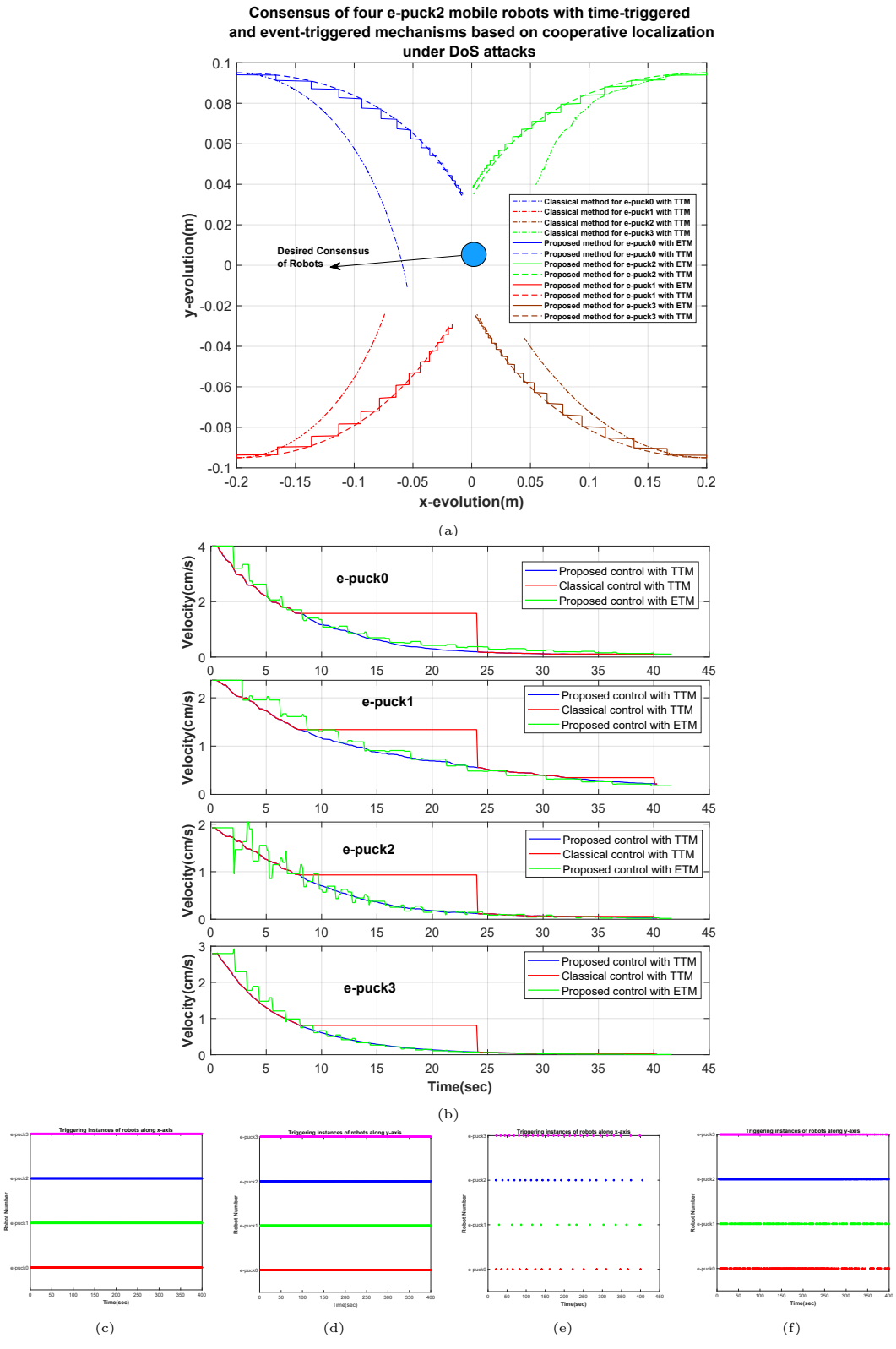

Figure 7.8: Consensus of e-puck2 robots with *time-triggered mechanism (TTM)* and *event-triggered mechanism (ETM)* based on CL algorithm in presence of DoS attacks (a) position of four robots on the xy-plane (b) velocities of four robots respect to time (c), (d) triggering times of robots along x-axis and y-axis in TTM (e), (f) triggering times of robots along x-axis and y-axis in ETM

Chapter 8

Summary and Conclusions

In this thesis, we propose to study multi-robot cooperative localization with its application to a fleet of mobile robots. Then, we investigate the consensus control problem for group of mobile robots where each robot use the position estimates from CL agorithm in order to perform consensus. Specifically, our interest is in the development of a decentralized algorithm that can remain operational under the following constraints:

1. limited communication resouces,
2. networked induced delays,
3. cyber attacks,

The outcomes of our research attempts are further summarized as follows:

1. In chapter 3, we propose a novel decentralized event-based cooperative localization algorithm for a team of mobile robots where the objective is to perform localization with limited communication resources. We show that by properly tuning the event-triggering condition, the estimation error remains bounded while the data transmission between the sensors and the filters reduced. The proposed algorithm was successfully applied to four e-puck2 robots and the comparison results showed the effectiveness of the proposed algorithm.
2. In chapter 4, we study the problem of DECL for a team of mobile robots assuming that random delays affect the communication flow between robots. We propose a DECL algorithm that can cope with the effect of random delays and derive two optimal filters that minimize the estimation variance under two separate assumption; namely with and without time stamps technology.

In both case, we provide sufficient conditions for the boundedness of the estimation error for both filters proposed. We show that by considering the proposed boundary for random delays and tuning the event-triggering parameters, the estimation error remains bounded while the number of transmission packets between sensor and filter is reduced. Simulation and experimental results show the effectiveness of the proposed approach.

3. In chapter 5, we study the problem of event-triggered cooperative localization with the specific objective of cyber attacks. For the attacks with limited resources, we design the optimal Kalman filter under both DoS and FDI attacks, and provided a sufficient condition to guarantee the convergence and resilience of the proposed filter. Moreover, we also propose an attack detection mechanism for the proposed algorithm when the attack signal are unbounded. Simulation and experimental results show the efficiency of the proposed algorithm.

4. In chapter 6, we study the problem of event-triggered consensus control for a multi-robot systems. In our framework, we consider cooperative localization (CL) to estimate the position of robots and employ the result of position estimates as input of consensus control. We design an event-triggered consensus control based on CL such that robots achieve a prescribed consensus while reducing unnecessary communication between robots. We derive an optimization framework where the control and filter gains as well as the event-triggered parameters can be designed simultaneously and minimize the consensus bound. Finally we present both simulation and experimental results to show the effectiveness of proposed approach.

5. In chapter 7, we investigate the event-triggered secure consensus control for multi-robot systems in the presence of DoS attacks. Specifically, we employ a cooperative localization algorithm to estimate the position of robots and design a consensus control for each robot based on position estimates and steer the position of robots to the desired agreement position under DoS attacks. We provide a relation between a secure consensus and attack parameters which then used to improve the tolerance and resilience of DoS attack intervals. Our simulations and experiments verify the effectiveness of proposed method.

I Directions for Future Work

The research results, provided in this thesis can be extended and pursued in the following areas:

1. **Event-triggered consensus control for multi-robot systems with cooperative localization under asynchronous behaviour of communication network:** In this thesis, we assume that each robot checks the event-triggering condition periodically using the same sampling period and that all robots are synchronized. For simplicity, our analysis ignores a small delay that accounts for the effect of the communication delays between robots. This delay is inevitable due to the unpredictable nature of the network. When the number of robots is small, this delay is typically negligible. However, as the number of robots increases, the delay might result in asynchronous behaviour that requires a more detailed analysis. The number of robots that can be tolerated under the presents assumptions, depends on the characteristics of the robots and the network. Therefore, how to design a triggering condition for asynchronous behaviour of multi-robot network will be our future work.

2. **Multi-rate consensus control for multi-robot systems with cooperative localization:** As we mentioned before, in cooperative localization exteroceptive and proprioceptive sensors needs to be fused to correct the navigation states. More specifically, laser, camera and IMU sensors usually run at quite different sampling rate, one of the challenges is the sensor data streams being multi-rate. To tackle this problem, we consider multi-rate EKF design to estimate the position of robots. Then, the consensus control in each robot determines the velocity feedback control signal based on the transmitted position estimates and steer the robot to the desired agreement position. Therefore, considering the effect of multi-rate on the design of the cooperative localization is an opening problem.

3. **Navigation for Mobile Robots in Dynamic and Uncertain Environments:** In recent years, the navigation of autonomous mobile robots have been received significant amount of attention from academia and industry. One of the interesting problem in autonomous navigation is to guide the mobile robot from the dynamic and uncertain environment to the destination. Specifically,

the main challenging task in the motion planning is to create a path for a mobile robot in the presence of dynamic objects. To navigate in such environments, each robot needs to make an optimal decision at each time so it can move safely and smoothly toward the desired destination. Although many research have been conducted in the field of motion planning and control, this problem remains a difficult challenge with the existing approaches.

References

[1] I. J. Cox, "Blanche-an experiment in guidance and navigation of an autonomous robot vehicle," in IEEE Transactions on Robotics and Automation, vol. 7, no. 2, pp. 193-204, April 1991

[2] Everett, H. R. (1995). Sensors for Mobile Robots. A K Peters/CRC Press.

[3] J. Borenstein and Liqiang Feng, "Measurement and correction of systematic odometry errors in mobile robots," in IEEE Transactions on Robotics and Automation, vol. 12, no. 6, pp. 869-880, Dec. 1996.

[4] C. F. Olson and L. H. Matthies, "Maximum likelihood rover localization by matching range maps," Proceedings. 1998 IEEE International Conference on Robotics and Automation (Cat. No.98CH36146), 1998, pp. 272-277 vol.1

[5] S. I. Roumeliotis and G. A. Bekey, "Bayesian estimation and Kalman filtering: a unified framework for mobile robot localization," Proceedings 2000 ICRA. Millennium Conference. IEEE International Conference on Robotics and Automation. Symposia Proceedings (Cat. No.00CH37065), 2000, pp. 2985-2992 vol.3

[6] R. Kurazume, S. Nagata and S. Hirose, "Cooperative positioning with multiple robots," Proceedings of the 1994 IEEE International Conference on Robotics and Automation, 1994, pp. 1250-1257 vol.2

[7] Rekleitis, I., Dudek, G., & Milios, E. (2001). Annals of Mathematics and Artificial Intelligence, 31(1/4), 7–40.

[8] S. I. Roumeliotis and G. A. Bekey, "Distributed multirobot localization," in IEEE Transactions on Robotics and Automation, vol. 18, no. 5, pp. 781-795, Oct. 2002.

[9] E. D. Nerurkar, S. I. Roumeliotis and A. Martinelli, "Distributed maximum a posteriori estimation for multi-robot cooperative localization," 2009 IEEE International Conference on Robotics and Automation, 2009, pp. 1402-1409.

[10] S. S. Kia, J. Hechtbauer, D. Gogokhiya and S. Martínez, "Server-Assisted Distributed Cooperative Localization Over Unreliable Communication Links," in IEEE Transactions on Robotics, vol. 34, no. 5, pp. 1392-1399, Oct. 2018.

[11] R. Madhavan, K. Fregene, and L. E. Parker, "Distributed cooperative outdoor multirobot localization and mapping," Auton. Robot, vol. 17, no. 1, pp. 23–39, 2004.

[12] Howard, A. (2006). Multi-robot simultaneous localization and mapping using particle filters. The International Journal of Robotics Research, 25(12), 1243–1256.

[13] A. Ahmad, G. Lawless and P. Lima, "An Online Scalable Approach to Unified Multirobot Cooperative Localization and Object Tracking," in IEEE Transactions on Robotics, vol. 33, no. 5, pp. 1184-1199, Oct. 2017.

[14] H. Li and F. Nashashibi, "Cooperative Multi-Vehicle Localization Using Split Covariance Intersection Filter," in IEEE Intelligent Transportation Systems Magazine, vol. 5, no. 2, pp. 33-44, Summer 2013.

[15] J. Kim, "Cooperative Localization and Unknown Currents Estimation Using Multiple Autonomous Underwater Vehicles," in IEEE Robotics and Automation Letters, vol. 5, no. 2, pp. 2365-2371, April 2020.

[16] Zhuang, Y., Wang, Z., Yu, H., Wang, W., & Lauria, S. (2013). A robust extended filtering approach to multi-robot cooperative localization in dynamic indoor environments. Control Engineering Practice, 21(7), 953–961.

[17] I. M. Rekleitis, G. Dudek and E. E. Milios, "Multi-robot cooperative localization: a study of trade-offs between efficiency and accuracy," IEEE/RSJ International Conference on Intelligent Robots and Systems, 2002, pp. 2690-2695 vol.3.

[18] S. I. Roumeliotis and I.M. Rekleitis, "Propagation of uncertainty in cooperative multirobot localization: Analysis and experimental results," Auton. Robot, vol. 17, no. 1, pp. 41–54, 2004.

[19] S. Safavi and U. A. Khan, "An Opportunistic Linear–Convex Algorithm for Localization in Mobile Robot Networks," in IEEE Transactions on Robotics, vol. 33, no. 4, pp. 875-888, Aug. 2017

[20] T. -K. Chang and A. Mehta, "Optimal Scheduling for Resource-Constrained Multirobot Cooperative Localization," in IEEE Robotics and Automation Letters, vol. 3, no. 3, pp. 1552-1559, July 2018.

[21] A. I. Mourikis and S. I. Roumeliotis, "Optimal sensor scheduling for resource-constrained localization of mobile robot formations," in IEEE Transactions on Robotics, vol. 22, no. 5, pp. 917-931, Oct. 2006.

[22] T. R. Wanasinghe, G. K. I. Mann and R. G. Gosine, "Distributed Leader-Assistive Localization Method for a Heterogeneous Multirobotic System," in IEEE Transactions on Automation Science and Engineering, vol. 12, no. 3, pp. 795-809, July 2015.

[23] A. I. Mourikis and S. I. Roumeliotis, "Performance analysis of multirobot Cooperative localization," in IEEE Transactions on Robotics, vol. 22, no. 4, pp. 666-681, Aug. 2006.

[24] Caglioti, V., Citterio, A., & Fossati, A. (2006). Cooperative, distributed localization in multi-robot systems: a minimum-entropy approach. IEEE Workshop on Distributed Intelligent Systems: Collective Intelligence and Its Applications (DIS'06).

[25] L. Zhang, X. Tao and H. Liang, "Multi AUVs Cooperative Navigation Based on Information Entropy," OCEANS 2018 MTS/IEEE Charleston, 2018, pp. 1-10.

[26] P. Singh, M. Chen, L. Carlone, S. Karaman, E. Frazzoli and D. Hsu, "Supermodular mean squared error minimization for sensor scheduling in optimal Kalman Filtering," 2017 American Control Conference (ACC), 2017, pp. 5787-5794.

[27] Zhang, H., Ayoub, R., & Sundaram, S. (2017). Sensor selection for Kalman filtering of linear dynamical systems: Complexity, limitations and greedy algorithms. Automatica: The Journal of IFAC, the International Federation of Automatic Control, 78, 202–210.

[28] Sullivan, N., Grainger, S., & Cazzolato, B. (2018). Analysis of cooperative localisation performance under varying sensor qualities and communication rates. Robotics and Autonomous Systems, 110, 73–84.

[29] J. Zhu and S. S. Kia, "Cooperative Localization Under Limited Connectivity," in IEEE Transactions on Robotics, vol. 35, no. 6, pp. 1523-1530, Dec. 2019.

[30] N. Trawny, S. I. Roumeliotis and G. B. Giannakis, "Cooperative multi-robot localization under communication constraints," 2009 IEEE International Conference on Robotics and Automation, 2009, pp. 4394-4400.

[31] K. Y. K. Leung, T. D. Barfoot and H. H. T. Liu, "Decentralized Localization of Sparsely-Communicating Robot Networks: A Centralized-Equivalent Approach," in IEEE Transactions on Robotics, vol. 26, no. 1, pp. 62-77, Feb. 2010.

[32] M. Ouimet, D. Iglesias, N. Ahmed, and S. Martínez, "Cooperative robot localization using event-triggered estimation," J. Aerosp. Inf. Syst., vol. 15, no. 7, pp. 427–449, Jul. 2018.

[33] Q. Yan, L. Jiang and S. S. Kia, "Measurement Scheduling for Cooperative Localization in Resource-Constrained Conditions," in IEEE Robotics and Automation Letters, vol. 5, no. 2, pp. 1991-1998, April 2020.

[34] C. Zhang and Y. Jia, "Distributed Kalman consensus filter with event-triggered communication: Formulation and stability analysis," J. Franklin Inst., vol. 354, no. 13, pp. 5486–5502, Sep. 2017.

[35] Q. Liu, Z. Wang, X. He, and D. H. Zhou, "Event-based recursive distributed filtering over wireless sensor networks," IEEE Trans. Autom. Control, vol. 60, no. 9, pp. 2470–2475, Sep. 2015.

[36] W. Qiao and R. Sipahi, "Consensus control under communication delay in a three-robot system: Design and experiments," IEEE Trans. Control Syst. Technol., vol. 24, no. 2, pp. 687–694, 2016.

[37] X. Jiang, G. Xia, Z. Feng, and X. Jing, "Distributed sampled-data non-fragile consensus filtering over sensor networks with topology switching and transmission delay," IEEE-ASME Trans. Mechatronics., pp. 1–1, 2021.

[38] H. Zhang, X. Zheng, H. Yan, C. Peng, Z. Wang, and Q. Chen, "Codesign of event-triggered and distributed H_∞ filtering for active semi-vehicle suspension systems," IEEE-ASME Trans. Mechatronics., vol. 22, no. 2, pp. 1047–1058, 2017.

[39] A. Wang, B. Mu, and Y. Shi, "Event-triggered consensus control for multiagent systems with time-varying communication and event-detecting delays," *IEEE Trans. Control Syst. Technol.*, vol. 27, no. 2, pp. 507–515, 2019.

[40] D. Liu, Z. Wang, Y. Liu, and F. E. Alsaadi, "Extended Kalman filtering subject to random transmission delays: Dealing with packet disorders," *Inf. Fusion*, vol. 60, pp. 80–86, 2020.

[41] X. Fu, H. Bi, and X. Gao, "Multi-UAVs cooperative localization algorithms with communication constraints," Math. Probl. Eng., vol. 2017, pp. –8, 2017.

[42] S. Zhang and Y. Cao, "Cooperative localization approach for multi-robot systems based on state estimation error compensation," *Sensors (Basel)*, vol. 19, no. 18, p. 3842, 2019.

[43] M. D. Phung, T. T. Van Nguyen, T. H. Tran, and Q. V. Tran, "Localization of networked robot systems subject to random delay and packet loss," in *IEEE Int. Conf. Advanced Intelligent Mechatronics.*, pp. 1442–1447, 2013.

[44] M. Shan, S. Worrall, and E. Nebot, "Delayed-state nonparametric filtering in cooperative tracking," *IEEE Trans. Robot.*, vol. 31, no. 4, pp. 962–977, 2015.

[45] Y. Yao, D. Xu, and W. Yan, "Cooperative localization with communication delays for MAUVs," in 2009 IEEE International Conference on Intelligent Computing and Intelligent Systems, vol. 1, pp. 244–249, 2009.

[46] Y. Zhang, F. Li, and Y. Chen, "Leader-following-based distributed Kalman filtering in sensor networks with communication delay," *J. Franklin Inst.*, vol. 354, no. 16, pp. 7504–7520, 2017.

[47] Y. Mo and B. Sinopoli, "Secure estimation in the presence of integrity attacks," *IEEE Trans. Autom. Control.*, vol. 60, no. 4, pp. 1145–1151, 2015.

[48] H. Fawzi, P. Tabuada, and S. Diggavi, "Secure estimation and control for cyber-physical systems under adversarial attacks," *IEEE Trans. Autom. Control.*, vol. 59, no. 6, pp. 1454–1467, 2014.

[49] Y. Shoukry and P. Tabuada, "Event-triggered state observers for sparse sensor noise/attacks," *IEEE Trans. Autom. Control.*, vol. 61, no. 8, pp. 2079–2091, 2016.

[50] Y. Li, L. Shi, P. Cheng, J. Chen, and D. E. Quevedo, "Jamming attacks on remote state estimation in cyber-physical systems: A game-theoretic approach," *IEEE Trans. Autom. Control.*, vol. 60, no. 10, pp. 2831–2836, 2015.

[51] H. Zhang, P. Cheng, L. Shi, and J. Chen, "Optimal DoS attack scheduling in wireless networked control system," *IEEE Trans. Control Syst. Technol.*, vol. 24, no. 3, pp. 843–852, 2016.

[52] Q. Su, Z. Fan, Y. Long, and J. Li, "Attack detection and secure state estimation for cyber-physical systems with finite-frequency observers," *J. Franklin Inst.*, vol. 357, no. 17, pp. 12724–12741, 2020.

[53] H. Lin, J. Lam, and Z. Wang, "Secure state estimation for systems under mixed cyber-attacks: Security and performance analysis," *Inf. Sci. (Ny)*, vol. 546, pp. 943–960, 2021.

[54] Liu, Y., & Yang, G. H. (2020). Y. Liu and G.-H. Yang, "Event-triggered distributed state estimation for cyber-physical systems under DoS attacks," *IEEE Trans. Cybern.*, vol. PP, pp. 1–12, 2020.

[55] Y. Liu and G.-H. Yang, "Resilient event-triggered distributed state estimation for nonlinear systems against DoS attacks," *IEEE Trans. Cybern.*, vol. PP, pp. 1–14, 2021.

[56] W. Chen, D. Ding, H. Dong, and G. Wei, "Distributed resilient filtering for power systems subject to denial-of-service attacks," *IEEE Trans. Syst. Man Cybern. Syst.*, vol. 49, no. 8, pp. 1688–1697, 2019.

[57] Y. Chen, S. Kar, and J. M. F. Moura, "Resilient distributed estimation: Sensor attacks," *IEEE Trans. Autom. Control.*, vol. 64, no. 9, pp. 3772–3779, 2019.

[58] L. An and G.-H. Yang, "Distributed secure state estimation for cyber–physical systems under sensor attacks," *Automatica*, vol. 107, pp. 526–538, 2019.

[59] A.-Y. Lu and G.-H. Yang, "Secure state estimation for multiagent systems with faulty and malicious agents," *IEEE Trans. Autom. Control.*, vol. 65, no. 8, pp. 3471–3485, 2020.

[60] L. Su and S. Shahrampour, "Finite-time guarantees for byzantine-resilient distributed state estimation with noisy measurements," *IEEE Trans. Autom. Control.*, vol. 65, no. 9, pp. 3758–3771, 2020.

[61] A.-Y. Lu and G.-H. Yang, "Distributed secure state estimation in the presence of malicious agents," *IEEE Trans. Autom. Control.*, vol. 66, no. 6, pp. 2875–2882, 2021.

[62] T. K. Tasooji and H. J. Marquez, "Cooperative Localization in Mobile Robots Using Event-Triggered Mechanism: Theory and Experiments," IEEE Trans. Autom. Sci. Eng., October 2021, doi: 10.1109/TASE.2021.3115770.

[63] T. K. Tasooji and H. J. Marquez, "Decentralized Event-Triggered Cooperative Localization In Multi-Robot Systems Under Random Delays: With/Without Time Stamps Mechanisms", Accepted for publication of IEEE-ASME Trans. Mechatronics.

[64] L. Cheng, Z. Hou, M. Tan and X. Wang, "Necessary and Sufficient Conditions for Consensus of Double-Integrator Multi-Agent Systems With Measurement Noises," *IEEE Trans. Autom. Control.*, vol. 56, no. 8, pp. 1958-1963, Aug. 2011.

[65] T. Li, F. Wu and J. Zhang, "Multi-Agent Consensus With Relative-State-Dependent Measurement Noises," *IEEE Trans. Autom. Control.*, vol. 59, no. 9, pp. 2463-2468, Sept. 2014.

[66] Y. Chen, H. Dong, J. Lu, X. Sun, and K. Liu, "Robust consensus of nonlinear multiagent systems with switching topology and bounded noises," *IEEE Trans. Cybern.*, vol. 46, no. 6, pp. 1276–1285, 2016.

[67] Z. Wang and H. Zhang, "Consensus error calculation for multiagent systems with both system and measurement noises," *IEEE Trans. Control Netw. Syst.*, vol. 5, no. 3, pp. 1457–1466, 2018.

[68] Z. Wang, H. Sun, H. Zhang, and X. Liu, "Bounded consensus control for stochastic multi-agent systems with additive noises," *Neurocomputing.*, vol. 408, pp. 72–79, 2020.

[69] L. Ma, Z. Wang and H. Lam, "Mean-Square $\mathcal{H}_\infty$ Consensus Control for a Class of Nonlinear Time-Varying Stochastic Multiagent Systems: The Finite-Horizon Case," *IEEE Trans. Syst., Man, Cybern., Syst.*, vol. 47, no. 7, pp. 1050-1060, 2017.

[70] J. Wang, G. Wen, Z. Duan and J. Lü, "Stochastic Consensus Control Integrated With Performance Improvement: A Consensus Region-Based Approach," *IEEE Trans. Ind. Electron.*, vol. 67, no. 4, pp. 3000-3012, 2020.

[71] L. Li, Z. Li, Y. Xia, and J. Yan, "Event-triggered bounded consensus for stochastic multi-agent systems with communication delay," *Int. J. Control*, pp. 1–24, 2021.

[72] X. Cao, C. Zhang, D. Zhao, B. Sun, and Y. Li, "Event-triggered consensus control of continuous-time stochastic multi-agent systems," *Automatica.*, vol. 137, no. 110022, p. 110022, 2022.

[73] W. Zou, P. Shi, Z. Xiang and Y. Shi, "Consensus Tracking Control of Switched Stochastic Nonlinear Multiagent Systems via Event-Triggered Strategy," *IEEE Trans. Neural Netw. Learn. Syst.*,, vol. 31, no. 3, pp. 1036-1045, 2020.

[74] D. Ding, Z. Wang, B. Shen, and G. Wei, "Event-triggered consensus control for discrete-time stochastic multi-agent systems: The input-to-state stability in probability," *Automatica*, vol. 62, pp. 284–291, 2015.

[75] L. Ma, Z. Wang, and H.-K. Lam, "Event-triggered mean-square consensus control for time-varying stochastic multi-agent system with sensor saturations," *IEEE Trans. Autom. Control.*, vol. 62, no. 7, pp. 3524–3531, 2017.

[76] Z. Feng and G. Hu, "Secure cooperative event-triggered control of linear multiagent systems under DoS attacks," IEEE Trans. Control Syst. Technol., vol. 28, no. 3, pp. 741–752, 2020.

[77] Y. Xu, M. Fang, Z.-G. Wu, Y.-J. Pan, M. Chadli, and T. Huang, "Input-based event-triggering consensus of multiagent systems under denial-of-service

attacks," IEEE Trans. Syst. Man Cybern. Syst., vol. 50, no. 4, pp. 1455–1464, 2020.

[78] Y. Yang, Y. Li, D. Yue, Y.-C. Tian, and X. Ding, "Distributed secure consensus control with event-triggering for multiagent systems under DoS attacks," IEEE Trans. Cybern., vol. 51, no. 6, pp. 2916–2928, 2021.

[79] Y. Xu, M. Fang, P. Shi, and Z.-G. Wu, "Event-based secure consensus of multi-agent systems against DoS attacks," IEEE Trans. Cybern., vol. 50, no. 8, pp. 3468–3476, 2020.

[80] T. Dong and Y. Gong, "Leader-following secure consensus for second-order multi-agent systems with nonlinear dynamics and event-triggered control strategy under DoS attack," Neurocomputing, vol. 416, pp. 95–102, 2020.

[81] T.-Y. Zhang and D. Ye, "Distributed event-triggered control for multi-agent systems under intermittently random denial-of-service attacks," Inf. Sci. (Ny), vol. 542, pp. 380–390, 2021.

[82] W. Xu, G. Hu, D. W. C. Ho, and Z. Feng, "Distributed secure cooperative control under denial-of-service attacks from multiple adversaries," IEEE Trans. Cybern., vol. 50, no. 8, pp. 3458–3467, 2020.

[83] W. Xu, D. W. C. Ho, J. Zhong, and B. Chen, "Event/self-triggered control for leader-following consensus over unreliable network with DoS attacks," IEEE Trans. Neural Netw. Learn. Syst., vol. 30, no. 10, pp. 3137–3149, 2019.

[84] J. Liu, T. Yin, D. Yue, H. R. Karimi, and J. Cao, "Event-based secure leader-following consensus control for multiagent systems with multiple cyber attacks," IEEE Trans. Cybern., vol. 51, no. 1, pp. 162–173, 2021.

[85] C. De Persis and P. Tesi, "Input-to-state stabilizing control under denial of-service," IEEE Trans. Autom. Control, vol. 60, no. 11, pp. 2930–2944, Nov. 2015.

[86] S. Feng, A. Cetinkaya, H. Ishii, P. Tesi, and C. De Persis, "Networked control under dos attacks: Tradeoffs between resilience and data rate," IEEE Transactions on Automatic Control, vol. 66, no. 1, pp. 460–467, 2020.

[87] D. Senejohnny, P. Tesi, and C. De Persis, "A jamming-resilient algorithm for self-triggered network coordination," IEEE Transactions on Control of Network Systems, vol. 5, no. 3, pp. 981–990, 2017.

[88] H. Sun, C. Peng, W. Zhang, T. Yang, and Z. Wang, "Security-based resilient event-triggered control of networked control systems under denial of service attacks," J. Franklin Institute, vol. 356, no. 17, pp. 10277–10295, 2019.

[89] M. Miskowicz, "Send-on-delta concept: An event-based data reporting strategy," *Sensors (Basel)*, vol. 6, no. 1, pp. 49-63, 2006.

[90] P. Tabuada, "Event-triggered real-time scheduling of stabilizing control tasks," *IEEE Trans. Autom. Control.*, vol. 52, no. 9, pp. 1680-1685, 2007.

[91] D. P. Borgers and W. P. M. H. Heemels, "Event-separation properties of event-triggered control systems," *IEEE Trans. Autom. Control.*, vol. 59, no. 10, pp. 2644-2656, 2014.

[92] D. Liu, Z. Wang, Y. Liu, and F. E. Alsaadi, "Extended Kalman filtering subject to random transmission delays: Dealing with packet disorders," *Inf. Fusion*, vol. 60, pp. 80–86, 2020.

[93] A. Wang, B. Mu, and Y. Shi, "Consensus control for a multi-agent system with integral-type event-triggering condition and asynchronous periodic detection," *IEEE Trans. Ind. Electron.*, vol. 64, no. 7, pp. 5629–5639, 2017.

[94] B. Mu, K. Zhang, F. Xiao, and Y. Shi, "Event-based rendezvous control for a group of robots with asynchronous periodic detection and communication time delays," *IEEE Trans. Cybern.*, vol. 49, no. 7, pp. 2642–2651, 2019.

[95] A. Wang, B. Mu, and Y. Shi, "Event-triggered consensus control for multiagent systems with time-varying communication and event-detecting delays," *IEEE Trans. Control Syst. Technol.*, vol. 27, no. 2, pp. 507–515, 2019.

[96] T. K. Tasooji and H. J. Marquez, "Event-Triggered Consensus Control for Multi-Robot Systems with Cooperative Localization" IEEE Trans. Ind. Electron., July 2022, doi: 10.1109/TIE.2022.3192673

[97] Soni A, Hu H. Formation control for a fleet of autonomous ground vehicles: A survey. Robotics. 2018 Nov 1;7(4):67.

[98] WIKIPEDIA. "Graph theory" [Online]. Available: https://en.wikipedia.org/wiki/ Graph_theory/ (visited on 8/9/2022).

[99] H. J. Marquez, Nonlinear Control Systems: Analysis and Design. New Jersey: John Wiley & Sons, Inc., 2003.

[100] Boyd, S., El Ghaoui, L., Feron, E. and Balakrishnan, V., 1994. Linear matrix inequalities in system and control theory. Society for industrial and applied mathematics.

[101] GCTronic. (2018). "E-puck," [Online]. Available: http: / / www. e - puck. org/ (visited on 11/12/2021).

[102] Fathinezhad, Fatemeh, Vali Derhami, and Mehdi Rezaeian. "Supervised fuzzy reinforcement learning for robot navigation." Applied Soft Computing 40 (2016): 33-41.

[103] M. Sugisaka, H. Tanaka, V. Trifa, C. Cianci, and D. Guinard, "Dynamic control of a robotic swarm using a service-oriented architecture," Jan. 2008.

[104] R. Visvanathan, S. M. Mamduh, K. Kamarudin, A. S. A. Yeon, A. Zakaria, A. Y. M. Shakaff, L. M. Kamarudin, and F. S. A. Saad, "Mobile robot localization system using multiple ceiling mounted cameras," in 2015 IEEE SENSORS, 2015, pp. 1–4.

[105] StereoLab. (2020). "Stereo lab," [Online]. Available: https://support.stereolabs. com/hc/en- us/articles/207616785-Getting-Started- with- your- ZED- camera (visited on 11/02/2021).

[106] H. Koki, Z. Tadanao, O. Noriaki, and L. Kang-Zhi, "Optimal formation control of two-wheeled vehicles using model predictive control," in 2015 10th Asian Control Conf. (ASCC), Chiba, Japan, 2015.

[107] M. Quigley, K. Conley, B. Gerkey, J. Faust, T. Foote, J. Leibs, R. Wheeler, and A. Ng, "Ros: An open-source robot operating system," vol. 3, Jan. 2009.

[108] J. Sch¨onberger, M. Pollefeys, A. Geiger, and T. Sattler, "Semantic visual localization," in 2018 IEEE Conf. Computer Vision and Pattern Recognition, Jun. 2018.

[109] M. Fiala, "Vision guided control of multiple robots," in Proc. First Canadian Conf. Computer. Robot. Vision., 2004, pp. 241–246.

[110] Q. Van Tran and H.-S. Ahn, "Distributed formation control of mobile agents via global orientation estimation," IEEE Trans. Control Network Syst., vol. 7, no. 4, pp. 1654–1664, 2020.

[111] B. Mu, J. Chen, Y. Shi, and Y. Chang, "Design and implementation of nonuniform sampling cooperative control on a group of two-wheeled mobile robots," IEEE Trans. Ind. Electron., vol. 64, no. 6, pp. 5035–5044, Jun. 2017.

[112] B. Wang, W. Chen, J. Wang, B. Zhang, Z. Zhang, and X. Qiu, "Cooperative tracking control of multiagent systems: A heterogeneous coupling network and intermittent communication framework," IEEE Trans. Cybern., vol. 49, no. 12, pp. 4308–4320, Dec. 2019.

[113] J. Hu, Z. Wang, H. Gao, and L. K. Stergioulas, "Kalman filtering with stochastic nonlinearities and multiple missing measurements," *Automatica*, vol. 48, no. 9, pp. 2007-2015, 2012.

[114] S. Weerakkody, Y. Mo, B. Sinopoli, D. Han, and L. Shi, "Multi-sensor scheduling for state estimation with event-based, stochastic triggers," *IEEE Trans. Autom. Control.*, vol. 61, no. 9, pp. 2695-2701, 2016.

[115] J. Fink, A. Ribeiro, and V. Kumar, "Robust control for mobility and wireless communication in cyber-physical systems with application to robot teams," *Proc. IEEE Inst. Electr. Electron. Eng.*, vol. 100, no. 1, pp. 164-178, 2012.

[116] B. Tao, H. Wu, Z. Gong, Z. Yin, and H. Ding, "An RFID-based mobile robot localization method combining phase difference and readability," *IEEE Trans. Autom. Sci. Eng.*, vol. 18, no. 3, pp. 1406-1416, 2021.

[117] R. M. Salinas and B. Magyar, "ArUco ROS library," 2015. [Online].Available: http://wiki.ros.org/aruco

[118] H. Rezaei, R. Mahboobi Esfanjani, and M. H. Sedaaghi, "Improved robust finite-horizon Kalman filtering for uncertain networked time-varying systems," *Inf. Sci. (Ny)*, vol. 293, pp. 263–274, 2015.

[119] Jacob Perron, Michael Carroll, "message filters ROS library," [Online].Available: http://wiki.ros.org/message_filters.

[120] K. Manandhar, X. Cao, F. Hu, and Y. Liu, "Detection of faults and attacks including false data injection attack in smart grid using Kalman filter," *IEEE Trans. Control Netw. Syst.*, vol. 1, no. 4, pp. 370–379, 2014.

[121] J. Huang, Y. Tang, W. Yang, and F. Li, "Resilient consensus-based distributed filtering: Convergence analysis under stealthy attacks," *IEEE Trans. Industr. Inform.*, vol. 16, no. 7, pp. 4878–4888, 2020.

[122] L. Li, H. Yang, Y. Xia, and H. Yang, "Event-based distributed state estimation for linear systems under unknown input and false data injection attack," *Signal Processing*, vol. 170, no. 107423, p. 107423, 2020.

[123] H. Gao, H. Dong, Z. Wang and F. Han, "Recursive Minimum-Variance Filter Design for State-Saturated Complex Networks With Uncertain Coupling Strengths Subject to Deception Attacks," in *IEEE Trans. Cybern*, doi: 10.1109/TCYB.2021.3067822

[124] D. Ding, Q.-L. Han, Z. Wang, and X. Ge, "A survey on model-based distributed control and filtering for industrial cyber-physical systems," *IEEE Trans. Industr. Inform.*, vol. 15, no. 5, pp. 2483–2499, 2019.

[125] X. -M. Li, D. Yao, P. Li, W. Meng, H. Li and R. Lu, "Secure Finite-Horizon Consensus Control of Multiagent Systems Against Cyber Attacks," in IEEE Trans. Cybern., doi: 10.1109/TCYB.2021.3052467.

[126] A. Sargolzaei, K. Yazdani, A. Abbaspour, C. D. Crane III and W. E. Dixon, "Detection and Mitigation of False Data Injection Attacks in Networked Control Systems," in IEEE Trans. Industr. Inform., vol. 16, no. 6, pp. 4281-4292, June 2020

[127] H. Gao, H. Dong, Z. Wang and F. Han, "Recursive Minimum-Variance Filter Design for State-Saturated Complex Networks With Uncertain Coupling Strengths Subject to Deception Attacks," in IEEE Trans. Cybern, doi: 10.1109/TCYB.2021.3067822

[128] Z. -H. Pang, G. -P. Liu, D. Zhou, F. Hou and D. Sun, "Two-Channel False Data Injection Attacks Against Output Tracking Control of Networked Systems," in IEEE Trans. Industr. Electron., vol. 63, no. 5, pp. 3242-3251, May 2016

[129] S. Liu, G. Wei, Y. Song, and Y. Liu, "Extended Kalman filtering for stochastic nonlinear systems with randomly occurring cyber attacks," Neurocomputing, vol. 207, pp. 708–716, 2016.

[130] B. Cui, X. Chen and X. Tang, "Improved Cubature Kalman Filter for GNSS/INS Based on Transformation of Posterior Sigma-Points Error," in IEEE Trans. Signal Process., vol. 65, no. 11, pp. 2975-2987, 2017

[131] K. Reif, S. Gunther, E. Yaz, and R. Unbehauen, "Stochastic stability of the discrete-time extended Kalman filter," IEEE Trans. Autom. Control., vol. 44, no. 4, pp. 714–728, 1999.

[132] J. Wang, G. Wen, Z. Duan and J. Lü, "Stochastic Consensus Control Integrated With Performance Improvement: A Consensus Region-Based Approach," *IEEE Trans. Ind. Electron.*, vol. 67, no. 4, pp. 3000-3012, April 2020

[133] B. Li, G. Wen, Z. Peng, T. Huang and A. Rahmani, "Fully Distributed Consensus Tracking of Stochastic Nonlinear Multiagent Systems With Markovian Switching Topologies via Intermittent Control," *IEEE Trans. Syst., Man, Cybern., Syst.*, vol. 52, no. 5, pp. 3200-3209, May 2022.

[134] Derui Ding, Zidong Wang, D. W. C. Ho, and Guoliang Wei, "Observer-based event-triggering consensus control for multiagent systems with lossy sensors and cyber-attacks," *IEEE Trans. Cybern.*, vol. 47, no. 8, pp. 1936–1947, 2017.

[135] H. Li, X. Liao, T. Huang, and W. Zhu, "Event-triggering sampling based leader-following consensus in second-order multi-agent systems," *IEEE Trans. Autom. Control.*, vol. 60, no. 7, pp. 1998–2003, Jul. 2015.

[136] X. Ge, Q.-L. Han, and F. Yang, "Event-based set-membership leader-following consensus of networked multi-agent systems subject to limited communication resources and unknown-but-bounded noise," *IEEE Trans. Ind. Electron.*, vol. 64, no. 6, pp. 5045–5054, 2017.

[137] H. Qu and J. Zhao, "Event-triggered H_∞ filtering for discrete-time switched systems under denial-of-service," IEEE Trans. Circuits Syst. I Regul. Pap., vol. 68, no. 6, pp. 2604–2615, 2021.

[138] Boyd, S., El Ghaoui, L., Feron, E. and Balakrishnan, V., 1994. Linear matrix inequalities in system and control theory. Society for industrial and applied mathematics.